A New Relaying Method for Third Zone Distance Relay Blocking During Power Swings

A Thesis Submitted

to the College of Graduate and Postdoctoral Studies

in

Partial Fulfillment of the Requirements

for the Doctor of Philosophy Degree

in the Department of Electrical and Computer Engineering
University of Saskatchewan

by

Don Kang

Saskatoon, Saskatchewan, Canada

Permission to Use

In presenting this thesis in partial fulfillment of the requirements for a Postgraduate degree from the University of Saskatchewan, it is agreed that the Libraries of this University may make it freely available for inspection. Permission for copying of this thesis in any manner, in whole or in part, for scholarly purposes may be granted by the professors who supervised this thesis work or, in their absence, by the Head of the Department of Electrical and Computer Engineering or the Dean of the College of Graduate and Postdoctoral Studies at the University of Saskatchewan. Any copying, publication, or use of this thesis, or parts thereof, for financial gain without the written permission of the author is strictly prohibited. Proper recognition shall be given to the author and to the University of Saskatchewan in any scholarly use which may be made of any material in this thesis.

Request for permission to copy or to make any other use of material in this thesis in whole or in part should be addressed to:

Head of the Department of Electrical and Computer Engineering
University of Saskatchewan
57 Campus Drive
Saskatoon, Saskatchewan S7N 5A9
Canada
OR

Dean of the College of Graduate and Postdoctoral Studies
University of Saskatchewan
116 Thorvaldson Building, 110 Science Place
Saskatoon, Saskatchewan S7N 5C9
Canada

Abstract

Due to the increasing complexity of modern bulk power systems, the power swing identification, blocking, and protection have become more challenging than they used to be. Among various transmission line protection methods, distance relays are the most commonly used type. One of the advantages of using distance relays is the zoned protection which provides redundancy. However, the additional redundancy comes with a problem that it increases the probability of incorrect operation. For example, the undesired operation of the third zone distance protection during power swing scenarios has been attributed as one of the major causes for creating large-scale blackouts. Some research works in the literature investigate proper identification of stable and unstable power swing conditions. Most research works dwell on identification of power swing conditions but do not address how the scheme could be used for blocking the third zone of distance relays during stable power swings. Also, the current power swing detection schemes are often very complex to implement for a relaying engineer or are not fast enough for blocking the third zone distance element.

This research proposes a reliable and fast methodology for the third zone blocking (TZB) during power swings. The new mathematical formulations and derivations are based on sound time tested power system theory and are simpler to understand for a relaying engineer to implement this technique. The algorithm proposed in the research can prevent unnecessary tripping of distance relays during power swings. The algorithm also overcomes the shortcomings of the conventional power swing identification methods when applied for the third zone blocking. A first zero-crossing (FZC) concept is introduced as the criteria for identifying stable power swing or out-of-step phenomena. The analysis is based on system stability point of view and utilizes power-angle equations. The proposed algorithm could be applied at every discrete time interval or time step of a distance relay to detect power swing points. It could also be applied to any transmission line in the power system by finding an

equivalent single machine infinite bus (SMIB) configuration individually for each line on a real-time basis, which is one of the primary advantages of the proposed method.

In the thesis work, the proposed technique is first demonstrated using a simple single machine infinite bus system. The TZB algorithm is then tested using a modified Western Electricity Coordinating Council (WSCC) power system configuration using Power System Analysis Toolbox (PSAT) simulations. The code is written in MATLAB. The TZB method is then further analyzed using electromagnetic simulations with Real-Time Digital Simulator (RTDS) on WSCC system. The proposed method uses small time step simulations (50 μs) to take various aspects of power system complexity into consideration, such as different harmonics presents in the system, synchronous machine operation at different speeds, travelling wave representation of transmission lines instead of purely lumped parameter representation, etc.

The investigations as mentioned above and the results show that the proposed TZB scheme is a straightforward and reliable technique, involving only a few calculation steps, and could be applied to any power system configuration. The main novelty of this technique is that it does not require a priori stability study to find the relay settings unlike conventional power swing identification or distance relay blocking techniques. The inputs to the relay are basic electrical quantities which could be easily measured locally on any transmission line. The local measurements would make the implementation of the proposed TZB simpler for relaying applications compared to Wide Area Measurement System (WAMS) based techniques. In a WAMS based relaying technique – the cost associated with the communication network, reliability of the communication network, impact of communication delay on relay, etc all become factors for actual industry use.

Acknowledgments

This research project and the thesis work was carried out in the Department of Electrical and Computer Engineering at the University of Saskatchewan and was under the supervision of Dr. Ramakrishna Gokaraju. First of all, my sincere appreciation goes to Dr. Ramakrishna (Rama) Gokaraju for his effort and help provided in my Ph.D. research. Especially, those days and nights he sat with me editing my reports, papers, as well as the thesis will never be forgotten.

My sincere appreciations also go to the Advisory Committee member Dr. Rajesh Karki for providing helpful advice in my research since the early stage of this project. My appreciation also goes to Department Graduate Chair Dr. Seok-Bum Ko for giving support at crucial junctures. Many thanks to Acting Department Graduate Chair Dr. Anh V. Dinh, Former Graduate Chair Dr. David M. Klymyshyn, Dr. Nurul A. Chowdhury, and Dr. Daniel X. B. Chen for sitting in my Advisory Committee and giving kind support. It has been an honour for me having Dr. Richard T. Burton sitting in my Advisory Committee as a Cognate Member. The thoughtful advice he gave not only motivated me to progress in the thesis work but also his advice will guide me in the future beyond my studies.

The author would like to thank Dr. M. Ramamoorty (Retired Director General, Central Power Research Institute, Bangalore, India & Formerly Professor of Indian Institute of Technology, Kanpur, India), Mr. Sivaramakrishnan Raman (Visiting Student under the supervision of Dr. Rama Gokaraju, University of Saskatchewan, Saskatoon, SK, Canada) for providing their inputs for the research work.

Thanks also go to Department Secretary Ms. Jan Compain, as well as to my current and previous lab mates, such as Dr. Eli Pajuelo for discussing the proposed methodology during development, Ms. Nataliia Petryshyn for teaching me PSAT software, and others like, Dr. Dipendra Rai, Mr. Binod Shrestha, Mr. Parikshit Sharma, Mr. Bikash Shrestha, Mr. Indra

Karmacharya, Mr. Shane Jin, Mr. Shea Pederson, Mr. Douglas Wagner, etc.

Thanks to March Consulting Associates Inc. the company I was working with for providing conveniences and flexibility during the period of my study. Special thanks go to my wife, Dr. Sue Li. Her understanding and financial support made it possible for me to self-support my graduate studies and to pursue my ambition of getting the highest degree.

Don Kang

Dedicated to

my mother Wang, Yiwen and father Kang, Jingliang

Table of Contents

List of Tables

List of Figures

List of Symbols and Abbreviations

$ADRS$	Adaptive Distance Relay Scheme
ANN	Artificial Neural Network
ATP	Alternative Transients Program
$AURORA$	Avoid Unwanted Reclosing On Rotating Apparatus
TZB	Third Zone Blocking
CCA	Critical Clearing Angle
CCT	Critical Clearing Time
COD	coefficient of determination
CTs	the current transducers
$CVTs$	the capacitor voltage transducers
DFT	Digital Fourier Transform
DSE	Dynamic State Estimation
EAC	Equal Area Criteria
EDT	East Daylight Time
$EEAC$	Extended Equal Area Criteria
EHV	Extra High Voltage
$EMTDC$	Electromagnetic Transients including DC
$EPRI$	Electric Power Research Institute
$FACTS$	Flexible AC Transmission System
FE	First Energy
FFT	Fast Fourier Transform
FIS	Fuzzy Inference System

FZC	First Zero Crossing
GPC	Giga Processor Card
GPS	Global Positioning System
GSF	generation shift factor
$GTWIF$	GT Workstation Interface
$GUIs$	graphical user interfaces
ICA	Independent Component Analysis
IEC	International Electrotechnical Commission
$IEEE$	Institute of Electrical and Electronic Engineers
$LGFLT$	line to ground fault
$LODF$	line outage distribution factor
LRI	Left Resistance Inner
LRO	Left Resistance Outer
$MISO$	Midwest Independent System Operator
MBP	Mobipocket Notes
$PB5$	PB5 Processor Card
$PCOA$	Partial Center of Angles
PLL	phase-locked-loop
PMU	Phasor Measurement Unit
$PSAT$	Power System Analysis Toolbox
$PSCAD$	Power Systems Computer Aided Design
$PSRC$	Power System Relaying and Control Committee
$P2P$	peer to peer
$QUAD$	Quadrilateral Characteristics

RMS	root mean square
RRI	Right Resistance Inner
RRO	Right Resistance Outer
$RSCAD$	Real-Time Digital Simulator Computer Aided Design
$RTDS$	Real-Time Digital Simulator
SCV	Swing Centre Voltage
SEM	Swing Equation Method
$SMIB$	single machine infinite bus
SOC	Second-of-Century
SPA	State Plane Analysis
SVM	Support Vector Machine
TE	electrical torque
TM	mechanical torque
UCA	Utility Communications Architecture
$UCTE$	Union for the Co-ordination of Transmission of Electricity
UKF	Unscented Kalman Filter
UTC	Universal Time Coordinated
$WSCC$	Western Systems Coordinating Council
WIF	Workstation InterFace

List of Publications

Following publications resulted from the work reported in this thesis.

List of Journal Papers:

D. Kang, R. Gokaraju, "A new method for blocking third-zone distance relays during stable power swings," *IEEE Transactions on Power Delivery (Special Issue: Frontiers of Power System Protection),* Vol. 31, Issue 4, pp. 1836-1843, January 2016.

List of Conference Presentations:

D. Kang, R. Gokaraju, "A new method for blocking third-zone distance relays during stable power swings," *IEEE Transactions on Power Delivery*, Presented at the IEEE PES General Meeting in Chicago, USA, July 16-20, 2017.

List of Poster Presentations:

D. Kang, R. Gokaraju, "A new method for blocking third-zone distance relays during stable power swings in power systems," Presented at the IEEE PES General Meeting in Vancouver, Canada, July 21-25, 2013.

Chapter 1

Introduction

1.1 Power System Protection

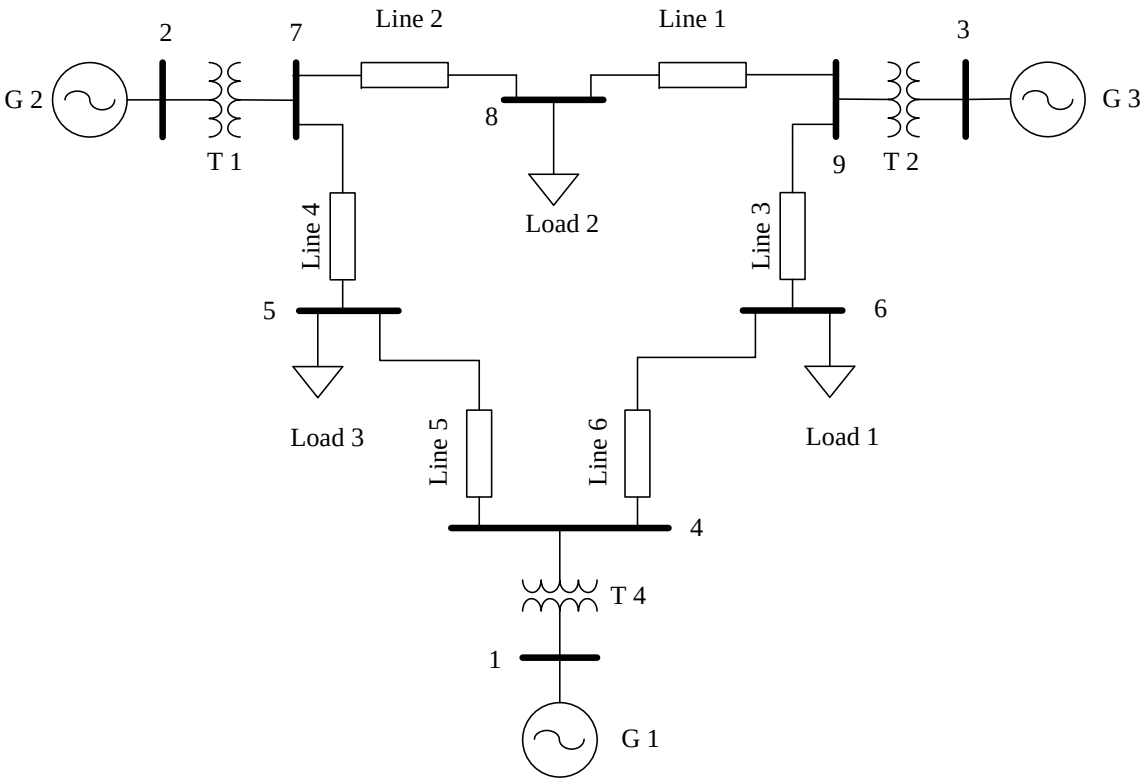

Figure 1.1: Typical Western Systems Coordinating Council 9 bus power system. [2]

In modern complex power system networks, the generating stations and subtransmission feed points are interconnected, therefore no radial or single-loop systems can be found [1].

A schematic diagram of a Western Systems Coordinating Council 9 bus power system is shown as an example in Figure 1.1. In this test system, the electrical power is generated from generating stations, and in step-up transformer substations it is converted from a lower voltage to 230kV high voltage to be delivered to step-down transformer substations, and to supply consumer loads. The primary objective of all power systems in general is to provide a highly reliable and continuous electricity supply to consumers. Nevertheless, with continuous increase in electrical loads, the transmission systems are often being operated under stressed conditions and as a result power systems of nowadays are more sensitive to disturbances than before, thus the modern interconnected networks are more likely losing stability that could lead to a partial or complete blackout [15].

Losing power, voltage drops in the power system and overcurrent situations can inevitably occur due to the natural events, physical accidents, equipment failures or misoperations [16]. The states in which a power system operates can be categorized as an alert state, an emergency state, and an in-extremis or islanding state [17]. In an alert state, the power system experiences an incident which often does not lead to an interruption. In an emergency state, the power system incident needs an immediate action. If the faulted portion of the power system is not isolated at the right time from the rest of the grid, the situation may deteriorate further due to the automatic protective device operation causing generation-load balance issues and lead to wider-scale power system instability. In the in-extremis or islanding state the large power network is separated into small areas or islands, where the loads are supplied from local generations. Once the system comes to this state, it cannot go back to the emergency mode without operator's intervention. As the chain of events happen in various sections of the grid, a flood of alarms occur and also there is incomplete information coming from some portions of the network creating a vastly complex situation for the operator to mitigate the fast developing disturbance situation in a manual mode [17]. This essentially means that the protective devices have to be prudently designed for their automatic operation to control the impact of the disturbance. For automatic operations, the proper sequential operation of local and back-up protection functions is also essential (i.e. in case of a local protection failure).

The five basic facets of all power system protection as described in [16] are: Reliability: the certainty that protection operates correctly; Selectivity: the ability of keeping continuity of service with the minimum amount of disconnection; Operational Speed: high speed fault clearance to prevent equipment damages and hazards to personnel; Simplicity of the Methodology: to achieve the protection reliability objectives; Economics: the maximum amount of protection at a least amount of total cost.

1.2 Power System Relaying

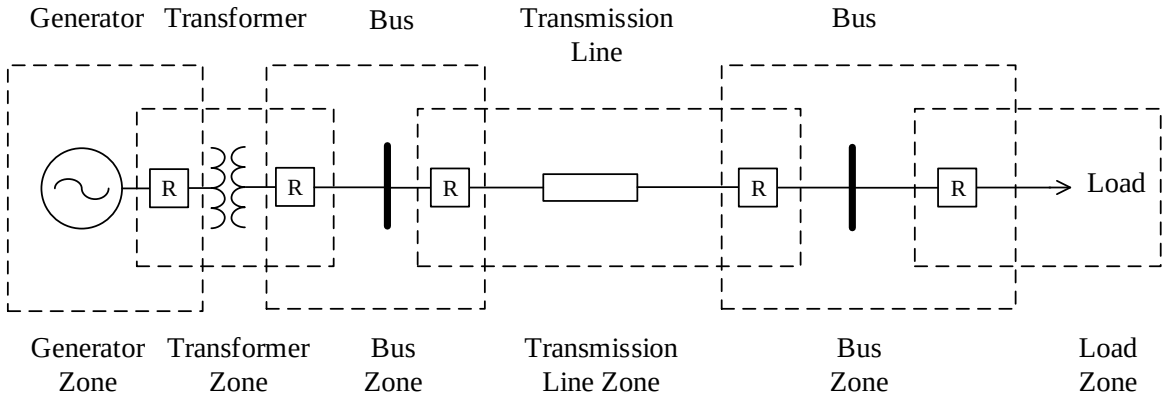

Figure 1.2: Protective relay overlapped protection zone.

A protective relay apart from its basic logical components also consists of other subsystems, such as circuit breakers, transducers, and batteries, etc [18]. Circuit breakers interrupt electric circuits at near current zero by energizing their operating coils [19]. The transducers, such as CTs and CVTs, convert the voltage and current to an acceptable lower level to drive relays as well as other logical devices.

Power system protective relays are implemented by dividing the power system into protection zones and contingencies can be removed by disconnecting a minimum proportion of the system [4]. To reduce the possibility of the unprotected section of the system, the adjacent protection zones are overlapped as shown in Figure 1.2. The boundaries of the protection zones are determined by the locations of current transformers (CTs). The protection

zones overlaps each other by locating CTs as shown in Figure 1.3. In order to ensure that the power system operates properly; the various protective relays need to be coordinated accordingly. For example, when a fault happens, the primary relay assigned to this zone is supposed to operate. If it does not operate, the backup relays that are available have to clear this fault. The postmortem analysis of many of the previous power system incidents have shown that the backup protective relays can cause cascading type events (i.e. backup relay operation in one portion of the network could make another portion of the network vulnerable) [15]. Generally, a good amount of redundancy is needed to achieve dependability. However, the additional redundancy comes with a problem: it increases the probability of incorrect operation even though that it improves dependability, therefore, a balance is needed between the dependability and the security [16].

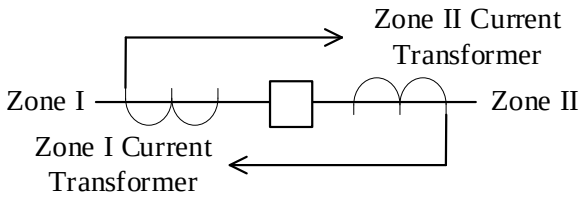

Figure 1.3: Protective relay CT placement for overlapped protection zone. [3]

The protective relays are of paramount importance to accomplish power system protection tasks. A protective relay is defined by Institute of Electrical and Electronic Engineers (IEEE) as "an electric device that is designed to respond to input conditions in a prescribed manner and, after specified conditions are met, to cause contact operation or similar abrupt change in associated electric control circuits." "Inputs are usually electric, but may be mechanical, thermal, or other quantities or a combination of quantities" [20].

The protective relays can be categorized by their input: current, voltage, power, frequency, and temperature, or the technology they use: electromechanical, solid-state, digital, numerical relays, or by their performance characteristics such as distance, reactance, directional overcurrent, inverse time, phase, ground, overcurrent, undervoltage, overvoltage, percentage differential relays etc. [16]. Whenever contingencies happen in a power system,

the various protection devices quickly operate to isolate the fault and also to minimize the extent of outage on the system.

1.3 Distance Relay

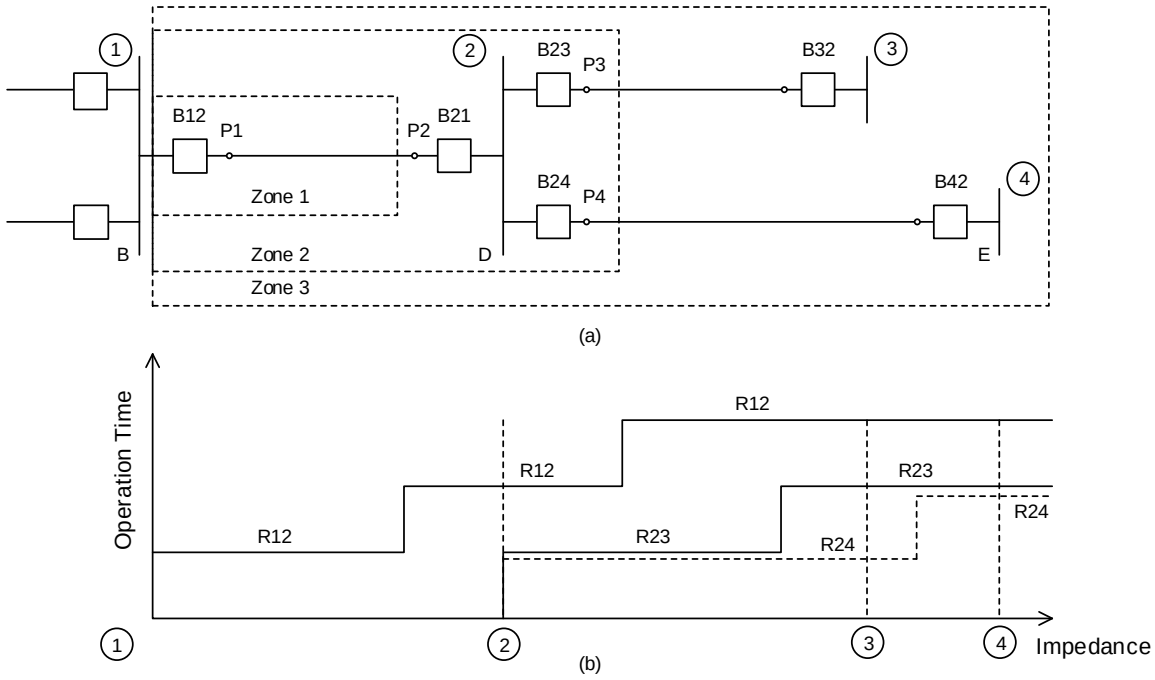

Figure 1.4: (a) Zone protection. (b) Time delays associated with different zones. [1]

1.3.1 Zone Protection

The distance relay started appearing around 1923 in an effort to overcome the problems associated with the simpler type of graded time overcurrent relays [21]. Well applicable to complex power system networks without radial or single-loop systems, the distance relay provides protection for the transmission lines connected to a network by measuring the impedance at the relay point, which is proportional to the distance to a fault and is inde-

pendent of the fault current level. This protection has a number of advantages compared to the overcurrent relay in power system network protection, e.g., greater trip coverage, greater sensitivity, easier setting, calculation and coordination, fixed zone of protection, and it is relatively independent of the system changes, requires less maintenance, has more independence for load changes [4].

The distance relay responds to the calculated electrical circuit distance between the relay location and the fault point as a function of its measured inputs. In other words, a distance relay measures the voltage and current of the power system at the relay point to determine whether a detected fault is within or outside its protection zones. That is

$$Z_{app} = E/I \tag{1.1}$$

where Z_{app} is the apparent impedance, E and I are the measured voltage and current at the relay point.

Generally for transmission line protections, three protection zones are applied to provide backup for the remote section. In Figure 1.4, a transmission line protection is described. In Figure 1.4a, Zone 1 of the relay B12 is designed to cover about 80% length of the section BD. Zone 2 is set to cover 120% length of BD. Zone 3 covers the section BD and 120% of the section DE. The transmission line in Figure 1.4 could be as long as hundreds of kilometers. Figure 1.4b shows the time delays for the relays in different zones.

1.3.2 Mho Relay

The impedance relays do not have a directional impedance characteristic, therefore a separate directional unit is required to limit the tripping area for line faults as shown in Figure 1.5a [4]. In the same fashion, the reactance relays can not work independently as well, since the load impedance may appear on the protection characteristics on an impedance plane. The reactance relay as shown in Figure 1.5b also needs a directional unit to confine the operational area.

The mho relay has a fixed protection coverage to prevent the load impedance intruding

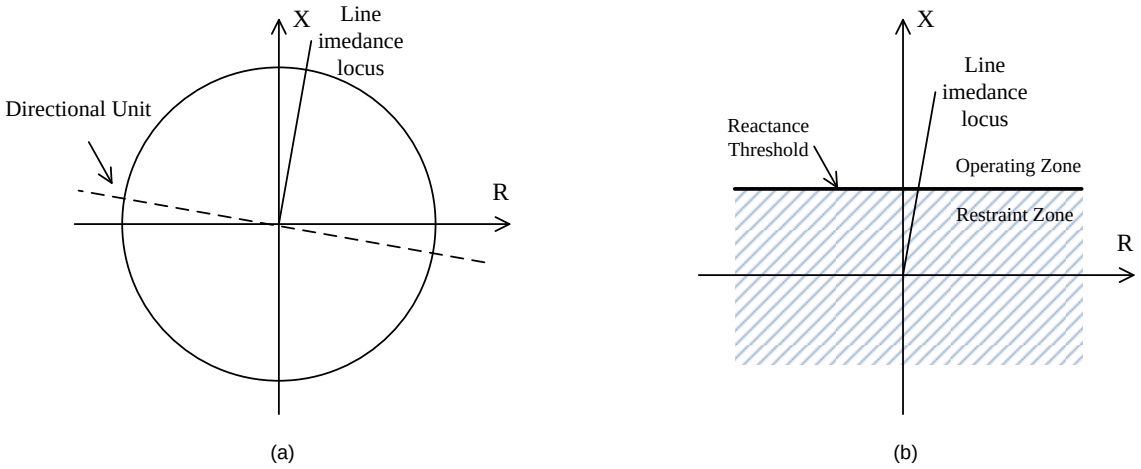

Figure 1.5: (a) Impedance relay characteristics. (b) Reactance relay characteristics. [4]

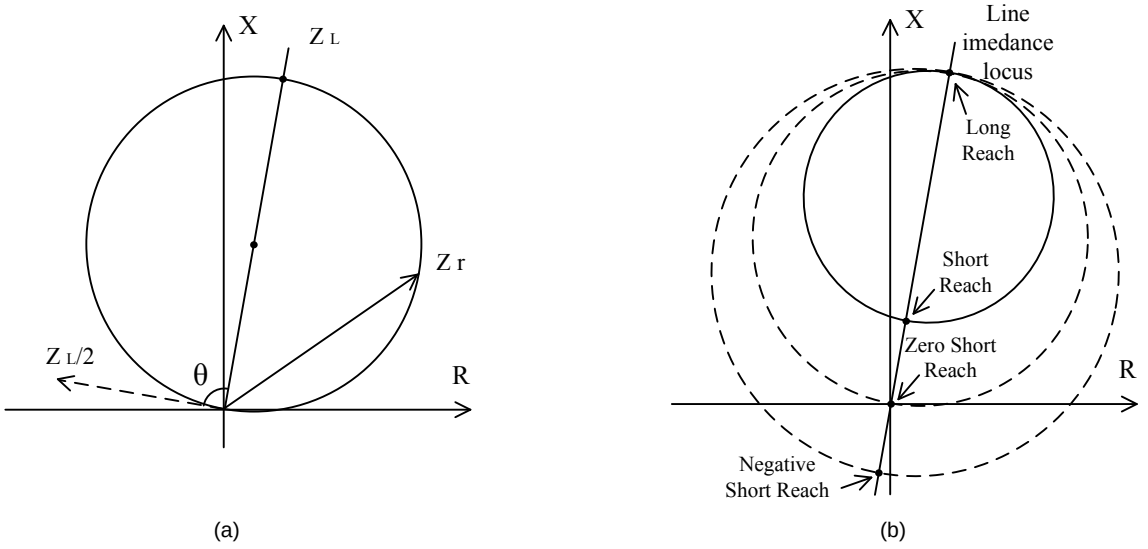

Figure 1.6: (a) Mho relay characteristics. (b) Offset mho relay characteristics. [4]

into the relay characteristics, and it has an inherent directional protection feature to limit the operation in response to the predefined zones as shown in Figure1.6a. The operating zone of a mho circle is defined by Equation 1.3 [4]

$$Z_r = \frac{Z_L - Z_L \angle \theta}{2} \tag{1.2}$$

where Z_r is the reach of the relay; Z_L is the protection reach impedance on the transmission line; θ varies from 0° to 360°, which works to define a circle whose center is at $\frac{Z_L}{2}$ and radius is the magnitude of $\frac{Z_L}{2}$.

The amplitude comparator and phase comparator can be employed to determine the operation of the mho relay [21]. The mho relay operates when the contingency is within the mho relay characteristics, i.e.

$$\left|C_O\right| \geq \left|C_R\right| \tag{1.3}$$

where C_O is the operation signal of the amplitude comparator, and C_R is the restraint signal of the amplitude comparator.

Or, expressed as a phase comparator

$$\left|\angle\phi_1 - \angle\phi_2\right| < 90^\circ \tag{1.4}$$

when

$$C_1 = C_O - C_R \tag{1.5}$$

$$C_2 = C_O + C_R \tag{1.6}$$

where C_1 is the difference phasor of C_O and C_R; and C_2 is the phasor sum of C_O and C_R; ϕ_1 is the angle of C_1; ϕ_2 is the angle of C_2.

The offsetting mho relay adjusts the relay characteristics to expand or shrink its coverage, in order to be less susceptible to a load encroachment or alternatively encompass the relay location into the protection zone, even providing reverse coverage to an adjacent line [14] as shown in Figure1.6b.

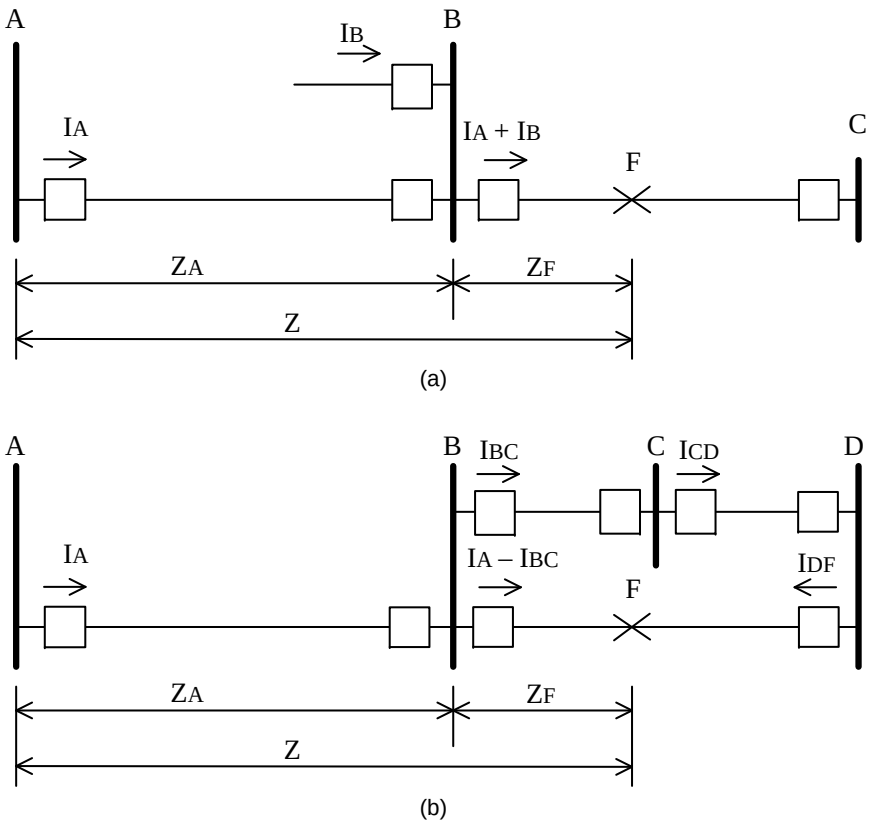

Figure 1.7: Infeed and outfeed impact on distance relay zone protection.

1.3.3 Infeed and Outfeed Impact on Distance Relays

The mho relay selectivity can be affected by contingency scenarios, fault impedance values, operating conditions, as well as due to different devices in the system, some of these issues are discussed in [22] [23]. For instance, when there is a source which could contribute to a fault current within the operating zone of a distance relay, its reach will be reduced and would be a function of the fault current [4]. This effect of infeed current can be analyzed using Figure 1.7a, where there is a source feeding current to a fault at F from Bus B. When there is a solid/bolted fault at F which is within the coverage of the relay at Bus A, the voltage measured by the relay at A is the drop along the lines from the relay to the fault [4],

$$V_A = I_A Z_A + (I_A + I_B) Z_F \tag{1.7}$$

The apparent impedance measured by the distance relay is

$$Z_{app} = Z_A + \frac{I_A + I_B}{I_A} Z_F \tag{1.8}$$

When I_B is not zero, the apparent impedance measured at Bus A, Z_{app}, is greater than the actual impedance, and the reach of the distance relay decreases.

When there is no source at a tap point except for a tie line to a remote bus, a fault current can flow out from this tap terminal for an internal fault near the remote bus as shown in Figure 1.7b. With no source at Bus C, the current will flow out of Bus C and over CD to the internal fault on the line BD, reducing the apparent impedance value to less than the actual impedance, so that the reach of the distance relay is increased in this scenario [4]. The infeed and outfeed effects are used for Zone 2 and Zone 3 remote back up protections.

The Zone 3 distance relay is an overreaching zone providing remote back up protection when the local primary protection fails for a local fault. The Zone 3 time delay is 1-2 seconds longer than the Zone 2 time delay to achieve the coordination [14]. The infeed at the remote bus may result in Zone 3 relays to underreach. Likewise, the outfeed may result in an overreaching effect. Distance relays may also operate falsely for transient and voltage instability [14], and sometimes the long reach of the distance relays even though useful in certain circumstances may conflict with the line load ability requirements.

1.4 Power System Stability

1.4.1 Power Swing Phenomena

A power balance exists between generated and consumed active and reactive powers in a power system under steady-state conditions. However, when a large disturbance happens,

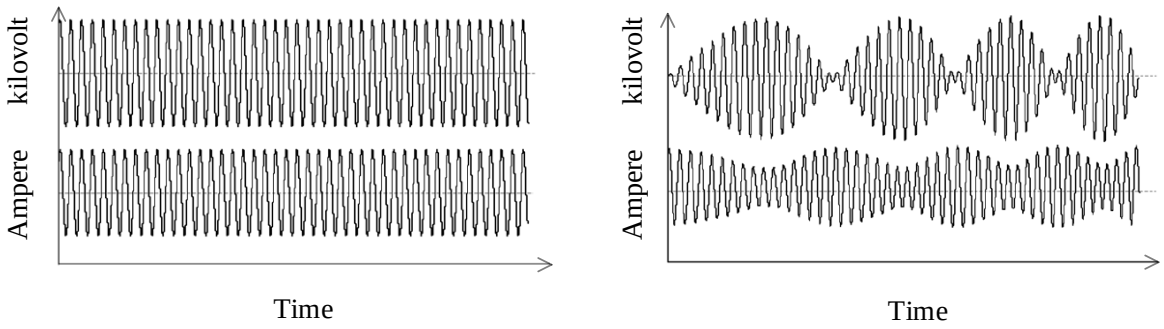

Figure 1.8: Voltage and current variations in power swing. [5]

e.g. faults, line switching, disconnection of generators, and the loss of large block of loads, it could result in sudden changes in the electric power consumptions. Since the mechanical power input to generator remains constant, these disturbances may trigger the machine rotor angle to oscillate and result in electrical power swings [6]. The generator rotor starts accelerating resulting in electromechanical oscillations in the system, which cause fluctuations in the magnitude and phase of the voltages and currents throughout the system [24] as shown in Figure 1.8. Consequently, the power flow between the interconnected portions of the system starts oscillating. Power swings are variations in power flow that occur when the internal voltages of generators at different locations of the power system start slipping relative to each other. If a new equilibrium is reached after the disturbance, the power swing is referred to as a stable power swing. If a new stable equilibrium is not reached then the swing is referred to as an unstable power swing or out-of-step phenomena. If the power swing is a severe power swing, it may cause large separations of generator rotor angles, losses of synchronism between generators and transmission systems, eventually tripping transmission lines, leading to cascading outages and the shutdown of large portion of the power grid.

For example, the large power swings were identified as the contributing factors to the July 2, 1996 WSCC (Western Systems Coordinating Council) blackout. This outage tripped 30,500 MW of load and 27,300 MW of generation and affecting 7.5 million customers over an area reaching 2,500 km from North to South and 2,000 km East to West in United States

and Canada [25] [26].

The postmortem analysis and the subsequent R&D in the industry, Electric Power Research Institute (EPRI), U.S.A. and the academic institutions helped in several cases preventing power swings from unnecessary tripping and causing wide scale blackouts. On November 4, 2006, the distance relay for Wehrendorf-Landesbergen 380 kV transmission line in North Germany operated during a severe power swing disturbance that occurred in Europe. Although more than 15 million European households lost power in order to isolate this disturbance and the Union for the Co-ordination of Transmission of Electricity (UCTE) system was split into 3 islands, the conclusion inferred from the later investigation was that the distance relay protection operated as designed and helped in an even more severe blackout by splitting the system [14]. The incidents reported above explain the importance and complexity of the problem.

1.5 Distance Relay Zone 3 Protection

Undesired Zone 3 tripping has often contributed to cascading outages. Once cascaded events are initiated for various reasons, the Zone 3 elements of distance relays play an important role during its propagation [14]. Contingencies such as temporary overloading on a remote transmission line may accidentally trigger the operation of a local backup Zone 3 distance relay. The power flow transfer to other lines due to this operation makes other Zone 3 distance relays vulnerable prone to further operation leading to a more serious situation. Despite that a defense system can collect all this information and make a decision to control the situation, it is very difficult to interrupt the propagation of cascaded events because of the quick operation of protective relays [27].

For example, the inappropriate Zone 3 protection settings of distance relay has been identified as one of the major contribution factors for the cascading large scale power system outage during the August 14, 2003 North America blackout that caused failure of the power grids in Northeast United States and Southeast of Canada, which affected an estimated 50 million people and 61,800 MW of electrical load [28] [29]. Power was not restored for 4 days

in some parts of the United States and for more than a week in parts of Ontario. Estimated total costs reached billions of dollars in both countries [30].

Therefore, the correct operation of remote protective relays (Zone 3 operation) is very important so that a large section of the power system does not fail unnecessarily. As explained before, stable power swing conditions, which are not detrimental to the power system, but they often intrude into the Zone 3 region of the distance relays and often cause maloperation due to sometimes non-accurate settings for new system configuration or unforeseen type contingency scenarios. The traditional way of setting these relays is using multiple time domain simulations for different fault conditions but these settings become inaccurate as the system evolves over years.

1.6 Literature Review

Despite Wide Area Measurement Systems (WAMSs) solution methodologies have become popular nowadays for relaying applications, still most of the relaying applications in actual industrial use such as out-of-step protection schemes, transmission line protections etc mainly use local measurements, because of the simplicity, security and dependability of a local measurement based method, as well as cost considerations. The local measurement based schemes are still considered as desirable solution methodologies for relaying purposes.

In the following section, the various power swing identification techniques reported in the literature are discussed under two broad categories: the local measurement based methods in Section 1.6.1 and the synchrophasor based wide area measurement methods in Section 1.6.2.

1.6.1 Local Measurement Based Methods

Equal Area Criteria (EAC) is a classical direct method for power system stability prediction [13] as discussed in Section 1.6.2 and 2.3.1. The equal area concept of EAC has been extended to the time domain, namely ***Time Domain Equal Area Criteria*** [5],

as discussed later in detail in Section 2.3.2. In this method, an incremental sum of area is calculated between the mechanical power input P_m and the electrical power output P_e on $(P-t)$ power vs. time characteristics, representing the accelerating energy obtained in a duration from the inception of a disturbance to the instant disturbance is removed. The second portion of the area is calculated between the electrical power output P_e and the mechanical power input P_m on $(P-t)$ domain representing the decelerating energy obtained in a time duration after removing the disturbance to the instant when power angle would become maximum i.e. δ_m. Consequently, the system stability is determined by comparing the two integrated areas same as EAC, but directly in the time domain. In other words, the system is stable if the accelerating energy gain during the fault period is equal to the decelerating energy for $\delta < \delta_m$. Otherwise, if the accelerating energy is still greater at $\delta = \delta_m$ then the system will become unstable.

The ***Swing Centre Voltage (SCV) Method*** is also a local measurement based method and has been reported in [31] and discussed in Section 2.3.7. For a two source equivalent system, SCV is defined as the voltage when the impedance locus reaches the swing center at which the power angle between the two sources is 180 degrees apart. A more convenient way for out-of-step detection is differentiating SCV with respect to time: the absolute value of the rate of change of SCV is at its minimum when the angle between the two sources is close to zero, and this value is at its maximum when the angle is around 180 degrees, as such the out-of-step phenomena could be distinguished from a recoverable disturbance. The swing centre voltage SCV can be approximated as a function of source voltage magnitude and the power angle difference can be approximated by half of the angle between the two source. Using these approximations, the SCV out-of-step detection is realized based on local measurements.

Blinder Scheme [6] [32] is the conventional approach of power swing detection by tracking the rate of change of the positive sequence impedance vector measured by a distance relay, as discussed in Section 2.4.1. The Blinder Scheme is based on the concept that, during a power swing, the swing impedance locus measured by a distance relay moves slower on the impedance plane of the relay characteristics than it does in a fault condition. A timer is

used distinguish a fault condition from a power swing condition by finding the time it takes for the impedance locus to traverse between the outer and inner blinders (impedance locus traverses significantly faster compared to a power swing condition). In order to differentiate an out-of-step condition from a recoverable power swing, the blinder positions are determined by multiple simulation studies so that the impedance locus enters the outer blinder only and does not enter the inner blinder during a stable power swing. For an unstable power swing the impedance locus enters both outer and inner blinders. The Blinder Scheme is a simple scheme for determining out-of-step conditions or for power swing blocking, although it is not an easy task to find correct timer settings as well as proper inner and outer blinder's position on relay characteristics, which may involve extensive stability studies on the system for diverse contingency conditions. Moreover, it is not a robust technique for system configuration changes, and the blinder methods are vulnerable that its operation can be affected by load changes, which can be a tedious work for relay setting in power system protection.

Quadrilateral Characteristics (QUAD) Schemes are the distance relay zone protection schemes with quadrilateral characteristics, as discussed in Section 2.4.2. The QUAD characteristic has a rectangular or trapezoidal shaped zone that is comprised of two reactance lines providing reactance boundaries and two resistance lines providing resistance boundaries. The major advantage of the QUAD scheme is its flexible resistance coverage with which the protection characteristics can either avoid load region to be immune from load encroachment, or extend fixed resistance boundary to cover high resistance phase-to-earth faults. One particular shape of quadrilateral characteristics is polygon characteristics whose paralleled boundaries cover the reach of transmission lines and the resistance limits.

Concentric Zone Characteristics Schemes [6] are the blinder type schemes combined with different types relay zone characteristics, as discussed in Section 2.4.2. The scheme has two impedance characteristics that the second characteristic is concentric around the first one. This can be accomplished with two additional characteristics specifically for the power swing function, or with one additional outer impedance characteristic concentric to one of the existing distance protection characteristics, such as ***Concentric Mho Scheme***, ***Concentric Quadrilateral Characteristics Scheme***, ***Concentric Polygon Characteristics***

Scheme, and ***Concentric Lens Scheme*** [6].

Basic Characteristics Repositioning Method [14] moves basic mho relay characteristics to improve the security of the relay operation during heavy load or power swing conditions, as discussed in Section 2.4.3. The basic mho characteristics repositioning can be done by rotating the mho circle at the origin of the impedance plane or offsetting mho circle along the line impedance, in order to optimize the resistive coverage for relay mal-operation due to stable power swings, heavy loads, close in faults, or to encompass the relay location into relay coverage.

Continuous Impedance Calculation Method [8] tracks the rate of change of the impedances for all three phases to differentiate power swing from fault condition. The ratio of two successive differences of R, X is verified. The difference has to be less than a limiting value to ensure that the impedance locus has a "continuous" or uniform movement with no abrupt variations. This criteria is fulfilled only during a power swing condition, whereas during a fault or an abrupt load change, the impedance vector jumps immediately to a fault impedance value or a new impedance value.

For power swings, impedance loci generally swing from the operating region towards lower impedance regions where protection zones are located, and then swing back and start oscillating. The impedance vectors move relatively quickly while entering but at the point of return the velocity of the impedance vectors could be very low, or almost zero. After passing the point of return, the impedance vectors again start moving with increasing velocity. One issue that can arise with this power swing characteristics is that at the point of return it just looks like a three-phase fault, because all impedance vectors are in the protection zone with almost no change. To distinguish this stable power swing condition with a three-phase fault, reference [8] uses a time delay criteria. The delay is calculated dynamically and is used in conjunction with the velocity of the impedance vectors. More details on the continuous impedance calculation are provided in Section 2.4.4.

Instead of monitoring the rate of change of measured impedance, ***R-dot Method*** uses rate of change of apparent resistance for out-of-step trip decision making [33] as discussed

later in Section 2.4.5. The conventional blinder based relay schemes usually use fixed values for resistance settings. In the R-dot Method, in addition to a fixed resistance threshold, the rate of change of resistance is also included to determine the relay operation output. While detecting a slow moving impedance trajectory for a power swing scenario, the R-dot relay functions similar to a conventional Blinder Scheme relay. When the rate of change of resistance is high, such as during a fault or out-of-step condition, an early tripping is initiated for the relay.

There are other advanced types of protection methods such as the ***Wavelet Transform Method*** [34], which has been used in power system analysis to identifying power swing or differentiate a fault condition during a power swing phenomena, as discussed in Section 2.3.8. The calculated wavelet energies appear to be different when the system is at fault, during the power swing conditions or in the normal operations of the grid. In the Wavelet Transform Method, the energy variations are compared at different frequency levels by applying a wavelet transform on local voltage and current measurements. Since the wavelet analysis can be performed with desirable frequencies as compared to Fourier techniques, it is more suitable in power swing or out-of-step determination which is characterized with frequency deviation of the system. On the other hand, the challenge exists to identify noises from faults or contingencies, since the wavelet transform can be affected by inaccurate classification due to noises in the system.

Support Vector Machine (SVM) Method [35] applies the Support Vector Machine to distinguish power swings from fault and normal operating conditions. SVM has been used in classification problems, e.g. pattern recognition, to find out a hyperplane to separate the data points according to their classes such as the separation between the classes is maximum, as discussed in Section 2.5.1. The parameters of the SVM model for power swing identification are determined by inputting a set of pre-labelled training data, i.e. the electrical quantities locally measured during power swings, faults, and normal operating conditions. Then the power swing or symmetrical fault data testing sets are input to the SMV model to predict the membership based on the training. It is reported [35] that the method is capable of identifying power swings from normal operating conditions and distinguishing

symmetrical faults from power swings.

Other pattern recognition approaches are reported such as the ***Fuzzy Inference System (FIS) Scheme*** [9] for power swing identification, as discussed in Section 2.5.2. At first, the FIS scheme defines linguistic variables, such as machine angular frequency deviation, as the inputs to FIS, and compares the input values with membership functions to obtain membership values of the linguistic terms, which are the inputs to fuzzy rules. By applying fuzzy reasoning, the output of each rule can be a linear combination of the input variables. The out-of-step determination decision is therefore made as the final output which equals weighted average of each rule's output.

Similar types of pattern recognition approaches are applied for power swing and out-of-step detection namely ***Artificial Neural Networks (ANNs)*** [10], as discussed in Section 2.5.3. ANNs have a large parallel network consisting of numerous highly interconnected processors called neurodes operating based on organizational principles similar to the human brain [36]. ANNs have three layers for out-of-step detection. The inputs to the input layer are typical local electrical local measurements collected in either steady state or transient durations, which have significant effect on stability. Calculated through the hidden layer, the output out of the neural network output layer is a value between 0 and 1. A measurement is classified when a sample is collected in stable or unstable power swing by comparing the output to a threshold, e.g. greater or less than 0.5, such that the out-of-step detection is achieved. Once ANNs are trained, the networks can quickly recognize a new pattern of power system condition which belongs to a predefined class of patterns [10].

Theoretically all the above mentioned power swing detection approaches can be utilized for blocking Zone 3 protection. Using it for Zone 3 requires prudence, because nonavailability of Zone 3 when it is needed could exacerbate the situation and lead to a cascading effect, as identifed in the large scale power network blackout event [30].

Reference [37] discusses a ***Transient Monitoring Function using a Phase Angle Method*** for power swing blocking with the focus on Zone 3 protection, as presented later in Section 2.7.2. The fundamental phasor components estimated by using the least square

method match the actual phasor signal measurements in steady state, whereas they are different during abnormal conditions. This method calculates the absolute difference between reconstructed current phasor components from the least square method and the actually measured current phasors to detect abnormal changes in power system.

1.6.2 Wide Area Measurement Based Methods

The ***Synchrophasor Based Technology*** [38] [15] based protection schemes can supplement conventional protection schemes. It helps in precisely locating a fault and also block unnecessary relay trips. The synchrophasor based protection is discussed in more detail in Section 2.6. The availability of GPS makes it possible to synchronize power system measurements over long distances (using Phasor Measurement Units – PMU). The measurements of the PMU technique are time stamped with high precision at the source end, so that the data transmission speed is not as critical as it used to be in phasor based calculations and PMU measurements collected with the same time stamp are used to calculate the state of the power system at the instant defined by the time stamp [38]. The synchrophasor based technology has broadened the capability & the scope of protection system with the recent advances in communication networks as well as the development of inter-substation and intra-substation communication standards.

The ***Equal Area Criteria(EAC)*** [13] discussed in Section 2.3.1 is a classical direct method for stability analysis derived from the swing equation. The electrical power output of a synchronous machine P_e moves on power vs. power angle $(P-\delta)$ curve from the initial operating power angle δ_0 on $(P-\delta)$ plane during a dynamic condition, and is equal to mechanical power input P_m at steady state. The system stability after a disturbance is determined by comparing the area under the input electrical power P_e and the output mechanical power P_m on $(P-\delta)$ plane during the disturbance interval and after the disturbance is cleared. Therefore, a stable power swing can be distinguished from an unstable one by comparing the acceleration energy and the deceleration energy gain before and after removing the disturbance. With wide area measurements possible nowadays, the EAC method can be applied for power swing and out-of-step detection.

The classical EAC method is derived for a single machine infinite bus system and can be also applied to a two machine system with a few reductions. The ***Extended Equal Area Criteria(EEAC)*** developed by Xue, Cutsem and Pavella in 1989 [39] extends EAC to a multi-machine system. The method is discussed in detail in Section 2.3.3. During the transient time interval, the multi-machine system is segregated into two portions, i.e. a Critical Cluster that includes the group of critical machines oscillating together, and the other portion of the segregated system comprising of the remaining machines, buses, transformers, and transmission lines, etc. At the separating location, the multi-machine system is represented by an equivalent single machine infinite bus system, where EAC is utilized for transient stability analysis. The EEAC criteria based distance relay prototype with PMUs had been installed for out-of-step prediction at the major connection substation from Georgia to Florida in United States, and the angle predictions of the improved algorithm were very close to the actual values for the captured contingency events [40].

There was recently another paper [41] on the application of EEAC. The method is named as ***Adaptive Extended Equal Area Criteria*** and is discussed in Section 2.3.4. The multi-machine system is segregated (i.e. the critical cluster of generators) are found by employing the Independent Component Analysis (ICA) method, and the equivalent SMIB system parameters are identified by a Dynamic State Estimation (DSE). Then an EAC stability analysis is carried out. The parameters of the equivalent single machine infinite bus (SMIB) system are adapted online to current system state and are used for setting the mho relay characteristics with a single blinder, for power swing and out-of-step detection.

An alternative method called ***State Plane Analysis Method*** is used in [42] to solve the swing equation numerically to predict stable or unstable conditions. The method is discussed in more detail in Section 2.3.5. The complex multi-machine system is at first approximated into a SMIB system by applying EEAC and its dynamics are described by a Swing Equation. The nonlinear swing equation is transformed in the form of state space equations. The paper [42] explains that the system stability at equilibrium points can be determined by applying Lyapunov's indirect method on linearized state space model without explicitly solving the differential equations. The system dynamics are demonstrated with state plane

trajectories, and the out-of-step phenomena is explained graphically in the paper. In the method described in the paper the critical clearing angle is computed using the principle that the total energy of the system at the instant the fault is cleared should be equal to the maximum potential energy of the system. The critical clearing time corresponding to the value of the critical clearing angle is obtained directly using the time calibration of the relative speed versus power-angle solution curve. The simultaneous calculation of the critical clearing angle and the time makes the proposed approach fast [42].

The ***State Deviation Method*** has been reported in [7], which is based on online measurement of the generator speed from local voltage measurements as discussed in Section 2.3.6. The multi-machine system is approximated by a SMIB system using the real time calculation of the equivalent parameters of the system. The stable state of the given system is distinguished from out-of-step condition by monitoring the sign of the generator relative speed at the energy equilibrium points. The equilibrium point is obtained using the difference of mechanical and electrical power signal, i.e. the point where $(P_m - P_e)$ goes from negative to positive with the assumption that P_m is constant [7]. If the relative machine rotor speed is negative at the equilibrium point, a stable power swing is detected. Whereas, if a positive relative machine rotor speed is measured, an unstable or out-of-step condition is confirmed. The major advantage of the State Deviation Method is that the variables that can be readily measured in the power system are used as inputs to the relay, i.e. the mechanical power inputs to the machines, the electrical power outputs from the machines, and the voltage phase angle (to calculate relative rotor speed of the generators).

The aforementioned power swing and out-of-step detection schemes utilizing synchrophasor based wide-area measurements can be applied for Zone 3 protections. Additionally, a few other schemes have been developed for Zone 3 blocking, for instance, the power flow analysis can be one of the options for detecting power swings such as the ***Adaptive Distance Relay Scheme(ADRS)*** [27] as discussed in Section 2.7.2. When a transmission line is removed by a protective relay due to a fault, the power flow of the line transfers to other lines and results in overloading of the other lines. The overload condition may make the operating point encroach into Zone 3 of distance relay and trip the relay, which leads to

a cascading situation. If the calculated difference between the measured and the estimated post-fault power flow is within a pre-determined tolerance on a particular transmission line after disturbance, a transmission line overflow is recognized as a line flow transfer due to the power swing, instead of an internal fault on the transmission line.

There is another recent research method on power swing detection for Zone 3 blocking include the ***Polynomial Curve Fitting Method*** [43], as discussed in Section 2.7.2. The rotor angle dynamics of each machine is represented by a polynomial function using the least square curve fitting method, and the rotor velocity of each machine is obtained as the differentiation of this polynomial function. If it is a stable power swing, a zero value of the differentiation of the polynomial function stands for a zero relative rotor speed of the synchronous machine, shortly after the contingency is cleared from the system. A time delay is consequently set up as a criteria to distinguish an out-of-step phenomenon from a stable power swing case on the basis of extensive posteriori power swing case analysis. If a zero velocity is detected within this pre-determined time interval, a stable swing instead of an unstable swing is determined, and the blocking command ought to be issued to the relay.

1.7 Research Objectives

The primary objective of my research is to develop a power swing identification and blocking scheme purely based on local measurements for transmission line protection, which can determine whether it is a stable or unstable power swing encroaching into Zone 3. The other objective is, unlike most of the computationally intensive schemes, the method can be easily applied to a multi-machine power system configuration.

To achieve the above overall objectives, the following sub-objectives are pursued in the research work:

1. To develop an algorithm that calculates the equivalent SMIB system impedance based on system approximation of a complex power system network at a distance relay location and calculates the equivalent synchronous machine relative speed of the SMIB system to

identify stable or unstable power swings.

2. To carry out phasor based/electromagnetic simulations under various disturbance scenarios in different power system configurations, in order to verify the validity of the proposed algorithm as well as the method in distance relay Zone 3 blocking during power swings.

1.8 Organization of the Thesis

The thesis is organized in six chapters.

Chapter 1 gives a general background on power system protection, protective relaying, distance relaying, mho relaying as well as its application. The power system stability and power swing phenomena are briefly reviewed. The distance relay Zone 3 protection using distance relays is discussed. An overview is provided on various power swing detection methods followed by a discussion on Zone 3 blocking methods. The objectives of the research are described followed by an organization of the thesis work.

The impedance measurement by distance relays is introduced followed by a discussion on the concept of the system electric centre at the beginning of Chapter 2. The characteristics are reviewed for a variety of traditional and existing power swing identification and blocking schemes that have been reported in research literature and in industry. The importance of blocking Zone 3 of the distance protection especially during a stable power swing scenario is emphasized for the security of a complex power system and for preventing large scale power system blackouts. The capacities and limitations are evaluated for the current Zone 3 protection schemes, which clarifies the motivation of the proposed work.

In Chapter 3, the SMIB system representation concept which serves as the basis for the proposed TZB method is developed. Subsequently, the Third Zone Blocking (TZB) method is presented step by step, and the significance of the First Zero Crossing (FZC) is explained for differentiating a stable power swing and an out-of-step condition. A SMIB model is developed in PSCAD/EMDTC for studying the TZB algorithm. The most promising features of the

proposed algorithm are summarized following the discussion on the SMIB system PSCAD simulations.

The proposed TZB method is tested for stable power swing blocking on a modified WSCC system in PSAT for detailed simulations, as presented in Chapter 4. The modified WSCC system is created by adding an additional synchronous machine to the power network of a typical WSCC 9 bus system for the distance relay Zone 3 blocking study. The conventional double blinder scheme for stable power swing blocking is set up for comparison on the tested distance relay in the TZB method validation.

The detailed characteristics of the TZB method is further analysed in RTDS simulations as presented in Chapter 5. A modified WSCC testing system is established for the testing along with Digital Fourier Transform (DFT) local measurement circuits in RTDS. The TZB method fictitious machine relative speed calculation is verified by comparing it to the classic synchronous machine dynamics representation Swing Equation Method (SEM).

The proposed TZB method research is summarized in Chapter 6, and the conclusions are inferred from the current study, while the significance of the research is discussed. Finally, the possible future work is outlined for further TZB method study.

Chapter 2

Power Swing Detection (Blocking) and Zone Protection

2.1 Introduction

As discussed in Section 1.7, during stable or unstable power swings, the locus of the apparent impedance measured at a distance relay can enter relay operating characteristics and appears as a fault. If it is a fault or an unstable power swing, tripping is necessary to isolate the disturbed portion of the network from the rest of the grid. However, for stable swings, the relay needs to be blocked, in order to maintain the maximum amount of power supply to the load. Therefore, detecting and blocking power swings is critical for proper operation of distance relays.

The various types of power swing detection methodologies have been classified into different categories based on the underlying theory used. Under the Energy Equilibrium method in Section 2.3, the classical *Equal Area Criteria (EAC)* is discussed. The EAC method has been also extended to large interconnected power networks and called *Extended Equal Area Criteria*. The *Time Domain Equal Area Criteria* is another extension of EAC published in 2010 and is an elegant method to use in protection applications at transmission or generator level for large interconnected power networks with purely local measurements. The other recent research work on *EAC* is the *Adaptive Extended Equal Area Criteria*. In the same category of Energy Equilibrium methods, there are also *State Plane Analysis Method*, and *State Deviation Method*. All these methods are discussed in this chapter.

There are also methods such as *Swing-Centre Voltage Method*, and *Wavelet Transform*

Method, etc. discussed in the literature review.

The Impedance Trajectory Tracking method is discussed in Section 2.4. The *Blinder Scheme* is one such conventional scheme and widely used for power swing detection and blocking. Under the same category, there are *Concentric Zone Characteristics schemes*, *Basic Characteristics Repositioning Method*, *Continuous Impedance Calculation method*, as well as *R-dot Method*, etc.

There are other research methodologies discussed in the literature such as the Pattern Recognition Techniques discussed in Section 2.5, such as *Support Vector Machine Method*, *Fuzzy Inference System Method*, and *Artificial Neural Network Method*, etc.

The *Synchrophasor Based Method* are also being used on wide-area backup protections nowadays for power system stability/out-of-step detection, which is discussed in Section 2.6. Some of the current research works for blocking Zone 3 distance relays are discussed in Section 2.7.

2.2 Impedance Measured by Distance Relay

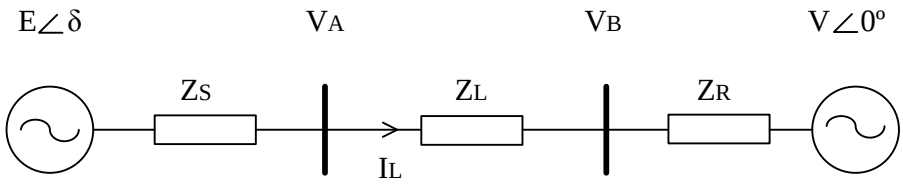

Figure 2.1: Two machine equivalent system.

The apparent impedance measured by a distance relay is formulated for a two machine example system shown in Figure 2.1 [6]. In the figure, E is the sending end generator voltage, V is the receiving end generator voltage, Z_S is the sending end generator internal impedance, Z_R is the receiving end generator internal impedance, Z_L is the transmission line impedance, V_A is the sending end bus voltage, V_B is the receiving end bus voltage, I_L is the transmission

line current measured at the sending end generator bus. The current I_L at Bus A is given by:

$$I_L = \frac{E - V}{Z_S + Z_L + Z_R} \tag{2.1}$$

The impedance measured by a relay at Bus A is:

$$Z = \frac{V_A}{I_L} = \frac{E - I_L Z_S}{I_L} = \frac{E}{I_L} - Z_S = \frac{E(Z_S + Z_L + Z_R)}{E - V} - Z_S \tag{2.2}$$

Assuming that E leads V by any angle δ and the voltage magnitude ratio is k. Then

$$\frac{E}{E - V} = \frac{k(\cos\delta + j\sin\delta)}{k(\cos\delta + j\sin\delta) - 1} = \frac{k\big[(k - \cos\delta) - j\sin\delta\big]}{(k - \cos\delta)^2 + \sin^2\delta} \tag{2.3}$$

When the two sources voltage magnitudes are equal or k is one, Equation 2.3 can be expressed as: [6]

$$\frac{E}{E - V} = \frac{1}{2}(1 - j\cot\frac{\delta}{2}) \tag{2.4}$$

The impedance measured at the relay is going to be: [6]

$$Z = \frac{V_A}{I_L} = \frac{Z_S + Z_L + Z_R}{2}(1 - j\cot\frac{\delta}{2}) - Z_S \tag{2.5}$$

Equation 2.5 can be expressed geometrically as shown in Figure 2.2. The two source voltages are going to vary during a power swing. The trajectory of impedance measured at the relay during a power swing corresponds to a straight line that intersects the segment A to B (The line AB is the system impedance.)at its middle point. This point is called as

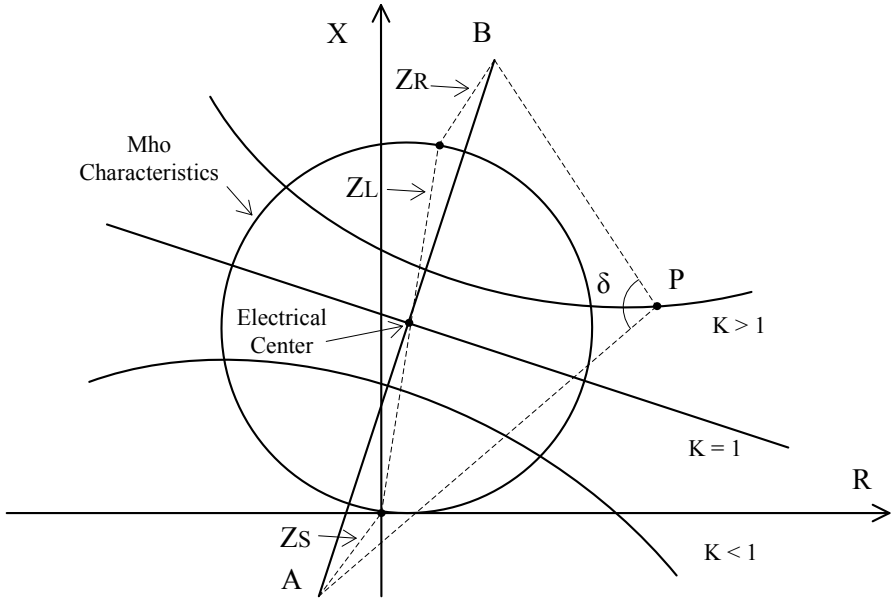

Figure 2.2: Impedance trajectories measured by distance relay during power swing for different k values [6]

.

the "*Electrical Center*" of the swing. When the angle δ reaches 180 degrees, the impedance is precisely at the electrical center. It can be seen that the impedance trajectory during a power swing will cross the relay characteristic that covers the line, provided the electrical center falls inside the line.

When k is not equal to one (i.e. when the two source voltages are unequal), it can be demonstrated that the impedance trajectory will correspond to a circle. This is shown in Figure 2.2. Another point to be noted is that in actual practice, the swing impedance seen from any given relay may be anywhere in the impedance characteristics plane and move in any direction during a power swing [16]. A number of factors may contribute to the complexity of the impedance trajectories and make them unpredictable, e.g. system configurations, grid connections, various contingency situations, device settings, equipment specifications, and environmental conditions, etc.

2.3 Power Swing Detection based on Energy Equilibrium

2.3.1 Equal Area Criteria(EAC)

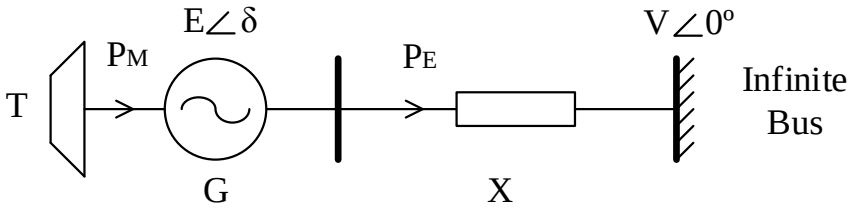

Figure 2.3: Single machine infinite bus representation of turbine power system.

The classical swing equation is a mathematical representation of the dynamics of synchronous machine rotor oscillations using the power balance between the mechanical power input and the electrical power output as the following:

$$M\frac{d^{\,2}\delta}{dt^2} = P_m - P_{max}\sin\delta \tag{2.6}$$

where

M the inertia constant of the machine, in $joule - seconds$ per mechanical $radian$

δ the angular variation of the rotor, in mechanical $radians$

t time, in $seconds$

P_m the mechanical power supplied by the prime mover, in $N - m$ per $second$

P_{max} the maximum electrical or electromagnetic power, in $N - m$ per $second$

The swing equation is a second order non-linear differential equation (since $P_{max}\sin\delta$ has a $\sin\delta$ term.) and is represented in terms of the fundamental frequency. Since it is a second-

order nonlinear equation, an explicit solution is not possible and a step-by-step approach numerical integration is used to obtain the solution. Consequently, the direct approach, such as EAC, is extensively utilized to determine the stability of a synchronous machine or a power network connecting two regions. Detailed explanation of the classical swing equation can be found in [13].

Consider the system shown in Figure 2.3 operating in steady state, the synchronous machine is at point a running at the synchronous speed, and its rotor angle is δ_0 in the $P-\delta$ curve shown in Figure 2.4. The input turbine mechanical power P_m is equal to the machine electrical power output P_e. When a fault happens somewhere in the system, the operating point moves down from a on the upper power angle curve to b on the lower power angle curve. During the fault, the mechanical input power P_m is greater than the electrical output power, the machine rotor speed becomes higher than the synchronous speed. Due to the fault, the rotor angle increases to δ_c at which the fault is cleared, the machine operating point moves from c to d back on the upper power angle curve. The machine starts decelerating since P_m is less than P_e, meanwhile the operating point moves from d to e at which the machine rotor speed decreases to the synchronous. The machine rotor speed continues decreasing to less than the synchronous speed, while its operating point begins to move from e back to a along the upper power angle curve.

The angular velocity of the rotor relative to the synchronous speed is

$$\omega_r = \frac{d\delta}{dt} = \omega - \omega_s \tag{2.7}$$

Replacing $\dfrac{d\delta}{dt}$ with ω_r in the above Swing Equation, Equation 2.6 becomes

$$M\frac{d\omega_r}{dt} = P_m - P_e \tag{2.8}$$

Multiplying ω_r and $\dfrac{d\delta}{dt}$ on both sides of Equation 2.8, the above Swing Equation can be written as

$$\frac{M}{2}\frac{d(\omega_r^2)}{dt} = (P_m - P_e)\frac{d\delta}{dt} \tag{2.9}$$

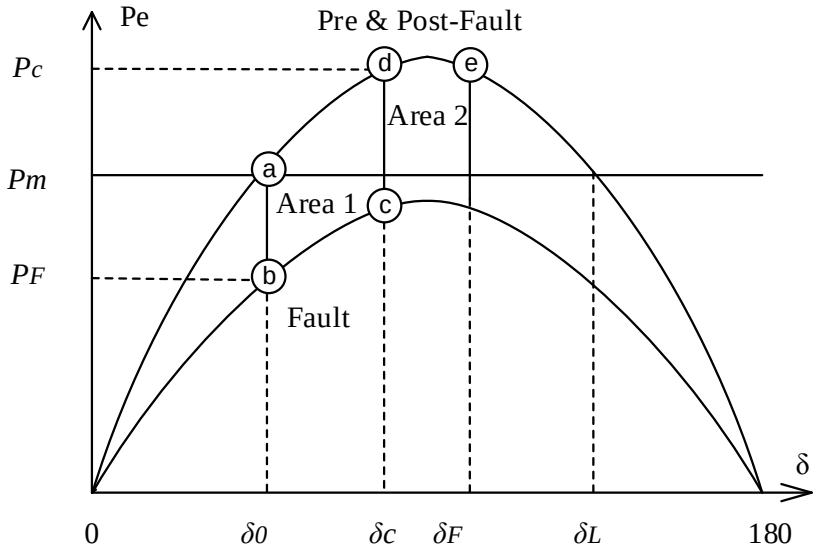

Figure 2.4: EAC $P - \delta$ curves showing a stable power swing condition.

Integrating Equation 2.9, then

$$\frac{M}{2}(\omega_{re}^2 - \omega_{ra}^2) = \int_{\delta_0}^{\delta_F} (P_m - P_e) d\delta \tag{2.10}$$

If the rotor speed is synchronous at δ_0 and δ_F, the corresponding machine rotor speed $\omega_{ra} = \omega_{re} = 0$, and

$$\int_{\delta_0}^{\delta_F} (P_m - P_e) d\delta = 0 \tag{2.11}$$

Dividing the integration to two portions at the fault clearing point where $\delta = \delta_c$, Equation 2.8 can be written as

$$\int_{\delta_a}^{\delta_c} (P_m - P_e) d\delta = \int_{\delta_c}^{\delta_F} (P_e - P_m) d\delta \tag{2.12}$$

Equation 2.12 shows mathematically Area 1 is equal to Area 2 in the power-angle diagram shown in Figure 2.4 for a stable power swing. It can be seen from Figure 2.4 that if the fault clearing time is increased, δ_c and δ_F moves to the right, and Area 1 and 2 increase to keep the system stable. When δ_F is equal to δ_L, and Area 1 is still greater than Area 2 then the system will become unstable or out-of-step. The basic derivation of EAC is for a single machine infinite bus system, but can be easily extended to a two machine system.

2.3.2 Time Domain EAC

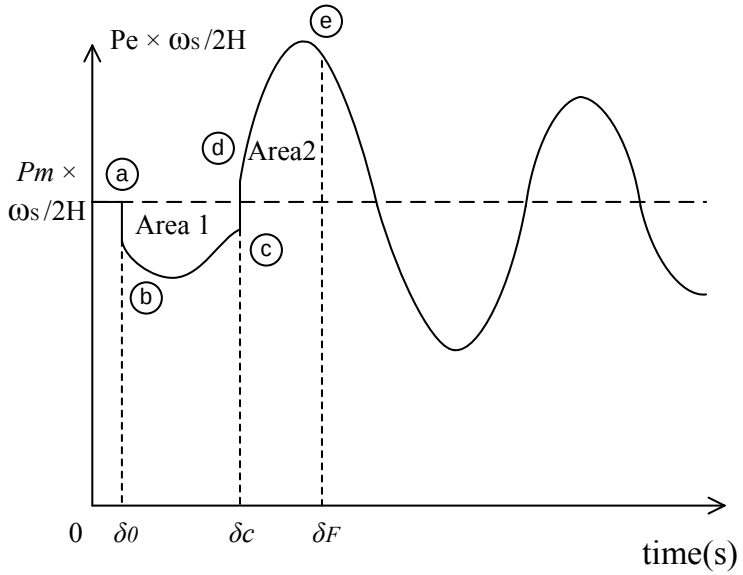

Figure 2.5: Time domain Equal Area Criteria $P-t$ curves.

The EAC obtained from the swing equation determines the power system stability in the δ domain. The concept and application has been extended to the time domain, i.e. EAC in time domain [5] [44]. Integrating the Swing Equation in the form of Equation 2.6 from the fault inception time t_0 to the fault clearing time t_c, the equation becomes

$$\left.\frac{d\delta}{dt}\right|_{t_c} - \left.\frac{d\delta}{dt}\right|_{t_0} = \int_{t_0}^{t_c} \frac{\omega_s}{2H}(P_m - P_e)dt \tag{2.13}$$

Referring to Equation 2.7, from t_0 to t_c where $P_m \geq P_e$, Equation 2.14 denotes the area of Area 1 in Figure 2.5.

$$Area1 = \int_{t_0}^{t_c} \frac{\omega_s}{2H}(P_m - P_e)dt = \omega_{tc} - \omega_s \tag{2.14}$$

where ω_{tc} is the speed of the rotor at the fault clearing time.

Integrating Equation 2.6 from t_c to t_F, the time corresponding to the maximum swing of δ, the area of Area 2 in Figure 2.5 is denoted by

$$Area2 = \int_{t_c}^{t_F} \frac{\omega_s}{2H}(P_m - P_e)dt = \omega_F - \omega_{tc} \tag{2.15}$$

where ω_F denotes the rotor speed at the maximum swing of δ, i.e. δ_F. At δ_F, the rotor speed ω_F equals to the synchronous speed for a stable swing. The total transient energy is the sum of Equation 2.14 and 2.15, i.e. [5]

$$A = Area1 + Area2 = \int_{t_0}^{t_c} \frac{\omega_s}{2H}(P_m - P_e)dt + \int_{t_c}^{t_F} \frac{\omega_s}{2H}(P_m - P_e)dt = 0 \tag{2.16}$$

For an out-of-step condition, the rotor speed ω_F at δ_F is greater than the synchronous speed. From Equations 2.14 and 2.15, the total transient energy becomes [5]

$$A = Area1 + Area2 = \int_{t_0}^{t_c} \frac{\omega_s}{2H}(P_m - P_e)dt + \int_{t_c}^{t_F} \frac{\omega_s}{2H}(P_m - P_e)dt > 0 \tag{2.17}$$

Equation 2.16 and 2.17 provide the expressions for EAC in time domain. During the transient, if Area 1 and Area2 are equal in a $(P-t)$ curve, the power swing is a stable one. However, if Area 1 is greater than Area 2, the swing becomes an out-of-step condition. Since the area in the $(P-t)$ curve represents energy, this EAC concept can be referred to as the energy equilibrium criteria in time domain [5].

2.3.3 Extended EAC

EAC represents the system stability based on areas under the power curve. EAC can only be applied to a SMIB system or equivalent two machine system, which restricts its usage for analyzing transient stability of a complex power network. The Extended Equal Area Criteria was developed to apply EAC to a multi-machine complex system in [39] in order to overcome this limitation. The criteria has been employed directly for out-of-step prediction on a distance relay prototype, which was installed at the major connection substation from

Georgia to Florida in United States in October 1993 and remained operational until January of 1995, as discussed in [40].

For a given time interval of power system transient dynamics, a given multi-machine system is decomposed into two portions. Critical Cluster consists of the group of the critical machines, and the other comprises the remaining system. The two portions of power system are represented by two equivalent synchronous machine systems. The machine dynamics of the separate portion of the system is expressed by a Partial Center of Angles (PCOA). The equivalent two-machine system is further reduced into a single machine infinite bus (SMIB) system. Thus, the transient stability of the multi-machine system can be analysed by applying EAC. The approximation to a SMIB system is formulated as shown in Appendix A.1.

There are two transient stability assessment measures provided by EEAC for stability evaluation of the given system. One of the margins is the Critical Clearing Time (CCT) τ corresponding to the given Critical Clearing Angle (CCA) δ_τ, and the other is the transient stability margin, η, expressed as [39]

$$\eta = A_{dec} - A_{acc} \tag{2.18}$$

where A_{acc} is the area where P_m is greater than P_e during fault from δ_0 to δ_C in Figure 2.4; A_{dec} is the area where P_e is greater than P_m after fault from δ_C to δ_L.

The correct determination of the transient stability by EEAC is based on appropriate approximation of the multi-machine system into a SMIB system. The factors include the correct identification and modelling of the critical cluster, representing the remaining system by an infinite bus system, and the calculation of critical clearing angle, etc. One of the assumptions for EEAC transient stability assessment is that the out-of-step phenomenon is determined only upon the angular separation between the Critical Cluster group and the group of the remaining system, which apparently relies on the representation of the SMIB system approximation of the two groups. Another assumption is that the rotor angle of the

fictitious machine of the remaining system can be represented by the PCOA of the aggregated system.

The identification of the critical cluster for a given disturbance is started by drawing a list of candidate critical clusters. The CCTs are calculated for the corresponding candidate critical clusters. The smallest CCT among the list of candidate critical clusters is considered as the actual CCT by EEAC, which indicates the stability threshold of the system to the particular disturbance.

2.3.4 Adaptive Extended EAC

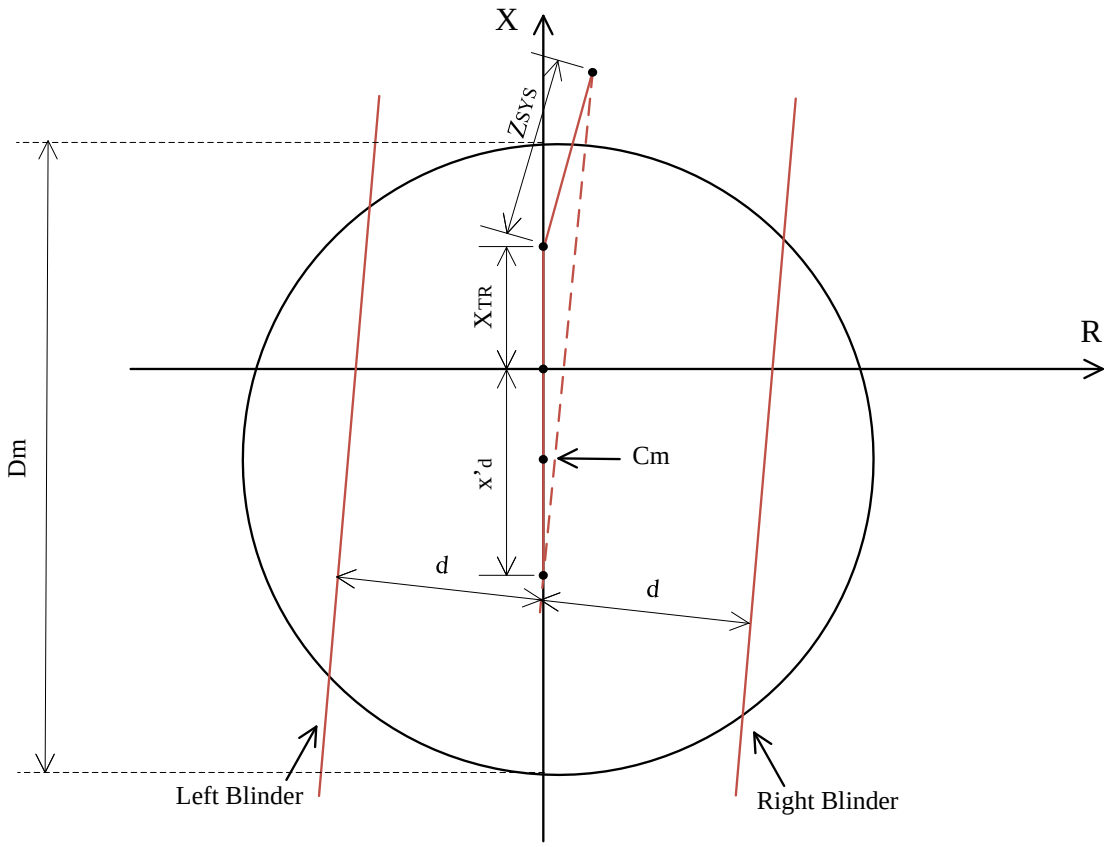

Figure 2.6: Diagram of single blinder Adaptive Extended EAC scheme.

EEAC provides a direct approach for out-of-step prediction based on a SMIB system

representation of the complex network. A power system configuration could evolve with time, and the state of the grid continuously changes, e.g. source units are disconnected, blocks of loads are dropped off or switched online temporarily, etc. Therefore, the system information needs to be gathered continuously by out-of-step protection scheme, e.g. the adaptive protection method discussed in [41].

The adaptive out-of-step protection method employs EEAC on setting a distance mho relay with a single blinder scheme discussed in [45]. As suggested in Figure 2.6, several system parameters are required for the calculation of the mho relay settings, such as the generator transient reactance x'_d, the unit transformer reactance X_{TR}, and the system impedance Z_{SYS}. The mho characteristics diameter D_m and center C_m are formulated as shown in the following equations [41]

$$D_m = 2 \times x'_d + 1.5 \times X_{TR} \tag{2.19}$$

$$C_m = 1.5 \times X_{TR} - \frac{D_m}{2} \tag{2.20}$$

The CCA δ_C between the generator and the rest of the system is empirically found as 120° [45]. The distance d of the parallel single blinder to the combined impedance is hence determined by the following equation [41]

$$d = \frac{x'_d + X_{TR} + Z_{SYS}}{2} \times tan(120° - \frac{\delta_C}{2}) \tag{2.21}$$

The timer settings (for traversing across blinders) can be found as long as the CCT is known. The CCA and CCT is calculated by utilizing EEAC based on the generator dynamic parameters that are estimated using the Unscented Kalman Filter (UKF) method [46]. The critical cluster of generators is identified by applying the Independent Component Analysis (ICA) method [47], instead of doing a simple CCT comparison among the candidate critical clusters in EEAC.

The calculation time of the Adaptive EEAC method is comparatively long, i.e. 2 to

3 seconds. The relay's operation time is a shortcoming of the Adaptive EEAC method, although it is still an acceptable time-frame for out-of-step detection for most of the outage cases.

A similar Adaptive EEAC study is reported for out-of-step detection in [48]. In this method, the generator rotor to grid angle separation is selected as a criteria for out-of-step detection.

2.3.5 State Plane Analysis Method

Several numerical methods have been reported for solving the nonlinear swing equations and analysing the transient responses of the power system under contingency conditions. A new method called State Plane Analysis (SPA) method which is different from the approach adopted in EAC is reported in [42] [7]. In the SPA method, the critical clearing time is computed at the same time as the critical clearing angle which makes the proposed method much faster than the EAC type method.

In stability analysis, the differential equations describing a nonlinear system can be written in the form of state space equations, and further linearized by applying Taylor expansion around equilibrium points. The stability of the linearized system at equilibrium points can be determined by applying Lyapunov's indirect method [49].

The state space equations representing the Swing Equation are converted in [7] as

$$\dot{\delta} = \omega \tag{2.22}$$

$$\dot{\omega} = P - \sin\delta \tag{2.23}$$

where δ and ω are the state variables and ω represents the machine relative speed with respect to the synchronous speed, and the rate of change of ω is derived from Equation 2.6 as explained in [7]

$$\dot{\omega} = \frac{d^2\delta}{dT^2} \tag{2.24}$$

and

$$P = \frac{P_m}{P_{max}} \tag{2.25}$$

$$T = t\sqrt{\frac{\pi \times P_{max}}{180 \times M}} \tag{2.26}$$

where P_m is the mechanical power input to the machine; P_{max} is the maximum electrical power output of the machine; T is the corresponding time variable.

The dynamics of a SMIB system can be demonstrated by plotting the state variable ω versus δ in a state plane. By applying the Lyapunov's indirect method, an equilibrium point can be recognized either as a vortex point or a saddle point. The machine potential energy is minimum at vortex point and the machine potential energy is maximum at the saddle point. If the sum of the kinetic energy gained during the fault condition and the potential energy obtained for the post-fault condition of the machine is less than the maximum potential energy (V_{max}) at the moment when the disturbance is cleared, the machine rotor speed becomes stable, otherwise, it becomes unstable [7]. These stable and unstable regions are separated by a critical trajectory on the state plane. Based on the assumption that the kinetic energy gained by the machine during fault equals to the potential energy gained after the fault condition at CCA, CCA can be located graphically on the post-fault critical trajectory in the state plane, and the corresponding time is CCT. By comparing the current fault clearing time to CCT, the out-of-step phenomena can be predicted. The SMIB system approximation introduced in [39] is empolyed for complex power network reduction.

2.3.6 State Deviation Method

The State Deviation Approach is proposed in [7] [50], which is based on the online measurement of the generator speed at the energy equilibrium points. Figure 2.7a shows ($P-$

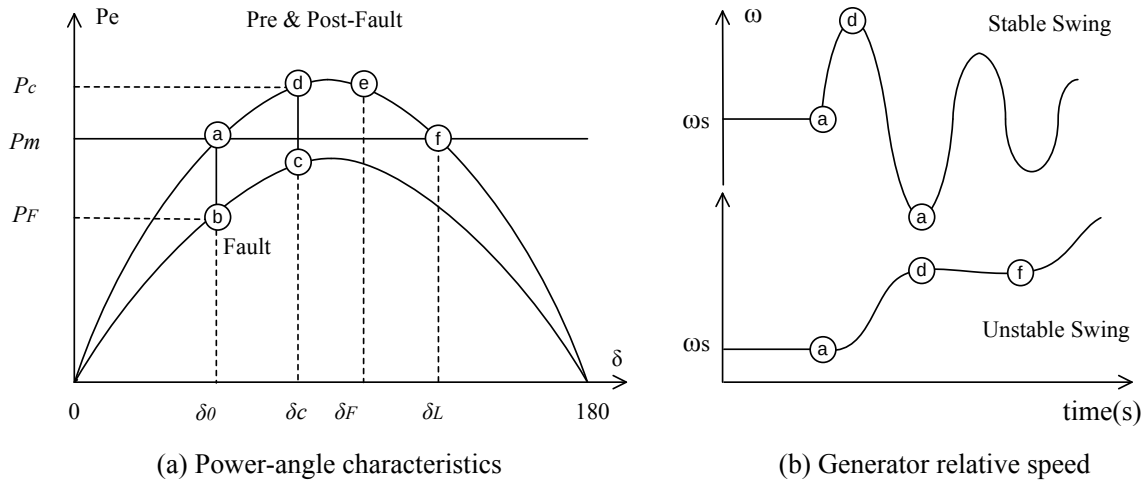

Figure 2.7: Diagram of State Deviation Technique [7].

δ) curves for pre-fault, during fault and post fault conditions on a power-angle characteristics. After the disturbance, the synchronous machine starts accelerating, and the machine speed increases. The machine starts decelerating after the fault is cleared. The pre-fault operating point is shown by the point a in steady state. When a fault occurs, the machine operating point jumps to the point b. At the point d at which the fault is cleared, the machine speed is higher than the synchronous speed, the rotor angle keeps separating while the machine starts decelerating. If the machine speed becomes synchronous at point e, it starts swinging backward. At the point a again, the machine state changes from deceleration to acceleration. Since the relative speed of the machine at a is less than 0, the rotor of the machine oscillates approaching to a steady state. If the machine rotor angle oscillates beyond the point e and reaches the point f at which the machine state changes from deceleration to acceleration, unstable condition is detected, when the relative speed of the machine is greater than 0 at the point f, as shown in Figure 2.7b.

The State Deviation Approach measures the electrical power and the generator speed online as inputs to locate the equilibrium point where $(P_m - P_e)$ changes from negative to positive. The primary advantage of this technique is that the parameters used by the relay are readily available and easy to measure, moreover, it does not require any network

admittance matrix reduction and dynamic model approximation, while it is applied to local generator out-of-step detection [7]. The State Deviation technique can be extended to a multi-machine system by conducting real-time SIMB system equivalenting.

2.3.7 Swing-Centre Voltage (SCV) Method

Benmouyal et al. [31] introduced another power swing detection method called as the Swing-Center Voltage (SCV) method, which detects the rate of change of the swing-center voltage of a power system to determine whether it is a stable power swing or an unstable condition. The SCV method originates from the concept that in a two-source system for a wide interval of power angle δ, the distance relay blocking signal is generated when a maximum negative value of $V_A \cos\varphi$ is reached at the vicinity of $\delta = \pi$ [51], where V_A is the locally measured voltage at the sending end of transmission line, and φ is the angle difference between V_A and the local current I as shown in Figure 2.8.

Swing-center voltage (SCV) is the voltage at the location of a two-source equivalent system where the voltage value is or close to zero when the phase angles between the two sources are 180 degrees apart [31]. When a two-source system goes into an out-of-step situation after disturbance, the angle difference of the two-source, $\delta(t)$, increases as a function of time. Figure 2.8 shows the voltage phasor diagram of a general two-source system, and SCV is the phasor from origin o to the point o'.

A SCV can be approximated through the use of locally available quantities as the following equation:

$$SCV = |V_A| \cos\varphi \tag{2.27}$$

In Figure 2.8, $V_A \cos\varphi$ is a projection of V_A onto the axis of the current I. In a homogeneous system with the system impedance angle θ close to 90 degrees, the magnitude of the swing-center voltage can be approximated by $V_A \cos\varphi$. From Equation 2.27 the relation between SCV and the phase-angle difference δ of the two-source voltage phasors can be simplified to the following equation by using local SCV estimation: [31]

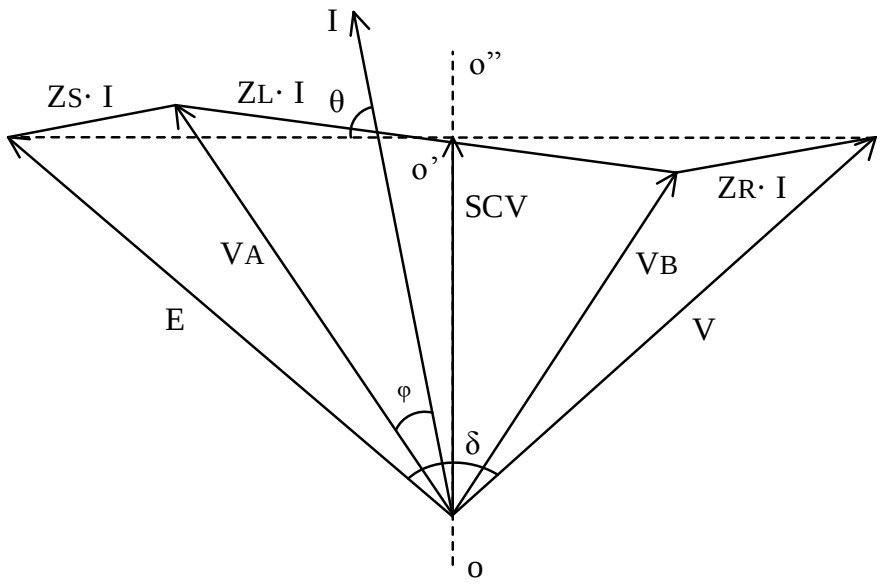

Figure 2.8: Voltage phasor diagram of a two-source system [6].

$$SCV_A = E_A \cos\frac{\delta}{2} \tag{2.28}$$

where E_A is the positive-sequence source magnitude equal to E approximately equal to V. SCV_A represents the positive-sequence swing-center voltage used in power swing detection.

The magnitude of SCV_A is maximum when the phase angle between the two sources is zero, and is at its minimum when the angle is 180 degrees. Based on this property, the rate of change of the swing center voltage can be used to detect power swings. The time derivative of SCV_A becomes the following: [31]

$$\frac{d(SCV_A)}{dt} = -\frac{E_A}{2}\sin(\frac{\delta}{2})\frac{d\delta}{dt} \tag{2.29}$$

In contrast to SCV, the absolute value of $\dfrac{d(SCV_A)}{dt}$ is at its minimum when the angle between the two sources is close to zero, and this value is at its maximum when the angle

is around 180 degrees. Equation 2.29 gives the relation between the rate of change of SCV and the two-machine system slip frequency $\frac{d\delta}{dt}$.

The SCV method is independent of the system source impedance and the line impedance, and its magnitude is directly related to the angle difference of sources δ, and is between 0 and 1 per unit [6]. The scheme is applicable for a two-source equivalent system.

2.3.8 Wavelet Transform Method

A power swing blocking scheme using the Wavelet Transform is reported in [52] [34]. The basic Wavelet Transform concept is to select an appropriate wavelet function and then perform analysis using shifted and dilated version of the wavelet. In contrast to Fourier analysis relying on a single basis frequency, a wavelet can be chosen with a desirable frequencies and time characteristics, i.e. compared to the Fourier transform which uses a single analysis window, the wavelet transform uses short windows at high frequencies and long windows at low frequencies [53].

By sequentially allocating the frequencies to levels, the energy difference of different levels distinguishes the fault and the power swings. The total energy of levels of a transient and a power swing condition are tracked for both the voltage and current signals. The calculated norm in each level gives the measurement of the amount of energy content D on the level as [52]

$$\|D\| = \left[\sum_{i=1}^{N}[D(i)]^2\right]^{1/2} \tag{2.30}$$

where N is the number of the detail coefficients at the level.

Despite its advantage that the Wavelet Transform Method can cover a wide range of system frequencies during pre-fault, during fault and post-fault conditions, it could be a challenge to identify the fault signature from noises, since the wavelet can be affected by inaccurate classification due to noises in the system.

2.4 Power Swing Detection based on Impedance Trajectory Tracking

2.4.1 Blinder Scheme

The traditional way of power swing detection is the Blinder Scheme, which detects the difference of the rate of change of the positive-sequence impedance vector [6] [32]. The Blinder Scheme uses the concept that during a power swing, it takes more time for the machine rotor angle to change due to its large inertia and also the apparent impedance measured at a distance relay during the power swing condition. On the contrary, during a faulted condition the rate of change of the apparent impedance is almost immediate. In the impedance plane shown in Figure 2.9, as soon as the detected impedance enters into the outer Z element blinder, a timer begins counting. The impedance locus does not enter the inner Z element blinder, if it is a stable power swing. However, the impedance locus enters the inner Z element blinder for an unstable power swing. The time counted for the impedance locus from outer Z element blinder to the inner Z element blinder is much longer for a power swing than for a fault. The counted time difference or the rate of change of the impedance distinguishes the power swing from the fault. Furthermore, the locus of the impedance locus determines whether it is a stable or unstable power swing.

The Blinder Scheme is simple, but it is not an easy task to find the correct settings of the distance relay for blocking during stable power swings and for tripping during unstable power swings. It requires detailed simulations on the given system for various contingency conditions. For example, the fastest rate of change of a possible power swing has to be decided based on a large number of stability studies. The Blinder Scheme setting procedure is discussed in Section 4.4.1.1 in a distance relay double blinder setup for power swing blocking. The main challenge with this method is that it is difficult to find all the power swing scenarios and operating conditions on a large power system, and the load change also has an impact on a blinder scheme relay operation. Apart from that, the best location to block the power swing or to separate the faulted portion of the power system also requires considerable amount of simulations. The Blinder Scheme is referred as an appropriate method for systems which slip

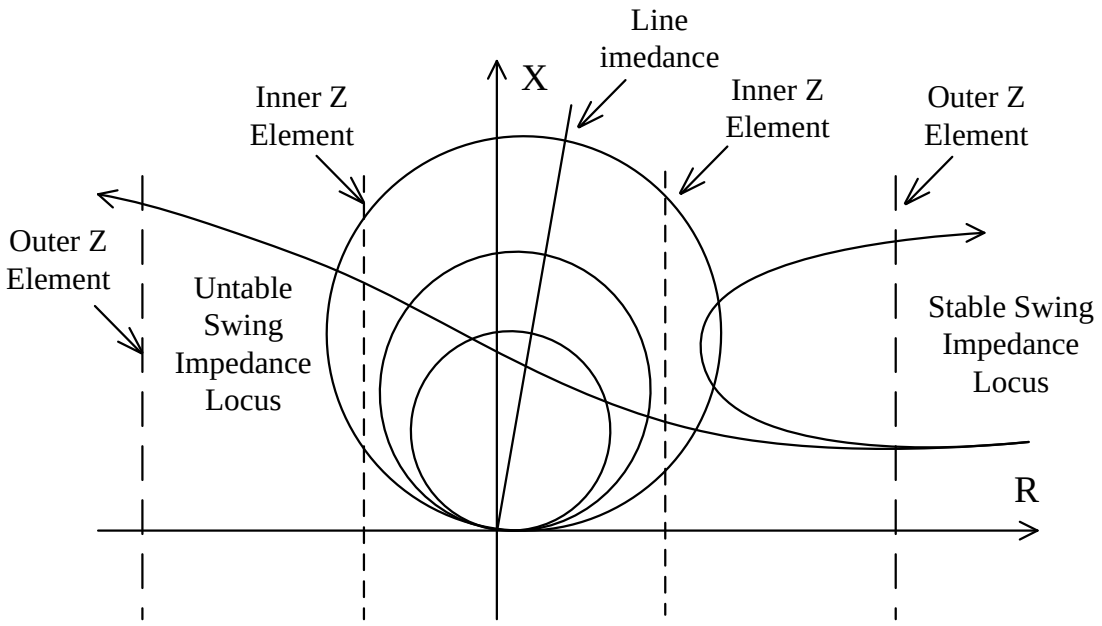

Figure 2.9: Double blinder impedance-based power swing blocking on Mho characteristics.

frequency does not change considerably when the systems go out-of-step. In many systems where the slip frequency increases considerably after the first slip cycle, a fixed impedance difference between the power swing blocking impedance elements and a fixed time delay may not be easily determined to provide a continuous blocking signal to a mho distance relay.

The above points have provided the motivation for developing a power swing blocking and out-of-step detection method for distance relays, including the proposed TZB method in this study. There are a few other schemes similar to the blinder scheme, such as Quadrilateral Characteristics (QUAD), Concentric Zone Characteristics, changing the zone shape of the distance relay, supervised zone tripping [14], and studying load encroachment characteristics schemes, etc.

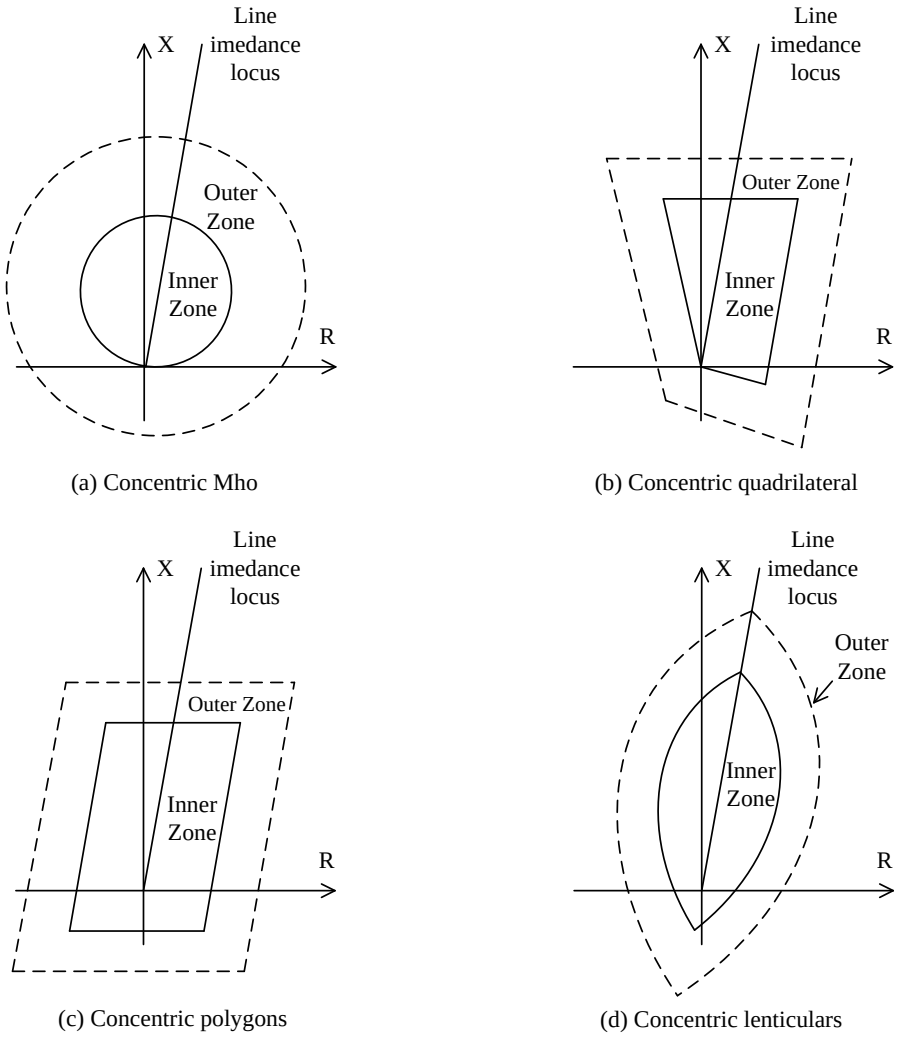

Figure 2.10: Impedance-based concentric power swing blocking characteristics. [6]

2.4.2 Concentric Characteristics Schemes

The ***Concentric Characteristic Schemes*** extend the basic blinder power swing blocking concept from the double blinder scheme for particular applications. The ***Concentric Mho Scheme*** is set up with the double mho circle characteristics and a timer counting the time during which the impedance locus traverses between the two impedance elements [54] [6], as shown in Figure 2.10a. If the swing impedance locus crosses both the concentric characteristics before the timer setting expires, a fault is detected, otherwise, a

power swing is identified. An impedance locus of a stable power swing only enters the outer mho circle (in dashline), whereas a locus of an unstable power swing sequentially enters both the outer and inner mho circles.

The ***Quadrilateral Characteristics (QUAD)*** are comprised of two lines of reactance boundaries and two lines of resistance boundaries. The angle of these lines relative to the R and X axes are based on a pre-fault load flow. The composite of these lines makes a rectangular or trapezoidal shaped impedance zone similar to that shown in solid lines in Figure 2.10b. This characteristic can limit the resistive reach to avoid load encroachments in a similar manner to that of the lens in Figure 2.10d, which provides a fixed resistive coverage from the relay location to the end of zone coverage [14]. The fault resistance varies in the range of 1 to 200Ω for phase-to-earth faults in overhead lines without earth wires. Mho characteristics cannot cover such a wide variation of resistance, especially on short lines [55], where the QUAD scheme can find its application. In the figure, dash-lines represent the concentric QUAD scheme outer characteristics.

The ***Concentric Polygon Characteristics Scheme*** can be classified into the quadrilateral characteristics scheme, which has paralleled boundaries to cover the reach of transmission line and the resistance limits, as shown in Figure 2.10c and in GE N60 distance relay application [56].

A distance element's charateristics can be set-up to form an intersection of two mho circles, i.e. the ***Concentric Lens Characteristics Scheme***, with the maximum sensitivity axis as shown in Figure 2.10d. The inner and outer lens are indicated with the solid and dash-lines. With the same impedance angle of the protected transmission line, the protection zone coverage maintains full reach for bolted faults in the forward direction, and the resistive coverage is significantly reduced [14]. The lens characteristics scheme reduces the chance for relay mal-operations comparing to a mho circle during power swings or steady state overload scenarios.

All these blinder based methods could be categorized in as changing of the zone characteristics schemes as well. However, similar to the blinder methods, the shortcoming of the

above alternate schemes is that the loci of the possible power swings have to be found based on extensive stability studies and not all power swing scenarios and operating conditions can be covered inclusively.

2.4.3 Basic Characteristics Reposition Method

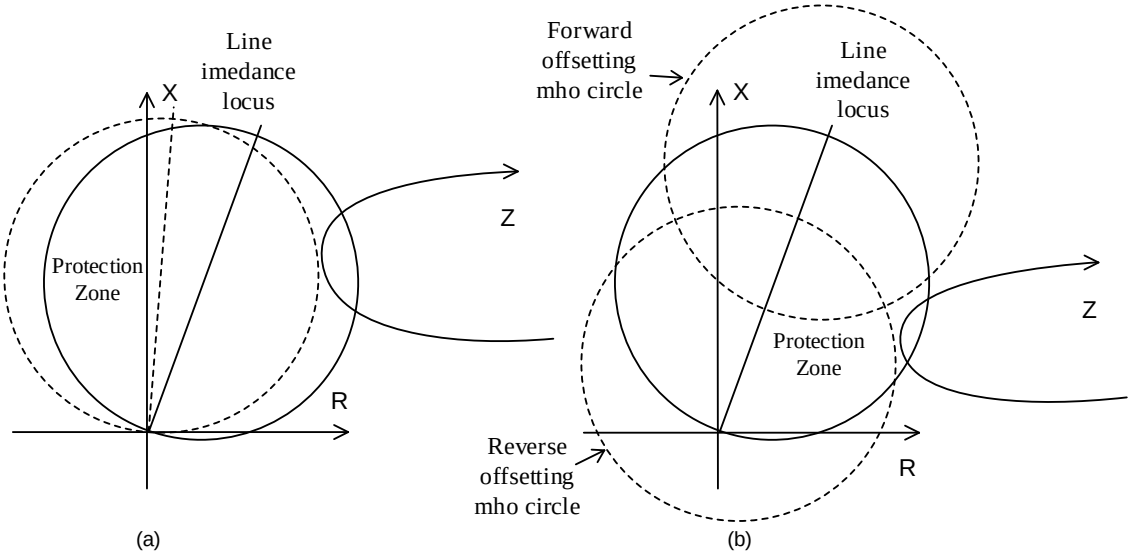

Figure 2.11: Basic mho relay characteristics reposition power swing blocking.

The Basic Characteristics Reposition method [14] is shown in Figure 2.11. The angle adjustment of the mho characteristics increases the maximum sensitivity angle to reduce the resistive coverage for a stable power swing, especially for the over-reaching zone protection as shown in Figure 2.11a. In contrast, with a lower maximum sensitivity angle it optimizes the resistive coverage for close-in faults (where a fault resistance has the greatest impact on a measured fault locus) for the under-reaching zone.

Likewise, the offsetting of the basic characteristics moves the mho circle away from the possible power swing loci in Figure 2.11b. The reverse offsetting pulls the mho circle back away from the main forward reach to encompass the relay's location as the lower dash-

line circle in the figure. As described in IEEE PSRC Working Group D4 report, a forward offsetting moves the circle along the protected line and place the relay location outside of the detection zone as the upper dash-line circle in the figure, therefore, a sensitive overreaching zone is moved beyond the range of steady state or transient load impedance loci. When a forward offsetting of mho characteristics is utilized to address loadability concerns, a shorter reaching distance zone must be placed to protect the close-in portion of the line not covered by the forward offset [14].

For distance relays, the susceptibility of the zone operation responding to load condition increases due to power swings during heavy and inductive load conditions, especially for Zone 3. Repositioning of the basic characteristic is one mechanism to improve the distance relay's operation during heavy loads and power swings. Nevertheless, the method is feasible for particular situations instead of being applicable to common situations.

2.4.4 Continuous Impedance Calculation

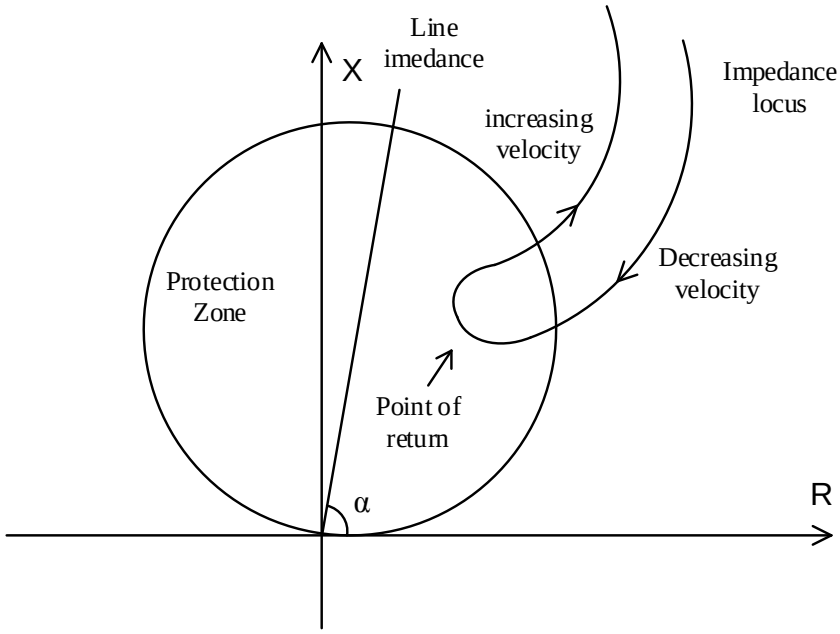

Figure 2.12: Impedance trajectory motion during stable power wings. [8]

A power swing detection function was proposed by J. Blumschein *et al.* from Siemens AG, which is based on continuous impedance calculations. The impedance loci are monitored continuously four times per cycle for each phase [8].

The criteria are based on the special features of the impedance trajectory motion during a power swing as shown in Figure 2.12. The impedance locus moves quite quickly towards the center of protection zone at the beginning of the power swing. The motion of the impedance vector becomes slow when it approaches to the returning point, and the velocity of the motion increases again when it swings back from the returning point.

The Continuous Impedance Calculation algorithm calculates the updated resistance and reactance values and compares them with the memorized values, meanwhile, the directions of the derivatives of resistance and reactance are monitored. The distance between two successive resistance or reactance values has to exceed a threshold value and the ratio of the differences of the resistance or reactance ought to be below a limit, and these criteria are only satisfied during power swing conditions when the impedance vector moves smoothly along an orderly path, instead of during load or fault conditions. Out-of-step condition can be identified by the same criteria combined with the direction at which impedance trajectory crosses a transmission line angle on a relay impedance plane [8].

The continuous impedance calculation criteria utilizes the characteristics of impedance trajectory motion during power swings to distinguish power swings from faults as well as load encroachment situations. However, due to the complex nature of power swings, the impedance loci are diverse. A few of these trajectories may have different motions not in compliance with the criteria. Therefore, an extensive system stability analysis is still inevitable for applying the method.

2.4.5 R-dot Method

An out-of-step relay described in the references [33] [57] was installed in the US Pacific NW-SW 500kV AC Intertie to prevent severe voltage dips due to uncontrolled loss of loads and loss of synchronism among sub-areas of utility networks. The function of out-of-step

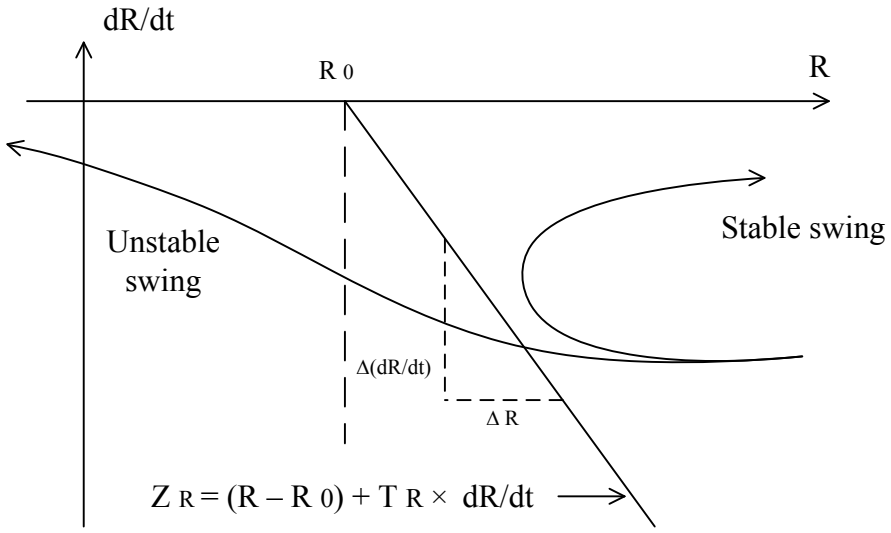

Figure 2.13: Illustration of Rdot scheme for distance relay power swings detection.

relay was enhanced with the rate of change of apparent resistance, which is called the R-dot scheme [6] [58].

In a resistance based control algorithm to describe the conventional out-of-step detection, distance relay control output Z_0 can be given by [6]:

$$Z_0 = (R - R_0) \leq 0, \tag{2.31}$$

Instead, in the R-dot out-of-step swing detection scheme, the control output Z_R is formulated by: [6]

$$Z_R = (R - R_0) + T_R \frac{dR}{dt} \leq 0, \tag{2.32}$$

where R is the apparent resistance measured by the relay; R_0 and T_R are the relay-setting parameters.

The characteristic of the R-dot relay can be illustrated in the R-Rdot plane shown in Figure 2.13. A conventional out-of-step relay is characterized by a vertical line offset by R_0 in the R-Rdot plane [6], which is similar to the R-Rdot scheme performance at low separate

rates with small dR/dt ratio. However, higher separation rates dR/dt cause a larger negative values of Z_R, and the system separation is initiated much faster when the calculated Z_R goes across a straight line having a slope T_R in the R-Rdot plane.

In the R-dot relay scheme, the resistance change rate during a power swing is taken into account in decision making. The R-dot relay can be set close to actual stability limits subject to circuit breaker duties and minimum voltage swing constraints, and it is intelligent to avoid tripping on recoverable swings, meanwhile initiating early tripping at a favourable circuit breaker angle during non-recoverable swings [33]. On the other hand, the involvement of the rate of change of resistance may also possibly trigger the relay operation during stable power swings, especially when its resistance changes fast.

2.5 Pattern Recognition Approaches

2.5.1 Support Vector Machine Method

A Support Vector Machine (SVM) based power swing identification scheme was introduced by Seethalekshmi K., et al. in 2010 [35]. It was reported in this paper that the method is capable of identifying a power swing and distinguishing the symmetrical faults during a power swing.

The support vector machine is one of the learning separating functions in pattern recognition and classification studies, or in performing function estimation in the regression problems. SVMs are used in classification problems to separate the data points according to their attributes by locating a hyperplane such that the identification of the classes is maximized [35], e.g. a linear discriminant function in the form of [35]

$$f(x) = W^T X + b = 0 \tag{2.33}$$

is a hyperplane dividing the input data space into two parts. Where W is known as the weight vector, X is the input data vector, and b is called the bias.

In Equation 2.33,

$$W^T X = \sum_{i=1}^{n} w_i x_i \tag{2.34}$$

where w_i is the i^{th} weight, x_i denotes the i^{th} input.

Because of the nonlinear nature of the power swing phenomena, the electrical quantities input to SVM are mapped to a higher dimensional space with the help of nonlinear transform to make the linear separation possible. The parameters of the SVM model are determined by inputting a set of pre-labelled training data collected during fault and power swing conditions, i.e. the locally measured electrical quantities, then the power swing or symmetrical fault testing data sets are input to the SMV model to predict the membership based on the training. 90% accuracy of power swing identification is reported by the SVM based classification [35].

Pattern recognition approaches require training using several offline simulation runs to determine model parameters. In the nature of statistic analysis, the testing accuracy reported can not be 100%, sequentially there are a percentage of the testing data not classified correctly. Even though the extensive case studies are inevitable, not all the power swing scenarios can be covered to ensure the security of the network.

2.5.2 Fuzzy Inference System Method

Fuzzy Logic techniques as well as Neural Networks are also reported in power swing and out-of-step phenomenon identification. As introduced in [9], the protection proposed makes use of an adaptive-network-based Fuzzy Inference System (FIS). The implementation of fuzzy criteria signals together with fuzzy settings provides a mechanism to handle measurement errors. The fuzzy algebra rules for aggregation enables easy realization of multi-criteria decision making [9].

The FIS scheme works in several steps: fuzzification-comparing the input values with membership functions to obtain membership values of each linguistic term; fuzzy reasoning-firing the rules and generating their fuzzy or crisp consequents; defuzzification-aggregating

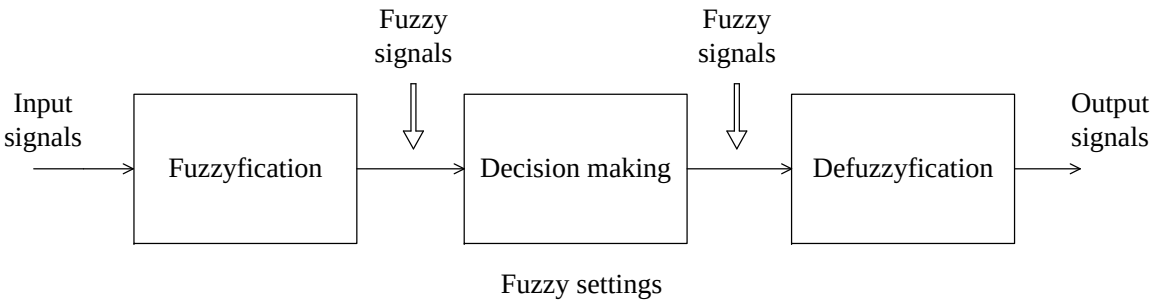

Figure 2.14: Typical Fuzzy reasoning system [9].

rule consequents to produce a crisp output [59].

The output of each rule $(y_1, ..., y_n)$ is a linear combination of input variables (x_1, x_2, x_3) plus a constant term, and the final output z is the weighted average of each rule's output. [9]

$$z = \frac{\beta_1 y_1 + \beta_2 y_2 + ... + \beta_n y_n}{\beta_1 + \beta_2 + ... + \beta_n} \tag{2.35}$$

$$y_k = a_k x_1 + b_k x_2 + c_k x_3 + d_k \tag{2.36}$$

$$\beta_k = \mu_{1k}(x_1)\mu_{2k}(x_2)\mu_{3k}(x_3) \tag{2.37}$$

where μ_{ik} is the membership function for the linguistic terms associated with the i^{th} input signal; a_k b_k c_k d_k are the parameters associating input signals to the k^{th} rule output; β_k is the weighting factor for the k^{th} rule consequent.

The network parameters of the FIS scheme are determined by a set of pre-labelled inputs in the reported research. The machine angular frequency deviation $\Delta\omega$ is selected as input signal because it carries the most recognized feature of out-of-step phenomena.

The average preciseness of the FIS scheme becomes high while the data acquisition window is enlarged in power swing and out-of-step identification, which is not favourable in protective relaying. It is not easy to make 100% accuracy examination for out-of-step detection.

2.5.3 Artificial Neural Network Detection Method

The Artificial Neural Network (ANN) method is another pattern recognition application in power swing and out-of-step detection. Neural networks are highly interconnected large numbers of simple structure processors, i.e. neurodes, that are the analogues of the neurons in the brain [10]. In the application described in [10], the neural networks algorithm has three-layers, i.e. an input layer, a middle layer and an output layer, and the layers work together with a sigmoidal activation function and supervised training using a back-propagation technique, as discussed in [36].

Three quantities are selected as inputs to ANNs scheme, i.e. the mechanical input power P_m, the kinetic energy deviation K_E at the fault clearing instant, and the average acceleration during fault α_{av} that is the mean values of the two rotor angular accelerations at the instant of applying the fault and at the fault clearing instant. The data of the quantities come from the power flow analysis and the transient stability study featured by the swing equation model of the machine.

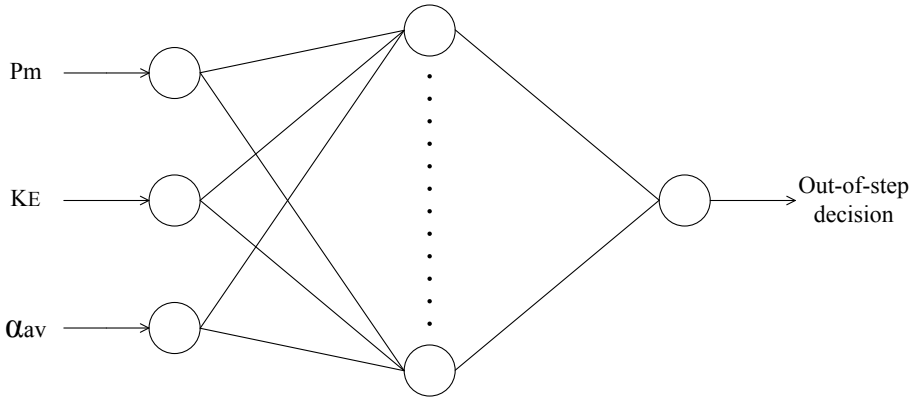

Figure 2.15: Artificial neural networks system for out-of-step detection [10].

The reported neural network approach is verified with unknown samples that include a wide spectrum of operation conditions and contingencies. The neural network used in this program shown in Figure 2.15 has an output value from the neural network between 0 and 1. The unstable can be identified if its output value from the neural network is less than 0.5, otherwise the stable can be distinguished. The maximum correct classification rate is in

the range of 85 to 98%. The prediction capability of the adaptive features of the proposed out-of-step relay is also studied by making some significant topology changes to the power network.

Although artificial neural network commonly require large volume of computational resources in its training and decision making process, compared to conventional power swing detection methods, the reported CPU time for the given method can be as fast as 0.19 to 0.37 ms in parallel or serial computer processing [10], which is fast enough for out-of-step detection. The comprehensive collections of training samples impact correct decision making output. Therefore, the extensive investigations of contingencies are indispensable for ANNs application for the given power system.

2.6 Synchrophasor Based Technology

Supplemental to conventional protective relaying, the advent of wide area backup protection systems minimizes the impact of an event on a network. The wide area backup protection can prevent cascading trips that are harmful to the network, in the way of precise locating of a fault so that only the circuit breakers necessary to isolate the fault are engaged in action, or distinguishing equipment failure or overloading to avoid unnecessary trips [15].

Synchronized phasor measurements have become optional measurement techniques for electric power systems. The positive sequence voltage and current measurements are synchronized to within a microsecond [38]. The availability of Global Positioning System (GPS) makes the measurements possible, and this system offered the effective way of synchronizing power system measurements over large distances. These systems can also be customized to measure harmonics, negative and zero sequence quantities, as well as the local frequency and the rate of change of frequency [60].

A signal $s(t)$ can be represented by a synchrophasor S of complex value given by Equation 2.38,

$$S = S_r + jS_i = (S_m/\sqrt{2})e^{j\phi} = S_m/\sqrt{2}(\cos\phi + j\sin\phi) \tag{2.38}$$

where S_m is the maximum magnitude of $s(t)$ and ϕ is its instantaneous phase angle relative to a cosine function at nominal system frequency refer to Universal Time Coordinate(UTC).

The measurements of Phasor Measurement Unit (PMU) technology are time stamped with high precision at the source, which make the data transmission speed no longer critical for the measurement. The state of the power system at the instant defined by the time stamp is inferred by the PMU measurements with the same time stamp [38].

A synchrophasor corresponding to the time of measurement are tagged with the UTC time. The time of measurement has three components, i.e. a Second-of-Century(SOC) count, a fraction-of-second count, and a time status value. The SOC count is a 4-byte binary number in seconds counting from midnight of January 1, 1970, to the current second. The fraction-of-second count is an integer by which the second is divided into a number of subdivisions by the specified time base integer. The synchrophasor measurements synchronized to UTC time shall be sufficiently accurate to meet the accuracy requirements of IEEE Standard C37.118 [61]. The time status value indicates the reliability of the local clock.

An example PMU synchrophasor measurement system [11] is shown in Figure 2.16. The high sampling rate data passing through a digital low-pass filter are acquired by the A/D converter before down sampling and resampling. The low pass filter outputs data at a higher rate for frequency estimation. One of the inputs to the resampler is the filtered signal, and the other input is the power system operating frequency. The filtered data are available to calculate the magnitude of the synchronized phasor, meanwhile they are also ready for distance protection applications.

Synchrophasor based wide area measurements provide alternatives to local out-of-step detections as well as stable power swing blockings as reported in [15] [6] [62] [63] [64]. Nowadays, the wide area measurement technologies have provided the capacity of broadening the scope of a protection system, with the help of the recent advances in communication, information and computer networks, and the significant development in inter-substation and intra-substation communication standards, such as UCA 2.0 and IEC 61850 [65] [66], 61968 [67] and 61970 [68]. [15]

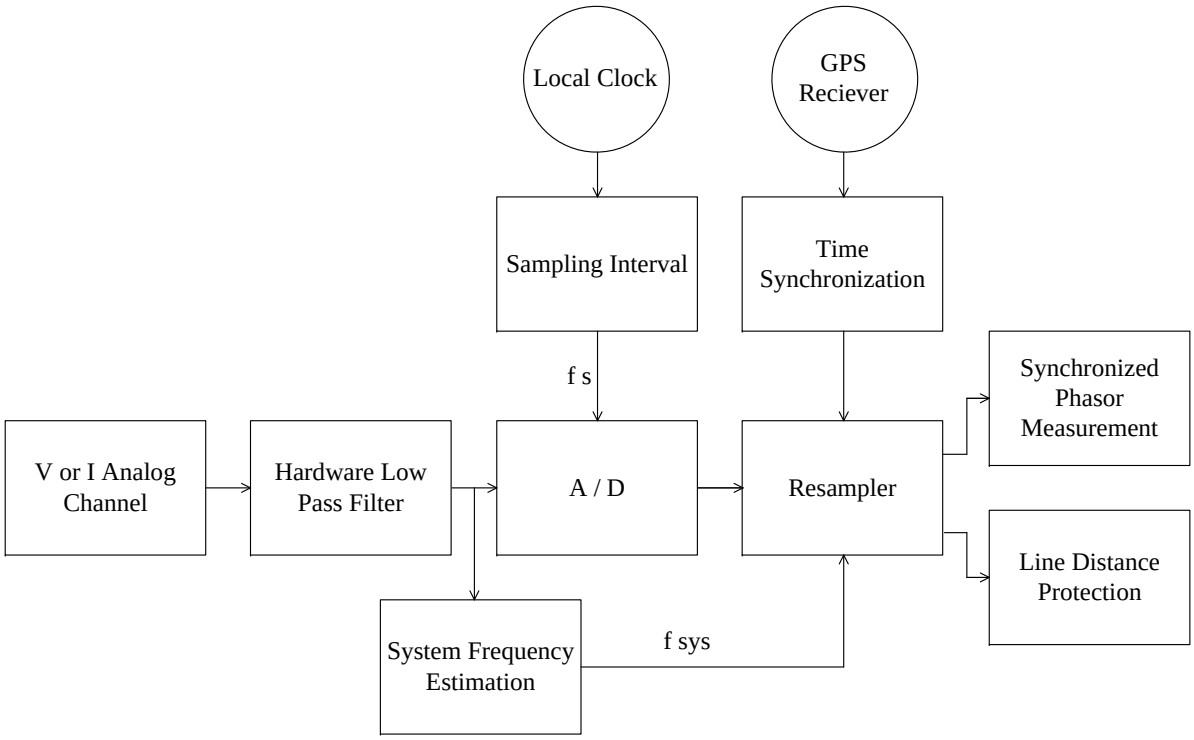

Figure 2.16: Example GPS and PMU synchrophasor measurement system associated with distance protection [11].

2.7 Distance Relay Zone 3 Blocking

2.7.1 Zone 3 Protection Overview

Either step or pilot scheme distance relay Zone 3 is designed originally for back-up protection to remote adjacent transmission lines or buses. The Zone 3 back-up protection is beneficial and prevalent especially for non-pilot distance relays, based on its sustainability and reliability to back up various contingencies happening due to incorrect operations, natural disasters, or due to the failures of components of the power system and its subsystems, such as batteries, relays, sensors, breakers, communication channels, etc. The Zone 3 time delay is typically between 1 to 2 seconds [14], longer than Zone 1 and Zone 2 time delay that is of the order of 15 to 30 cycles [28]. While the distance relay Zone 1 reach usually covers approximately 80% to 90% of the transmission line, and Zone 2 covers 120% of the

local transmission line, it is a normal practice that Zone 3 covers the whole length of the local transmission line plus 120% of the adjacent transmission line [14].

The step distance protection is one of the most commonly used schemes for HV and EHV transmission lines back-up protection. Being an over-reaching zone of protection, Zone 3 is considered the protection of the last resort if particular elements of the protection chain fail. Zone 3 occasionally trip under heavy and unusual loading conditions, and contribute to cascading failures of the power system as specified in [28]. When transmission lines are disconnected for some contingencies, the power flow of the faulted line will be transferred to other lines in operation. The Zone 3 element of a distance relay may trip to clear the overload, which actually aggravates the propagation of cascaded events.

The August 2003 blackout in the eastern U.S. and Canada is an example event of the above cascading sequence [69]. In the afternoon of August 14, the loss of the Eastlake 5 unit in North Ohio at 13:31 EDT was a significant factor in the later outage. Even though the trip of Stuart-Atlanta 345kV line afterwards at 14:02 EDT had no direct electrical effect on the system network, it affected the reliability coordinator Midwest Independent System Operator's (MISO) not being aware the loss of Eastlake 5 unit, and MISO's state estimator was unable to assess system conditions for most of the initial period of the outage, due to a combination of human error and the effect of the loss of Stuart-Atlanta line. Starting around 14:14 EDT, the local utility operating company First Energy's (FE) control room operators lost the alarm function of the primary server computer. Without the knowledge of the alarm function failure, FE's system operator remained unaware that their electrical system condition was beginning to degrade. From 15:05:41 EDT to 15:41:35 EDT, three more 345kV lines failed as the result of a tree contact in the control area. As each of the line failed, its power flow shifted to other transmission lines, voltages on the rest of FE's system degraded further. Starting at 15:39 EDT, the first of an eventual sixteen 138kV lines began to fail. The wide spread catastrophic outage became irremediable.

In the sequence of the cascading event, the Zone 3 operation is not a mis-operation because it trips the line according to the pre-designed protective scheme. However, its operation could be a challenge because it may contribute to the causes of a major outage [27].

Therefore, Zone 3 must not operate under extreme loading conditions. On the other hand, the specific contingencies and other situations must be evaluated prudently before the removal of the Zone 3 protection from a distance relay takes place.

2.7.2 Current Zone 3 Researches

In one of the Zone 3 blocking research efforts, a three-phase fault is distinguished from stressed conditions for distance relay Zone 3 protections by employing the maximum value of the transient monitoring function combined with a phase angle of positive sequence impedance [37]. The second criteria is used to identify a three-phase fault from perceived abnormal changes detected by the first criteria. The locally measured current signal is reconstructed by the Least Square Method introduced by M. S. Sachdev and et al. in [70]. The differences between the actual current and the reconstructed signal are calculated by the transient monitoring function over one cycle sampling period, that is [37]

$$TMF = \sum_{k=1}^{N} |d_k| \tag{2.39}$$

$$g = max(TMF_a, TMF_b, TMF_c) \tag{2.40}$$

where $|d_k|$ is the absolute value of the difference of the k^{th} element between the actual and the reconstructed current signals; N is the number of samples per cycle, k varies from 1 to N; TMF_a, TMF_b, TMF_c are the values of the transient monitoring function for phase a, b and c, and g is the maximum value.

The positive sequence impedance angle limit can be set as a criteria to distinguish the three-phase fault out of the stressed system conditions in compliance with the recommendations stated in [71]. The effectiveness of the differentiation may be susceptible in the application of the aforementioned technique, in case that there is other abnormal condition in which the positive sequence impedance angle also reaches the limit, such as in severe power swings.

Another distance relay Zone 3 blocking method was reported in [27], namely Adaptive Distance Relay Scheme (ADRS). The proposed scheme is based on the fact that when a transmission line is correctly removed by the protective relay due to a fault on the line, the power flow on this line will be transferred to other lines. The Zone 3 element of the distance protective relay could trip the line as a result of overload, leading to a more serious situation. In order to identify whether the overload is caused by the line flow transferred from the removed line, the post-fault flow can be measured on-line and compared to the estimated post-fault flow calculated from pre-fault line flow, line outage distribution factor (LODF) and generation shift factor (GSF). If the difference is within a tolerance, it is confirmed that the overload is caused by the transmission line power transfer. Otherwise, it is due to an internal fault. The criterion can be presented as follows: [27]

$$\left|\hat{P}_l^M - \hat{P}_l^E\right| < \varepsilon \tag{2.41}$$

where

$\hat{P}_l^M$ the measured post-fault line flow

$\hat{P}_l^E$ the estimated post-fault line flow

ε the error margin

The error margin ε in Equation 2.41 is a preset tolerance to separate overload from internal fault. The peer to peer (P2P) communication is the pre-requisite for the ADRS implementation. The cost and reliability of P2P communication could be a crucial evaluator for the scheme to be applied into practice, especially if the local measurement based scheme is available to determine the internal fault from overload conditions.

To improve the distance relay Zone 3 power swing blocking, there are other methods reported, including the Polynomial Curve Fitting Method [43]. In a given system network, the curves of the rotor angle change with respect to time for each synchronous machine and

may have diverse shapes during machine operation, and each of them can be represented by a polynomial function. The relative rotor angle changes can be approximated by voltage phase angles measured at generator bus during power swings. The estimated relative rotor angle velocity can be obtained by differentiating this voltage phase angle. Therefore, the approximate rotor velocity in turn can be represented by a polynomial function with one order less than the rotor angle polynomial function. For instance, if the rotor angle is expressed by a 6^{th} order polynomial function as [43]

$$\delta(t) = P_6 t^6 + P_5 t^5 + P_4 t^4 + P_3 t^3 + P_2 t^2 + P_1 t + P_0 \tag{2.42}$$

where P_i is the coefficient of the i^{th} element of the polynomial.

Thus, the change of the relative rotor velocity is given by a 5^{th} order polynomial function as

$$\frac{d\delta(t)}{dt} = 6P_6 t^5 + 5P_5 t^4 + 4P_4 t^3 + 3P_3 t^2 + 2P_2 t + P_1 \tag{2.43}$$

The rotor velocity curve calculated from the voltage phase angles is fitted with the rotor velocity polynomial function using the least square curve fitting method in Appendix A.2. In a post-fault power swing condition, a zero value of the regression polynomial function represents a zero crossing of the relative rotor speed of the synchronous machine, indicating a stable power swing scenario is detected, otherwise, if a zero crossing is not detected, an out-of-step phenomena is identified. A time interval after the contingency removal from system is selected for setting the optimal tripping time for distance relay. Within this time interval, a stable or an unstable power swing can be predicted.

2.8 Summary

The concept of *Electrical Center* was discussed in Section 2.2 for revealing the basic character of the apparent impedance measured by a distance relay. The existing techniques were categorized into three categories afterwards, based on the nature of methodologies for power swing detection and distance relay blocking, such as the *System Equilibrium Method*

in Section 2.3; the *Impedance Trajectory Tracking Method* in Section 2.4; the *Pattern Recognition Approaches* in Section 2.5. The wide area backup protection becomes available with the advent of the advanced synchrophasor based technology as discussed in Section 2.6.

The advantages and shortcomings of the conventional and existing methodologies were discussed. As the main focus of this research is the methodology for blocking Zone 3 protection during power swings so the methods pertaining to this were discussed in detail. The current research works on the same subject were discussed.

From the review of the methods in this chapter it is clear that a simple method without the need for setting parameters could be quite a useful advancement with practical applications to industry, especially if it could be applied to both generator and at transmission line level using purely local measurements. The new method is discussed in the next chapter.

Chapter 3

Proposed Third Zone Blocking (TZB) Algorithm for Detecting Power Swings

3.1 Introduction

Chapter 1 discussed the need for identifying the power swing type. Chapter 2 discussed the existing methodologies and conventional schemes for power swing blocking. As discussed in Chapter 1, the primary motivation for this research work was to develop a method for power swing identification to overcome the shortcomings of the current methodologies. The focus of this research work is mainly for blocking Zone 3 distance relays during power swing conditions, which often results in large scale blackouts. The proposed algorithm is referred to as "third zone distance relay blocking (TZB)" method and will be referred to as the TZB method in the subsequent discussions in this chapter.

The first step of the TZB method is power system equivalenting, which is based on a concept that at any bus (where the distance relay is placed), the complex power system network can be represented by an equivalent two-machine system and can be further reduced to a single machine infinite bus (SMIB) system. The SMIB equivalenting concept [39] was discussed in Section 2.3.3.

The TZB algorithm is introduced step-by-step in Section 3.2. Section 3.2.3 discusses the phase one of the TZB algorithm which calculates the equivalent system impedance by a non-linear iterative solver using the locally obtained voltage, active power, and reactive power. Section 3.2.4 discusses the phase two of the TZB algorithm to calculate the fictitious synchronous machine relative rotor speed with the acquired equivalent system impedance.

By checking for the first zero crossing (FZC) of the relative rotor speed, the type of power swing can be differentiated as discussed in Section 3.2.5.

The TZB algorithm is demonstrated on a SMIB system created in Power System Computer Aided Design (PSCAD) in Section 3.3. The simulation studies for verifying the TZB method are carried out for both stable power swing and out-of-step conditions. The calculated fictitious synchronous machine relative rotor speed with the TZB algorithm is compared to the actual system generator relative rotor speed to evaluate its correctness/accuracy.

3.2 TZB Algorithm

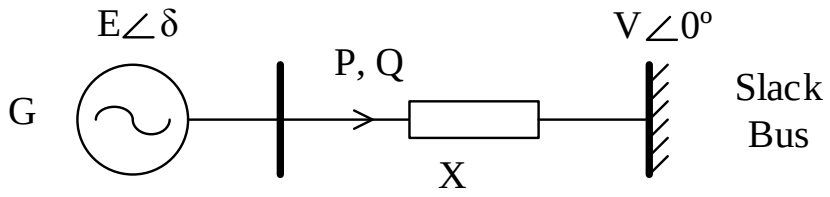

Figure 3.1: Equivalent single machine infinite bus representation of a complex power system.

3.2.1 Single Machine Infinite Bus (SMIB) System Representation

Due to the highly complex behavior of electrical power systems, building detailed models is difficult or could be time-consuming even with nowadays powerful computers. Therefore, it is essential to develop an equivalent model for static or dynamic analysis of the full order models. The power system reduction techniques can be categorized into modal equivalent, estimated equivalent and coherency equivalent methods as summarized in [72]. One of the techniques is introduced in [39] based on a concept of a single machine infinite machine equivalenting of a complex power system network. In this formulation, regardless of the complications of the given grid, at the relay location, the system can be approximated into a SMIB system with a couple of approximations as discussed in Section 2.3.3, so that the

dynamic analysis can be simplified in the form of a Swing Equation. The SMIB provides a simplified model of the power system for the stable/unstable power swing analysis using the TZB scheme.

3.2.2 Power Flow Equations

The TZB algorithm has been developed in this thesis from the basic power angle equations. The power-angle equations can be obtained from the basic power flow equations. The power flow can be demonstrated on a SMIB system model as shown in Figure 3.1. The bus admittance matrix of the SMIB system is written as

$$Y_{bus} = \begin{bmatrix} Y_{11} & Y_{12} \\ Y_{21} & Y_{22} \end{bmatrix} \tag{3.1}$$

where Y_{ii} and Y_{ij} are the self-admittances and the mutual admittances of the nodes.

The active and reactive power can be formulated by the node voltages, the system impedance, and the node phase angle difference. According to the admittance Y_{bus} matrix, on the sending terminal of the transmission line at the generator bus, we have

$$P + jQ = E(Y_{11}E)^* + E(Y_{12}V)^* \tag{3.2}$$

$$= E(G_{11} - jB_{11})E^* + E|Y_{12}|\angle(-\theta_{12})V^* \tag{3.3}$$

$$= |E|^2 G_{11} - j|E|^2 B_{11} + |E||V||Y_{12}|\angle(\delta - \theta_{12}) \tag{3.4}$$

where P Q are the active and reactive power measured at the sending end; the sending end voltage $E = |E|\angle\delta$; the receiving end voltage $V = |V|\angle 0°$; the self-admittance $Y_{11} = G_{11} + jB_{11} = |Y_{11}|\angle\theta_{11}$; the mutual admittance $Y_{12} = |Y_{12}|\angle\theta_{12}$.

Thus

$$P = |E|^2 G_{11} + |E||V||Y_{12}|\cos(\delta - \theta_{12}) \tag{3.5}$$

and

$$Q = -|E|^2 B_{11} - |E||V||Y_{12}|\sin(\delta - \theta_{12}) \tag{3.6}$$

Considering system resistance is insignificant for the power network, Equation 3.5 and 3.6 can be approximated by

$$P = |E||V||Y_{12}| \sin \delta \tag{3.7}$$

$$Q = |E|^2 B_{12} - |E||V||Y_{12}| \cos \delta \tag{3.8}$$

or

$$P = \frac{EV}{X_{12}} \sin \delta \tag{3.9}$$

$$Q = \frac{E^2}{X_{12}} - \frac{EV}{X_{12}} \cos \delta \tag{3.10}$$

where E V X_{12} are the absolute values of the quantities. The above two power angle equations are the basic equations from which the TZB algorithm is developed.

3.2.3 Phase One of TZB Algorithm

Considering a WSCC 9-bus system shown in Figure 3.2, the system has three machines, nine buses and six transmission lines. A three-phase fault occurs in a close proximity to Bus 7. Once it is cleared, the third zone of the distance relay R98 at Bus 9 must not operate due to a post-fault power swing. For the sake of illustration, only the fault F and the relay R98 have been taken into account. The concept can be extended to other distance relays on other lines as well.

Let us consider the voltage magnitude, active and reactive power measured by the relay R98, which are obtained from the measurements of instantaneous voltages and currents as the derivation in Appendix A.3 and denoted by E, P and Q, respectively. The relay measurements are used in an equivalent SMIB system arrangement as shown in Figure 3.1.

From the derivation in Section 3.2.2, the power angle equation for the SMIB system are given by:

$$P = \frac{EV}{X} \sin \delta \tag{3.11}$$

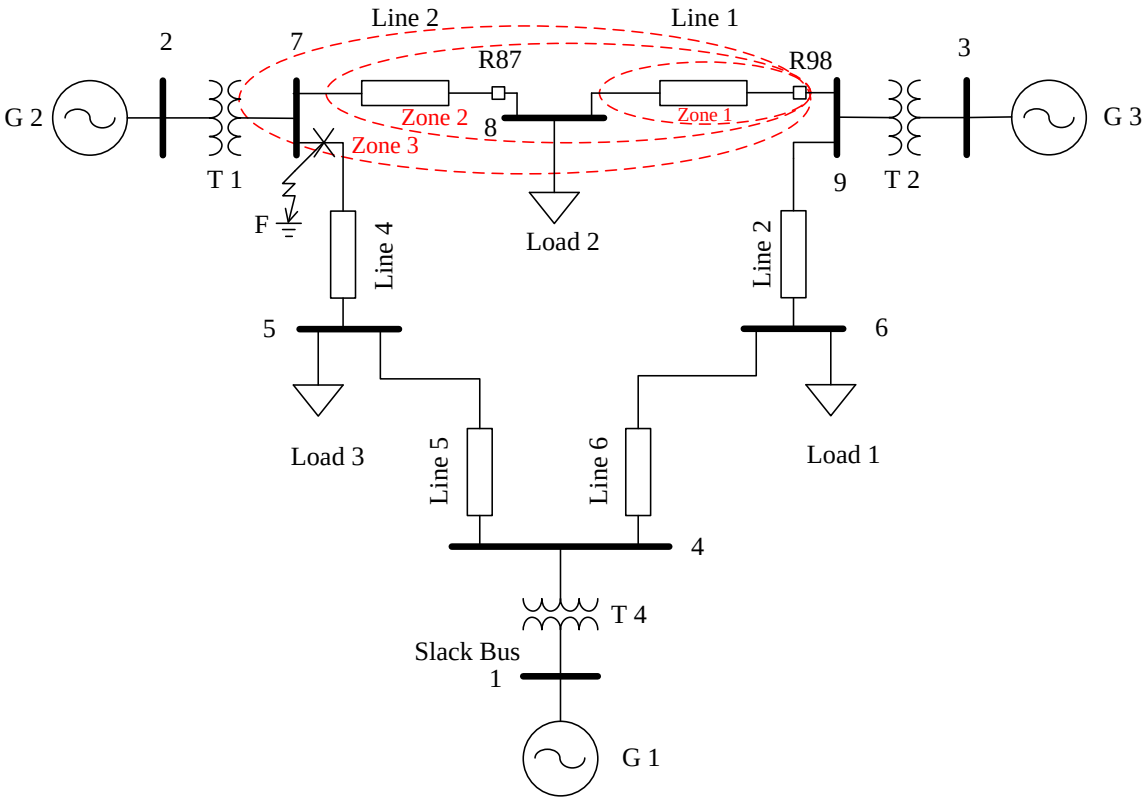

Figure 3.2: TZB methodology illustrated on a typical WSCC 9-bus system. [2]

Then

$$\sin\delta = \frac{XP}{EV} \tag{3.12}$$

And

$$Q = \frac{E^2}{X} - \frac{EV}{X}\cos\delta \tag{3.13}$$

Then

$$\cos\delta = \frac{E^2 - XQ}{EV} \tag{3.14}$$

The two unknown parameters in this arrangement are δ and X. δ is the source phase angle of the SMIB system voltage and X is the equivalent reactance magnitude of the fictitious system. From the derivation in Section 3.2.2, the system reactance X in power angle

equations is an approximation of the system impedance. The system impedance magnitude Z is used instead of X in the following derivation and calculation.

Eliminating δ from Equation 3.11 and Equation 3.13, we have

$$\left(\frac{PZ}{EV}\right)^2 + \left(\frac{E^2 - QZ}{EV}\right)^2 = 1 \tag{3.15}$$

And

$$P^2Z^2 + (E^2 - QZ)^2 = E^2V^2 \tag{3.16}$$

Thus, the following polynomial is obtained

$$(P^2 + Q^2)Z^2 - 2QE^2Z + E^4 - E^2V^2 = 0 \tag{3.17}$$

Only Z is unknown in Equation 3.17.

Using a non-linear iterative solver, i.e. the Laguerre's method discussed in Appendix A.4, Z can be obtained from the above equation. δ can be found from Equation 3.12 and Equation 3.14, once Z is solved for.

This completes the calculations for the first phase of the algorithm.

3.2.4 Phase Two of TZB Algorithm

From Equation 3.11, knowing the phase angle δ of the power source of the SMIB system and the equivalent impedance Z of the fictitious system, the electrical power input P to the system can be found. By differentiating Equation 3.11, the fictitious machine rotor relative speed can be expressed as the function of the rate of change of the electrical active power output from the fictitious machine and the rate of change of voltage magnitude measured at the relay location as the following:

$$\frac{d\left(\frac{P}{E}\right)}{dt} = \left(\frac{V}{Z}\right)\cos\delta\left(\frac{d\delta}{dt}\right) \tag{3.18}$$

Since the synchronous machine rotor relative speed ω_r equals to the rate of change of rotor angle, that is

$$\omega_r = \frac{d\delta}{dt} \tag{3.19}$$

Bringing Equation 3.13 and Equation 3.19 into Equation 3.18, it becomes

$$\frac{d\left(\frac{P}{E}\right)}{dt} = \left(\frac{V}{Z}\right)\left(\frac{E^2 - QZ}{EV}\right)\omega_r. \tag{3.20}$$

Thus

$$\frac{d\left(\frac{P}{E}\right)}{dt} = \left(\frac{E^2 - QZ}{EZ}\right)\omega_r. \tag{3.21}$$

In Equation 3.21, the variables *P, E, Q, V* and *Z* are known.

Therefore, the frequency or the rotor relative speed of the fictitious synchronous machine can be obtained for the equivalent system as the following:

$$\omega_r = \frac{\left(\frac{dP}{dt}\right)E - \left(\frac{dE}{dt}\right)P}{E\left(\frac{E^2 - QZ}{Z}\right)} \tag{3.22}$$

In order to determine $\frac{dP}{dt}$ and $\frac{dE}{dt}$, a numerical differentiation can be used as expressed below.

$$\frac{dP}{dt} \approx \frac{\triangle P}{\triangle t} = \frac{P_t - P_{t-1}}{\triangle t} \tag{3.23}$$

$$\frac{dE}{dt} \approx \frac{\triangle E}{\triangle t} = \frac{E_t - E_{t-1}}{\triangle t} \tag{3.24}$$

where P_t is the power and E_t is the voltage measured at the current simulation time instant t, and P_{t-1} is the power and E_{t-1} is the voltage measured at the previous time instant in the simulation.

Substituting Equation 3.23 and 3.24 into 3.22,

$$\omega_r = \frac{\left(\frac{P_t - P_{t-1}}{\triangle t}\right)E - \left(\frac{E_t - E_{t-1}}{\triangle t}\right)P}{E\left(\frac{E^2 - QZ}{Z}\right)} \tag{3.25}$$

The time step $\triangle t$ in the simulation is generally constant and is considered to be a small value. If ω is the actual rotor speed of the fictitious machine, then the relative speed ω_r is going to be

$$\omega_r = \omega - \omega_S \tag{3.26}$$

where ω_S is the synchronous speed equal to $2\pi f_S$, f_S is the synchronous frequency.

ω_r gives the relative speed of the fictitious machine over time as the simulation progresses. Plotting it over time will give an idea as to how the system is reacting to a disturbance.

3.2.5 Significance of First Zero Crossing (FZC)

A stable swing is distinguished from an unstable one from the fact that the speed ω of the machine G reaches a synchronous value, called First Zero Crossing (FZC) in this research in

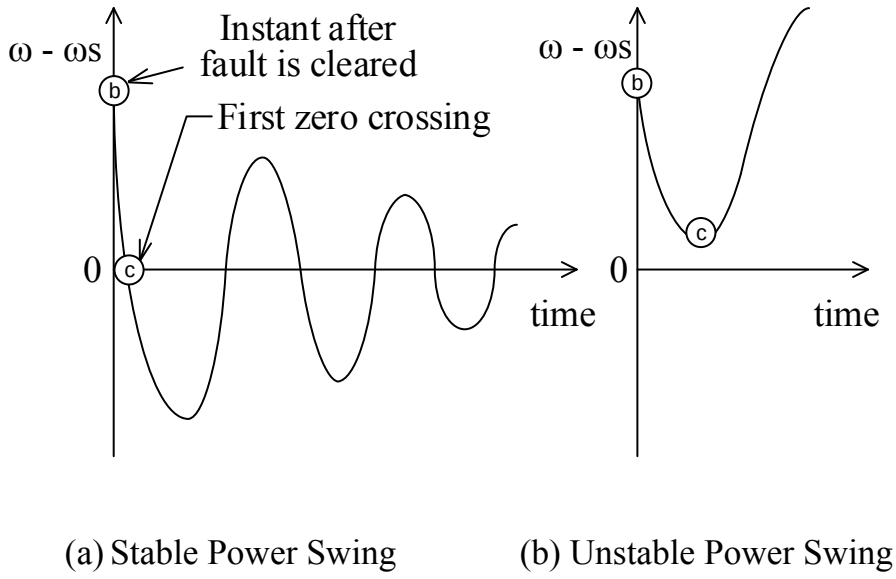

Figure 3.3: Relative speed of the equivalent machine due to a stable and unstable power swing. [12]

the equivalent SMIB system in Figure 3.1, before the machine starts accelerating again, if it is stable [12]. The stable or unstable swing identification with the relative speed $\omega_r = \omega - \omega_s$ is graphically illustrated in Figure 3.3. In a stable power swing scenario, after the contingency is cleared from the system at time instant b, the calculated fictitious synchronous machine relative speed decreases across zero at time instant c, and approaches to steady state as demonstrated in the equivalent machine relative speed curve in Figure 3.3(a). In the case of an unstable swing, the machine decelerates and starts accelerating again before the relative speed becomes zero or the speed becomes synchronous, as in Figure 3.3(b). From Figure 3.3, FZC can be determined easily. Finding FZC of the equivalent system is the crux of the proposed algorithm.

Figure 3.4 demonstrates the stable and unstable swings shown in Figure 3.3 from the physics point of view, i.e. using the equilibrium points. The point a corresponds to the instant at which a fault happens, when the relative speed is zero, the point b corresponds

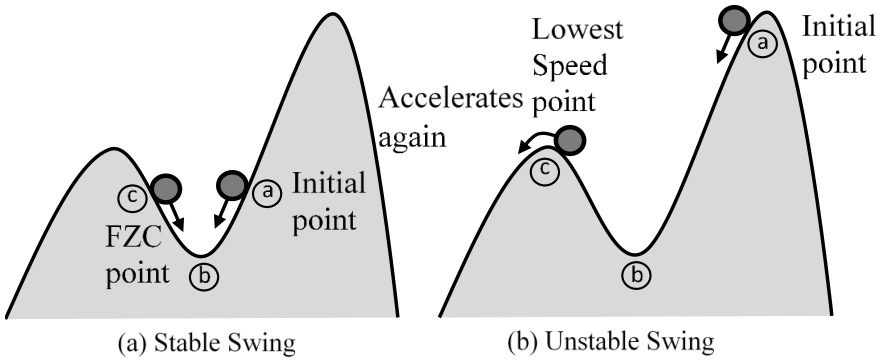

Figure 3.4: Physical interpretation of stable and unstable equilibrium points for power swings shown in Figure 3.3. [12]

to the instant at which a fault is cleared, i.e. the speed is at its maximum value, the point c corresponds to the zero crossing point for a stable swing as shown in Figure 3.4a, or the lowest speed point for an unstable swing as shown in Figure 3.4b [12].

The identification of stable or unstable power swings using the TZB method can also be interpreted using the concept described for Equal-Area Criteria in Section 2.3.1. In Figure 2.4, a is the steady state point where the equivalent synchronous machine is running at the synchronous speed ω_S. b is the fault instant at which the machine starts accelerating. d is the instant after fault is cleared. At this point the electrical power output of the synchronous machine is greater than the mechanical power input, and the machine decelerates until the synchronous speed is reached again at the point e in Figure 2.4, i.e. the first zero crossing point c in Figure 3.3(a). Therefore, if there is a first zero crossing in the curve plotted in Figure 2.4, the rotor angle of the synchronous machine oscillates approaching to a steady state value. In the case of an unstable swing, the speed of the machine starts increasing before it touches the synchronous speed ($\omega - \omega_S = 0$). There is no first zero crossing, i.e. the e point will never be reached. Before the machine rotor speed decreases to synchronous, the machine mechanical power input becomes greater than its electrical power output, and the machine starts accelerating again.

Consequently, for a fault occurring at some point in the system, the nature of power swing (post-fault) can be studied within the line distance relay module using the proposed algorithm to decide whether to block Zone 3 or not [12]. This decision is based on the first zero-crossing point, i.e. if the power swing encroaches into Zone 3, it need not trip the breaker using this arrangement. The Zone 3 relay generally has a time delay of 1-2 seconds. The first zero crossing can be detected much before that, so the proposed scheme is going to be very useful when used for a real application.

The algorithm proposed can be applied at every time interval or time step chosen to detect the FZC point. It can be applied to the distance relay module in the system by finding the equivalent system individually on a real-time basis for each case.

3.3 SMIB System Power Swing Detection

3.3.1 Introduction

The proposed TZB scheme in distance relays has been modeled in Power Systems Computer Aided Design /Electromagnetic Transients including DC (PSCAD/EMTDC) environment available in Electrical & Computer Engineering Department in University of Saskatchewan. EMTDC simulates the time domain instantaneous response of electrical systems, and solves differential equations for both electromagnetic and electromechanical systems in the time domain [73] [74]. The circuits are essentially representations of a number of the ordinary differential equations, numerically solved for discrete intervals.

PSCAD is a powerful and flexible graphical user interface to EMTDC solution engine. It enables graphically assembling the circuits, running the simulations, analyzing the results, and managing the data in a completely integrated graphical environment [73]. PSCAD comes with a component library of pre-programmed and tested models which range from simple passive elements and control functions, to more complex models, such as electric machines, FACTS devices, transmission lines and cables [75]. One of the features of PSCAD is its allowance for the custom design of models.

The purpose of PSCAD simulation is to evaluate the feasibility of the proposed TZB algorithm by employing a SMIB system available. The testing SMIB system model has one synchronous machine, a simple transmission system connected to infinite bus, and miscellaneous measurement devices, etc. The outputs of the simulation are displayed in PSCAD and are collected in MATLAB for detailed analysis.

3.3.2 SMIB System Setup

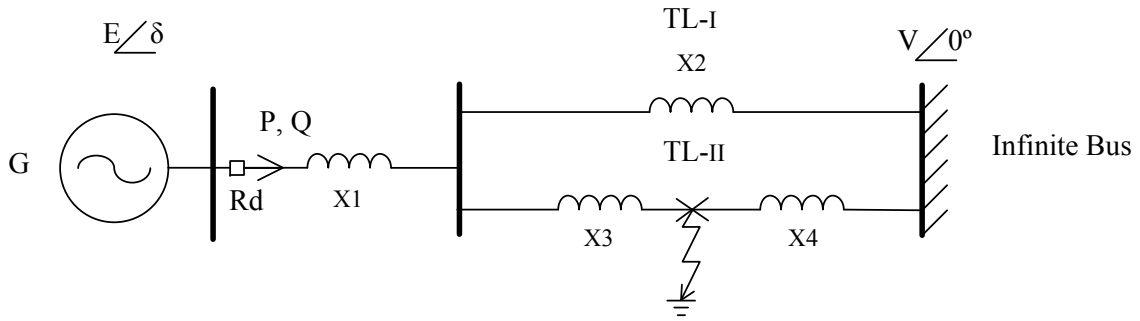

Figure 3.5: PSCAD Equivalent SMIB system schematic for TZB algorithm study.

A 24kV SMIB system has been modeled in PSAT and PSCAD to differentiate stable and unstable power swings using the TZB algorithm. The SMIB system schematic is seen in Figure 3.5. In the figure, E is the voltage on the bus of the generator G, and $\angle\delta$ is its angle. V is the voltage at the infinite bus. P and Q is the active and reactive power output of the generator bus. X_1 is the reactance of a measurement component. X_2 is the reactance of transmission line TL_I. The reactance of transmission line TL_{II} is identically divided into to two segments X_3 and X_4 for introducing contingency in the following study. The parameters of the system are as presented in Appendix B.1.

The SMIB system has been created in PSAT to conduct Load Flow study, which is shown in Appendix B.2. The outcome of the Load Flow results is attached in Appendix B.3.

The SMIB system PSCAD model with the same settings is shown in Appendix B.4 for the TZB algorithm study. In the figure, an IEEE Type I hydro-turbine is employed as the

prime mover converting the kinetic energy of water to the mechanical energy input to the synchronous generator. The inputs to the turbine are the per-unit speed ω, the per-unit speed reference ω_{ref} and the gate position z. The outputs are the mechanical torque T_m and the initial gate position zi [73]. The prime mover governor provides turbine control to regulate the power and the frequency. Both ω and T_m are input to the synchronous machine model. The synchronous machine Source Machine Transition time instant $S2M$ is set at 0.5 s which is provided by a Timer. The synchronous machine Locked-Rotor Normal Mode Transition time instant LRR is set at 1.0 s which is provided by another Timer.

The instantaneous current and voltage output of the generator G are measured by Multimeter component in series within the circuit close to the generator bus. Fast Fourier Transform (FFT) is applied to extract the 3-phase magnitude and phase quantities. The instantaneous active power P and reactive power Q are measured by Real/Reactive Power Meter element on X_1. The distance relay module R_d is located at the downstream of the generator bus before the power meter component, at which the fictitious synchronous machine relative speed is calculated.

3.3.3 Stable Power Swing Detection in SMIB System

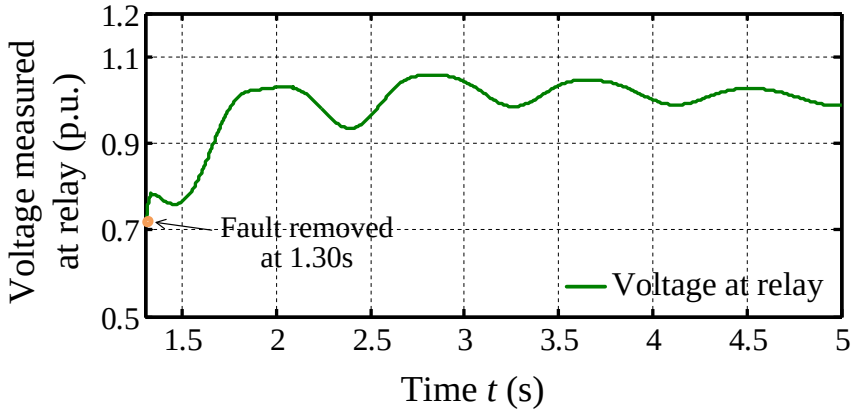

Figure 3.6: Measured voltage at relay location under stable power swing in SMIB system.

In a stable power swing study case, the contingency scenario is created by introducing

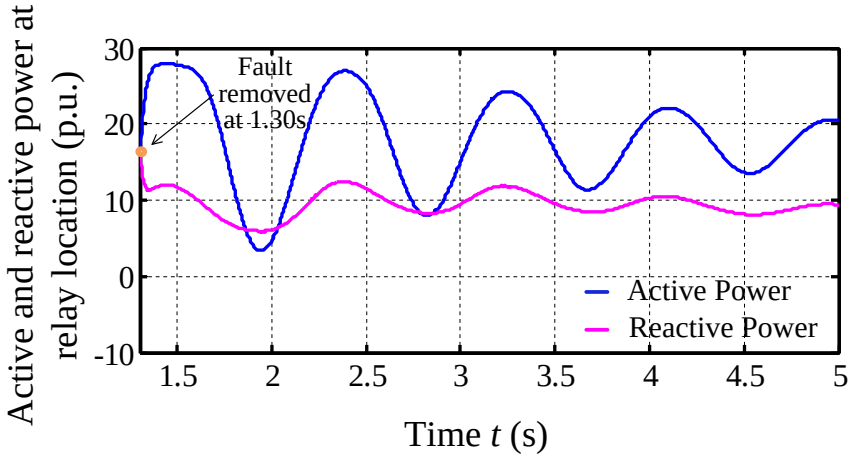

Figure 3.7: Measured active and reactive power at relay location under stable power swing in SMIB system.

a three phase to ground fault at the middle of the second transmission line, i.e. between $X3$ and $X4$, as shown in Figure 3.5. In the SMIB model shown in Appendix B.4, a Timed Fault Logic component is employed to control the type and duration of the fault. The stable power swing is observed after the three-phase fault is applied at 1.00 s and cleared at 1.30 s, i.e. the fault duration is 0.30 s.

The voltage E magnitude increases and oscillates approaching to the steady state value as shown in Figure 3.6, which is measured after the fault is removed at 1.30 s. The active and reactive power out of the generator bus, P and Q, are shown in Figure 3.7. The equivalent system impedance Z_r is calculated using Equation 3.17 of the phase one of the algorithm, as shown in Figure 3.8. Applying Equation 3.25 of the phase two of the algorithm, the equivalent SMIB system fictitious synchronous machine relative speed ω_r is calculated by the TZB method as shown in Figure 3.9. After the fault is removed at 1.30 s, the TZB calculated fictitious machine relative speed ω_r oscillates approaching to equilibrium around 0. The FZC is detected at 1.45 s.

The TZB calculated fictitious machine relative speed is validated by comparing it to the measured synchronous machine G relative speed ω_a as shown in Figure 3.10. It is observed

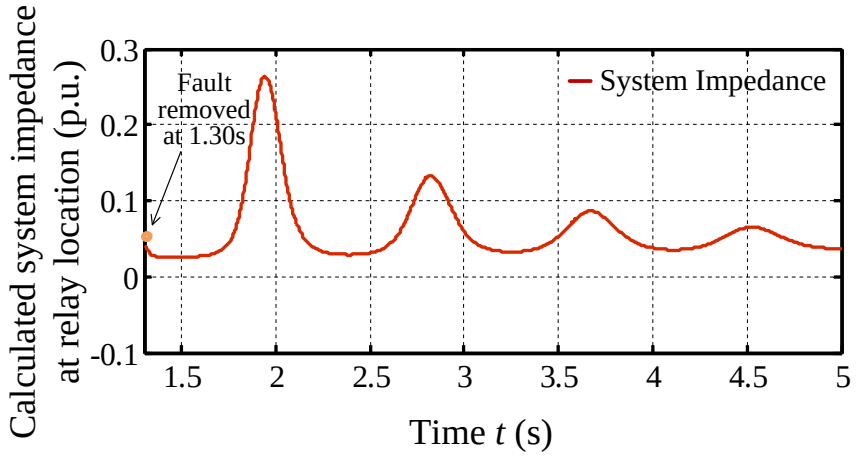

Figure 3.8: TZB calculated system impedance at relay location under stable power swing in SMIB system.

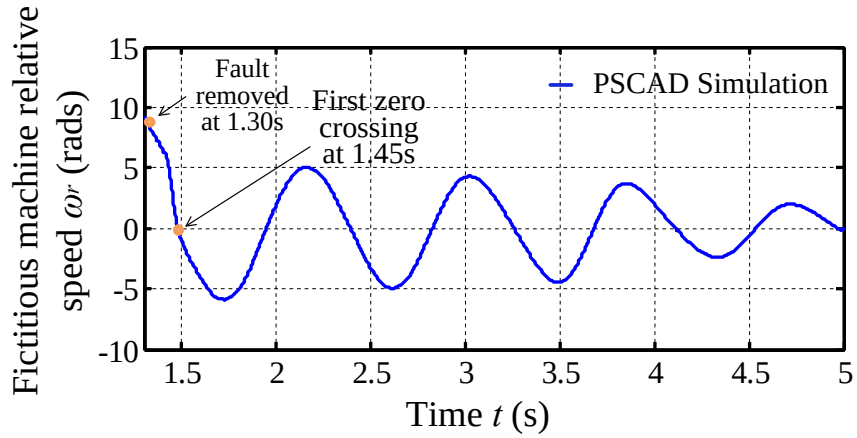

Figure 3.9: Calculated fictitious synchronous machine speed Case 1 under stable power swing in SMIB system.

that the two speed curves are not only generally in phase, but the FZCs happen at exact same time instant. The calculated relative speed magnitude ω_r is in the same scale with the measured generator G relative speed ω_a as well.

In another stable power swing scenario when a single phase to ground fault is applied in

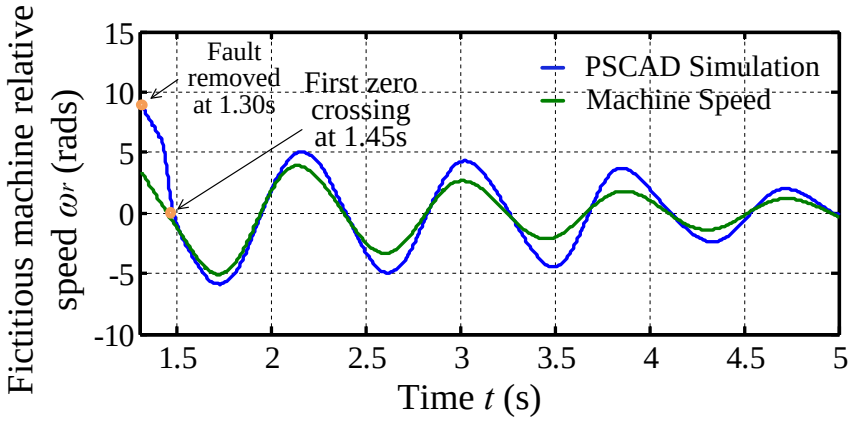

Figure 3.10: Calculated fictitious synchronous machine speed compared with measured actual machine speed in Case 1 under stable power swing in SMIB system.

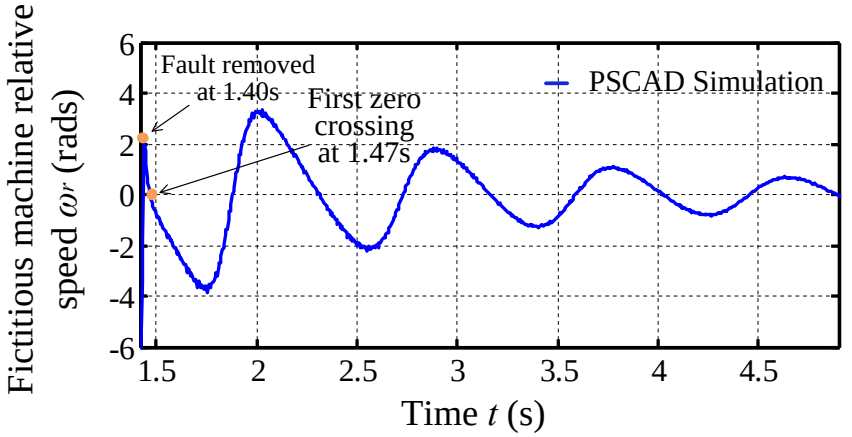

Figure 3.11: Calculated fictitious synchronous machine speed Case 2 under stable power swing in SMIB system.

the system, the equivalent SMIB system fictitious synchronous machine relative speed ω_r is calculated by the TZB method as shown in Figure 3.11. After the fault is removed at 1.40 s, the TZB calculated fictitious machine relative speed ω_r oscillates approaching to equilibrium around 0. The FZC is detected at 1.47 s.

The TZB calculated fictitious machine relative speed is validated by comparing it to the

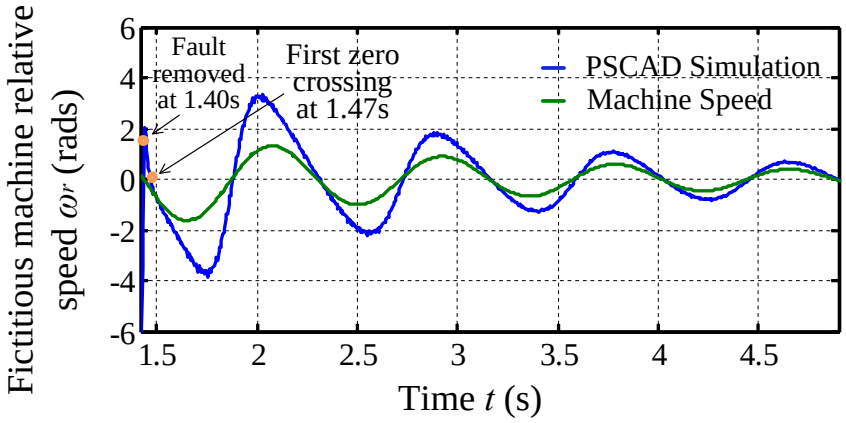

Figure 3.12: Calculated fictitious synchronous machine speed compared with measured actual machine speed in Case 2 under stable power swing in SMIB system.

measured synchronous machine G relative speed ω_a as shown in Figure 3.12. It is observed that the two speed curves are also in phase. The calculated relative speed magnitude ω_r is in the same scale with the measured generator G relative speed ω_a.

3.3.4 Unstable Power Swing Detection in SMIB System

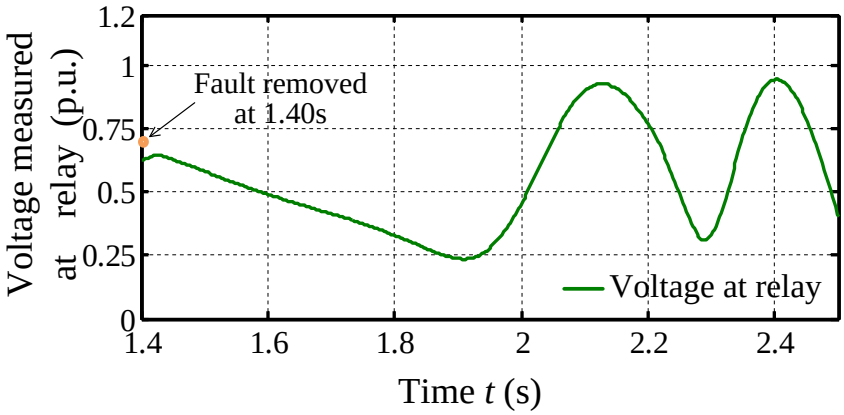

Figure 3.13: Measured voltage at relay location under unstable power swing in SMIB system.

In an unstable scenario study case, the same PSCAD SMIB system settings are kept as

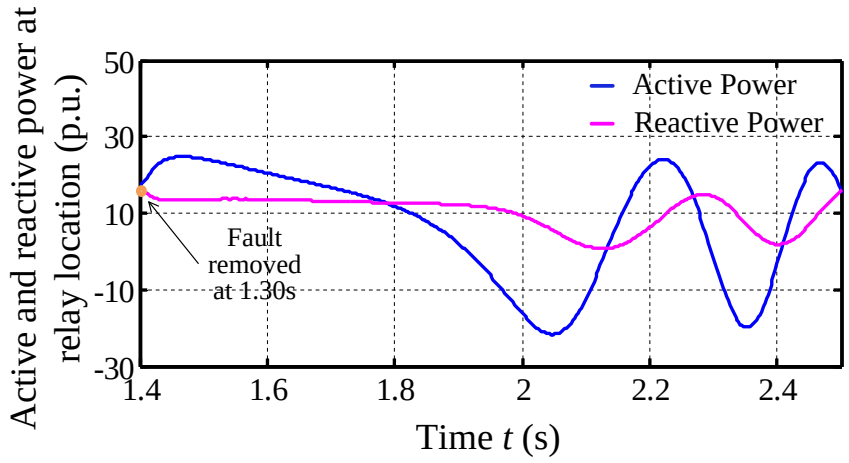

Figure 3.14: Measured active and reactive power at relay location under unstable power swing in SMIB system.

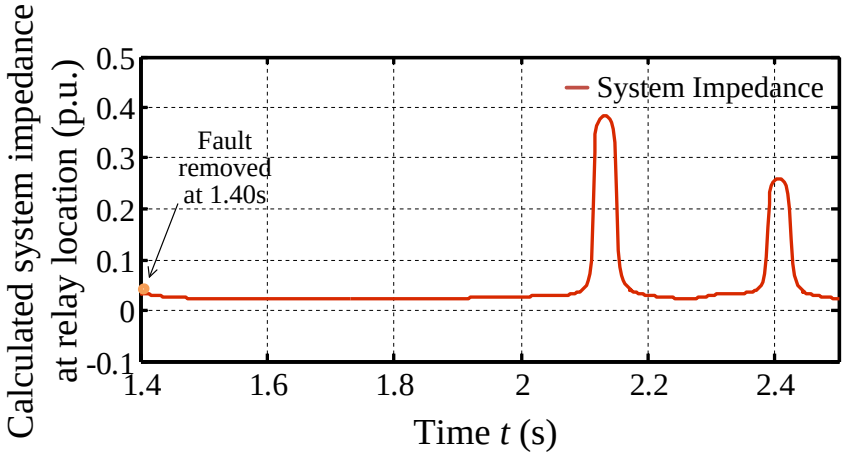

Figure 3.15: TZB calculated system impedance at relay location under unstable power swing in SMIB system.

in Appendix B.4. The unstable power swing is observed by postponing the three-phase fault clearing time to 1.40 s, i.e. the fault duration extending to 0.40 s.

The measured voltage magnitude E decreases after the fault is removed and starts fluctuating, instead of approaching to an equilibrium like in the stable case, as shown in Figure

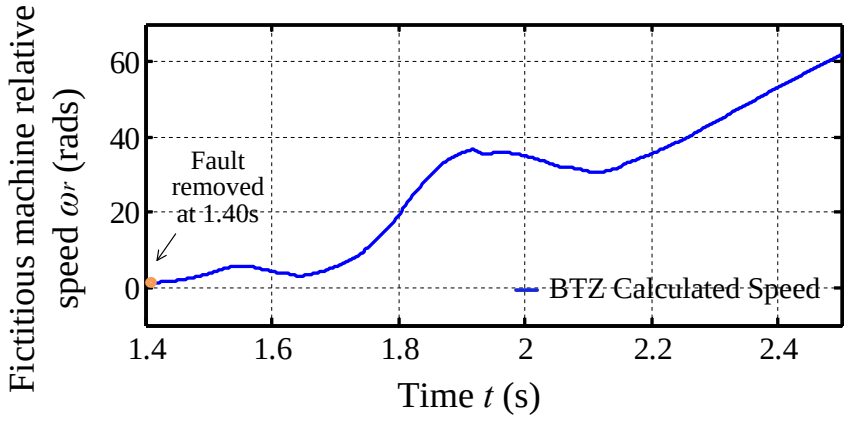

Figure 3.16: Calculated fictitious synchronous machine speed under unstable power swing in SMIB system.

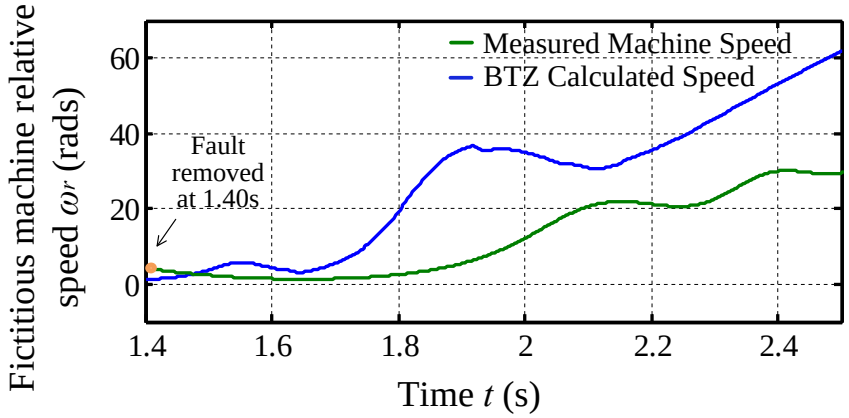

Figure 3.17: Calculated fictitious synchronous machine speed compared to measured actual machine speed under unstable power swing in SMIB system.

3.13. The measured active and reactive power P and Q also fluctuate and do not approach to steady state as shown in Figure 3.14. Based on the measurements, the equivalent system impedance Z_r is calculated by applying Equation 3.17 of the phase one of the algorithm as shown in Figure 3.15.

The fictitious machine relative speed ω_r is calculated by Equation 3.25 of the phase two

of the algorithm as shown in Figure 3.16. After the fault is cleared at 1.40 s, the TZB calculated relative speed ω_r increases and decreases, but does not cross zero and increases again. The equilibrium speed is not reached for the synchronous machine G after the fault is cleared, and the out-of-step condition can be identified.

The TZB calculated fictitious machine relative speed is compared to the actual synchronous machine G relative speed ω_a as shown in Figure 3.17. It can be observed that both the TZB calculated and the measured machine relative speed increase away from the synchronous value and the machine becomes unstable. The temporary decelerations can be observed on both the actual and the calculated speed curves. Neither the actual speed ω_a nor the calculated speed ω_r crosses zero, i.e. there is no FZC happening.

3.3.5 Discussion of SMIB Results for Proposed Algorithm

The SMIB example consisted of two parallel transmission lines. The stable and unstable power swing scenarios were generated applying the three-phase and single-phase fault in the middle of one of the transmission line. The proposed TZB algorithm calculates with the measurements at a distance relay location at the generator bus.

The TZB algorithm is developed in Fortran, and the algorithm can be executed in less than 1 ms on computer clock of a 64-bit operating system computer with an Intel Core i5-2400 CPU @ 3.10 GHz. FZC of the calculated relative speed ω_r was obtained for the fictitious synchronous machine for the stable cases. The calculated relative speed ω_r does not have the FZC point for an unstable swing scenario. A stable power swing scenario can therefore be differentiated from an unstable one. For a stable power swing, the calculated fictitious machine relative speed is in phase with the actual measured machine speed value. However, for an unstable power swing condition, there is magnitude difference between the calculated relative speed value and the measured generator G relative speed.

From the above SMIB studies/results, the following conclusions can be drawn for the proposed TZB algorithm.

- The TZB method does not require offline studies to find its parameters. The fictitious SMIB representation and the relative machine rotor speed calculations can be done in a real-time fashion.

- The proposed TZB method is very accurate in terms of finding a stable power swing condition and can be used for blocking third zone distance relays during stable power swings.

- Since it identifies power swings from a system equilibrium point of view, there is no need to do extensive stability studies.

- The TZB method does not require detailed information for the network so it can be applied to any sized system and grid configuration. The inputs to TZB method are local measurements available at the distance relay location which provides significant advantages.

3.4 Summary

The derivation steps for the proposed TZB algorithm were discussed in this chapter. Firstly, a SMIB equivalent of the power network was obtained. The equivalent SMIB parameters were obtained purely from local measurements. The fictitious synchronous machine relative speed was calculated, and the calculated fictitious synchronous machine relative speed (whether it went through an FZC or not) was used to differentiate stable power swing from out-of-step condition. The significance of FZC was explained from a physics point of view and the classical Equal-Area Criteria theory.

A 24kV SMIB system model in PSCAD/EMTDC was used for the SMIB studies in this chapter. The simulation studies showed that the proposed method was practical, and could be reliably used for blocking distance relays during stable power swings. If it was a stable power swing, the relay could be blocked irrespective of whether it encroached into protection zones or not. The proposed TZB method also could detect out-of-step conditions correctly.

Chapter 4

Testing of the Proposed Third Zone Blocking (TZB) Method by Phasor Based Simulations Using PSAT

4.1 Introduction

The TZB algorithm, as well as the FZC concept, was introduced in Chapter 3. The proposed scheme was demonstrated using a SMIB system as an example. In this chapter, the TZB method is tested on a multi-machine test system to validate the method further.

As discussed in Chapter 1, the power system static and transient response can be produced/generated using digital computer simulations. For this purpose, the power systems components need to be modeled e.g. synchronous machines, transmission lines, transformers, etc, and their behavior is investigated during disturbances and system parameter variations. Section 4.2 discusses the power system modeling and the electrical representation of basic components.

This chapter uses Power System Analysis Toolbox (PSAT) for computer simulations. PSAT is selected for the TZB method testing, because PSAT is a phasor based software and provides a straightforward power system simulation environment for testing. Section 4.3 discusses the PSAT toolbox (an application tool developed in MATLAB). It uses the fundamental frequency modeling to study the dynamic response of the power system.

WSCC 9-bus system is utilized for the purpose of testing the TZB method. The system setup is shown in Section 4.3.2. Section 4.3.3 and Section 4.3.4 describe the testing of the

TZB method on the distance relay R98 and R78 respectively at different locations in the WSCC system for different power swing scenarios.

The proposed TZB method is further compared with a conventional Double Blinder scheme, and the results are presented in Section 4.4. Setting up of a basic Double Blinder procedure is first discussed in Section 4.4.1.1. A discussion of the Double Blinder concentric polygons scheme for the relay R98 is discussed in Section 4.4.1.2. The comparative results using the proposed TZB method and the conventional Double Blinder scheme are discussed in the following Section 4.4.2.

The impedance loci calculated at distance relay locations are basic quantities used for the TZB method power swing blocking. Finally in Section 4.5, the transmission line current calculation for the distance relay is verified to confirm the impedance locus calculation at the relay location.

4.2 Power System Modelling

The proposed power swing blocking scheme is tested utilizing power system stability analysis software, which are designed for power system planning, protective device testing, new concept developing, etc. for utilities, manufacturers, consultants, research and academic institutes. In software, the power system elements are modeled by equivalent impedance networks. The solution of the entire network connected by individual elements is obtained by solving the nodal equations established for any arbitrary system. The power system element models for transient stability study are discussed in the following sections for synchronous machines, transformers and transmission lines. The power system simulation can be enhanced with the understanding of the modelling of power grids, electrical machines and apparatuses.

4.2.1 Synchronous Machine

A synchronous machine is a device that performs electromechanical energy conversion through the medium of the electric and the magnetic field interaction. The simplified synchronous machine can be represented by a Thevenin voltage source for the fundamental frequency. The machine terminal voltage E_r can be expressed by

$$E_r = E_{IN} - I_a(R_a + jX_S), \tag{4.1}$$

where E_r is the resultant armature coil winding potential; E_{IN} is the machine no-load source voltage; I_a is the armature current; R_a is the armature resistance; X_S is the synchronous reactance equal to the armature reactance X_a plus the leakage reactance X_l, as derived in [13].

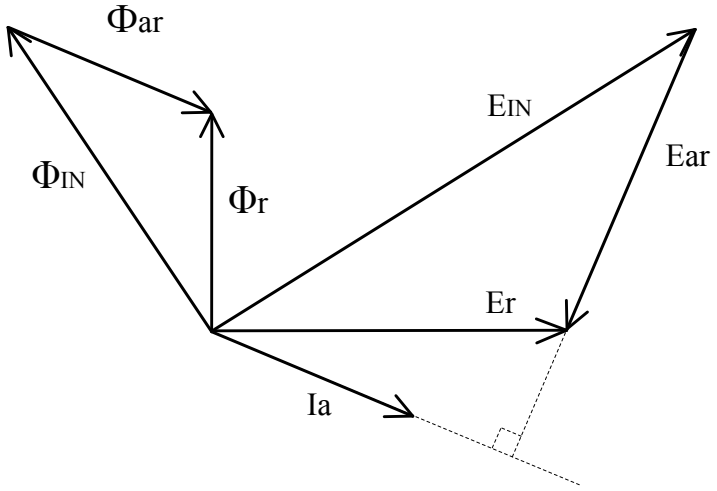

Figure 4.1: Phasor diagram of voltage source. [13]

In general practices, the armature resistance R_a is small enough to be negligible as shown in the phasor diagram Figure 4.1, in which E_{ar} is the voltage drop across the phase armature winding reactance. If I_a is lagging the machine no-load voltage E_{IN} by 90°, the resultant flux Φ_r, equal to the rotor flux Φ_{IN} less than the armature flux Φ_{ar}, is largely reduced. If

a highly-inductive load is connected then the terminal voltage E_r generated by Φ_r is going to be much lower than the machine no-load voltage E_{IN}. Whereas, if I_a is leading the machine no-load voltage E_{IN} by 90°, the resultant flux Φ_r equals to the rotor flux Φ_{IN} plus the armature flux Φ_{ar}, and is greatly increased. If a highly capacitive load is connected to the machine terminal, the resulting E_r is going to be considerably higher than the machine no-load voltage E_{IN}.

In power system analysis software, the synchronous machine is modeled utilizing the Park's ($dq0$) transformation [76] [77] equations (given in Appendix B.5) to describe its transient and dynamic performance. It transforms the armature (stator) side *abc* currents into *d-axis* and *q-axis* currents in phase with the amortisseur direct-axis and quadrature-axis windings.

The machine stator instantaneous $dq0$ voltages and currents are obtained from three phase instantaneous voltages and currents, respectively. Then the *d-axis* and *q-axis* flux linkages are derived from the corresponding instantaneous currents. From the flux linkage, voltage and current equations, the machine electric torque and rotor speed can be obtained and the static and dynamic responses of the synchronous machine can be simulated.

4.2.2 Transmission Line

There is no shunt admittance that needs to be considered for a short transmission line, so that the current is same at the sending and the receiving end. The nominal π circuit is the conventional representation of the medium length line. The sending end current I_{SL} is the sum of the current in series arm and shunt admittances,

$$I_{SL} = V_{SL}\frac{Y_L}{2} + V_{RL}\frac{Y_L}{2} + I_{RL}, \tag{4.2}$$

where V_{SL} is the sending end voltage; V_{RL} is the receiving end voltage; Y_L is the shunt admittance; I_{RL} is the receiving end current.

The sending end voltage V_{SL} can be calculated as [13]

$$V_{SL} = \left(Z_L\frac{Y_L}{2} + 1\right)V_{RL} + Z_L I_{RL}, \tag{4.3}$$

where Z_L is the impedance in the series arm.

Thus, the sending end current I_{SL} can be expressed as the function of V_{RL} and I_{RL}, as [13]

$$I_{SL} = \left(Z_L \frac{Y_L}{4} + 1\right) V_{RL} Y_L + \left(Z_L \frac{Y_L}{2} + 1\right) I_{RL}, \tag{4.4}$$

4.2.3 Transformer

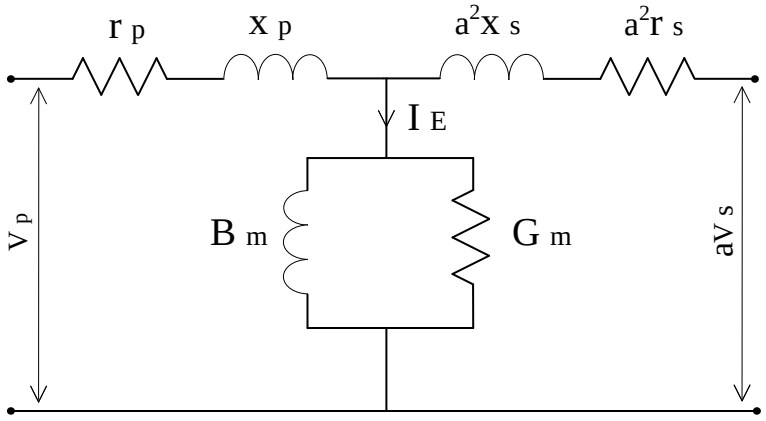

Figure 4.2: Practical transformer equivalent circuit.

Unlike the ideal transformer, in a practical transformer, a portion of the flux linking to the primary winding not linking the secondary creates a voltage drop, which is called the leakage reactance x_P in series with the primary winding. Similarly, the leakage reactance x_S on the secondary is in series with the secondary winding. Additionally, the winding resistance r_P and r_S are considered for the primary side and the secondary side respectively. The magnetizing current I_E is represented by an inductive reactance x_M and a resistance r_C to account for the hysteresis loss and the eddy current loss as in Figure 4.2.

For a practical transformer, its secondary voltage is formulated as follows [1], if its secondary winding is open-circuited.

$$aV_S = \frac{jx_M}{r_P + j(x_P + x_M)} V_P \tag{4.5}$$

where $a = N_P/N_S$ is the ratio of the transformer windings.

When a finite impedance burden is on the secondary side, the load impedance converted to the primary side z'_b, the converted secondary winding resistance r'_S to the primary side, the converted secondary leakage reactance x'_S to the primary side are formulated as follows [1], given the primary side equivalent impedance z_{eq}.

$$z_{eq} = \frac{(r_P + jx_P)jx_M}{r_P + j(x_P + x_M)} \tag{4.6}$$

$$z'_b = a^2 z_b \tag{4.7}$$

$$r'_S = a^2 r_S \tag{4.8}$$

$$x'_S = a^2 x_S \tag{4.9}$$

where z_b is the load impedance.

Thus, the practical transformer voltage becomes as follows, [1]

$$aV_S = \frac{z_{eq} z'_b}{(r_P + jx_P)(z_{eq} + z'_b + r'_S + jx'_S)} V_P \tag{4.10}$$

The equivalent circuit of a practical transformer takes into account of the issues, such as the finite permeability, the winding resistances, the iron core losses, and the incomplete flux linkage between the primary and the secondary winding, etc.

4.3 TZB Studies with Modified WSCC System in P-SAT

4.3.1 Power System Analysis Toolbox (PSAT)

The TZB method testing in PSAT is facilitated by the ability of numerical computing, the power of matrix manipulation of MATLAB, as well as by the flexibility of graphically system construction of SIMULINK. The power system is constructed graphically in PSAT by using the components from a specified PSAT library in the SIMULINK environment.

Apart from that, the test data can be easily collected and analysed in MATLAB after each simulation run in PSAT.

Initially written as a MATLAB toolbox, PSAT provides user friendly tools for the analysis and the control of electric power systems. Its functions called routines include Power Flow, Continuation Power Flow, Optimal Power Flow, Small Signal Stability Analysis, and Time Domain Simulation, etc. [78] The routines can be accessed and operated by means of graphical user interfaces (GUIs). All components for network design are selectable from a SIMULINK-based library. By launching the command line version, the routines of PSAT can be easily called from a user defined MATLAB program. Apart from the mathematical routines and models, PSAT also includes the following utilities: single-line network diagram editors and user defined model constructions; GUIs for system settings and routine parameters; GUIs for plotting results; filters for converting data to and from other formats; command logs, etc. [79]

Among the PSAT routines, the Power Flow is the core function which also takes care of the state variable initialization. Further static or dynamic analysis can be performed, once the Power Flow is solved. The Time Domain Simulation routine has been extensively used on the purpose of power swing analysis in the TZB study. The power system component modelings are simplified in PSAT. For instance, it is assumed that the speed variations of synchronous machines are small, thus the mechanical power is approximately equal to the mechanical torque in per unit. The transmission lines are represented by nominal π circuits in PSAT, including long transmission lines.

The parameters of the general settings for the Time Domain Simulations can be customized in the GUI main window, including the initial and final times, the convergence tolerances, the maximum number of iterations of the Newton-Raphson technique for each time step, and etc. The settings for the Time Domain routine are saved in the structure of *Settings*, which also contains the general PSAT settings and the parameters for power flow studies [79].

In the Time Domain Simulations, the output variables are named by the structure of

$Varout$. In the command line version of PSAT, the output variable can be selected by assigning a vector of indexes to $Varout.idx$. The selection is done after running the Power Flow analysis and before running the Time Domain Simulations.

Disturbances can be inserted in power networks in PSAT. In the Time Domain Simulations, three phase faults are defined in the $Fault$ structure. In the TZB study, after the power network is established in SIMULINK, the static operation conditions are determined by running the Power Flow analysis. Three phase faults are applied in order to create power swing scenarios in the given network in the PSAT Time Domain Simulations. The system outputs as well as the transient/dynamic intermediate data are collected by $Varout$, and transferred to the MATLAB workspace for further examination and calculation.

4.3.2 Modified WSCC System Setup

The proposed TZB scheme has been tested on a modified WSCC system that is constructed based on a typical WSCC 9-bus system, as shown in Figure 4.3. The modified WSCC system PSAT model is shown in Appendix B.6. An additional 250MVA generator G4 has been connected to the load Bus 8 of the original WSCC 9-bus system [2] to introduce an infeed current into distance relay apparent impedance calculations. The infeed current makes a distance relay under-reach, therefore the reach of the distance relay Zone 3 is enlarged to keep the Zone 3 coverage. The system parameters are given in Appendix B.7.

Moreover, for the distance relay R98 study, the transmission line L78 is extended to simulate the power system transient scenarios when the impedance loci enters into Zone 3. The transmission line parameters are given in Appendix B.7. The reach of Zone 3 of R98 is determined by Equation 1.8. Considering a three-phase fault happens on Bus 7, the current ratio $\frac{I_A + I_B}{I_B}$ is 5.9762. The Zone 3 reach Z_{Z3} is 0.2557 + 2.1662i in p.u. that is calculated by the following equation.

$$Z_{Z3} = Z_{l1} + 1.2 \times 5.9762 \times Z_{l2} \tag{4.11}$$

where Z_{l1} is 0.0119 + 0.1008i; Z_{l2} is 0.0340 + 0.2880i from Appendix B.7.

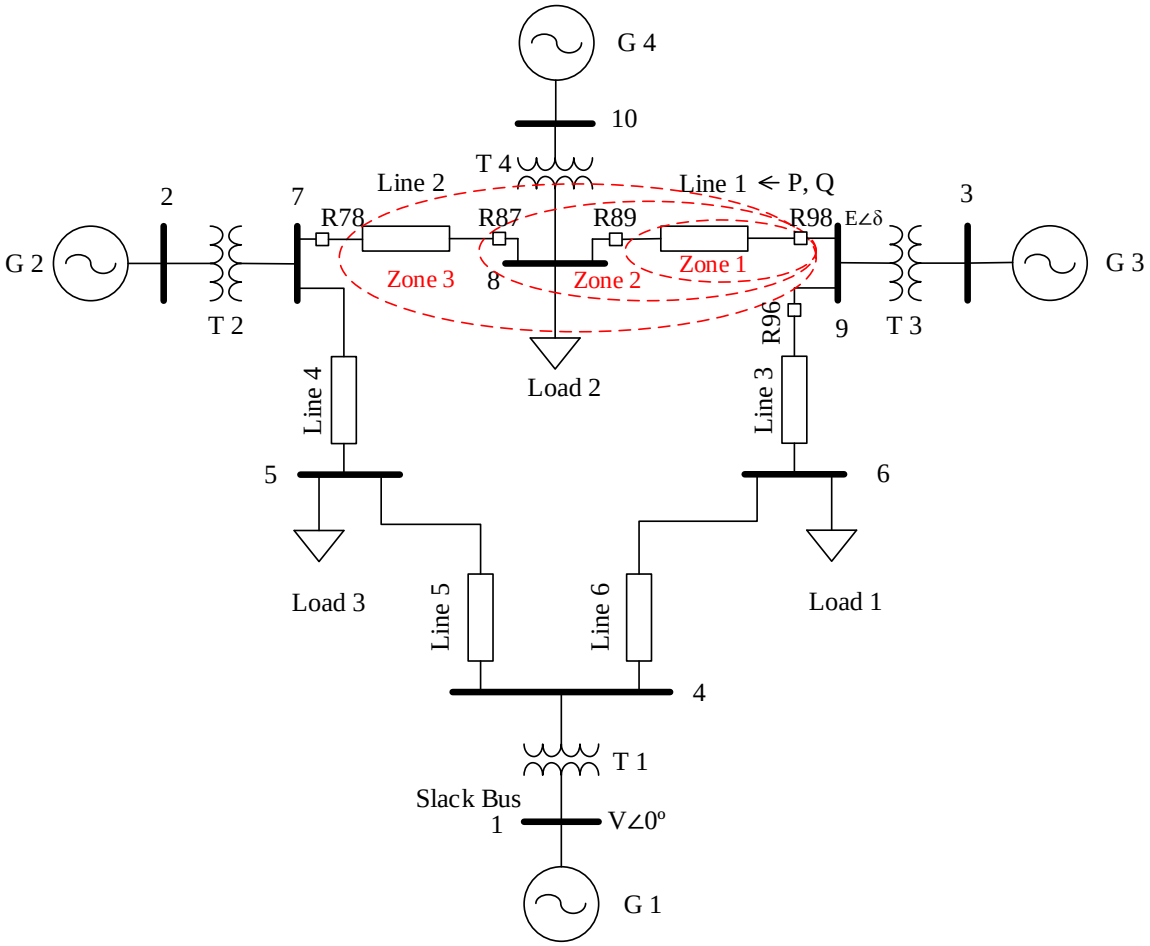

Figure 4.3: WSCC 9-bus system modified with infeed generator G4. [2]

Similarly, in the distance relay R78 study, the transmission line L98 is extended. The transmission line parameters are given in Appendix B.7. Considering a three-phase fault happens on Bus 9, the current ratio $\frac{I_A + I_B}{I_B}$ is 3.1202. The Zone 3 reach Z_{Z3} is 0.1422 + 1.2043i calculated by the following equation.

$$Z_{Z3} = Z_{l2} + 1.2 \times 3.1202 \times Z_{l1} \tag{4.12}$$

where Z_{l2} is 0.0085 + 0.0720i; Z_{l1} is 0.0357 + 0.3024i from Appendix B.7.

4.3.3 Stable Swing Studies for Distance Relay R98

In order to simulate the power swing encroaching into Zone 3 of the distance relay, three phase to ground faults are applied at different locations in the system. A numerical optimization procedure (Laguerre method) is used to solve the polynomial of Equation 3.17 and to calculate the system impedance Z of the equivalent SMIB system. The system impedance Z and the rate of change of active power $\frac{dP}{dt}$ is utilized to find the relative speed ω_r of the equivalent synchronous machine G in Figure 3.1. The apparent impedances are calculated at the relay location R98, and their loci are obtained and shown on mho relay Zone 3 characteristics.

The distance relay R98 is located at the sending end of transmission Line 1 at Bus 9. Three protection zones of R98 are shown in red dash-line ovals in Figure 4.3 in which Zone 3 here covers Line 1 plus 120% of Line 2. The Zone 3 characteristics is placed forward along the transmission line impedance with the transmission line impedance passing through its center. The transmission Line 2 distance relay R87 at Bus 8 is backed up by the relay R98.

4.3.3.1 Stable Swing Studies for Distance Relay R98 Case 1

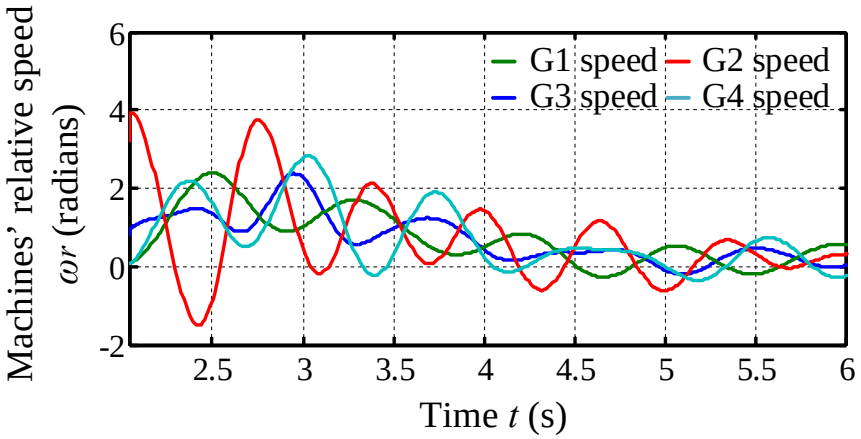

Figure 4.4: G1 to G4 synchronous machine actual relative speed for R98 study Case 1.

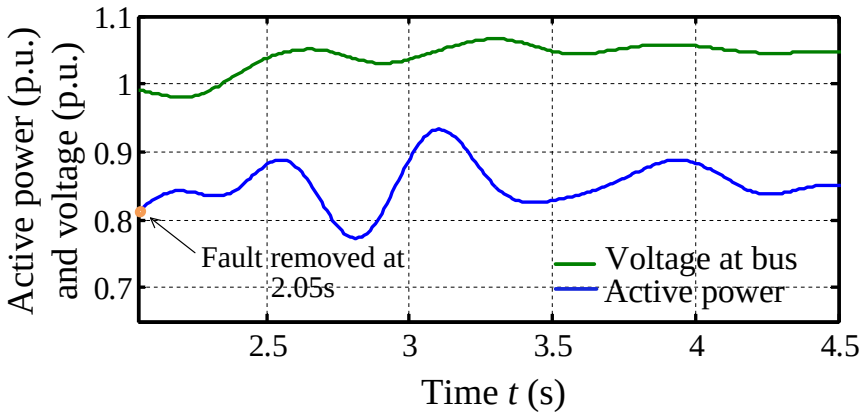

Figure 4.5: Active power and voltage magnitude measured at Bus 9 for study Case 1 on distance relay R98.

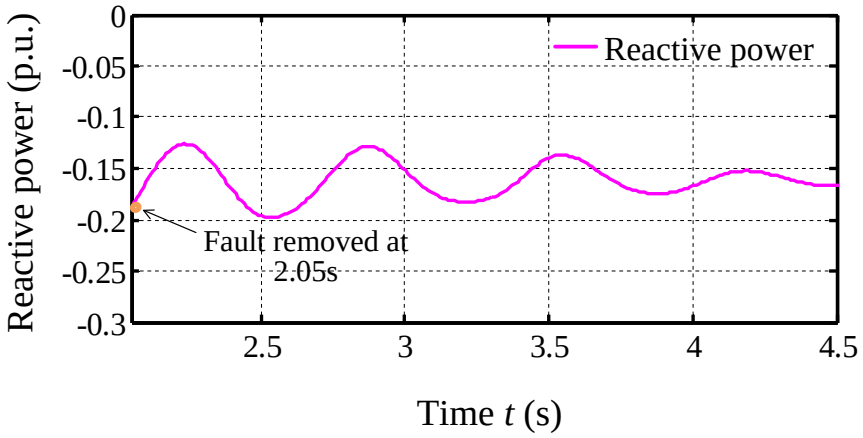

Figure 4.6: Reactive power measured at Bus 9 for study Case 1 on distance relay R98.

In the first case study (Case 1) of R98, the three phase fault is applied at 2.00 s at Bus 7 and removed at 2.05 s. Figure 4.4 shows the measured actual synchronous machine relative speeds of G1 to G4. It oscillates after the fault removal and approaches to steady-state value of 0 radians. The active power P from Bus 3 to Bus 9 and the voltage E_B is measured by R98 at Bus 9 as shown in Figure 4.5. Both P and E_B decreases sharply away from steady state value at the fault instant. The reactive power Q from Bus 3 to Bus 9 is measured at Bus 9 as shown in Figure 4.6. In contrast to P and E_B, Q increases sharply at the fault

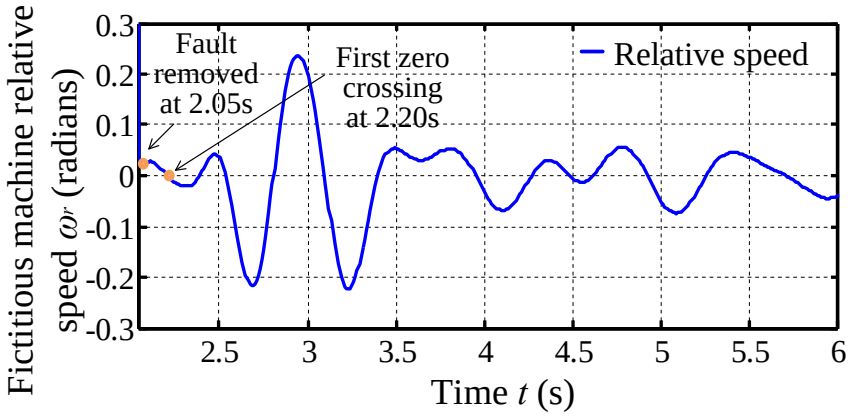

Figure 4.7: Fictitious synchronous machine relative speed for study Case 1 on distance relay R98.

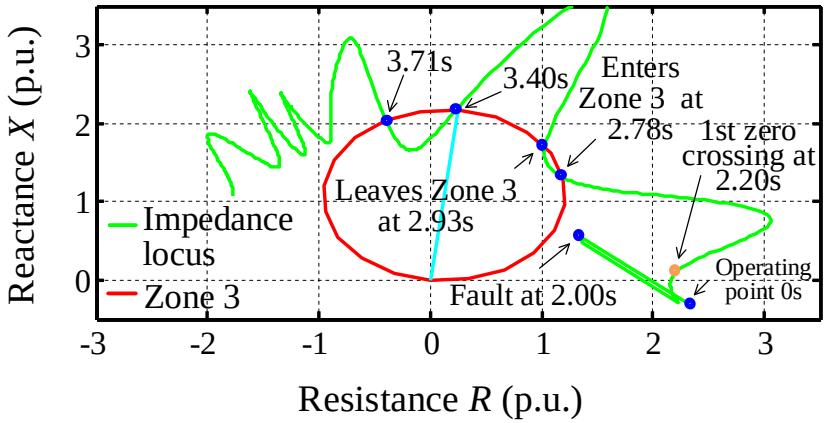

Figure 4.8: Impedance locus measured at distance mho relay R98 on Zone 3 characteristics for study Case 1.

instant. After the disturbance is cleared, P, E_B and Q start oscillating and approaches to an equilibrium.

The 0.05 s fault duration is less than the time delay setting for Zone 3, i.e. 1.5 s (90 cycles). For this case study, the primary protection is Zone 2 of the distance relay R87. The TZB calculated fictitious synchronous machine relative speed ω_r is shown in Figure 4.7 for

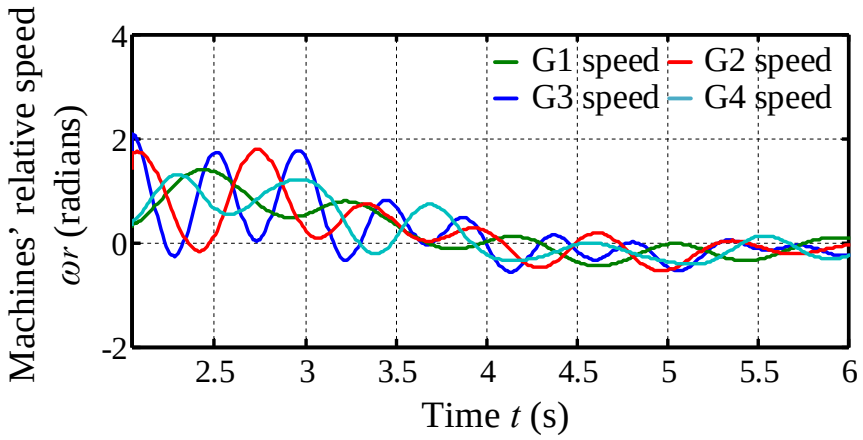

Figure 4.9: G1 to G4 synchronous machine actual relative speed for R98 study Case 2.

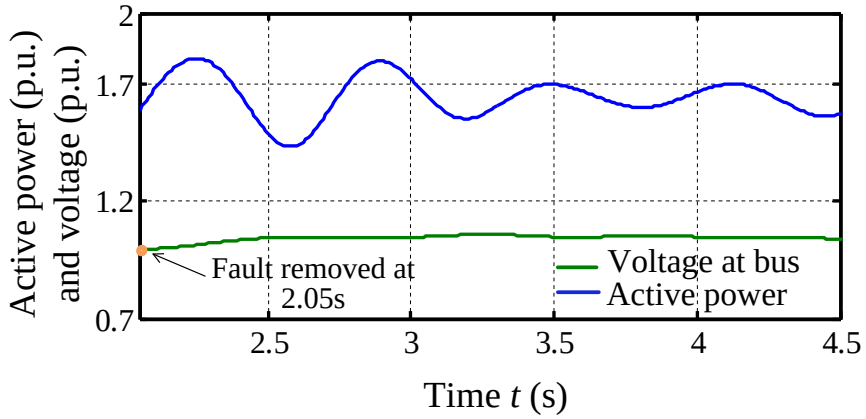

Figure 4.10: Active power and voltage magnitude measured at Bus 9 for study Case 2 on distance relay R98.

the study Case 1 of R98. It can be seen from Figure 4.7 that the fictitious machine speed ω reaches the synchronous value at 2.20 s (the relative speed is zero), i.e. 0.15 s after the fault is removed. The trace of the impedance locus change is shown in Figure 4.8. The first time the locus enters Zone 3 is at 2.78 s, i.e. 35 cycles after FZC. So there is adequate room for blocking the third zone of R98 after the stable power swing is detected.

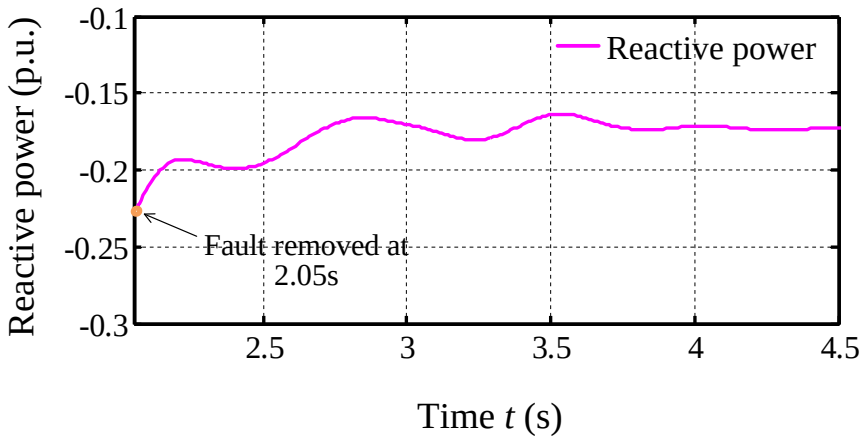

Figure 4.11: Reactive power measured at Bus 9 for study Case 2 on distance relay R98.

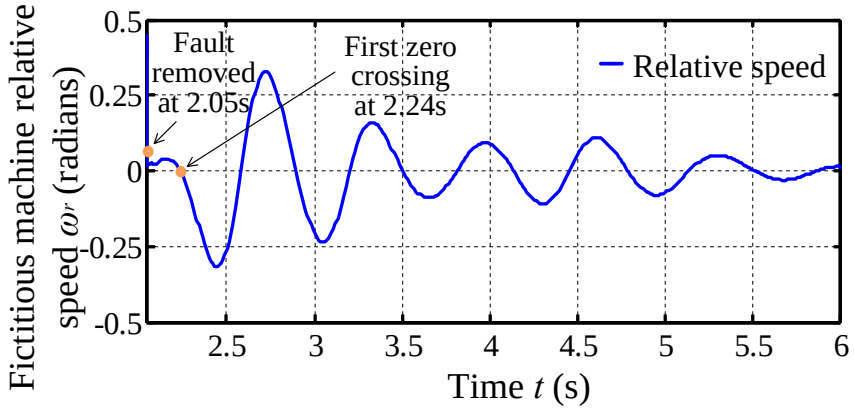

Figure 4.12: Fictitious synchronous machine relative speed for study Case 2 on distance relay R98.

4.3.3.2 Stable Swing Studies for Distance Relay R98 Case 2

For the relay R98 Case 2 study, the fault is applied at Bus 6, which is outside the reach of Zone 3 of the relay, as shown at 2.0 s on the mho relay characteristics in Figure 4.13. Figure 4.9 shows the measured actual synchronous machine relative speeds of G1 to G4, which are oscillating after the fault removal and approaching to an equilibrium gradually with time increment. The active power P from Bus 3 to Bus 9 and the voltage E_B is measured by R98

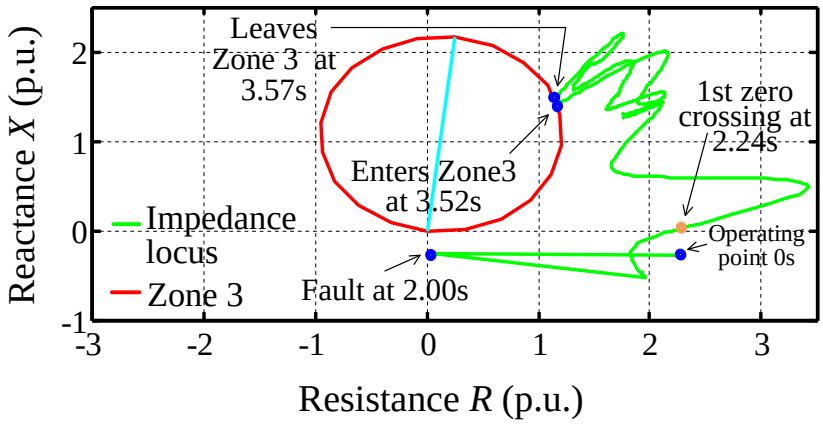

Figure 4.13: Impedance locus measured at distance mho relay R98 on Zone 3 characteristics for study Case 2.

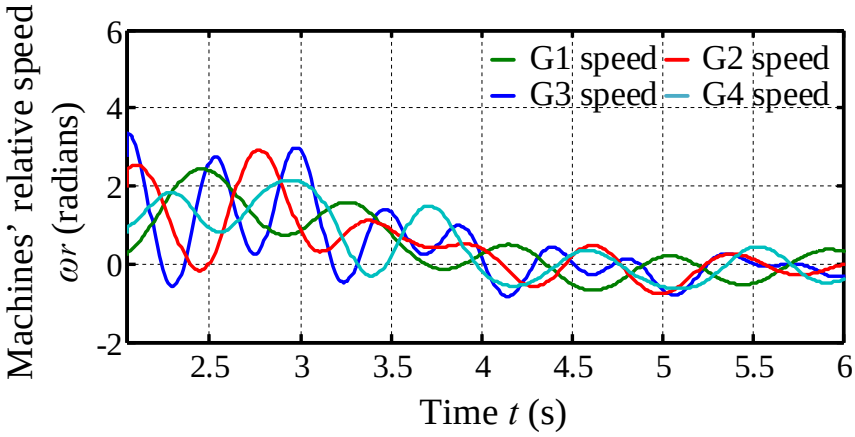

Figure 4.14: G1 to G4 synchronous machine actual relative speed for R98 study Case 3.

at Bus 9 as shown in Figure 4.10. The reactive power Q from Bus 3 to Bus 9 is measured at Bus 9 as shown in Figure 4.11. The primary protection, Zone 2 of the distance relay R96, is assumed to fail to respond to the fault. Figure 4.12 shows the plot of the relative speed of the equivalent machine, which approaches to an equilibrium with time after the fault removal. Figure 4.13 gives the plot of the impedance locus. The first zero crossing of the relative speed is obtained at 2.24 s, whereas the instant at which the impedance locus enters Zone 3

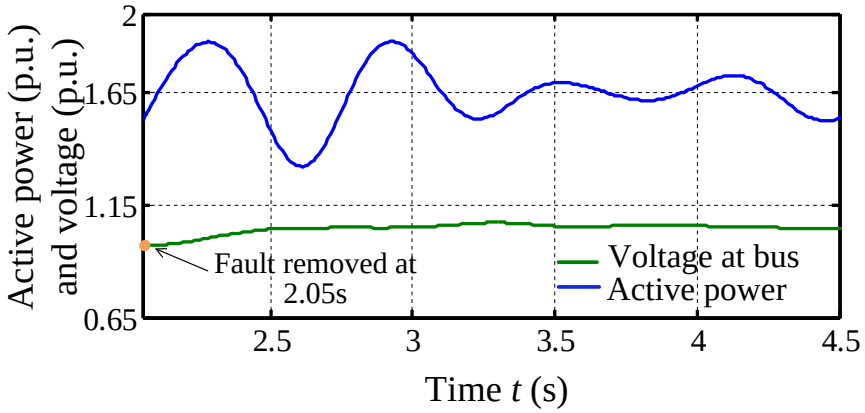

Figure 4.15: Active power and voltage magnitude measured at Bus 9 for study Case 3 on distance relay R98.

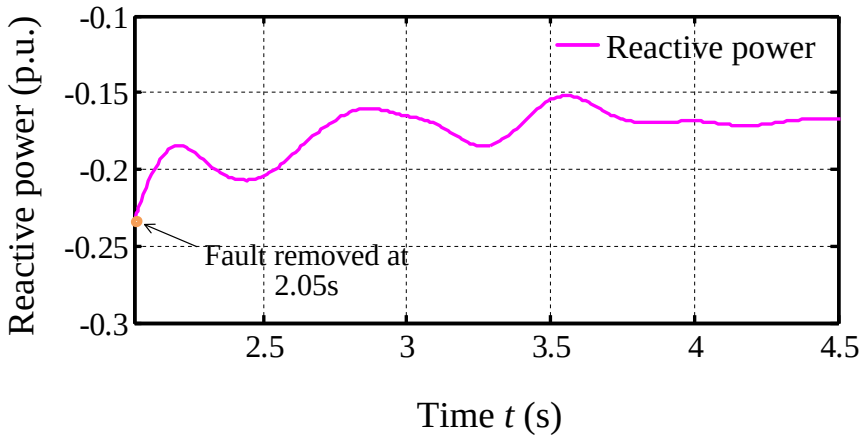

Figure 4.16: Reactive power measured at Bus 9 for study Case 3 on distance relay R98.

is at 3.52 s, i.e. 77 cycles after FZC, on the impedance characteristics in Figure 4.13. Thus it gives sufficient time to block the third zone of the relay R98.

4.3.3.3 Stable Swing Studies for Distance Relay R98 Case 3 to Case 6

Similar studies have been done for the relay R98 when the faults are applied at other locations in the system, i.e. at the location of Bus 5 with 0.05 s fault duration and at

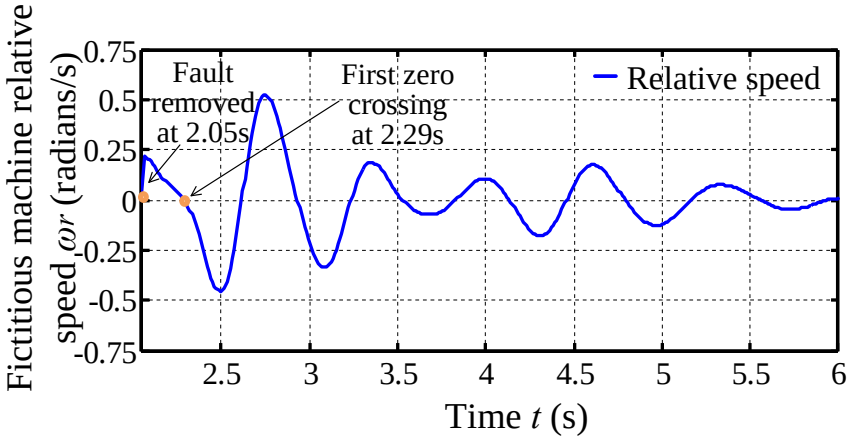

Figure 4.17: Fictitious synchronous machine relative speed for study Case 3 on distance relay R98.

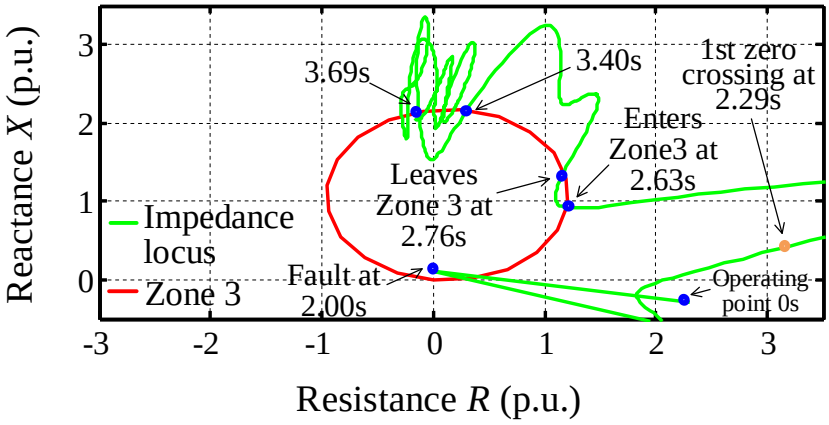

Figure 4.18: Impedance locus measured at distance mho relay R98 on Zone 3 characteristics for study Case 3.

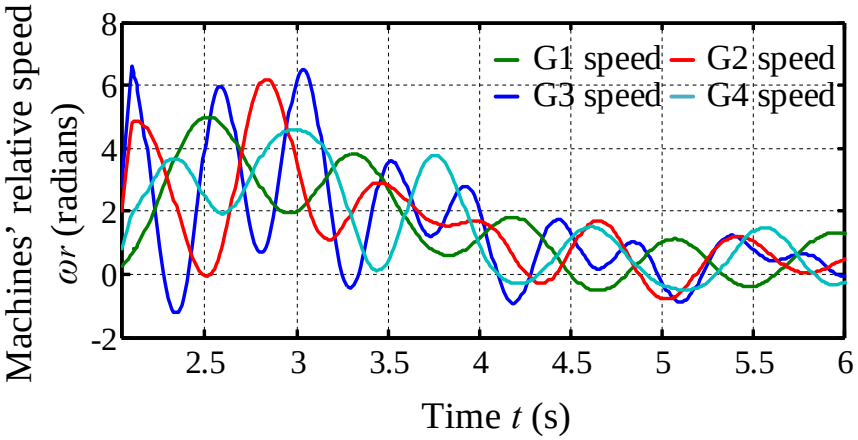

Figure 4.19: G1 to G4 synchronous machine actual relative speed for R98 study Case 4.

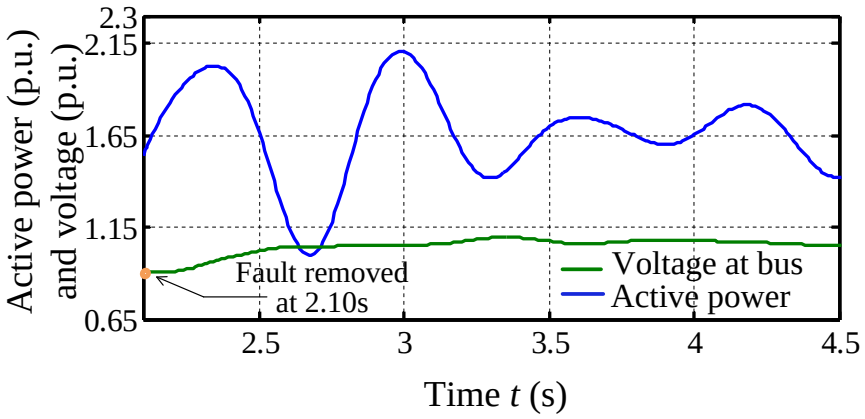

Figure 4.20: Active power and voltage magnitude measured at Bus 9 for study Case 4 on distance relay R98.

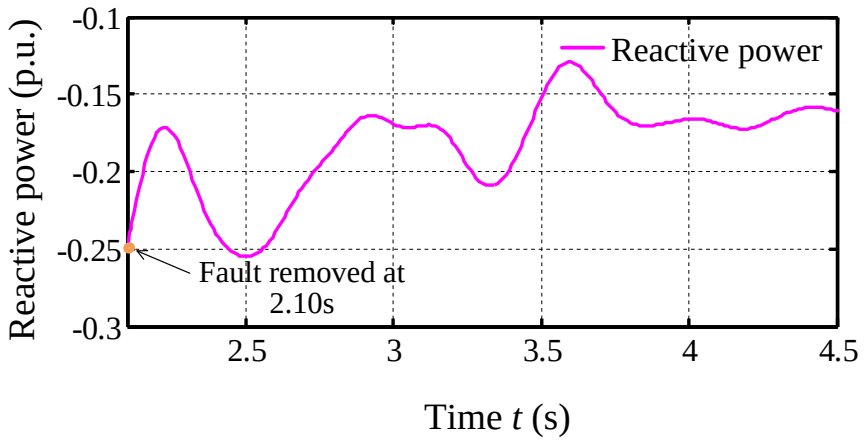

Figure 4.21: Reactive power measured at Bus 9 for study Case 4 on distance relay R98.

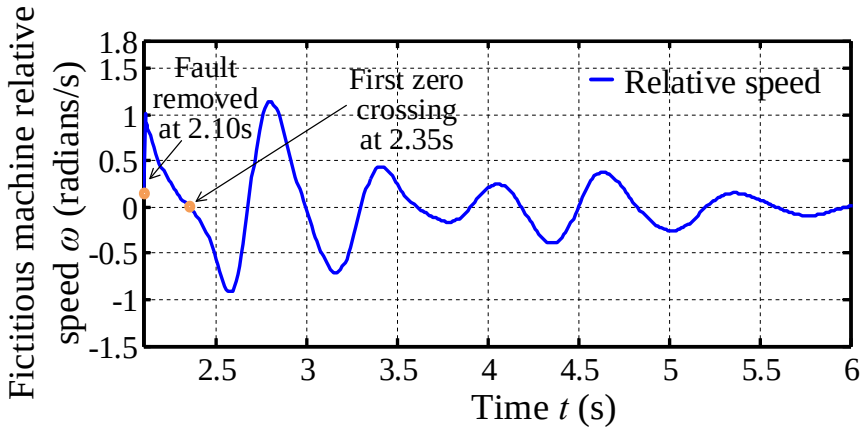

Figure 4.22: Fictitious synchronous machine relative speed for study Case 4 on distance relay R98.

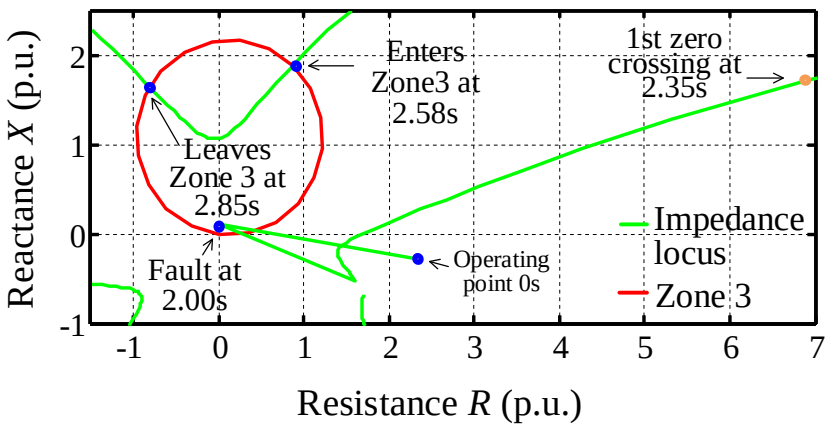

Figure 4.23: Impedance locus measured at distance mho relay R98 on Zone 3 characteristics for study Case 4.

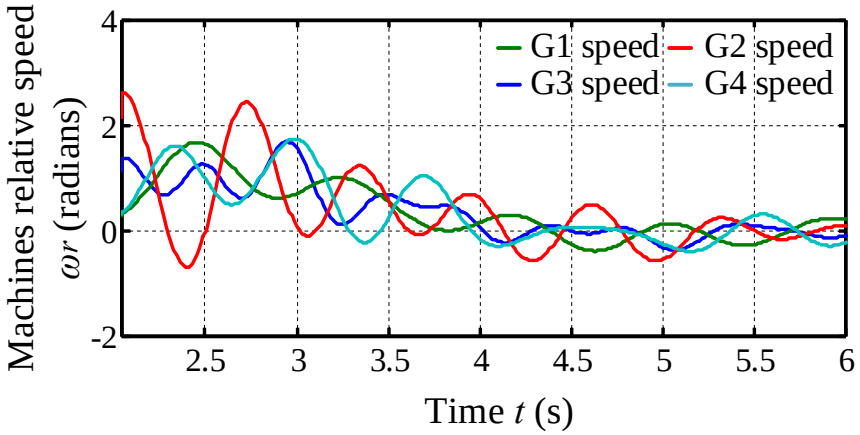

Figure 4.24: G1 to G4 synchronous machine actual relative speed for R98 study Case 5.

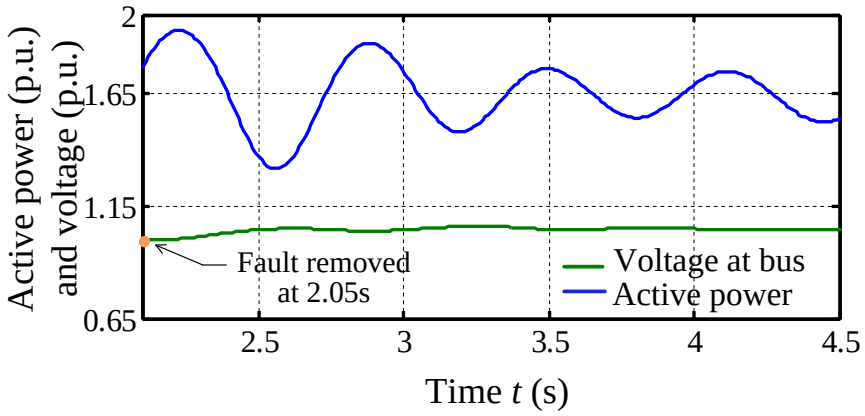

Figure 4.25: Active power and voltage magnitude measured at Bus 9 for study Case 5 on distance relay R98.

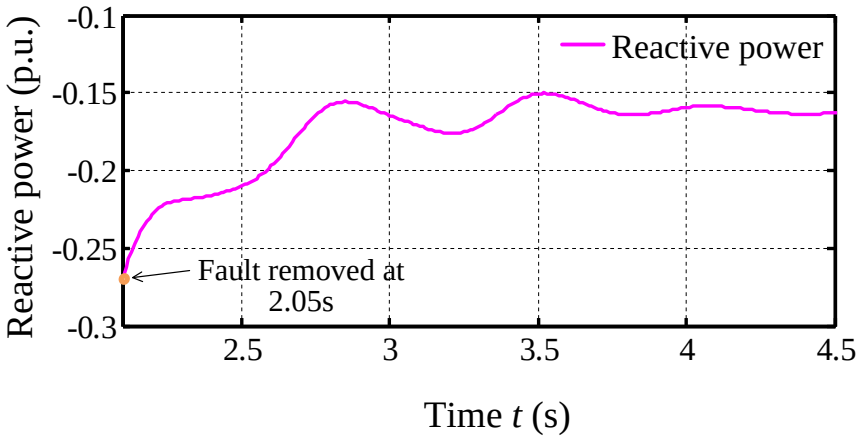

Figure 4.26: Reactive power measured at Bus 9 for study Case 5 on distance relay R98.

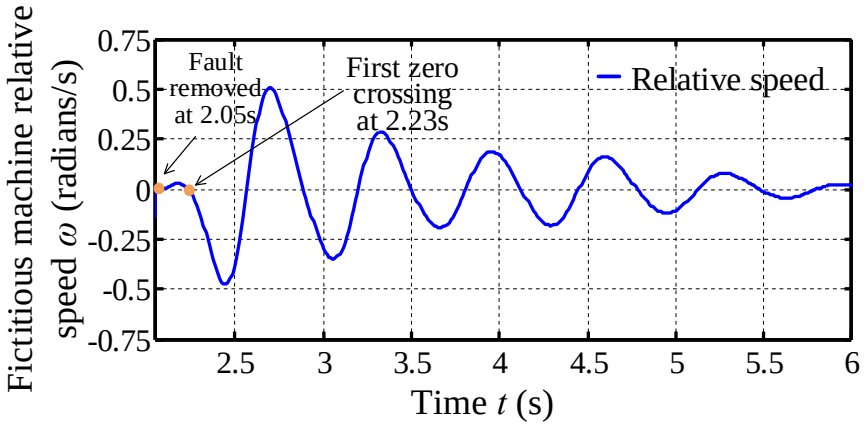

Figure 4.27: Fictitious synchronous machine relative speed for study Case 5 on distance relay R98.

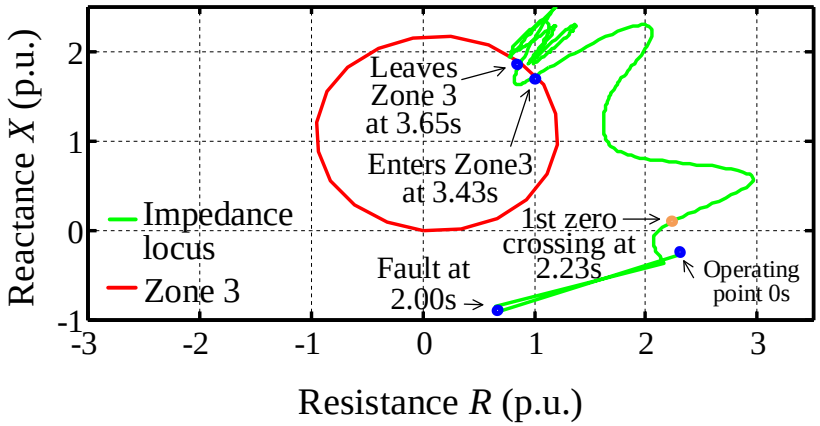

Figure 4.28: Impedance locus measured at distance mho relay R98 on Zone 3 characteristics for study Case 5.

the location of Bus 8 with 0.05 s, 0.10 s and 0.15 s fault durations, for four more cases. Figure 4.14, Figure 4.19, Figure 4.24 and Figure 4.29 show the measured actual synchronous machine relative speeds of G1 to G4 in Case 3 to Case 6. The active powers P from Bus 3 to Bus 9 and the voltages E_B are measured by R98 at Bus 9 as shown in Figure 4.15, Figure 4.20, Figure 4.25, Figure 4.30 in Case 3 to Case 6. The reactive powers Q from Bus 3 to Bus 9 are measured at Bus 9 as shown in Figure 4.16, Figure 4.21, Figure 4.26, Figure 4.31.

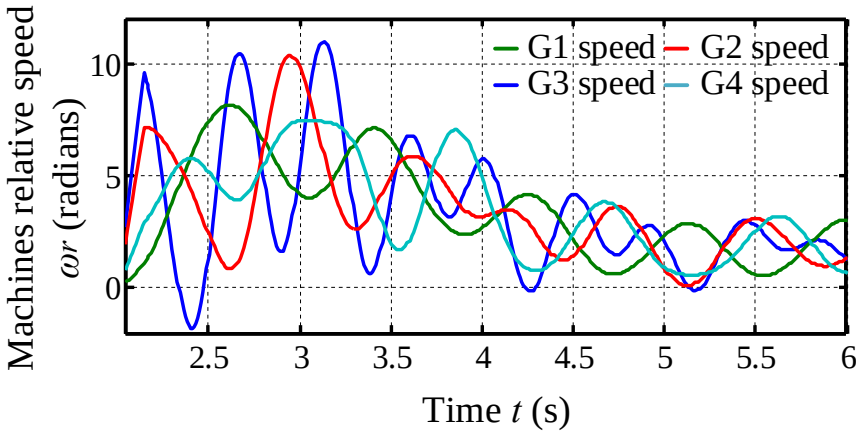

Figure 4.29: G1 to G4 synchronous machine actual relative speed for R98 study Case 6.

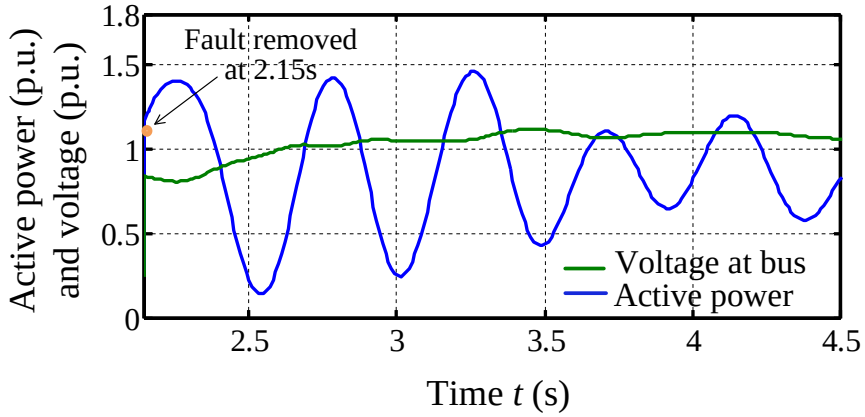

Figure 4.30: Active power and voltage magnitude measured at Bus 9 for study Case 6 on distance relay R98.

The test results for Case 3 to Case 6 are shown in Figure 4.17, Figure 4.22, Figure 4.27 and Figure 4.32 for the TZB calculated fictitious synchronous machine relative speeds ω_r, and shown in Figure 4.18, Figure 4.23, Figure 4.28, and Figure 4.33 for the impedance loci measured at the distance mho relay R98 on Zone characteristics planes. The same promising results have been obtained in these study cases as well.

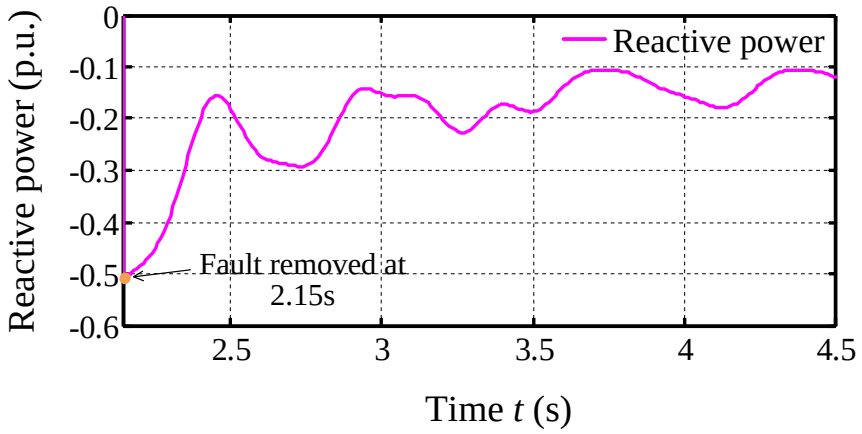

Figure 4.31: Reactive power measured at Bus 9 for study Case 6 on distance relay R98.

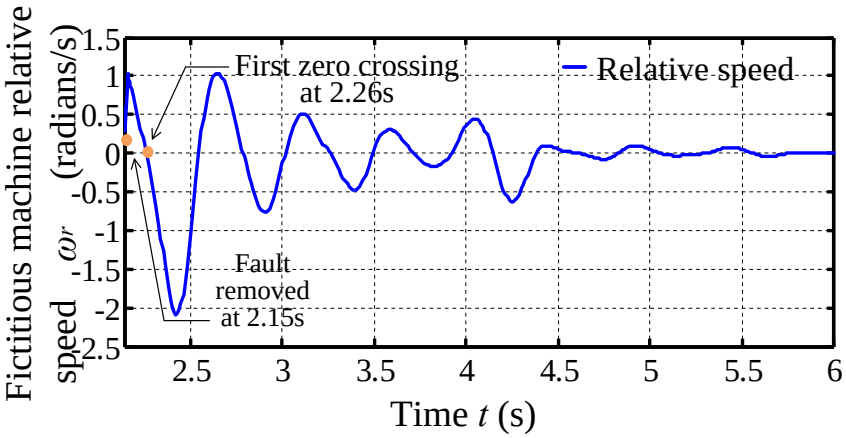

Figure 4.32: Fictitious synchronous machine relative speed for study Case 6 on distance relay R98.

Similar to Cases 1 and 2, the results here show that FZC can be detected much before the time at which the impedance locus enters Zone 3. So for all cases there is sufficient time for safely blocking Zone 3 for the relay R98, no matter whether the fault is within Zone 3 of the relay or not.

The proposed TZB scheme is also tested for different fault durations for the purpose of examining the TZB method for contingencies of different severity levels, i.e. when fault applied at Bus 8 is 0.05 s, 0.10 s and 0.15 s, respectively. The results are shown in Cases 3, 5 and 6. From the results, it can be seen that the TZB method works correctly in all cases.

The results are summarized in Table 4.1.

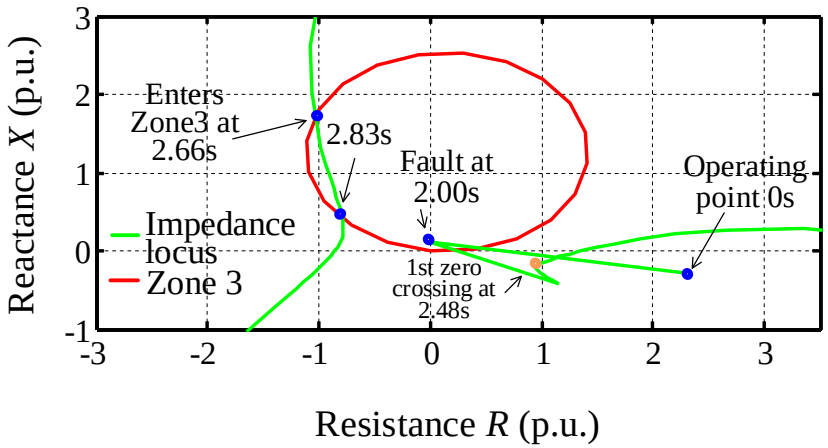

Figure 4.33: Impedance locus measured at distance mho relay R98 on Zone 3 characteristics for study Case 6.

4.3.4 Stable Swing Studies for Distance Relay R78

4.3.4.1 Stable Swing Studies for Distance Relay R78 Case 1

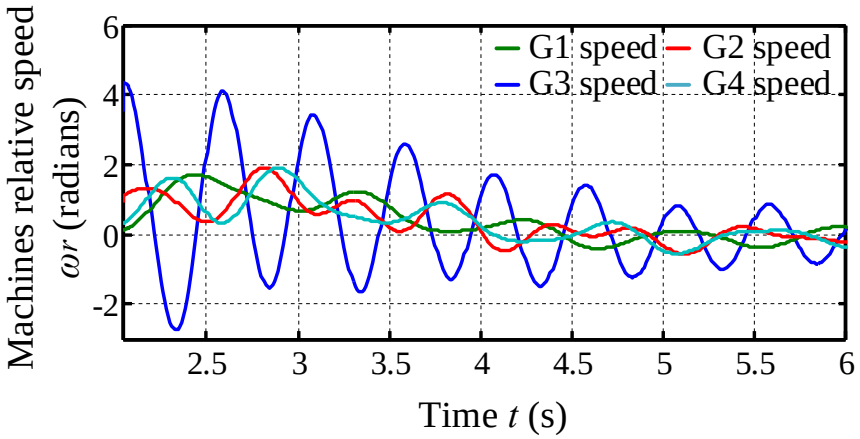

Figure 4.34: G1 to G4 synchronous machine actual relative speed for R78 study Case 1.

The distance relay R78 is selected for additional TZB method testings, which is located on the end of transmission Line 2 at Bus 7. The protection zones of R78 are not drawn in Figure 4.3 for clarity. Its protection Zone 3 covers the full length of Line 2 plus 120% of Line 1. The distance relay R89 on the end of Line 1 at Bus 8 is backed up by R78.

For the R78 Case 1 study, the fault is applied at Bus 9 at 2.00 s and removed at 2.05 s. The relay R89 is assumed not to operate for this case study. Figure 4.34 shows the measured actual synchronous machine relative speeds of G1 to G4, which oscillate after the

Table 4.1: Summary of stable power swing studies on distance relay R98 in Modified WSCC system.

Case No.	1	2	3	4	5	6
Fault Location Bus No.	7	6	8	8	5	8
Fault in Protection Zones (Y/N)	N	N	Y	Y	N	Y
Fault Duration (cycle)	3	3	3	6	3	9
Fault Duration (s)	0.05	0.05	0.05	0.10	0.05	0.15
FZC After Fault Removal (s)	0.15	0.19	0.24	0.25	0.18	0.11
First Zone 3 Entering (s)	0.73	1.47	0.58	0.48	1.38	0.51
Relay Reaction Time After FZC (cycle)	35	77	20	14	72	24
Zone 3 Blocking decision (Y/N)	Y	Y	Y	Y	Y	Y

fault removal and approach to an equilibrium value with time. The active power P from Bus 2 to Bus 7 and the voltage E_B is measured by R78 at Bus 7 as shown in Figure 4.35. The reactive power Q from Bus 2 to Bus 7 is measured at Bus 7 as shown in Figure 4.36.

The relative speed of the equivalent machine reaches a zero value at 2.23 s that can be seen in Figure 4.37, i.e. 0.18 s after the fault is removed. The plot of the impedance locus is shown in Figure 4.38. The impedance locus enters Zone 3 at 3.42 s, i.e. 71 cycles after FZC.

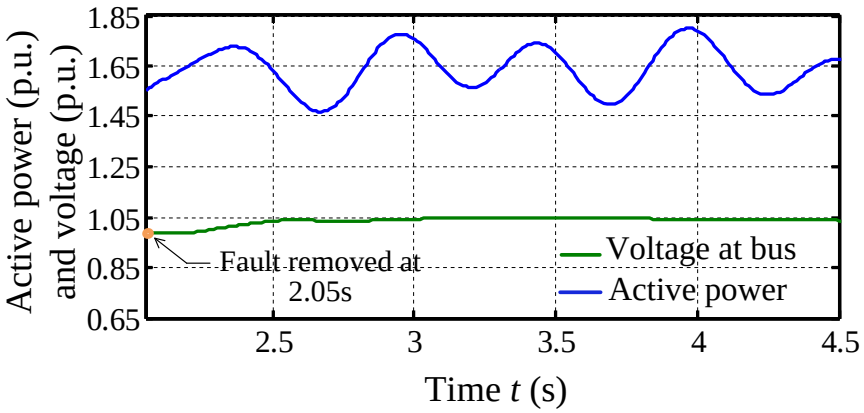

Figure 4.35: Active power and voltage magnitude measured at Bus 9 for study Case 1 on distance relay R78.

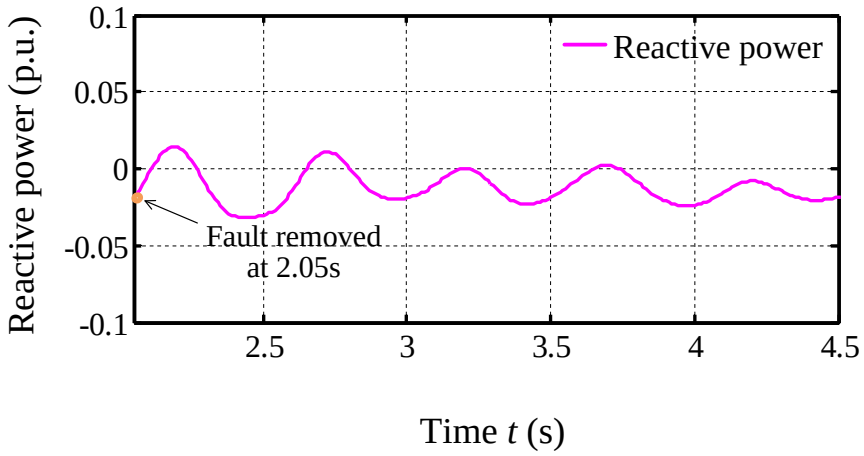

Figure 4.36: Reactive power measured at Bus 9 for study Case 1 on distance relay R78.

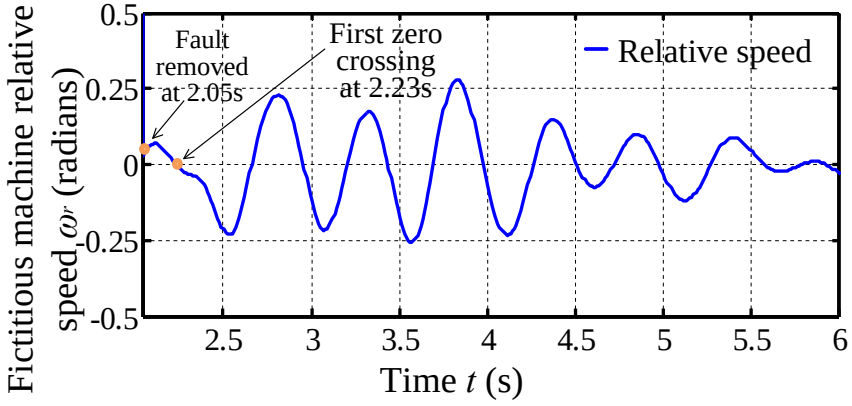

Figure 4.37: Fictitious synchronous machine relative speed for study Case 1 on distance relay R78.

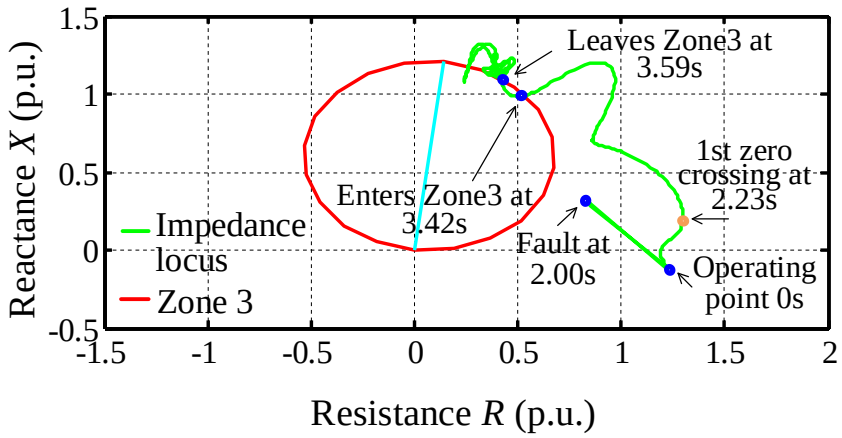

Figure 4.38: Impedance locus measured at distance mho relay R78 on Zone 3 characteristics for study Case 1.

So in this case it can be seen again that there is sufficient time for blocking Zone 3 during a stable power swing.

4.3.4.2 Stable Swing Studies for Distance Relay R78 Case 2 to Case 5

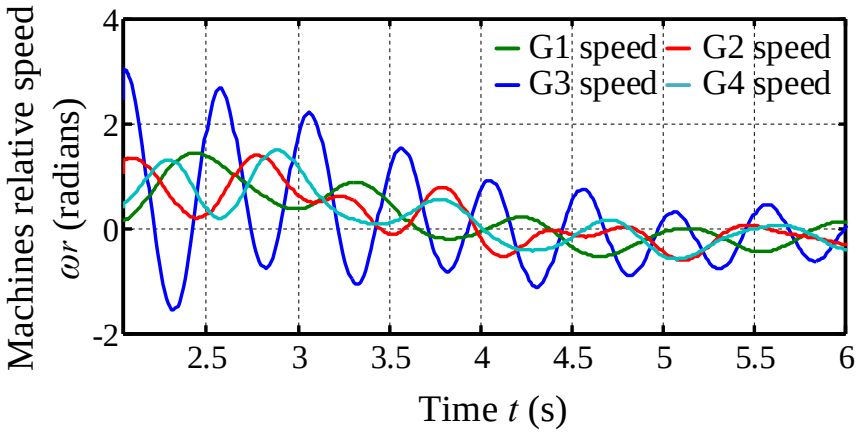

Figure 4.39: G1 to G4 synchronous machine actual relative speed for R78 study Case 2.

Additional four case studies are reported for R78 with the faults applied at different locations in the system at Buses 5, 6 and 8. Figure 4.39, Figure 4.44, Figure 4.49 and Figure 4.54 show the measured actual synchronous machine relative speeds of G1 to G4 in Case 2 to Case 5. The active powers P from Bus 2 to Bus 7 and the voltages E_B are measured by R78 at Bus 7 as shown in Figure 4.40, Figure 4.45, Figure 4.50, Figure 4.55 in Case 2 to Case 5. The reactive powers Q from Bus 2 to Bus 7 are measured at Bus 7 as shown in

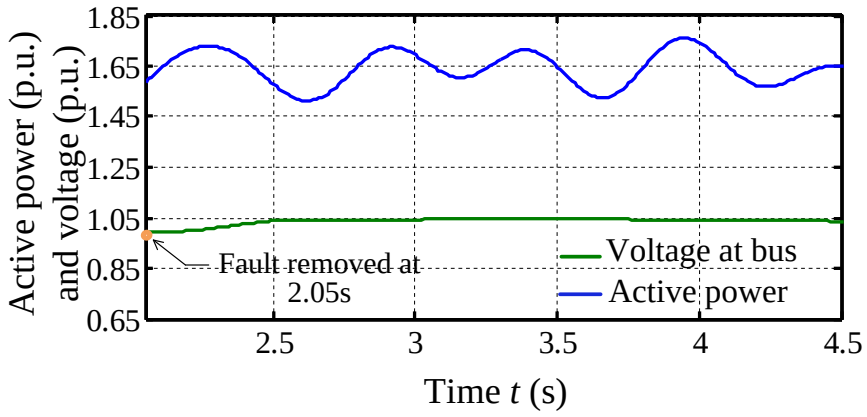

Figure 4.40: Active power and voltage magnitude measured at Bus 9 for study Case 2 on distance relay R78.

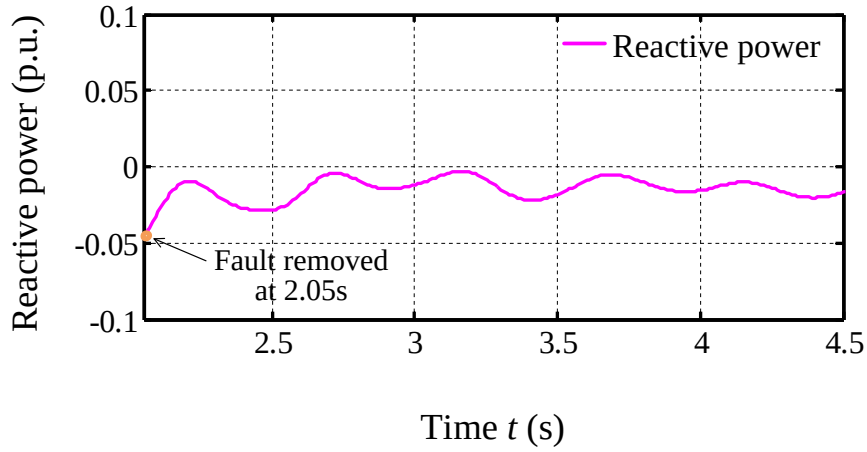

Figure 4.41: Reactive power measured at Bus 9 for study Case 2 on distance relay R78.

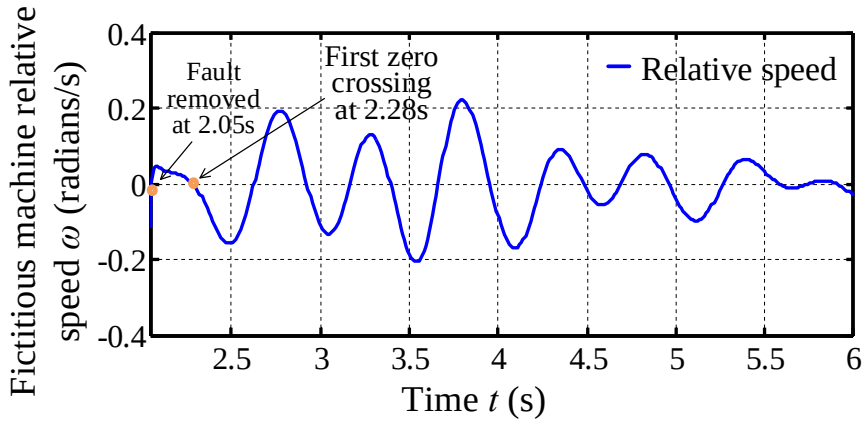

Figure 4.42: Fictitious synchronous machine relative speed for study Case 2 on distance relay R78.

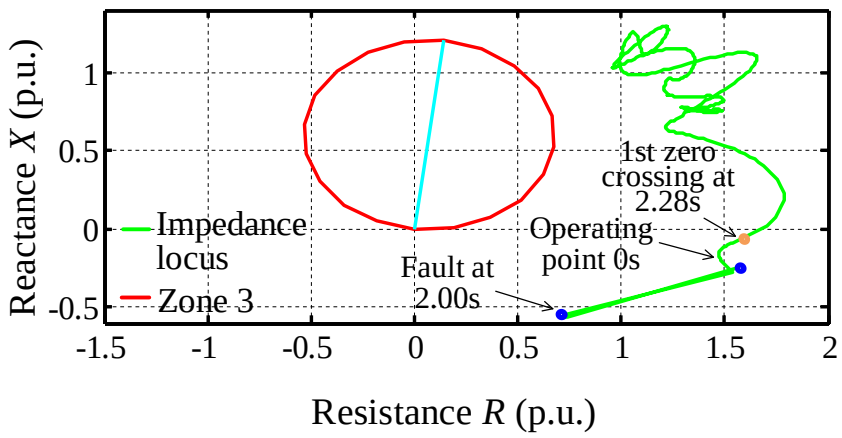

Figure 4.43: Impedance locus measured at distance mho relay R78 on Zone 3 characteristics for study Case 2.

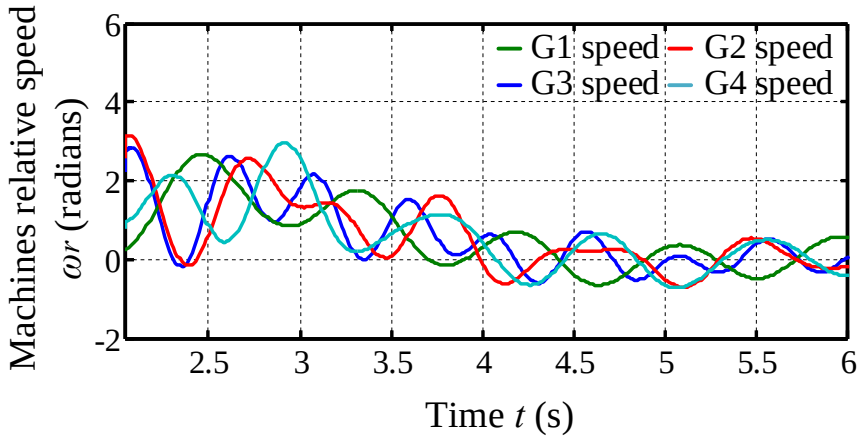

Figure 4.44: G1 to G4 synchronous machine actual relative speed for R78 study Case 3.

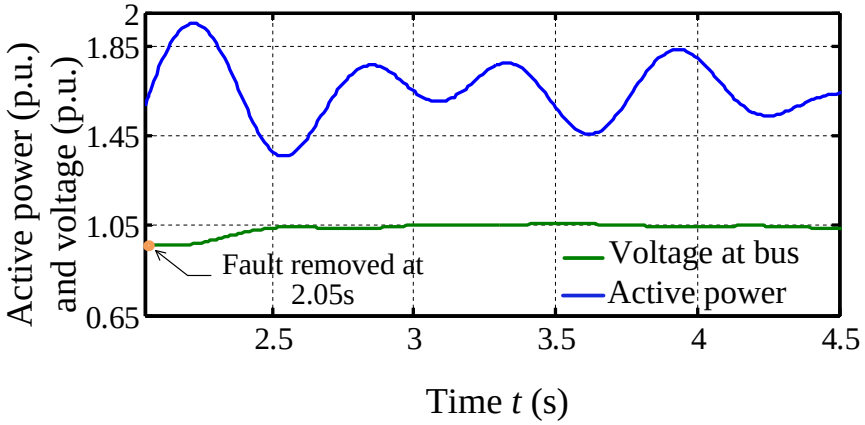

Figure 4.45: Active power and voltage magnitude measured at Bus 9 for study Case 3 on distance relay R78.

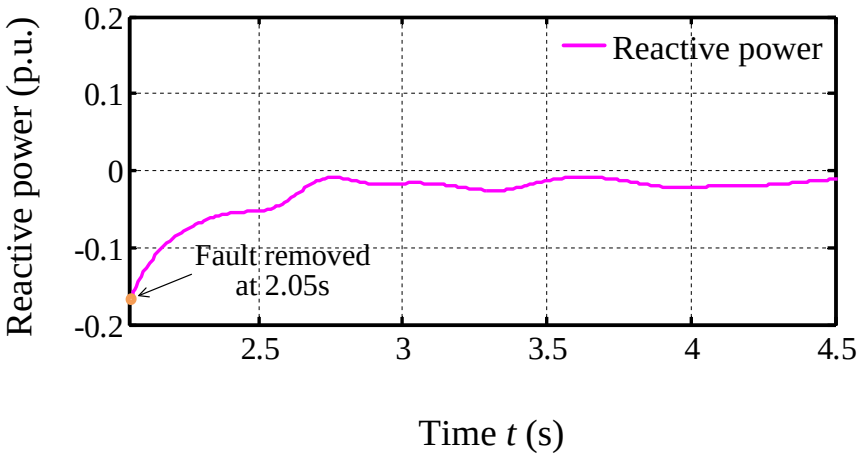

Figure 4.46: Reactive power measured at Bus 9 for study Case 3 on distance relay R78.

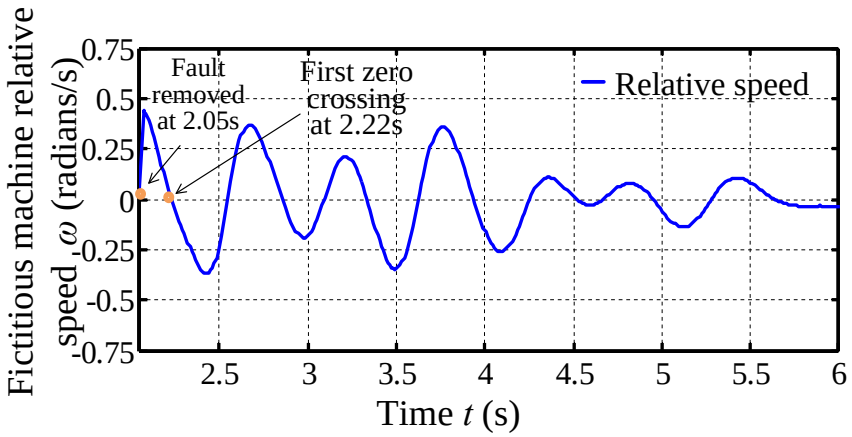

Figure 4.47: Fictitious machine relative speed for study Case 3 on distance relay R78.

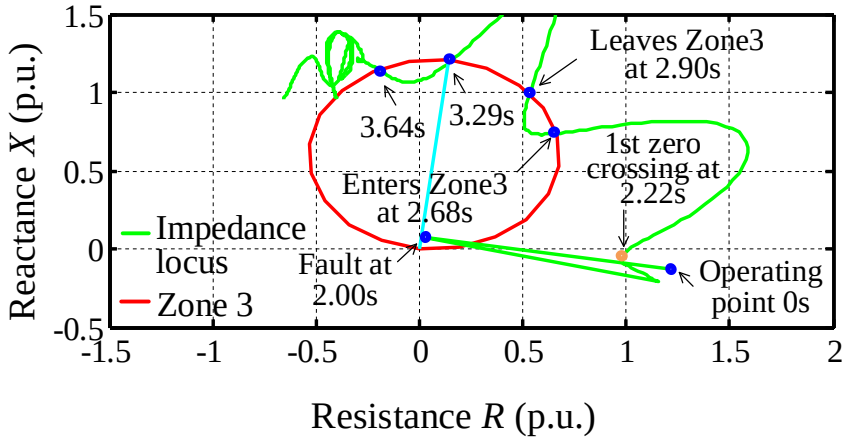

Figure 4.48: Impedance locus measured at distance mho relay R78 on Zone 3 characteristics for study Case 3.

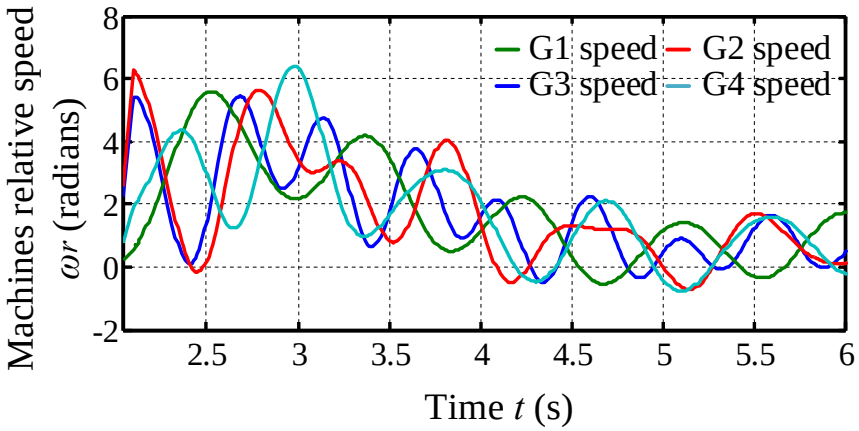

Figure 4.49: G1 to G4 synchronous machine actual relative speed for R78 study Case 4.

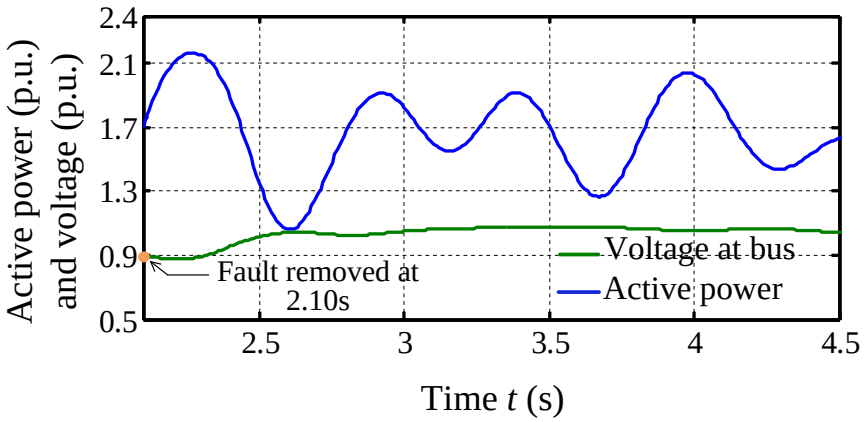

Figure 4.50: Active power and voltage magnitude measured at Bus 9 for study Case 4 on distance relay R78.

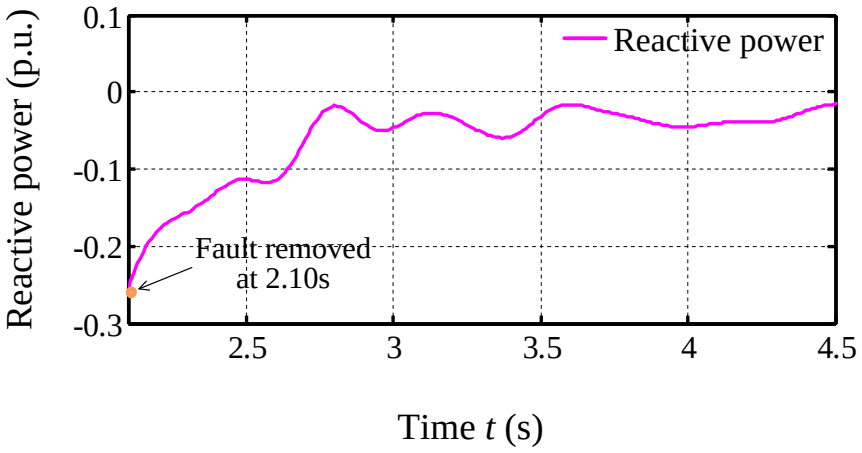

Figure 4.51: Reactive power measured at Bus 9 for study Case 4 on distance relay R78.

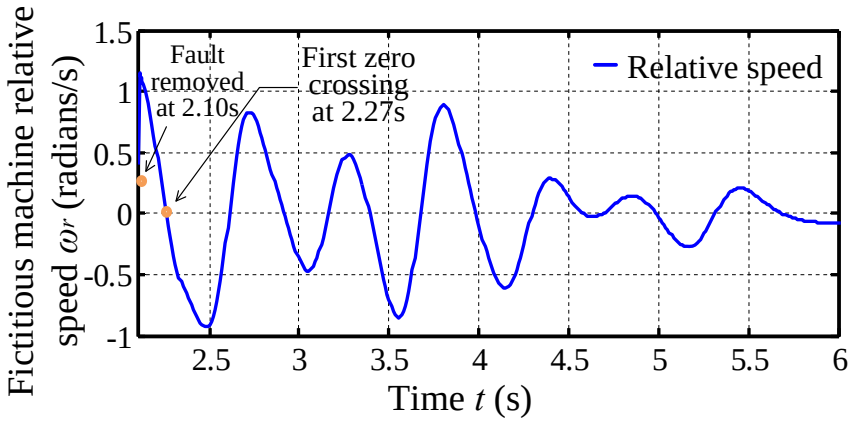

Figure 4.52: Fictitious synchronous machine relative speed for study Case 4 on distance relay R78.

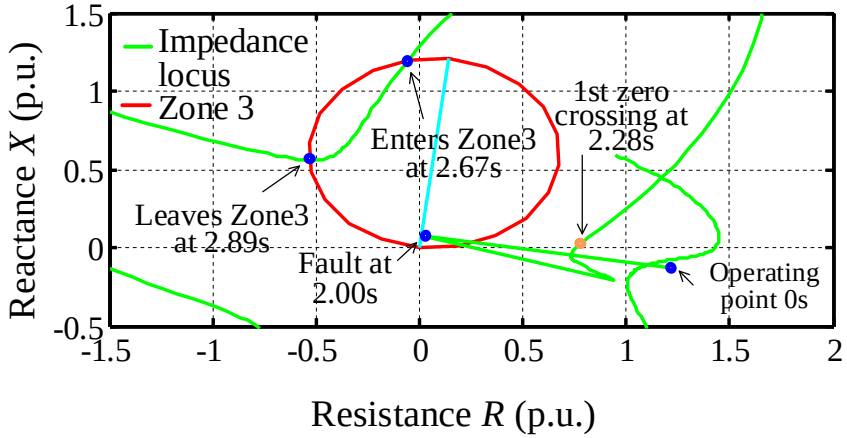

Figure 4.53: Impedance locus measured at distance mho relay R78 on Zone 3 characteristics for study Case 4.

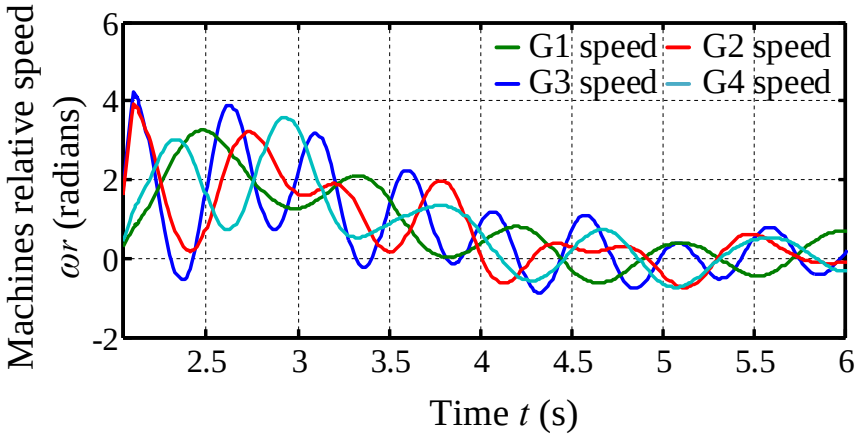

Figure 4.54: G1 to G4 synchronous machine actual relative speed for R78 study Case 5.

Figure 4.41, Figure 4.46, Figure 4.51, Figure 4.56.

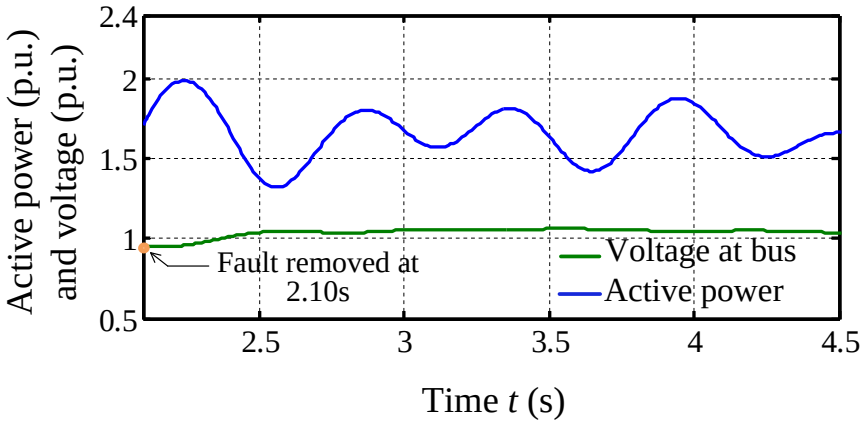

Figure 4.55: Active power and voltage magnitude measured at Bus 9 for study Case 5 on distance relay R78.

The test results from Case 2 to Case 5 are shown in Figure 4.42, Figure 4.47, Figure 4.52 and Figure 4.57 for the TZB calculated fictitious synchronous machine relative speeds ω_r, and shown in Figure 4.43, Figure 4.48, Figure 4.53, and Figure 4.58 for the impedance loci measured at the distance mho relay R78 on the Zone characteristics planes. The results similar to the study Case 1 have been obtained in these study cases as well.

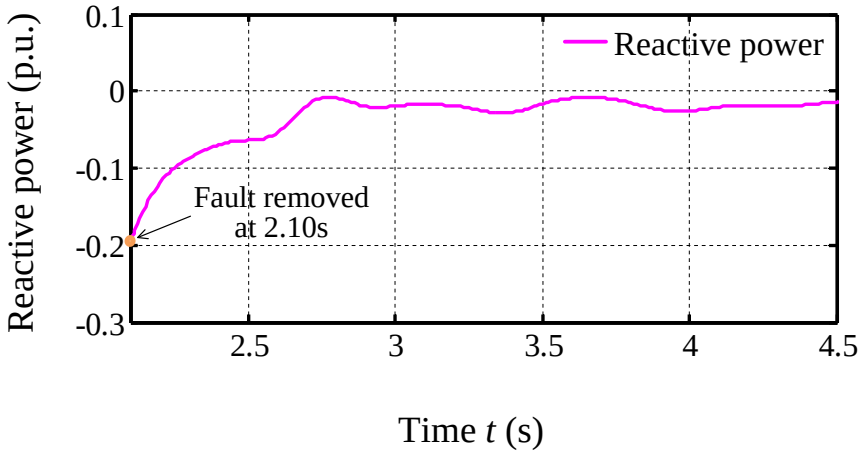

Figure 4.56: Reactive power measured at Bus 9 for study Case 5 on distance relay R78.

The effectiveness of the TZB scheme for different three phase fault durations are also examined, i.e. the fault durations of 0.05s and 0.10s respectively at Bus 8. The results show that FZC can be detected much before the impedance locus enters Zone 3. The study case

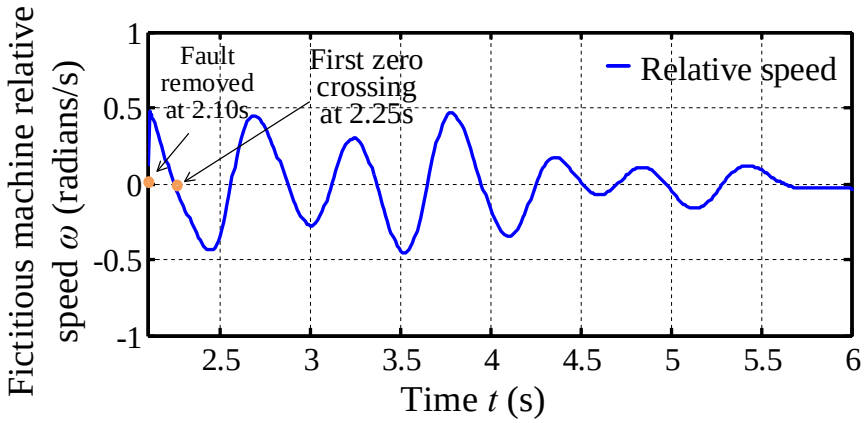

Figure 4.57: Fictitious synchronous machine relative speed for study Case 5 on distance relay R78.

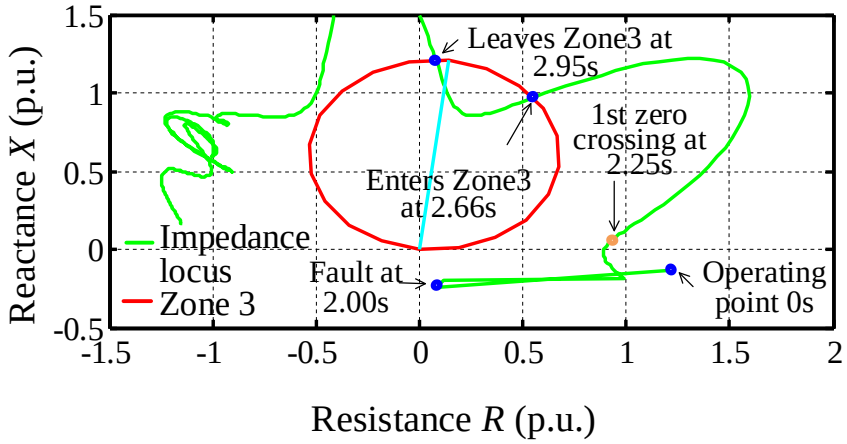

Figure 4.58: Impedance locus measured at distance mho relay R78 on Zone 3 characteristics for study Case 5.

results are summarized in Table 4.2 and the additional cases are numbered from Case 2 to Case 5.

4.3.5 Discussion of the Results

In all simulation cases, the first zero crossing is obtained much earlier (less than 0.33 s) than the impedance trajectory enters in Zone 3, so Zone 3 could be blocked. If a fault happens during a power swing that is a three-phase balanced phenomenon, then it is important to unblock Zone 3. In a practical application of distance relaying, additional logics would have to be included to handle these scenarios. Majority of the faults happening in power system are

Table 4.2: Summary of stable power swing studies on distance relay R78 in Modified WSCC system.

Case No.	1	2	3	4	5
Fault Location Bus No.	9	6	8	8	5
Fault in Protection Zones (Y/N)	N	N	Y	Y	N
Fault Duration (cycle)	3	3	3	6	6
Fault Duration (s)	0.05	0.05	0.05	0.10	0.10
FZC After Fault Removal (s)	0.18	0.23	0.17	0.17	0.20
First Zone 3 Entering (s)	1.37	NA	0.63	0.57	0.56
Relay Reaction Time After FZC (cycle)	71	NA	28	24	22
Zone 3 Blocking decision (Y/N)	Y	N	Y	Y	Y

unbalanced type, e.g. single-line-to-ground faults or double-line faults. A negative sequence component monitor can be used for unblocking the relay for unbalanced faults. However, when it is a three-phase fault that the negative sequence monitor cannot obviously detect, the rate of change of impedance would be also monitored by the relay. If the swing progresses into a three-phase fault, the rate of change of impedance is going to be very fast, which could be used for unblocking the relay for symmetrical three-phase faults as stated in [8]. From the simulation results presented in the above study cases, the impedance locus at fault moves

instantaneously, whereas the one of power swing moves at a much slower rate. Moreover, other reported schemes are also applicable to unblock the relay such as the Blinder schemes discussed in Section 2.4.1, the Concentric Zone Characteristics schemes in Section 2.4.2, the Support Vector Machine method in Section 2.5.1, the Wavelet Transform method in Section 2.3.8, etc.

4.4 TZB and Traditional Zone Blocking Blinder Scheme Comparison in Modified WSCC System

4.4.1 Double Blinder Scheme Setup

4.4.1.1 Double Blinder Scheme Setup Procedure

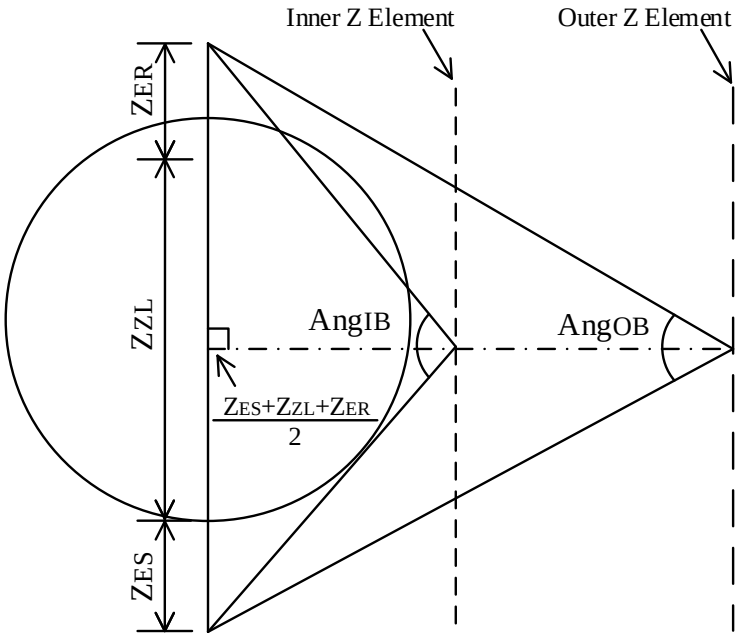

Figure 4.59: Double Blinder scheme setup with equivalent two source machine angles. [14]

The effectiveness of the developed TZB scheme has been verified by comparing it to the conventional power swing identification and blocking blinder based scheme. A two concentric

polygons blinders are established inclined at the transmission line angle, i.e. 81 degrees, in the power swing studies for the distance relay R98 as shown in Figure 4.60, 4.61, 4.62 and 4.63.

The blinder settings procedures are referred to [6], [14], [80] and [81], which are used for the test system and illustrated in Figure 4.59. In Figure 4.59, Z_{ES} is the local source impedance; Z_{ZL} is the line impedance; Z_{ER} is the remote source impedance; Ang_{IB} is the machine angle at the inner blinder reach; Ang_{OB} is the machine angle at the outer blinder reach. The inner blinder must be placed covering the maximum protection zone to keep the optimal room for stable power swing blocking. The absolute value of the outer blinder impedance must be less than the magnitude of maximum possible load impedance whose trajectories may be regarded as power swings triggering blocking action of the relay. In order to differentiate a fault from a power swing whose trajectories move much slower on the impedance plane of the distance relay, a timer is established to count the time difference that the measured impedance locus travels from the outer blinder to the inner blinder under fault conditions or in out-of-step phenomenon. The setting of the timer, T_R in cycles, can be calculated in the following Equation 4.13 with the system information [6].

$$T_R = \frac{(Ang_{IB} - Ang_{OB}) \times f_S}{360 \times f_{SLIP}} \tag{4.13}$$

where, f_S is the nominal system frequency; f_{SLIP} is the maximum slip frequency.

4.4.1.2 R98 Double Blinder Scheme Setup

The local and remote end equivalent source impedance is calculated for the concentric polygon Double Blinder scheme setup of the relay R98 in the modified WSCC system shown in Figure 4.3. The calculated remote end equivalent source impedance Z_{ER} equals to $0.0511+0.1844i$ in p.u., and the local end equivalent source impedance Z_{ES} equals to $0.0567+0.2198i$.

Considering the impedance of transmission Line 1 and Line 2, the total Zone 3 impedance

Z_{EZ} of the relay R98 is

$$Z_{EZ} = Z_{ER} + Z_{ZL} + Z_{ES} = 0.1537 + 0.7930i \tag{4.14}$$

The system operating point is at (1.514, -0.11) in per unit. Taking 5% margin of the outer blinder resistive setting into account, the perpendicular distance from the outer blinder is

$$Douter = Router \times sin81^\circ = 1.4305 \tag{4.15}$$

where $Douter$ is the perpendicular distance from the outer blinder to Z_{EZ}; $Router$ is 95% of the resistance of operating point in per unit.

The machine angle at the outer blinder reach, Ang_{OB}, equals to 31.5°.

Taking 5% margin of the inner blinder resistive setting into account, the perpendicular distance from the inner blinder is

$$Dinner = Rdiff \times sin81^\circ = 1.1292 \tag{4.16}$$

where $Dinner$ is the perpendicular distance from the inner blinder to Z_{EZ}; $Rdiff$ is 105% of the maximum resistive reach of Zone 3 of R98 in per unit.

The machine angle at the inner blinder reach, Ang_{IB}, equals to 39.4°.

The maximum slip frequency is about 2 Hz. The minimum block duration timer setting T_R is 0.65 cycles calculated from Equation 4.13, which is equal to 11 ms [81]. From the TZB and the blinder scheme comparisons it can be seen that the impedance trajectory moves instantaneously at the instant of the fault as shown in Figure 4.60, 4.61, 4.62 and 4.63. The fault conditions can be differentiated from the power swing scenarios by applying the calculated timer setting.

The inner blinder of the concentric polygon is placed outside the protection Zone 3 characteristics. The outer blinder settings are considered to keep 5% security margin resistively away from the possible maximum load, and 20% margin reactively away from the maximum mho relay reach [12]. The settings are given below [12].

Right Resistance Inner (RRI): 1.1451 p.u.

Right Resistance Outer (RRO): 1.4506 p.u.

Left Resistance Inner (LRI): - 1.1451 p.u.

Left Resistance Outer (LRO): - 1.4506 p.u.

4.4.2 TZB and Blinder Scheme Comparison

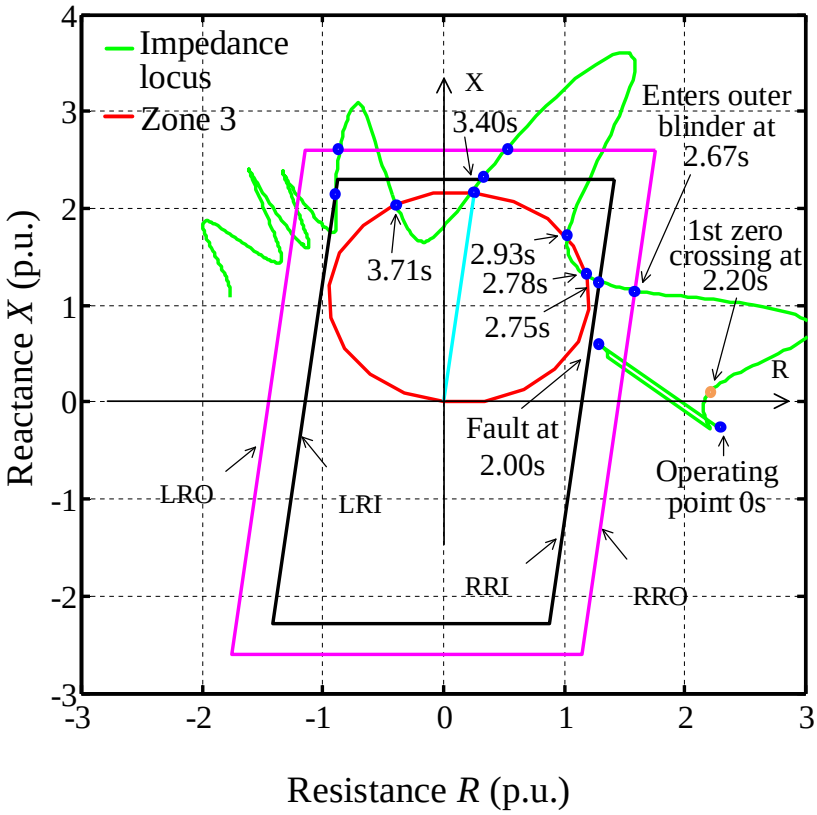

Figure 4.60: TZB and Blinder scheme comparison for study Case 1 on relay R98.

For the Case 1 studies for the distance relay R98, the impedance locus enters the outer blinder when the fault happens at 2.00 s. Since for a fault, the rate of change of impedance is instantaneous, the blinders settings do not classify it as a swing trajectory during the fault duration. Once the fault is removed, the swing impedance locus enters the outer blinder

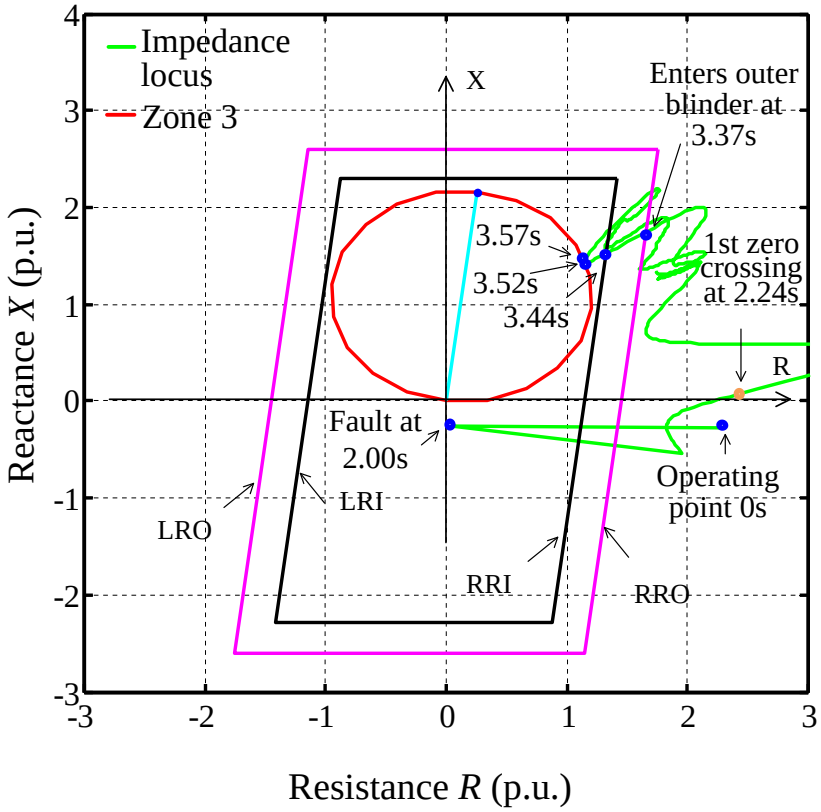

Figure 4.61: TZB and Blinder scheme comparison for study Case 2 on relay R98.

at 2.67 s, and then enters into the inner blinder as well. It is identified incorrectly as an out-of-step phenomenon by the conventional two blinder scheme. The proposed TZB scheme correctly identifies it as a stable power swing as shown in the results in Figure 4.7. In Figure 4.60, it can be seen that the impedance locus reenters both the outer and the inner blinders from the top of the concentric polygons.

For Case 2 for R98, the fault is again applied at 2.00 s. The impedance locus during the short fault duration of 0.05 s is obviously not picked up by the blinders. Similar to the Case 1 study, the power swing is identified as a stable one as shown on the relative speed trajectory in Figure 4.12. However, in Figure 4.61 the impedance locus of the swing enters into the inner blinder of the double blinder scheme and results in an incorrect classification as an unstable swing.

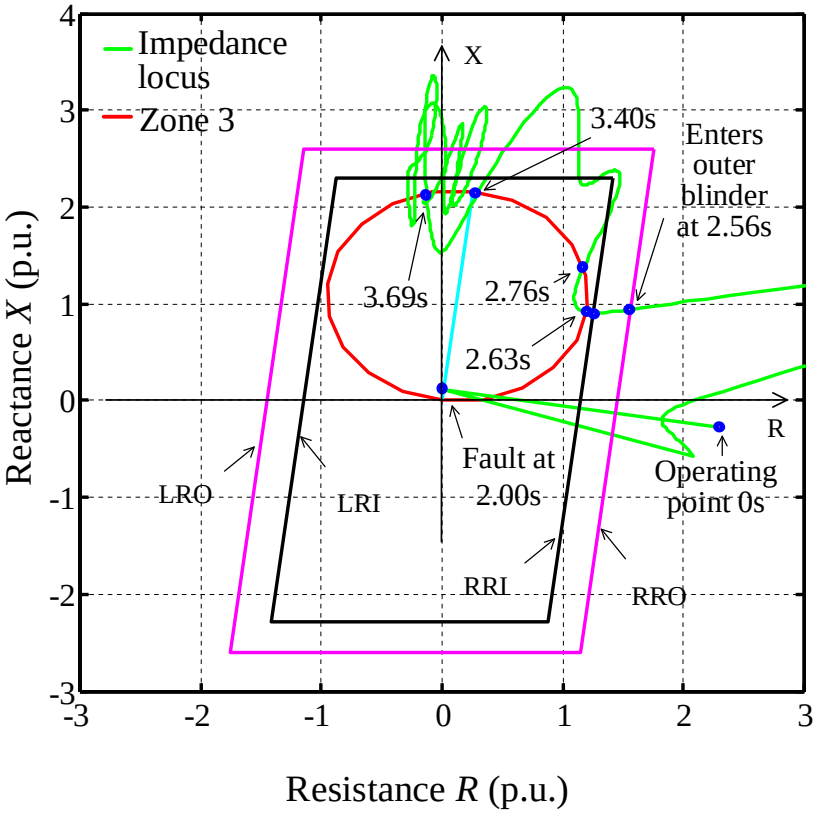

Figure 4.62: TZB and Blinder scheme comparison for study Case 3 on relay R98.

Similar results are also observed in the other two case studies for R98, i.e. Case 3 and Case 4, when the fault is applied on Bus 8 with 0.05 s and 0.10 s fault durations. In the stable Case 3, FZC is detected at 2.29 s by the TZB method as shown in Figure 4.17 and 4.18. Whereas, the impedance locus enters the outer and the inner blinder afterwards at 2.56 s and 2.63 s respectively, such that the swing is distinguished as an unstable one by the Blinder scheme. The locus is also observed entering both the outer and the inner blinders again later from the top of the concentric polygons in Figure 4.62. In the stable Case 4, the power swing is found being stable one since FZC is detected at 2.35 s by the TZB method as shown in Figure 4.22 and 4.23. Nevertheless, the impedance locus enters both the outer and inner blinder at 2.55 s and 2.56 s as shown in Figure 4.63. Due to the Double Blinder scheme 0.65 cycles timer setting, although the swing is not falsely identified as a three phase

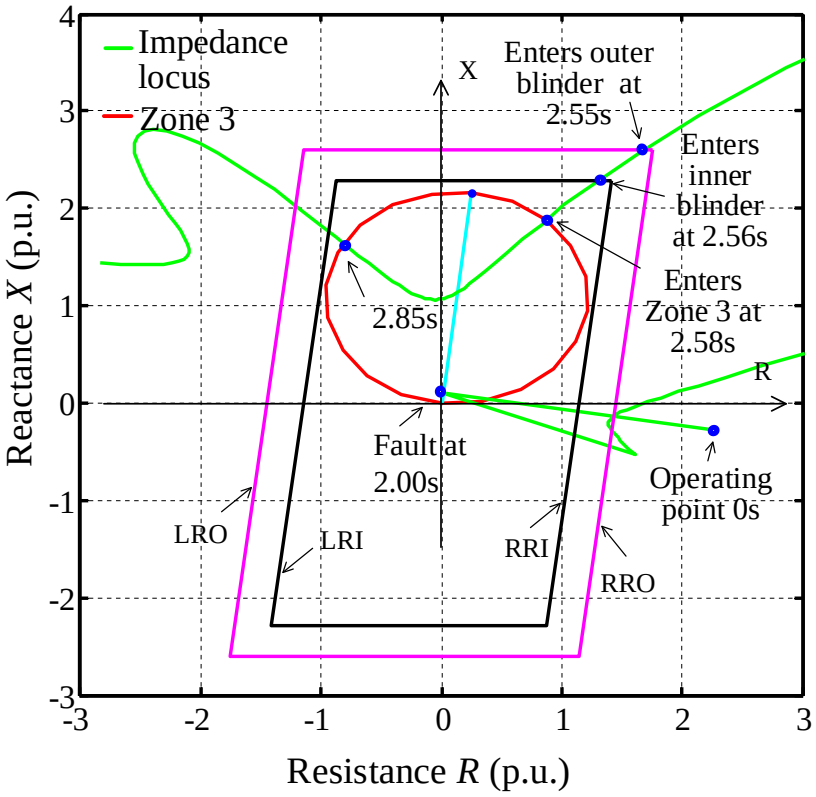

Figure 4.63: TZB and Blinder scheme comparison for study Case 4 on relay R98.

fault by the Blinder scheme, instead it is seen as an unstable swing.

The Blinder scheme is straightforward and practical, however it is not an easy task to find the appropriate settings for stable power swing blocking and tripping of the distance relay during unstable power swings. The power swings are so diverse that can be a result of various of contingency situations, e.g. various faults, line switchings, disconnections of generators, losses of large block of loads, and etc. In spite of extensive stability studies, not all of the power swing scenarios can be predicted in advance. Even if the blinder scheme is properly established for the distance relay R98 studies in this project, there is a chance that impedance loci measured by the relay enter into concentric double polygons and trip the relay unnecessarily as shown in the study Case 1 to Case 4.

The traditional blinder scheme tracks the difference of the rate of change of the positive

Table 4.3: Summary of TZB And Blinder Scheme Comparison on Distance Relay R98 in Modified WSCC system.

Case No.	1	2	3	4
Fault Location Bus No.	7	6	8	8
Fault in Protection Zones (Y/N)	N	N	Y	Y
Fault Duration (s)	0.05	0.05	0.05	0.10
FZC After Fault Removal (s)	0.15	0.19	0.24	0.25
First Outer Blinder Entering (s)	0.62	1.32	0.51	0.45
Zone 3 Blocking Decision (Y/N)	Y	Y	Y	Y
Swing Entering Outer Blinder (Y/N)	Y	Y	Y	Y
Swing Entering Inner Blinder (Y/N)	Y	Y	Y	Y

sequence impedance vector, so that the precise timer setting is vital for distinguishing power swing. Although it can be inferred from the studies that the Double Blinder scheme is capable of differentiating fault from slow power swing, its differentiation capacity is susceptible for fast moving swings.

The Blinder scheme application is under the influences of system configurations, e.g. the

infeed currents brought in by additional sources, the outfeed current by connecting extra line, the extension of existing transmission lines, etc. For instance, the additional power source G4 in the modified WSCC system provides an infeed current reducing the R98 and the R78 Zone 3 reach, which impacts on the Blinder scheme proper operation.

Apart from that, the reaches of the outer and the inner blinders are required to be less than maximum possible load impedance and greater than largest protection zone. Thus the scheme implementation is apparent system specified and needs to be upgraded accommodating any system changes, e.g. the switching on or off of a block of customer loads, disconnecting an unit of generation source, the loss of a transmission line, etc. The temporary system alternation can result in incompatible blinder settings and lead to distance relay mal-operations.

On the contrary, power swing blocking by the TZB method is subject to neither different system configurations nor temporary system changes. Moreover, FZCs for the reported four blinder scheme comparisons are detected much earlier than the impedance loci cross the outer blinder entering the polygons. The primary benefit of the proposed method in current research is that it can detect power swings correctly and faster than the conventional type two blinders scheme [12]. The four comparison case results are summarized in Table 4.3.

4.5 Verification of Distance Relay Current Calculation

In the TZB method studies, the impedance trajectories are displayed on distance mho relay Zone 3 characteristics to determine if the relay should be tripped or blocked. The apparent impedance seen by the relay is calculated as the ratio of voltage and current obtained at relay locations by Equation 1.1.

The magnitude and phase angle of the local voltage V_{A9C} of the relay R98 is provided by PSAT in the system output variables $Varout$. Since only the magnitude of the local current I_{ASC} of the relay R98 is given by the system output variables $Varout$, the I_{ASC} vector is calculated from the bus voltage difference over the transmission line impedance modeled in

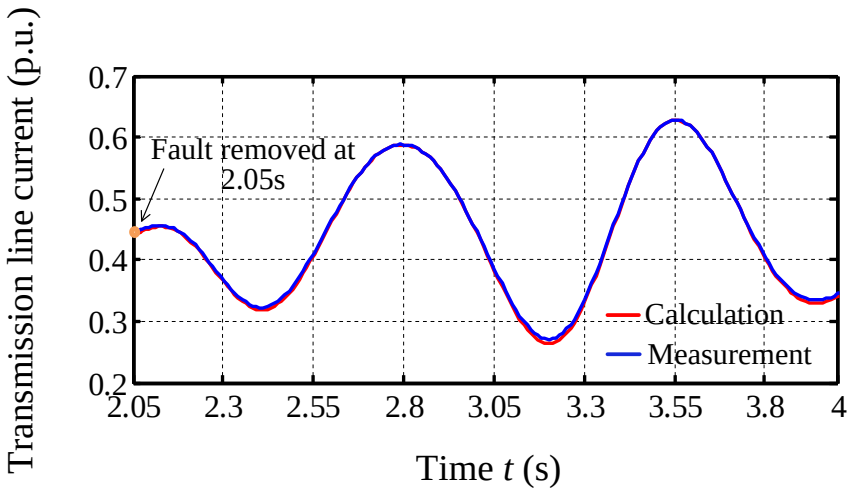

Figure 4.64: Calculated compared to measured transmission line L98 sending end current at Bus 9 for study Case 1 on relay R98.

the lumped parameters.

$Vinterm1$ is given as an intermediate variable for the receiving end current I_{RL1} calculation as

$$Vinterm1 = (Z_{L1} \times \frac{Y_{L1}}{2} + 1) \times Veb8 \tag{4.17}$$

where Z_{L1} gives the transmission Line 1 reactance and resistance; Y_{L1} is the Line 1 shunt capacitance; $Veb8$ is the measured voltage at Bus 8.

Then, the receiving end current I_{RL1} of transmission Line 1 at Bus 8 can be expressed as

$$I_{RL1} = (Veb9 - Vinterm1)/Z_{L1} \tag{4.18}$$

where $Veb9$ is the measured voltage at Bus 9.

The sending end current I_{SL1} of Line 1 is the sum of the receiving end current and the current in the equivalent shunt capacitors as

$$I_{SL1} = Veb9 \times \frac{Y_{L1}}{2} + Veb8 \times \frac{Y_{L1}}{2} + I_{RL1} \tag{4.19}$$

The accuracy and reliability of impedance trajectories calculation is determined by the accuracy of the sending end current of the transmission Line 1 at Bus 9. The calculated I_{SL1} magnitude is compared to the sending end current magnitude available in the system output variables $Varout$ as shown in Figure 4.64 for the stable Case 1 after the fault is applied on Bus 7 in the modified WSCC system. The calculated magnitude is in agreement with the measured result for the static and transient dynamic current magnitude.

4.6 Summary

In this chapter, the phasor based simulation of the TZB method has been discussed by employing PSAT in detail for distance relay Zone 3 blocking during power swings in power system network. Complexities such as synchronous machine non-rated speed responses, traveling wave modelings of transmission lines, local measurement implementations, etc. were not included in the PSAT simulations, which will be further addressed in Chapter 5 with the RTDS Electromagnetic Transient (EMT) simulation.

The power system components modelling was at first reviewed for the purpose of understanding power system simulation. In the modified WSCC system simulations, conditions were generated when the impedance loci measured by the distance relays enters the Zone 3 characteristics.

The proposed TZB method has been tested at different distance relay locations and analyzed under different power swing situations. The obtained simulation results demonstrated the validity of the TZB method. The testing results were summarized for comparison. The TZB method was further compared to a conventional power swing blocking concentric polygons type Double Blinder scheme, which was set according to the procedure laid out in IEEE PSRC document. The features/benefits of the TZB method are evident from the comparative studies. The shortcomings of the conventional scheme have also been discussed. Moreover, the impedance calculations were verified provided at the end of the chapter.

Chapter 5

Testing of Third Zone Blocking (TZB) Method Using RTDS/Electromagnetic Simulations

5.1 Introduction

In the previous chapter, the TZB method for power swing was tested with Power System Analysis Toolbox (PSAT) software. The PSAT is a phasor based program (60 Hz) and does not include other frequency behavior of the power system.

In this chapter, electromagnetic time-domain simulations with Real-Time Digital Simulator (RTDS) (Section 5.2) are used for the purpose of verifying the proposed TZB method. The RTDS simulations take into account the synchronous machine behavior for off-nominal frequencies, the transmission line is modeled in detail with a traveling wave model, and the system noise can be taken into consideration in the analysis. The instantaneous voltage and current samples are passed through a Discrete Fourier Transform (DFT) block to find the voltage and current phasors just like an actual numerical relay. The RTDS hardware as well as its graphical user interface RSCAD are briefly described in the next section.

The modified WSCC system is modeled in RTDS. The modeling details are discussed in Section 5.3. Section 5.4 discusses the detailed case studies for power swing detection and Zone 3 distance relay blocking. In the subsequent Section 5.5, the TZB method results are verified and compared with the Swing Equation Method by calculating the fictitious synchronous machine speed. The impedance locus obtained from the DFT calculations are

presented in Section 5.6.

5.2 Real-Time Digital Simulator (RTDS)

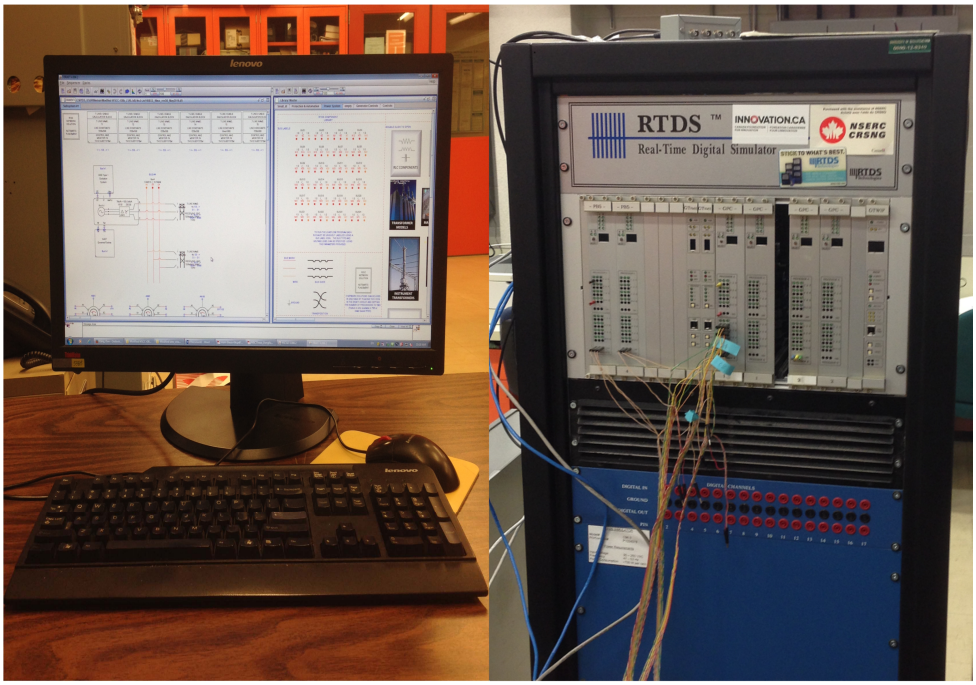

Figure 5.1: RTDS setup in Real Time Power System Simulation Lab.

RTDS is a digital real time power system simulator extensively used in electric power industries, equipment manufacturers and research institutes. The simulator provides facilities for continuous real time electromagnetic transient simulations. More specifically, electric power utilities have used the system for close-loop protective relay testings, in training on controllers for HVDC, Static Var Compensators and generators, and in large scale real time simulations [82].

The RTDS hardware is built on parallel processing structure to solve the electromagnetic transient simulation algorithm. The size of power systems can be expanded modularly on RTDS by adding hardware units (racks) which consist of both communication and processor cards linked through a shared backplane. Workstation InterFace (WIF) card enables Ethernet communication between racks and the graphical user interface, synchronizes calcu-

lations, and cordinates communications among processor cards and racks during real time simulations [82].

The processor cards calculate power network responses including the network nodal analysis and the auxiliary components solution, which solves the node voltages and branch currents on the matrix of network impedances plus the contribution of the auxiliary components [82]. The combination of the solutions becomes the overall network response. The typical simulation time step for real time operation of RTDS is in the order of 50 μs.

There are 4 GPC cards, 2 PB5 cards, 1 GTWIF card on the RTDS rack available in Real-Time Power System Simulation Lab in Electrical & Computer Engineering Department at U of S, as shown on the right of Figure 5.1. Both GPC and PB5 cards solve the equations representing the power network and control system models in RTDS. The GTWIF card provides functions of communication between the RTDS rack and the computer workstation running the RSCAD software, and of communication of the data between processors over the rack's backplane, etc. [83]

The graphical user interface known as RSCAD runs on the computer workstation, as shown on the left of Figure 5.1. The power network and its components for the RTDS simulation are constructed and connected graphically in the RSCAD Draft module. The parameters of individual components can be selected or input through a component data menu. The constructed network is compiled to create the simulation code downloaded to the processor cards on the simulator rack. RunTime of the graphical user interface of RSCAD operates on the computer workstation, and communicates back and forth with the simulator GTWIF cards. The simulation results are transferred back to the graphical user interface on the computer workstation. Details of transient responses can be recorded and displayed with a resolution as high as time step in the RunTime plots by the simulator GTWIF cards.

Real time simulations in RTDS provide a more detailed representation of the network behaviour than standard transient stability simulations. For instance, RTDS simulations have a much better frequency response (DC to 3 kHz). Even though the following is not in the scope of the current study: RTDS also provides a detailed representation of power

electronic installations in the system (as opposed to a nominal frequency approximation), the real time feedback, and the ability to interconnect with physical devices.

5.3 Modified WSCC System Setup in RTDS

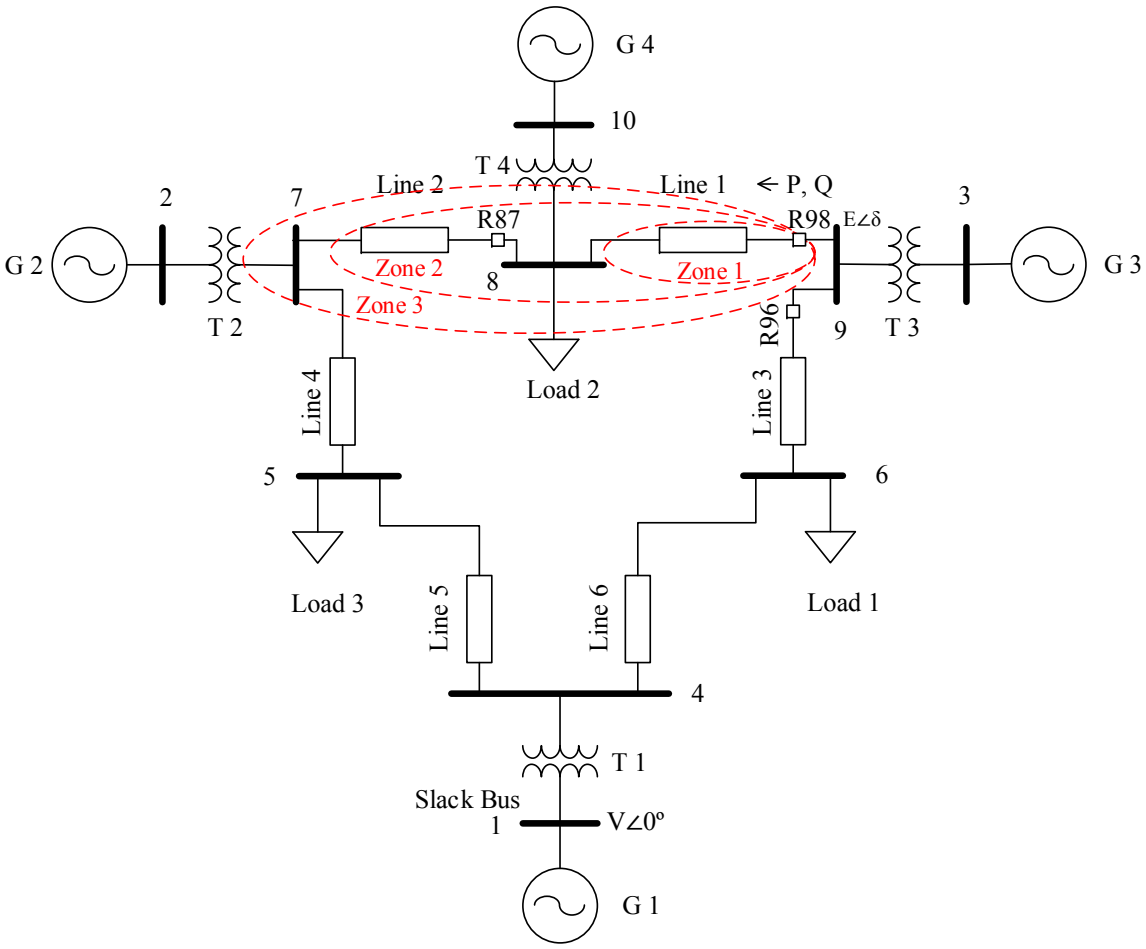

Figure 5.2: Modified WSCC 9-bus system for TZB testing in RTDS. [2]

5.3.1 Modified WSCC System Simulations

The modified WSCC system is developed in the Draft module in RSCAD as shown in Appendix B.8, which is compiled and downloaded from RSCAD to the processors on the

RTDS rack for real time simulation. The schematic of the modified WSCC system created in RTDS is shown in Figure 5.2.

In RTDS, generator does not necessarily run at the nominal speed, instead the speed is determined by the sum of the torques that act on the total inertia of the machine in a free speed mode, which includes the mechanical torque (T_m), the electrical torque (T_e), and the damping torque [84]. Both the static operating condition and dynamic response of the power network change from the scenario when the machine is running at the nominal speed as in PSAT. Because the system responses are different at the off-nominal frequency of operation and in order to simulate the conditions at which the impedance trajectory enters Zone 3 during power swings, the system configuration and some of the settings are changed from those used in the PSAT testing. Therefore, the RTDS studies are more practical by including generator off-nominal frequency operational behaviors. The new frequency is 393 rad/s at steady state, i.e. 1.04 $p.u.$ of the nominal frequency.

The transformers and machines parameters are listed in Appendix B.9. One 400 MVA generator G4 is connected to the load Bus 8 to introduce infeed currents in the RSCAD simulation in the modified WSCC system.

Due to energy inputs mismatch to consumer loads in a large power network or the incorrect system configuration, the network may be initially unable to reach to a steady state operating point. In order to run a large network in steady state, the stable operating condition has to be defined by a load flow analysis. The Load Flow Analysis is embedded in RSCAD and interfaced with the Draft module. The four menu entries, i.e. *load flow voltage magnitude, load flow voltage phase angle, load flow real power, and load flow reactive power*, at the top of the *MACHINE INITIAL LOAD FLOW DATA* menu specifies the initial terminal conditions of the machine [84]. These initial terminal conditions are available from the output of the load flow program. The Load Flow Analysis results of the modified WSCC system are listed in Appendix C.1.

Note that if the configuration of the modified WSCC system is same as in PSAT, i.e. the same parameters of the system and ancillary components are kept the same in system

setup in RTDS, then the static initial operating conditions are same for both the RSCAD and the PSAT Load Flow Analysis in Appendix C.2. However since generators run at free speed mode in RTDS, the operating conditions at steady state move away from the initial states defined by the Load Flow.

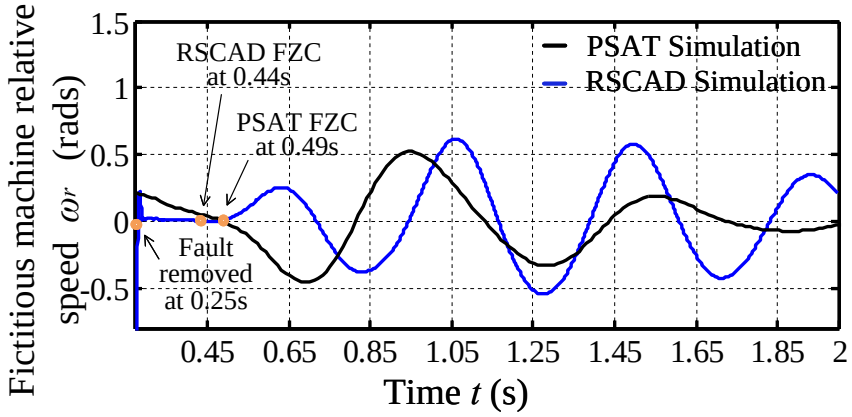

Figure 5.3: Relative speed of fictitious machine for stable swing study with distance relay R98 in PSAT and in RTDS.

The phasor based PSAT simulation was carried out as a preliminary step to cope with the complexity of the TZB study. While the conventional phasor based simulation is prevalent for both static and dynamic studies of power system in industry, the electromagnetic simulation includes more complex features of power networks in analyses, such as off-nominal frequencies, distributed parameter modelings of transmission lines, and local DFT measurements, etc.

A comparison is made to demonstrate the difference of the fictitious synchronous machine relative speeds calculated by the TZB algorithm in PSAT and in RTDS. The system parameters of the RTDS modified WSCC system are kept same as the ones in the stable Case 3 study in the modified WSCC system in PSAT. After the 0.05 s fault is cleared at 0.25 s, both the calculated relative speeds in PSAT and in RTDS oscillate approaching to steady state, as shown in Figure 5.3. FZC of the relative speed at 0.44 s in RTDS is detected

earlier than FZC detected at 0.49 s in PSAT, and the oscillation frequency difference is also observed, due to the fast electromagnetic responses.

5.3.2 Transmission Line Modeling

The six transmission lines are modeled by TLINE program as travelling wave transmission lines in kilometers instead of lumped parameters representations, such as in the PSAT simulation in Chapter 4. The TLINE program is one of the inherent tools of RSCAD for network module construction in the Draft module [85]. The distributed parameter representations of transmission lines in a traveling wave model gives more accurate solution for a long transmission line network analysis.

In the distributed parameters modeling of a long transmission line, the voltages and currents of each small line element are different on the two sides of the element in the distributed parameters modeling, and they vary along the line. With known line parameters, the sending end voltage and current of the line can be written as a function of the receiving end voltage and current, as derived in [13]

$$V_{SL} = \frac{V_{RL} + I_{RL}Z_c}{2}e^{\gamma x} + \frac{V_{RL} - I_{RL}Z_c}{2}e^{-\gamma x}, \tag{5.1}$$

and

$$I_{SL} = \frac{V_{RL}/Z_c + I_{RL}}{2}e^{\gamma x} - \frac{V_{RL}/Z_c - I_{RL}}{2}e^{-\gamma x}, \tag{5.2}$$

where Z_c is the characteristic impedance of the line; γ is the propagation constant; V_{RL} and V_{SL} are the receiving and the sending end voltage; I_{RL} and I_{SL} are the receiving and the sending end current; x is the line distance measured from the receiving end.

The first term of Equation 5.1 diminishes in magnitude and retards in phase angle with the distance increasing from the sending end of the line. It is named as the incident voltage that elucidates the travelling wave characteristic of the transmission line. Whereas, the second term of Equation 5.1 increases in magnitude and advances in phase angle from the sending end of the line. It is named as the reflected voltage. An actual voltage of the line

is the sum of the incident voltage and the reflected voltage at the specified point along the line.

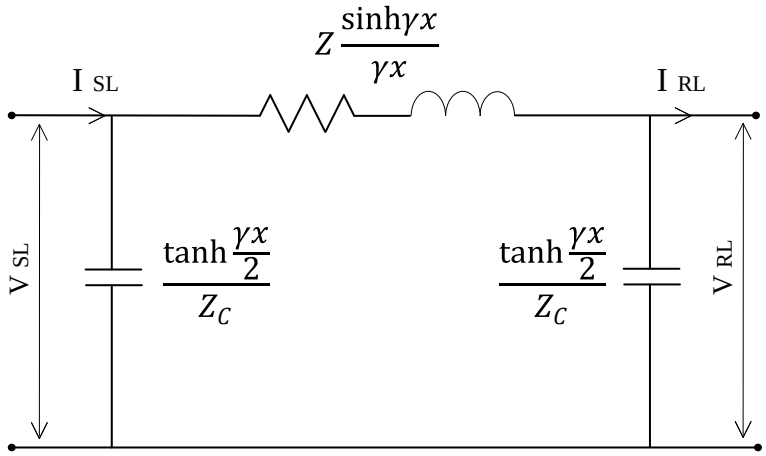

Figure 5.4: Long length transmission line nominal π equivalent circuit. [13]

The Equation 5.1 and 5.2 can be rearranged by introducing the hyperbolic function *sinh* and *cosh* as follows, [13]

$$V_{SL} = \cosh\gamma x V_{RL} + Z_c \sinh\gamma x I_{RL}, \tag{5.3}$$

and

$$I_{SL} = \frac{\sinh\gamma x V_{RL}}{Z_c} + \cosh\gamma x I_{RL}, \tag{5.4}$$

For simplification, the distributed parameter expression of the long transmission line can be written into a nominal π formula by combining the terms of Equation 5.3 and 5.4 as follows, [13]

$$Z' = Z_c \sinh\gamma x, \tag{5.5}$$

and

$$\frac{Y'}{2} = \frac{1}{Z_c}\tanh\frac{\gamma x}{2}, \tag{5.6}$$

where Z' is the equivalent line impedance; $\frac{Y'}{2}$ is the equivalent admittance at the sending or the receiving end of the line.

The sending end voltage and current can be calculated by the equivalent nominal π model in Figure 5.4 in term of Z' and $\frac{Y'}{2}$ as follows, [13]

$$V_{SL} = \left(1 + \frac{Z'Y'}{2}\right) V_{RL} + Z' I_{RL}, \tag{5.7}$$

and

$$I_{SL} = Y' \left(1 + \frac{Z'Y'}{4}\right) V_{RL} + \left(1 + \frac{Z'Y'}{2}\right) I_{RL}, \tag{5.8}$$

5.3.3 DFT Local Measurement Setup

The local electrical quantities are measured by applying the DFT technique, which is also used in state-of-the-art filtering techniques in many distance relays such as GE Multilin N60 relay [56]. The DFT technique is briefly discussed in Appendix C.3. Compared to other filtering techniques, the advantage of DFT technique are – reduces noise effectively; attenuates all higher harmonic components effectively; rejects the non-decaying part of the dc component. The disadvantages of the DFT Technique are – the transient response is slower compared to the transient response of the short data window measurement, e.g. Mann and Morrison Algorithm; the decaying part of the dc component affects accuracy of the DFT calculation; more computations are required compared to the computations required by the Mann and Morrison algorithm [1].

In the DFT calculations, one thing that can be seen is that when the decaying part of the dc component is present in the current measurement, then the derived value of the relative rotor speed using the DFT calculated phasors has a bias compared to the actual rotor speed value. The disadvantages of DFT discussed in the previous paragraph are tolerable in the TZB study. For instance, the timing wise impedance locus caused by power swing enters Zone 3 more than 400 milliseconds after the fault removal, so the power swing blocking is affected

by the inaccuracies that could be present in the first few cycles of the DFT calculations (e.g. the decaying dc component of current etc would have subsided by then).

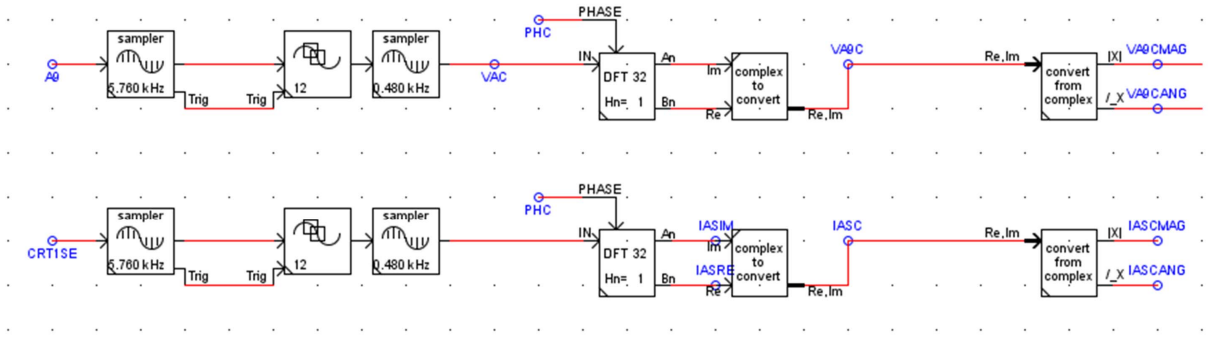

Figure 5.5: DFT measurement blocks of distance relay in Draft module of RSCAD^{TM} (created in RSCAD^{TM}).

The first component of the DFT block is a sampling unit as given in Figure 5.5. The phase voltage and current are sampled at 96 samples per cycle. The sampled data are received by a 12 point moving average filter. Eight data per cycle are output from a moving average filter to a down sampler to avoid aliasing and distortion. The fundamental frequency value of the sampled signal is extracted by a full cycle (32 points) Discrete Fourier Transform unit to obtain real and imaginary parts of the phasor that are used for impedance calculation [86].

The PHASE input of the DFT unit signal receives a sawtooth waveform locked to the input signal fundamental frequency generated from a phase-locked-loop (PLL) unit [87]. The PLL unit input is the voltage measured by the distance relay R98 located at Bus 9 in the modified WSCC system. The PHASE input is also the phase reference for the DFT measurement. The DFT output can be specified as either A_n, B_n in the real and imaginary format, or as C_n, Phi in the magnitude and angle format. A_n, B_n and C_n, Phi are expressed in terms of the following formula:

$$C_n = \sqrt{(A_n^2 + B_n^2)},\ Phi = \arctan(\frac{B_n}{A_n}) \tag{5.9}$$

The measured impedance by the distance relay R98, Z_{A9C}, is obtained based on the DFT

measured V_{A9C} and I_{ASC} as given by the following equation:

$$Z_{A9C} = \frac{V_{A9C}}{I_{ASC}} \tag{5.10}$$

The calculated impedance Z_{A9C} is converted from complex to real and imaginary segments for plotting and recording for further analysis.

5.4 TZB Method Testing with RTDS

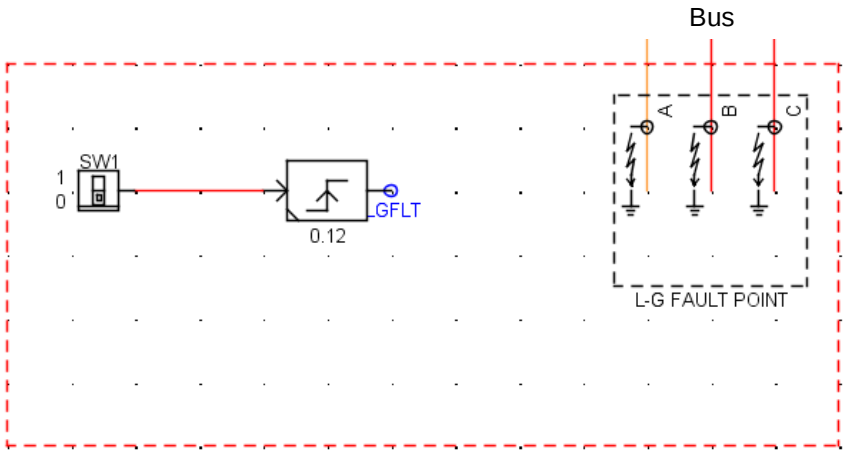

Figure 5.6: Three-phase to ground fault generation circuit in Draft module of RSCAD^{TM} (created in RSCAD^{TM}).

The proposed TZB method has been tested on the modified WSCC system using the configuration and settings described in previous sections. For the purpose of simulating measured impedance locus encroaching into Zone 3 of the distance relay R98 mho characteristics, three-phase faults are applied at different locations in the modified WSCC system.

The three-phase to ground fault is initialized by a Signal Switch that creates 1 or 0 signal controlled by the corresponding unit in the RunTime, as shown in the Draft module circuit

in Figure 5.6. A pulse generator receives the Switch signal and generates a fixed width rising edge pulse defined by its Duration Timer, Timer Mode and Trigger on Edge parameter. The L-G Fault Switch is attached to the fault point and triggered by a LGFLT pulse signal to produce a fixed time duration temporary three-phase to ground fault.

Similar to the TZB study with PSAT, the distance relay R98 is located at the sending end of the transmission line L1 at Bus 9. However the difference compared to the PSAT simulation model is that Zone 3 of the relay R98 has a further reach covering Bus 7 as shown in Figure 5.2, which is also indicated on the mho relay characteristics on the impedance planes as shown in Figure 5.10, 5.15, 5.20, 5.25, and 5.29. Zone 3 of R98 covers Line 1 plus 120% of Line 2. In the duration when the three-phase to ground fault happens on Bus 7, the current magnitude ratio $I_{A87SM}/I_{A98SM} = 4.08$. I_{A87SM} and I_{A98SM} are the sending end current magnitudes of Line 2 (Bus 8 to Bus 7) and Line 1 (Bus 9 to Bus 8) respectively. Thus, the Zone 3 impedance is calculated as $40.06\ \Omega + 4.08 \times 137.79\ \Omega = 602.18\ \Omega$. The transmission line impedance is $(0.03478 + i0.2198)\ \Omega/km$ calculated from [88].

After the simulation is finished in RTDS, the experimental data are saved in the RunTime of RSCAD and transferred to MATLAB for analysis.

5.4.1 Stable Power Swing Scenario for Relay R98

A three-phase to ground fault is applied at 0.12 s and removed at 0.24 s at Bus 7. Zone 2 of R87 operates for this fault. The relay R87 on Line 2 at Bus 8 is backed up by R98 at Bus 9. The fault duration is 0.12 s and is less than the time delay setting for Zone 3 of R98, i.e. 1.5 s (90 cycles).

Figure 5.7 shows the actual relative speed values of G1 to G4 measured in the system. The stable oscillations reaching to an equilibrium value after the fault is removed are shown in the figure. The active power P, reactive power Q from Bus 3 to Bus 9 and the voltage E_B measured by R98 at Bus 9 are shown in Figure 5.8. It can be seen from Figure 5.9 that the fictitious machine ω_r oscillates after the fault is removed, and approaches to a steady state value. The first time that the machine speed goes through the synchronous speed value is

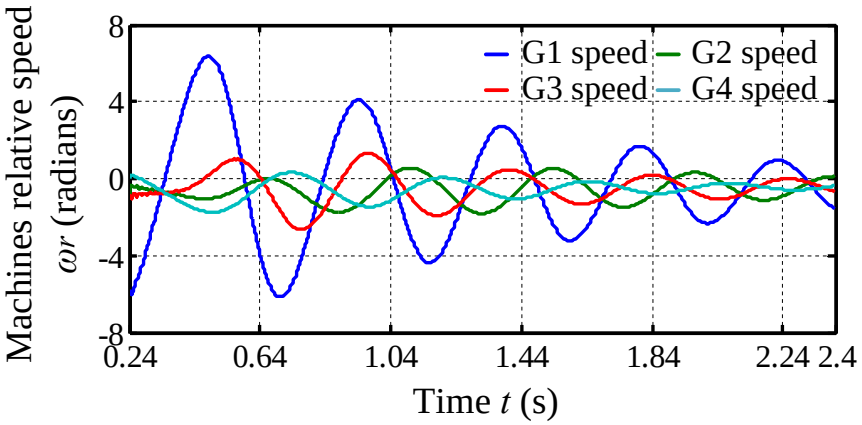

Figure 5.7: Actual relative speeds measured for G1 - G4 (Case 1 Studies for R98 - stable scenario).

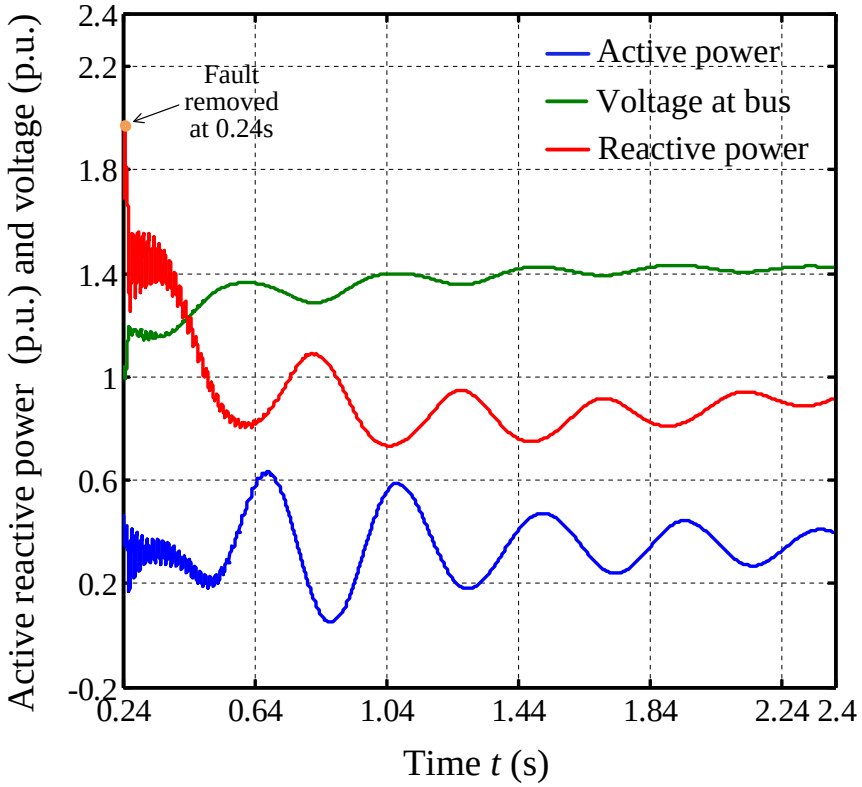

Figure 5.8: Measured active and reactive power values, and voltage for Case 1 (stable case) studies with RTDS for distance relay R98.

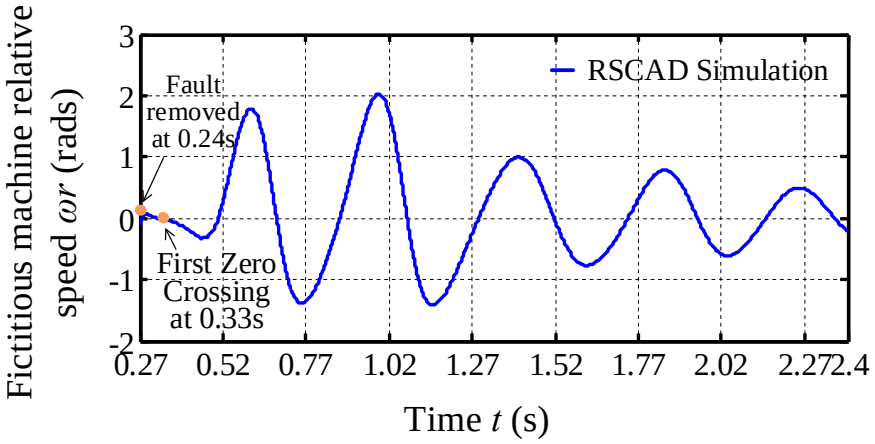

Figure 5.9: Relative speed of fictitious machine for Case 1 studies with distance relay R98 in RTDS.

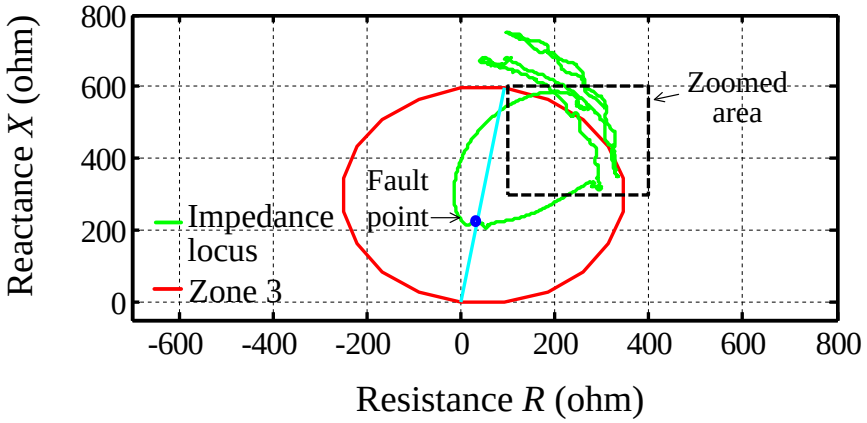

Figure 5.10: Impedance locus superimposed on mho characteristics of distance relay R98 (Case 1 studies with RTDS - stable scenario).

at 0.33 s, at which the relative speed ω_r equals to zero, i.e. 0.09 s after the fault is removed.

The trajectory of impedance locus measured at R98 is shown in Figures 5.10 and 5.11. During the fault interval, the impedance locus is seen residing at the center of the protection Zone 3. After the fault is cleared from the system at 0.24 s, the impedance locus moves away from the low impedance position towards the steady state operating point that is out

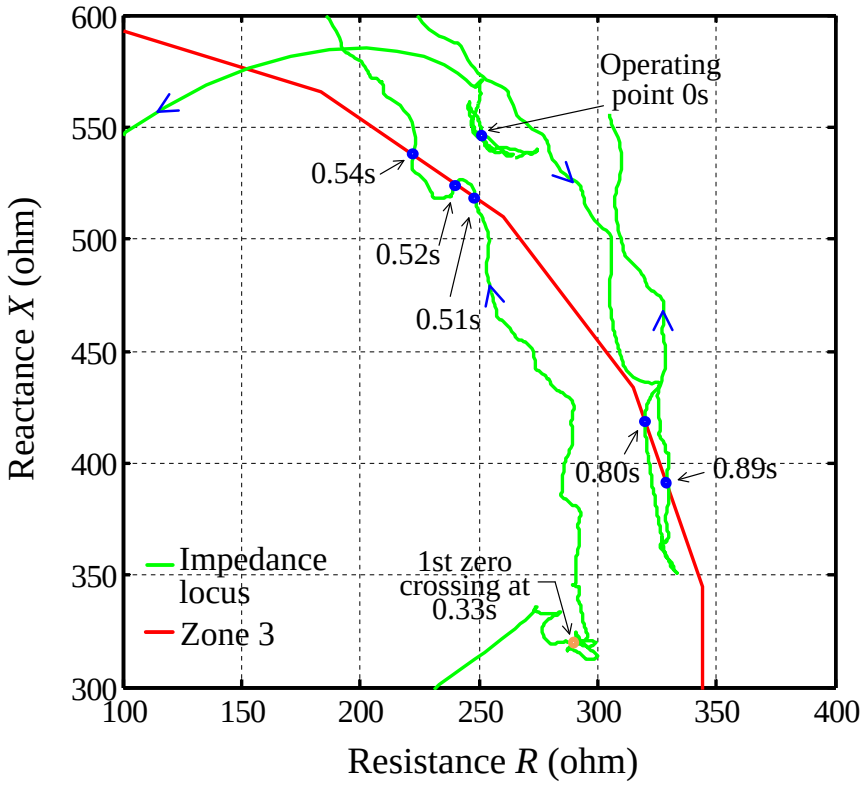

Figure 5.11: Impedance locus superimposed on the zoomed mho characteristics shown in Figure 5.10 (shown for R98 for Case 1 studies).

of Zone 3. The swing locus is detected re-entering the Zone 3 characteristics at 0.52 s, which is caused by system transient instability. Zone 3 operating time delay is 1.5 s which is much greater than 0.52 s, so that Zone 3 is going to be secure during this period. The impedance trajectory again enters Zone 3 at 0.80 s, when the system starts post-fault oscillating after the removal of the fault, which is 0.47 s (28 cycles) after the FZC point (at 0.33 s) shown in Figure 5.11. It can be seen from the figure that there is adequate room for blocking Zone 3 when the swing locus oscillates back and forth during the post-fault condition.

In Case 2 – another stable case scenario for R98, the fault is applied at 0.12 s and removed at 0.24 s at Bus 8. In this scenario, Zone 2 of R98 operates for the fault. The fault duration is less than Zone 2 operating time for R98, which is typically in the range 0.25 s to 0.5 s (15 to 30 cycles) [28].

Figure 5.12 shows the measured actual synchronous machines' relative speeds of G1 to G4.

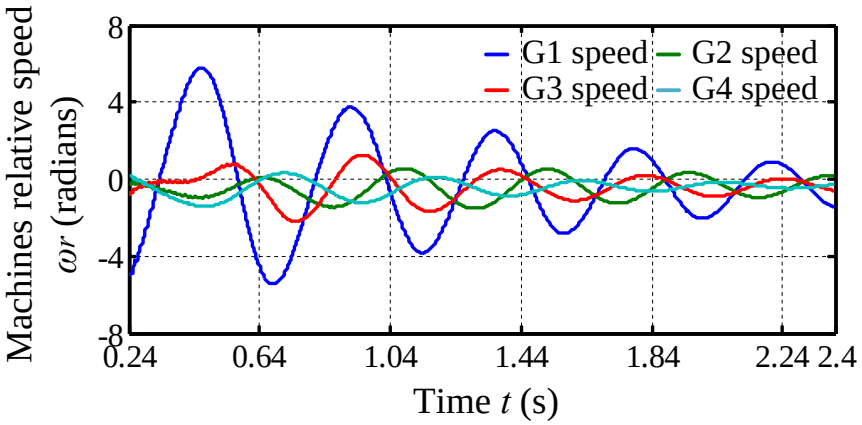

Figure 5.12: Actual relative speeds for G1 - G4 for Case 2 studies with R98 - stable scenario.

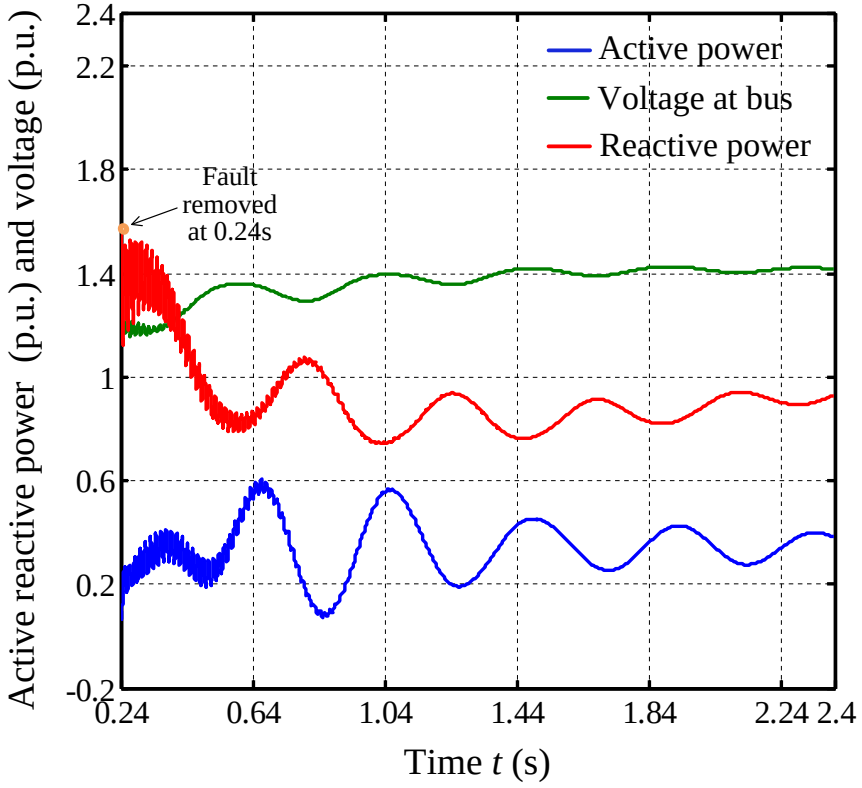

Figure 5.13: Measured active, reactive power and voltage for R98 for Case 2 - stable scenario.

The active power P, reactive power Q from Bus 3 to Bus 9 and the voltage E_B is measured by R98 at Bus 9 as shown in Figure 5.13. The TZB calculated fictitious synchronous machine

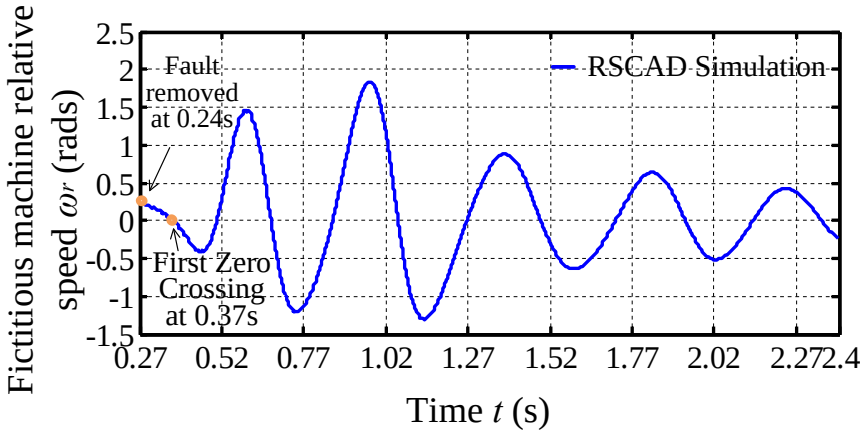

Figure 5.14: Relative speed of the equivalent fictitious machine for R98 - Case 2 stable scenario.

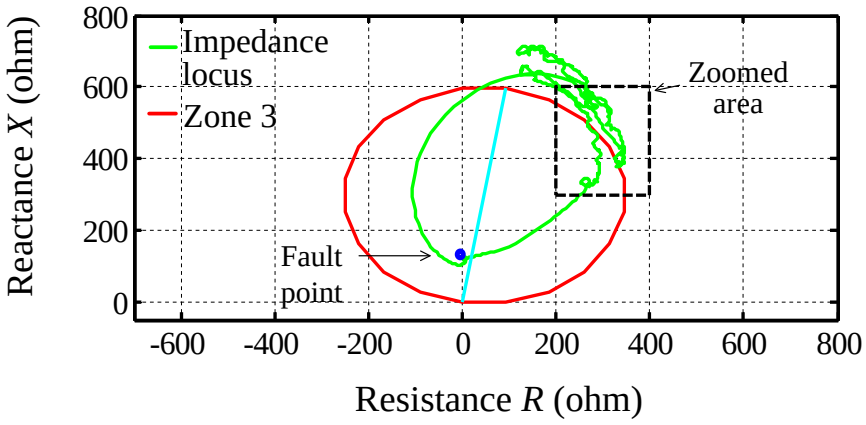

Figure 5.15: Impedance locus with mho characteristics of R98 for Case 2 – stable scenario.

relative speed ω_r oscillates after the fault is cleared, and approaches to a steady state value as shown in Figure 5.14. FZC is observed at 0.37 s, i.e. 0.13 s after fault removal. The impedance locus first enters Zone 3 at 0.81 s that is 0.44 s (26 cycles) after FZC as shown in Figures 5.15 and 5.16. There is adequate room for blocking the relay R98 with Zone 3.

In the stable Case 3 study of R98, the fault is applied at 0.12 s at Bus 6 which is not in the relay's protection zone, and removed after 0.12 s at time instant of 0.24 s. Figure 5.17

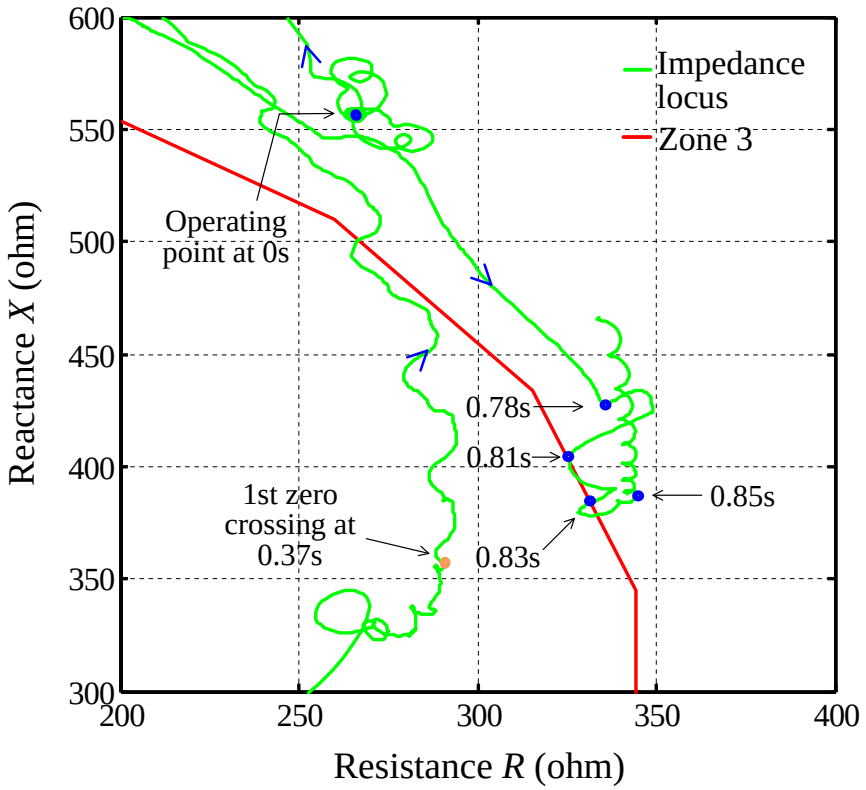

Figure 5.16: Impedance locus with zoomed-in mho characteristics shown in Figure 5.15 for R98 for Case 2 – Stable scenario.

shows the measured actual synchronous machines' relative speeds of G1 to G4. The active power P, reactive power Q from Bus 3 to Bus 9 and the voltage E_B measured by R98 at Bus 9 are shown in Figure 5.18.

Similar to previous study cases, the calculated fictitious machine relative speed decreases after the fault removal. FZC is observed at 0.27 s, i.e. 0.03 s after the fault is removed as marked in Figure 5.19. A high impedance value is measured by R98 during the fault interval, which is away from the protection Zone 3 on the relay characteristics as shown in Figure 5.20. The locus is observed entering Zone 3 at 0.34 s (not shown in Figure 5.21), i.e. 0.07 s after FZC, as a result of the system transient instability similar to the scenario in Case 1. It will not trip the relay because of the Zone 3 time delay. The impedance locus enters Zone 3

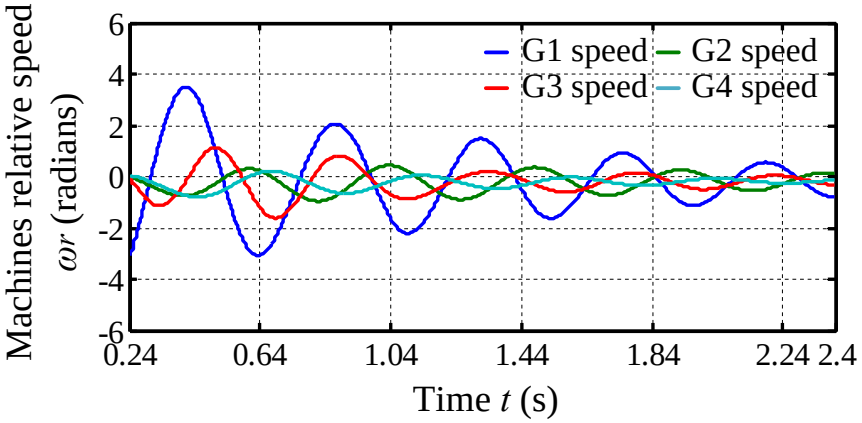

Figure 5.17: Actual relative speeds for G1 - G4 for Case 3 studies with R98 - stable scenario.

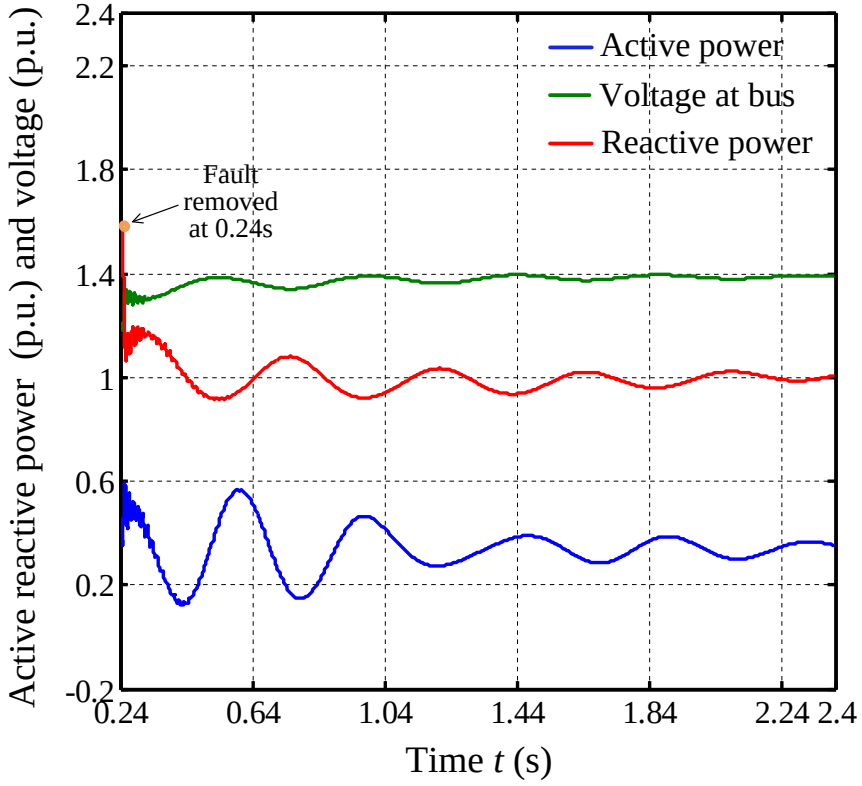

Figure 5.18: Measured active reactive power and voltage for R98 for Case 3.

at 0.76 s that is caused by the first power swing, i.e. there is 0.49 s (29 cycles) time interval adequate for blocking Zone 3 as marked in Figure 5.21.

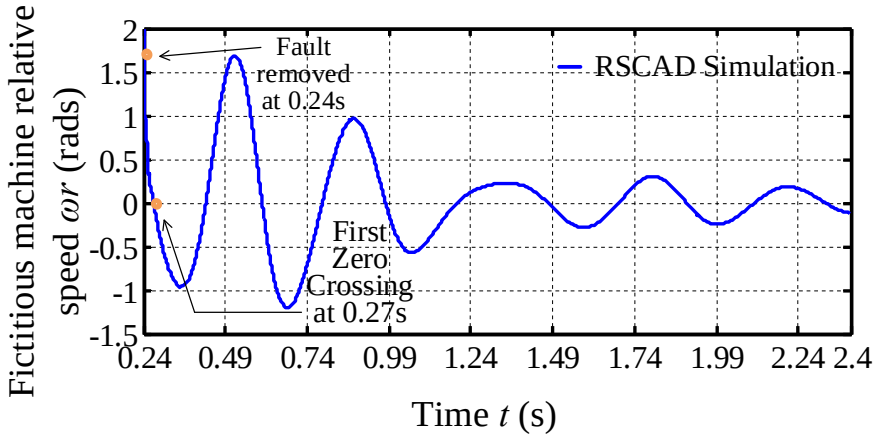

Figure 5.19: Fictitious synchronous machine relative speed for relay R98 for Case 3 studies.

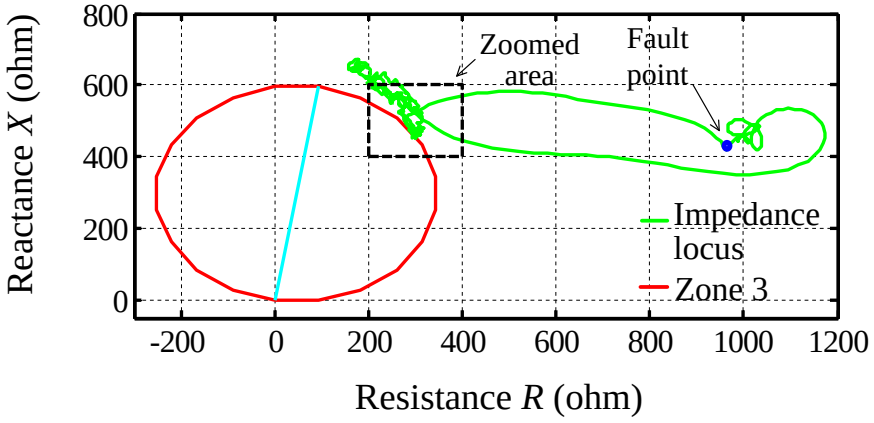

Figure 5.20: Impedance locus superimposed on mho characteristics of distance relay R98 for Case 3 studies (Stable Case).

In Case 4 study for R98, the fault is applied at 0.12 s to Bus 5 which is out of the reach of relay's protection zone, and is removed after 0.12 s at 0.24 s. Figure 5.22 shows the measured values of the actual synchronous machines' relative speeds of G1 to G4. The active power P, reactive power Q from Bus 3 to Bus 9 and the voltage E_B are measured by R98 at Bus 9 as shown in Figure 5.23. Similar to previous study cases, the calculated fictitious machine relative speed decreases after the fault is removed. FZC is observed at 0.26 s, i.e. 0.02 s after the fault removal, as marked in Figure 5.24. The impedance locus first enters Zone

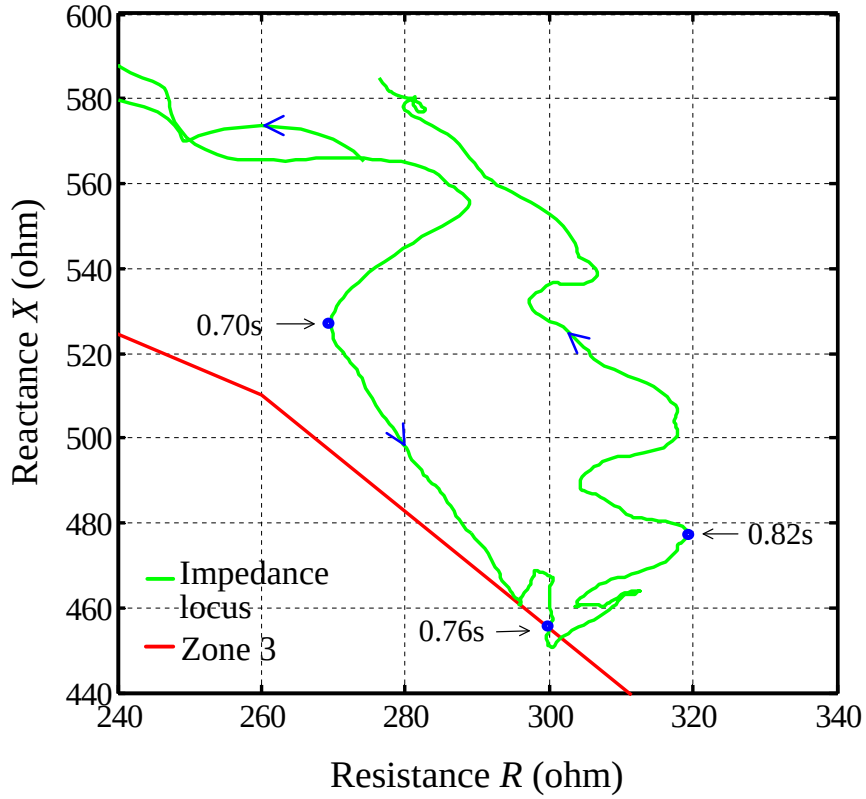

Figure 5.21: Impedance locus on zoomed mho characteristics in Figure 5.20 of distance relay R98 for stable Case 3 in RTDS.

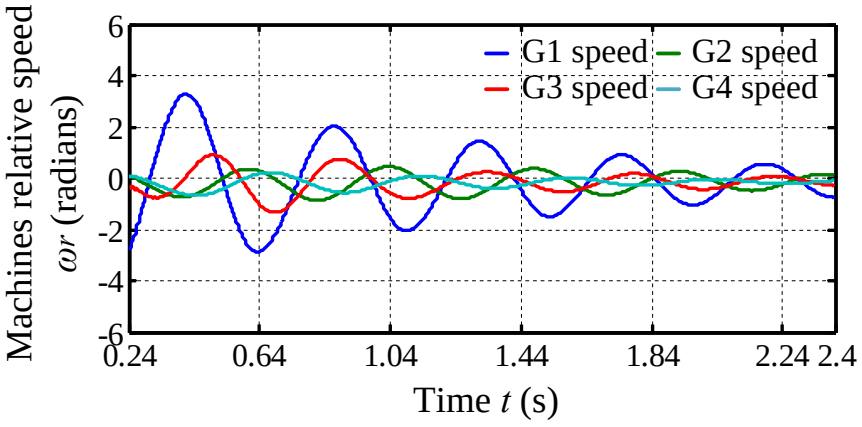

Figure 5.22: Actual relative speeds for G1 - G4 for Case 4 studies with R98 - stable scenario.

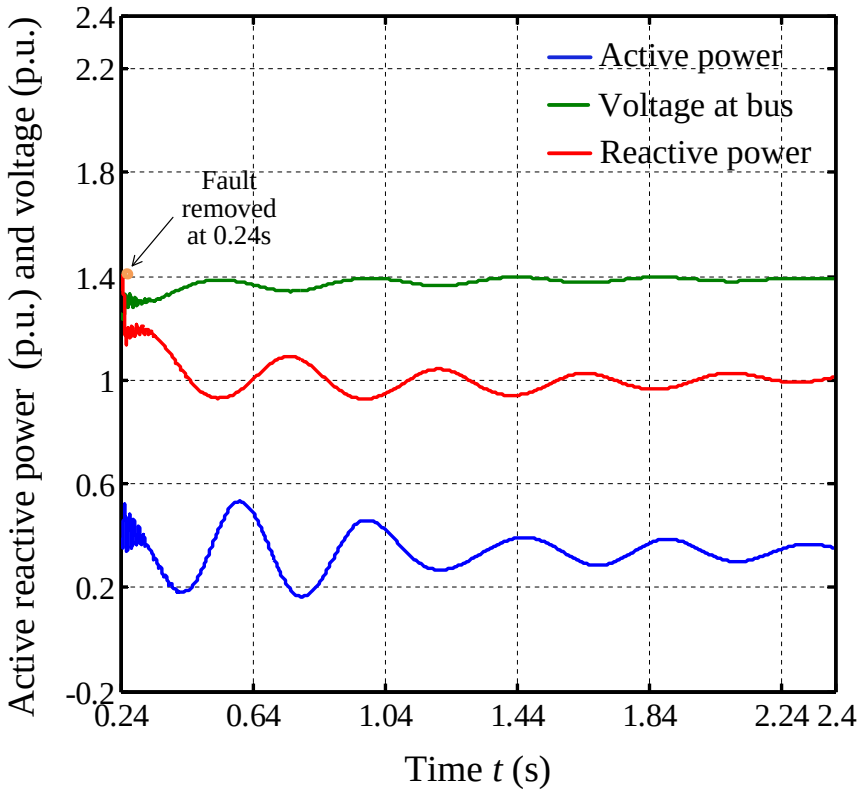

Figure 5.23: Measured active, reactive power and voltage for stable swing studies with relay R98 (Case 4 studies).

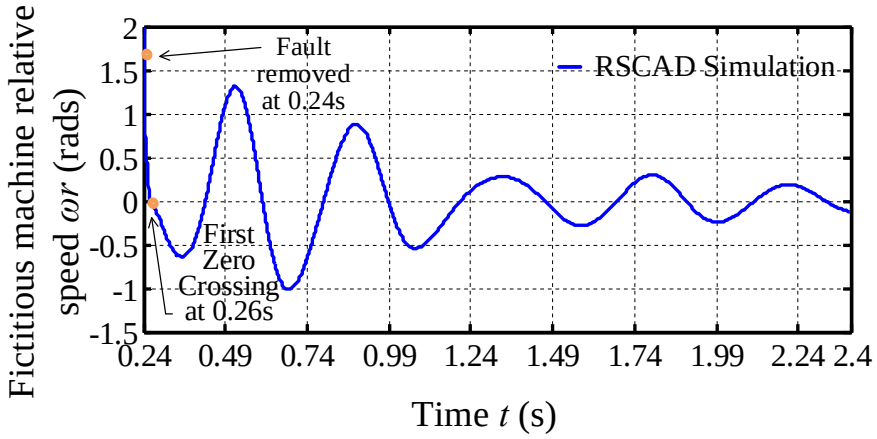

Figure 5.24: Fictitious synchronous machine relative speed for relay R98 (Case 4 studies).

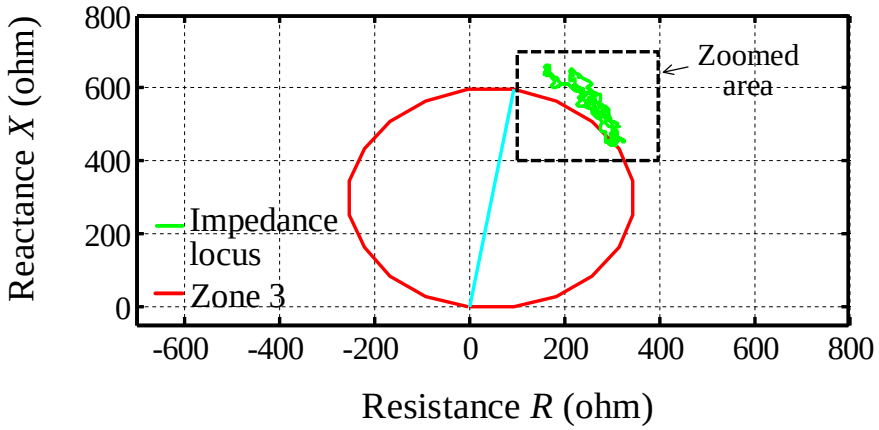

Figure 5.25: Impedance locus superimposed on mho characteristics of R98 (Case 4 stable scenario).

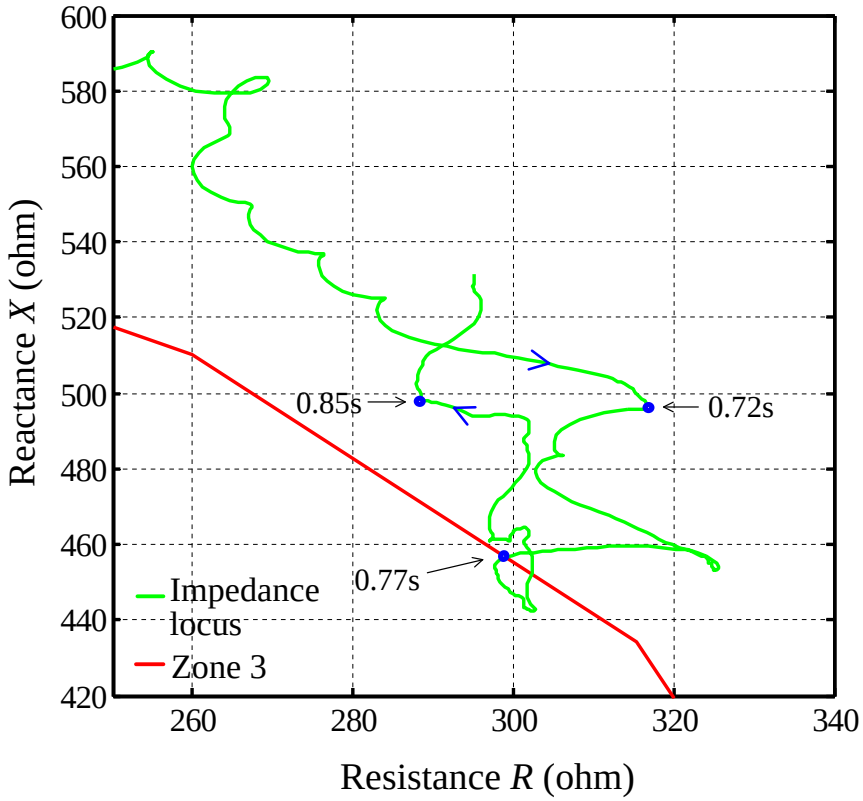

Figure 5.26: Impedance locus superimposed on the zoomed-in mho characteristics in Figure 5.25 for R98 (Case 4 stable scenario).

3 at 0.30 s (not shown in Figure 5.26) which is 0.04 s after FZC, and the relay is blocked from tripping by the Zone 3 time delay. The impedance locus enters Zone 3 caused by power swing at 0.76 s as shown in Figure 5.25 and in Figure 5.26, i.e. there is 0.50 s (30 cycles) time interval after FZC for blocking Zone 3.

Table 5.1: Summary of stable power swing studies for relay R98 in the modified WSCC system.

Case No.	1	2	3	4
Fault Location Bus No.	7	8	6	5
Fault in Protection Zones (Y/N)	Y	Y	N	N
Fault Duration (cycle)	7	7	7	7
Fault Duration (s)	0.12	0.12	0.12	0.12
FZC After Fault Removal (s)	0.09	0.13	0.03	0.02
First Swing Zone 3 Entering after FZC (s)	0.47	0.44	0.49	0.50
Zone 3 Blocking decision (Y/N)	Y	Y	Y	Y

For all four stable power swing study cases reported, the results show that FZC can be detected much before the time instant at which the first swing impedance locus enters into Zone 3, so that there is sufficient time for safely blocking Zone 3 for the relay R98. The results are summarized in Table 5.1.

5.4.2 Unstable Power Swing Study

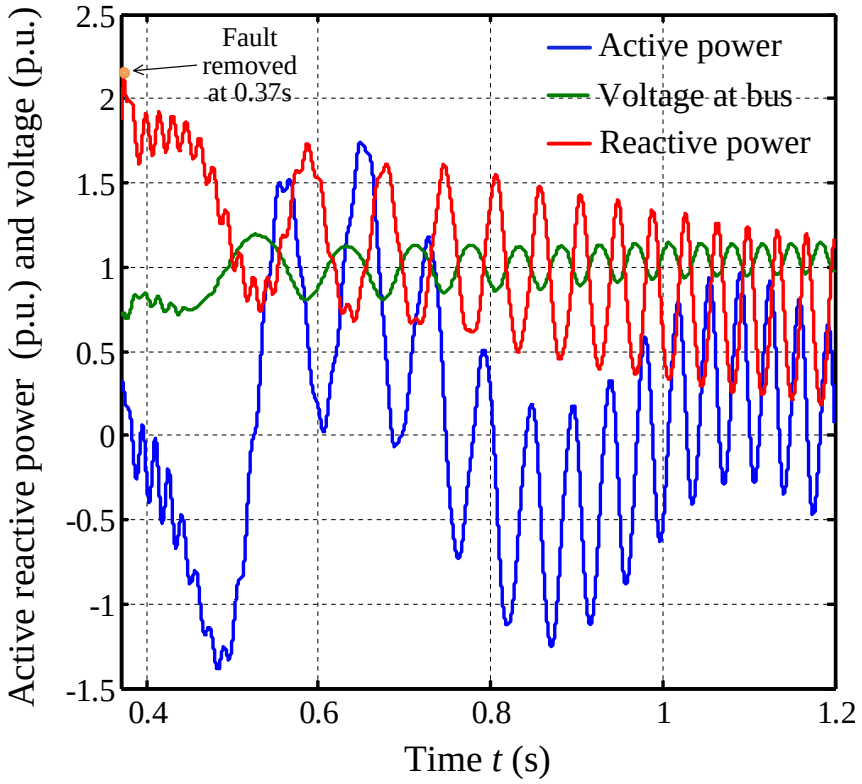

Figure 5.27: Measured active, reactive power and voltage for unstable swing study for relay R98.

For the Case 2 swing scenario, if the fault duration is prolonged to 0.25 s, more specifically, a three-phase to ground fault is applied to Bus 8 at 0.12 s and removed at 0.37 s, an unstable power swing is identified by the distance relay R98 in the RTDS modified WSCC system. The measurements are carried out at Bus 9 and the TZB calculation is performed at the R98 location, i.e. the sending end of transmission Line 1 in Figure 5.2.

The active power P, reactive power Q from Bus 3 to Bus 9 and the voltage E_B is measured by R98 at Bus 9 as shown in Figure 5.27. The TZB method calculated relative speed is shown in Figure 5.28 for the fictitious synchronous machine. After the fault is cleared, the calculated machine relative speed continuously increases from the synchronous speed instead of oscillating as in the stable swing cases. The first deceleration of the fictitious synchronous machine is detected at 0.55 s, i.e. machine speed decreases somewhat but does

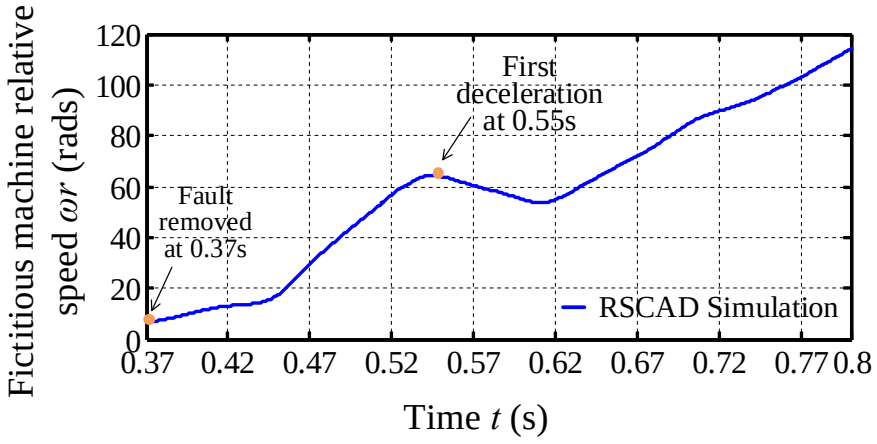

Figure 5.28: Calculated fictitious synchronous machine relative speed for R98 for unstable power swing study in MWSCC system.

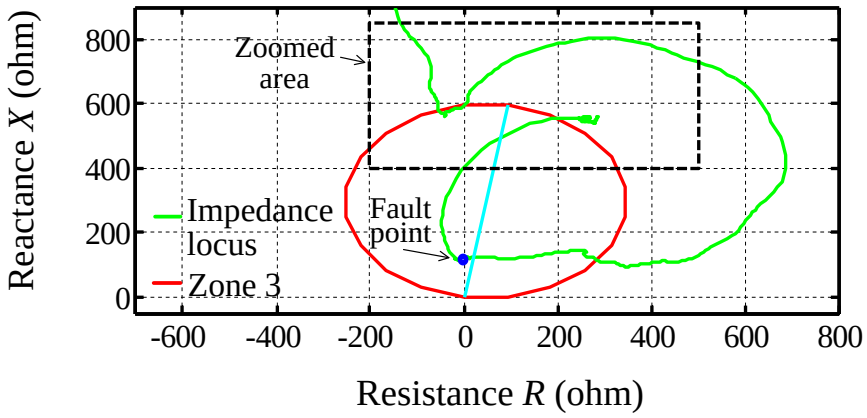

Figure 5.29: Impedance locus superimposed on mho characteristics of relay R98 for unstable study case.

not reach the synchronous speed value and then increases again.

The local measurement of the impedance locus is shown in Figure 5.29 and Figure 5.30. After the fault is cleared, the impedance trajectory leaves the protection zone and fluctuates across the impedance plane. The locus when it enters Zone 3 is detected at 0.52 s as shown in Figure 5.30. The unstable power swing is identified, due to the fact that FZC is not detected

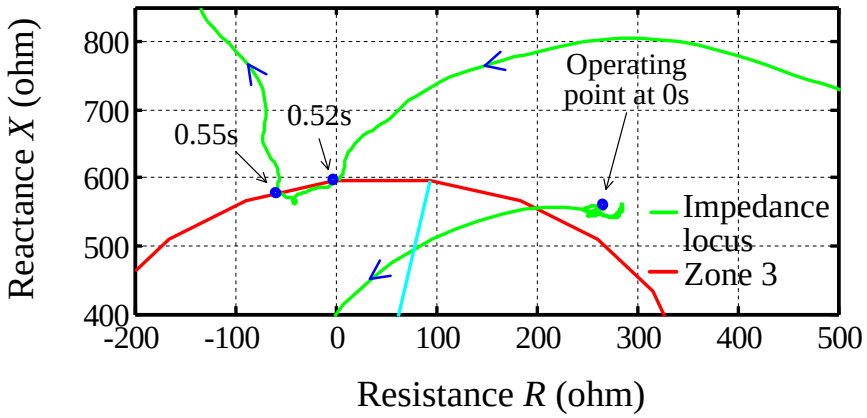

Figure 5.30: Impedance locus shown along with zoomed mho characteristics in Figure 5.29 for R98 for unstable study case.

on the TZB calculated machine relative speed curve as shown in Figure 5.28. When the impedance trajectory is found entering into Zone 3 of R98, as observed in Figure 5.30, the distance relay can be tripped or kept blocked, which depends upon the optimally selected locations for network separation.

5.4.3 Discussions of the Results for Case Studies

In the previous four stable power swing case studies, the TZB testings are carried out under different power swing scenarios when the three-phase faults are applied at different locations in the modified WSCC system in RTDS. In all testing cases FZCs are detected in the short time intervals, i.e. 0.02 s to 0.14 s, after the faults are removed. They are much before the impedance trajectories enter into Zone 3 of the mho relay characteristics as the results of the power swings, as shown in Table 5.1. Therefore, during a stable power swing there is sufficient time to safely block Zone 3 of the distance mho relay R98.

In case the power swing is an unstable one (for example the case study described in Section 5.4.2), FZC of the machine relative speed ω_r does not happen but the relative speed starts increasing again. This is categorized as an out-of-step condition. When the impedance

locus enters into the Zone 3 mho relay characteristics for an out-of-step condition, Zone 3 could still be blocked. This faciliates tripping at selected points to ensure adequate load-generation balance.

It is also observed in Figure 5.10, 5.15, 5.20, 5.25, and 5.29 that the impedance loci of fault are inherently different to the ones during power swings. If a three-phase fault happens during a power swing, the blocked distance relay Zone 3 can be unblocked and let the relay trip as discussed in Section 4.3.5 in Chapter 4.

5.5 TZB and Swing Equation Method(SEM) Comparison

The features of the TZB method have been discussed in the previous sections in the RTDS simulation. The fictitious machine relative speed calculation is also examined by comparing it to the conventional Swing Equation Method to evaluate the validity of the TZB method.

5.5.1 Swing Equation Method

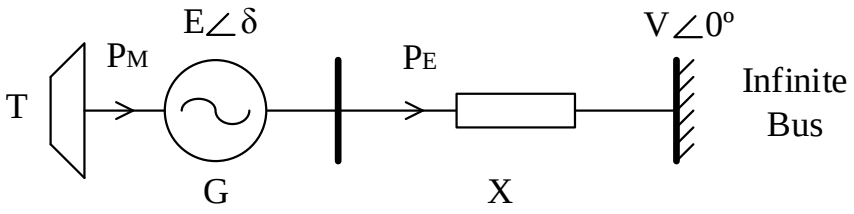

Figure 5.31: Equivalent single machine infinite bus representation of complex power system.

The Swing Equation for rotor motion is based on the simple principle in dynamics that the accelerating torque is equal to the moment of inertia of the rotor times its angular acceleration, as derived in [13].

$$J\frac{d^{\,2}\alpha_m}{dt^2} = T_m - T_e \tag{5.11}$$

where

J the total moment of inertia of the rotor mass, in $kg - m^2$

α_m the angular displacement of the rotor, in mechanical *radians*

t time, in *seconds*

T_m the mechanical torque supplied by the prime mover, in $N - m$

T_e the net electrical or electromagnetic torque, in $N - m$

Since α_m is measured with respect to a stationary reference axis on the stator, it continuously increases with time even at constant synchronous speed. Therefore,

$$\alpha_m = \omega_S t + \sigma_m \tag{5.12}$$

where σ_m is the angular variation with respect to a rotating reference axis on the stator at the synchronous speed.

Multiplying Equation 5.11 by the angular velocity of the rotor, $\omega_m = \dfrac{d\alpha_m}{dt}$, Equation 5.11 becomes

$$M\frac{d^{\,2}\delta}{dt^2} = P_m - P_e \tag{5.13}$$

where $M = J\omega_m$ is the inertia constant of the machine in joule-seconds per mechanical radian; the angular variation σ_m is replaced with δ in electrical radians; P_m is the power supplied by the prime mover and P_e is the electrical power crossing the air gap, when the machine rotational losses and the armature internal resistance losses are neglected.

Swing Equation governs the rotational dynamics of a synchronous machine in stability study, as illustrated on a SMIB system in Figure 5.31. The other form of the Swing Equation 5.13 is written as given by the following

$$\frac{2H}{\omega_S}\frac{d^{\,2}\delta}{dt^2} = P_m - P_e \tag{5.14}$$

or in its equivalent form

$$\frac{2H}{\omega_S}\frac{d\omega}{dt} = P_m - P_e \tag{5.15}$$

where $H = \dfrac{M\omega_S}{2S_{mach}}$ is called the H constant in seconds, provided P_m and P_e is in per unit on the same base as H, and ω_S is the synchronous speed.

From Equation 5.15, replacing $\dfrac{\omega}{\omega_S}$ with ω_{PU}, and by applying Euler's method, the synchronous machine speed can be obtained by integration, then

$$\omega_{PU} = \frac{1}{2H}\int_0^t (\mathrm{P_m} - \mathrm{P_e})\,\mathrm{d}t \tag{5.16}$$

where ω_{PU} is the synchronous machine rotor speed in per unit.

Therefore, the fictitious synchronous machine relative speed ω_r calculated in the TZB method study can also be obtained by the Swing Equation Method and equals to $(\omega_{PU} - 1)$ in per unit.

5.5.2 Parameters Identification for Swing Equation

In order to determine the corresponding Swing Equation, H constant of the equation needs to be identified. Case 2 of the TZB stable swing study is selected as the base case in which the TZB calculated relative speed data are utilized for the regression study.

On the basis of the Swing Equation model of the fictitious machine, the H is identified by employing the $nlinfit$ MATLAB function. The $nlinfit$ function returns a vector of the estimated coefficients for the nonlinear regression of the responses on the predictors using the specified model. The coefficients are determined using the iterative least squares estimation.

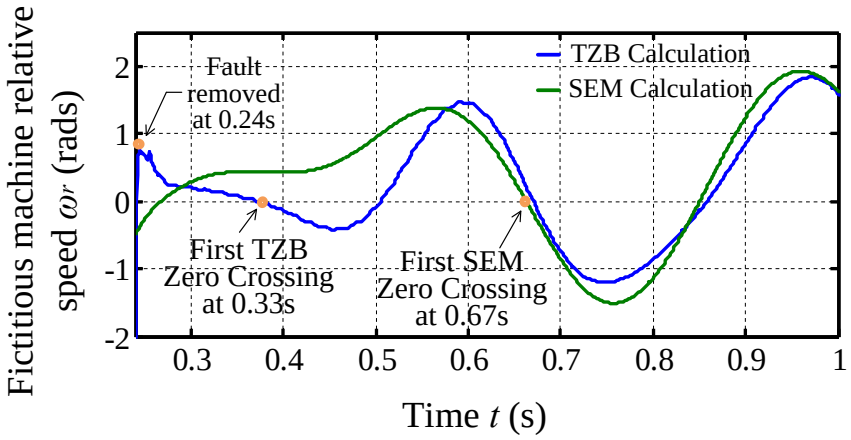

Figure 5.32: TZB compared to SEM calculated fictitious synchronous machine speed at R98 under stable power swing Case 2 in the modified WSCC system.

The group of the data between 0.24 s to 1 s are cut off from the original data for regression. The function starts the parameter estimation with an initial guess and then altering the guess value until the difference between the responses and the model predictors converges and becomes minimum. By doing so, the estimated $H = 1.81$ s.

In Figure 5.32, the blue curve is the TZB method calculated fictitious machine relative speed. After the fault is removed at 0.24 s, FZC is detected at 0.33 s. The green curve in the figure is the machine relative speed out of the SEM model regression with the estimated H constant. The SEM regression is performed under the same system settings as discussed in Section 5.3.1, as well as the same simulation conditions of the TZB method testing discussed in Section 5.4.1.

5.5.3 TZB and Swing Equation Method Comparison

Comparisons are also made to validate the developed TZB method in three stable swing cases, i.e. Case 1, 3, 4, and one unstable swing case by comparing the TZB method calculated machine relative speeds and the Swing Equation model outputs.

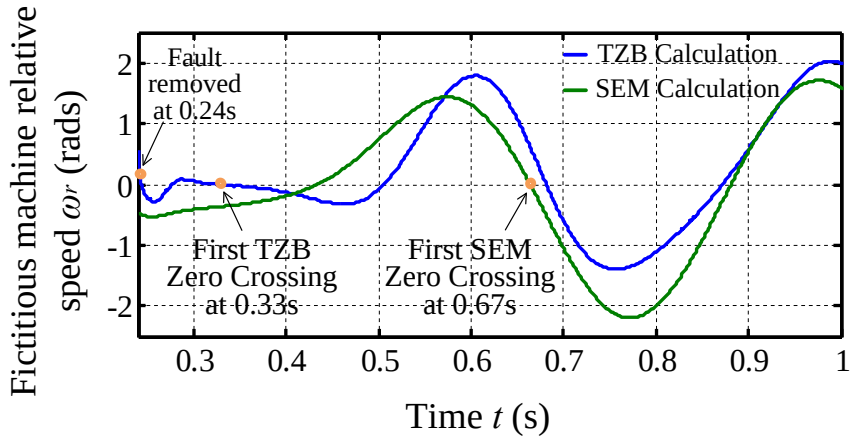

Figure 5.33: TZB compared to SEM calculated fictitious synchronous machine speed at R98 under stable power swing Case 1 in the modified WSCC system.

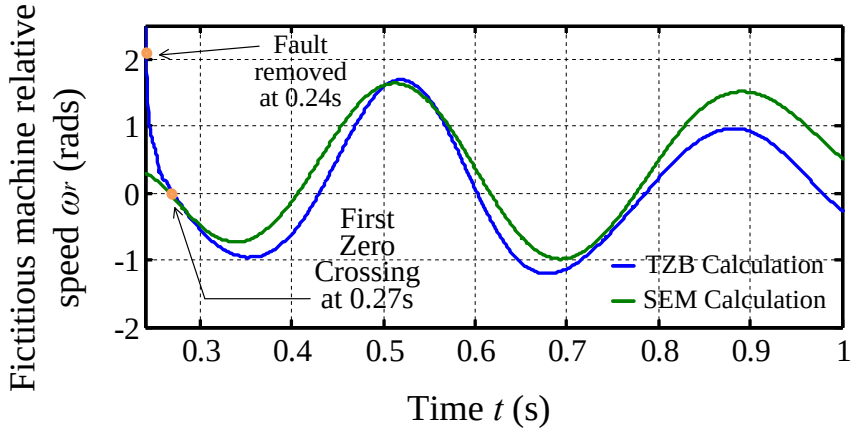

Figure 5.34: TZB compared to SEM calculated fictitious synchronous machine speed at R98 under stable power swing Case 3 in the modified WSCC system.

The SEM calculated ω_r magnitude and phase in the stable Case 1 matches the TZB method calculation in most of the selected duration as shown in Figure 5.33. The SEM calculated ω_r drifts down slightly at the end of the duration, because the electrical power P_e slightly reduces at equilibrium after the disturbance is removed.

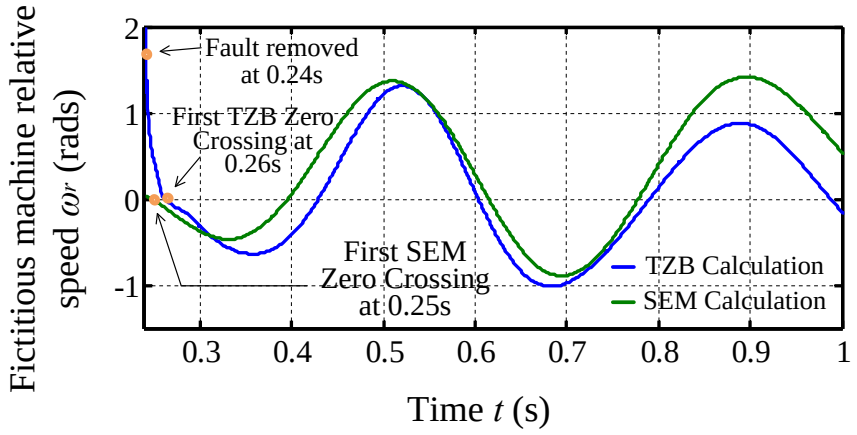

Figure 5.35: TZB compared to SEM calculated fictitious synchronous machine speed at R98 under stable power swing Case 4 in the modified WSCC system.

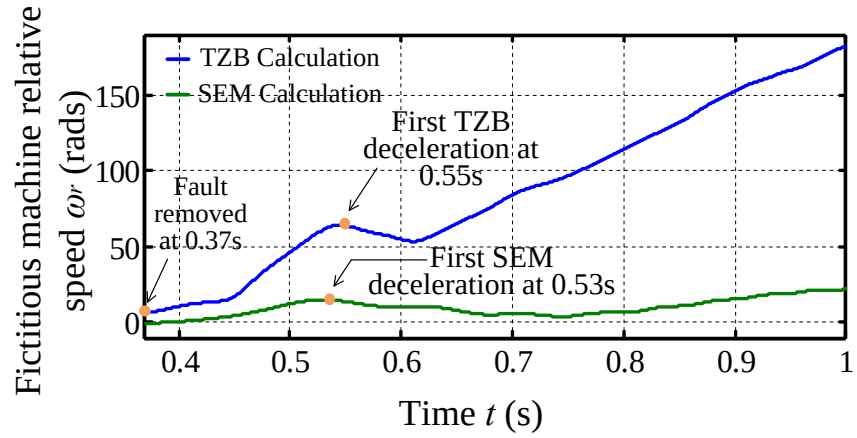

Figure 5.36: TZB compared to SEM calculated fictitious synchronous machine speed at R98 under unstable power swing case in the modified WSCC system.

The correlation of coefficient R is a unitless value to measure how strong a regression is in fitting a observation data curve. The square of the correlation of coefficient, R^2, the coefficient of determination is generally used in the regression results evaluation, which is

formulated as [89]

$$R^2 = 1 - \frac{SS_{res}}{SS_{tot}} \tag{5.17}$$

where SS_{res} is the residual sum of squares; SS_{tot} is the total sum of squares. R^2 is a value between 0 and 1. The closer is R^2 to 1, the stronger is the regression correlated to the observation.

The calculated Coefficient of Determination (COD) R^2 is 0.7943 in the time period from 0.24 to 1.0 s for the Case 1 study, when the TZB method calculation is treated as the observation and the SEM calculation is treated as the prediction. FZC of SEM calculated ω_r is observed at 0.67 s, i.e. 0.34 s behind FZC of the TZB calculation that is at 0.33 s.

In Case 3 (stable scenario), the SEM calculated ω_r magnitude and phase matches the ω_r calculated by the TZB method as shown in Figure 5.34. But at 1.0 s the SEM calculated ω_r drifts because of the electrical power P_e change at equilibrium due to the fault. The calculated R^2 is 0.8046 between the TZB method and the SEM. FZC of the SEM calculated ω_r detected overlaps FZC of the TZB calculated ω_r at 0.27 s.

In Case 4 (stable scenario), the SEM calculated ω_r magnitude and phase matches the ω_r calculated by the TZB method as shown in Figure 5.35. The slight drifting up of the SEM calculated ω_r is observed similar to Case 3 (stable scenario). The calculated R^2 is 0.7840 between the TZB calculation method and the SEM calculation. FZC of the SEM calculated ω_r is found at 0.25 s, close to FZC of the TZB calculation method that is at 0.26 s.

The TZB calculation is also compared to the output of the parameter estimated SEM model in the unstable case study. In the out-of-step scenario, the SEM calculated relative speed ω_r increases away from the synchronous value after the fault is removed at 0.37 s, similar to the TZB method. The first machine deceleration is found at 0.53 s, which is close to the first machine deceleration at 0.55 s obtained from the TZB method. In other words, the machine relative speeds ω_r calculated by the SEM and by the TZB method are in phase.

In summary, the TZB method has been verified by comparing it to the classic SEM calculated ω_r in the stable swing Case 1, 3, 4 and the unstable case of the RTDS TZB

simulations. Following observations can be inferred from the above verification:

- The TZB method is capable of separating stable and unstable power swings and safely blocking the distance relay.
- The fictitious machine relative speed ω_r calculated by the TZB method is generally accurate in stable power swing scenarios.
- The TZB calculated machine relative speed ω_r is not affected by steady state electrical power change due to synchronous machines' velocity drifting after fault, as observed in the ω_r calculation in the SEM application, which makes the TZB method power swing blocking reliable.
- FZC detected by the TZB method can be much earlier than the SEM calculation.

The ω_r magnitude difference is apparent at the instant when a fault is removed between the TZB and the SEM calculated relative speed in above study cases. The inertia term of the Swing Equation plays a vital role so that the ω_r amplitude is damped being smoother than the one calculated by the TZB method. For example, in the stable power swing study, Case 2, the TZB algorithm calculated relative rotor speed decreases after the fault is removed at 0.24 s, and FZC is detected at 0.33 s, i.e. 0.09 s after the fault removal. Whereas, because of the inertia term the oscillations of the relative rotor speed calculated by SEM are reduced, such that FZC is not detected around 0.33 s instead at 0.67 s, i.e. 0.43 s after the fault removal instant, which coincides with the second zero crossing of the TZB calculation. The bottom-line is that both the TZB method and the SEM are able to detect unstable power swings also correctly even though they are at different time instants, which is the primary objective of this research work.

Although it has been proved that the proposed TZB method is fast and reliable, additional precaution should still be taken to ensure the security for the power swing blocking and the correct system separation. In a real industry practice, another power swing identification and blocking scheme can be used as the backup plan to the TZB method, e.g. EAC etc.

5.6 Verification of the DFT Calculations

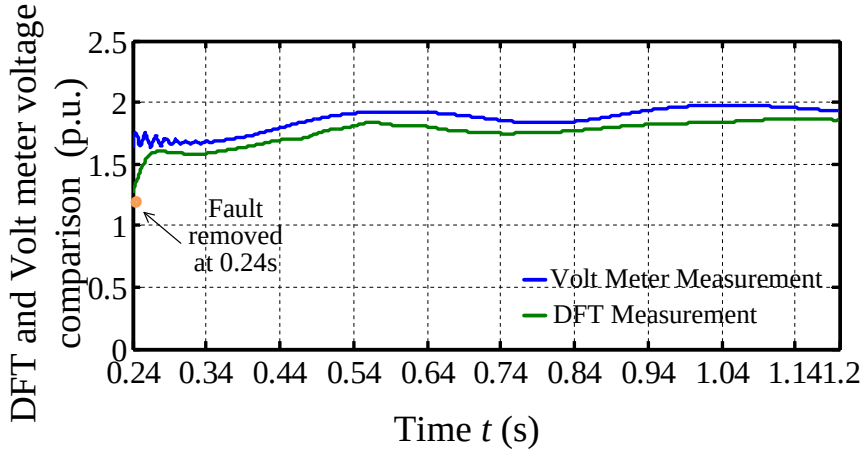

Figure 5.37: DFT compared to Volt meter on voltage measurement of distance relay R98 under power swing in the modified WSCC system.

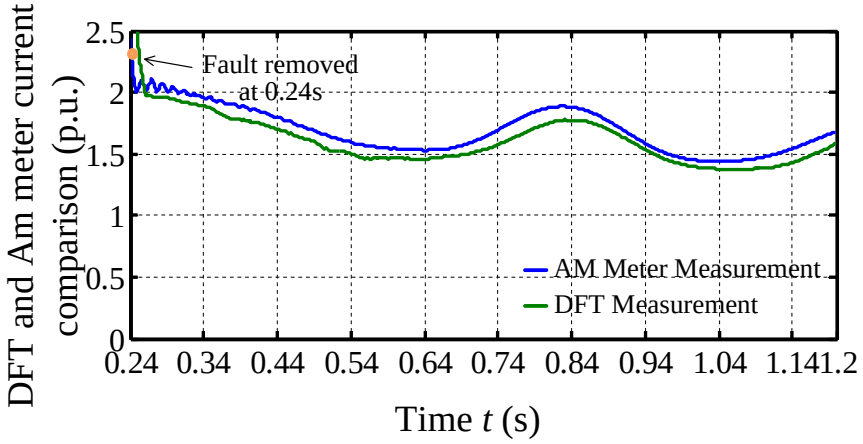

Figure 5.38: DFT compared to Ammeter on current measurement of distance relay R98 under power swing in the modified WSCC system.

The impedance trajectories obtained by the DFT calculations and the distance mho relay Zone 3 characteristics are shown to determine if the relay should be tripped or blocked. The apparent impedance obtained by the relay is the ratio of the voltage and the current measured

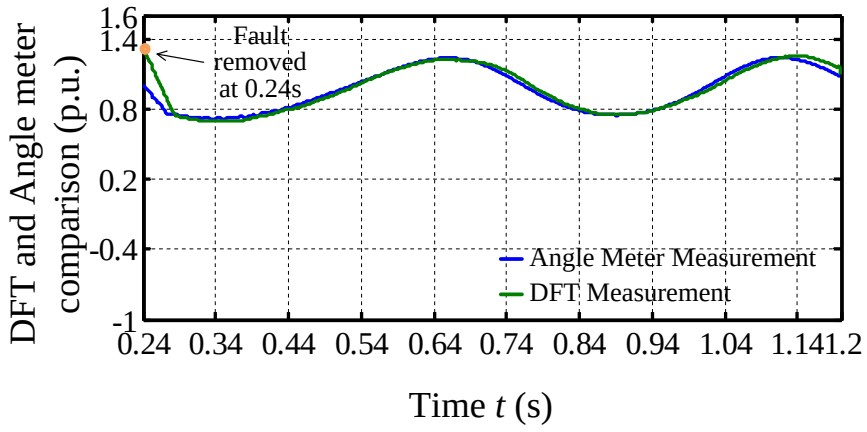

Figure 5.39: DFT compared to Angle meter on phase angle measurement of distance relay R98 under power swing in the modified WSCC system.

at the relay location, as calculated by Equation 5.10. The local sample measurements of V_{A9C} and I_{ASC} are passed through a DFT filter block as discussed in Section 5.3.3.

The accuracy of the phasor values obtained from the DFT calculations is evaluated by comparing it to the voltage/current values obtained from the RMS meter and the phase angle meter measurement available in the Draft module in RSCAD. The local voltage V_{A9C} measured by the DFT and the RMS voltage magnitude of the Voltmeter of R98 at Bus 9 are shown in Figure 5.37 during a stable power swing after a 0.12 s three-phase to ground fault is applied and removed at Bus 8 in the modified WSCC system. The local DFT current I_{ASC} and the RMS Ammeter output measured at the sending end of the transmission Line 1 are shown in Figure 5.38 in the same case study after the fault is removed. The DFT measured impedance angle of Z_{A9C} is compared to the phase angle measured by the Angle Meter between V_{A9C} and I_{ASC} as shown in Figure 5.39.

The results match well over transient and steady-state for both the voltage and the current magnitude. The DFT voltage outputs are slightly less than the values obtained from the RMS meters (the same thing happens for the DFT current outputs as well). This is because of the losses in the sampling and averaging effect in the DFT circuits. Nevertheless, the measured impedance Z_{A9C} from the distance relay matches well with the RMS meter

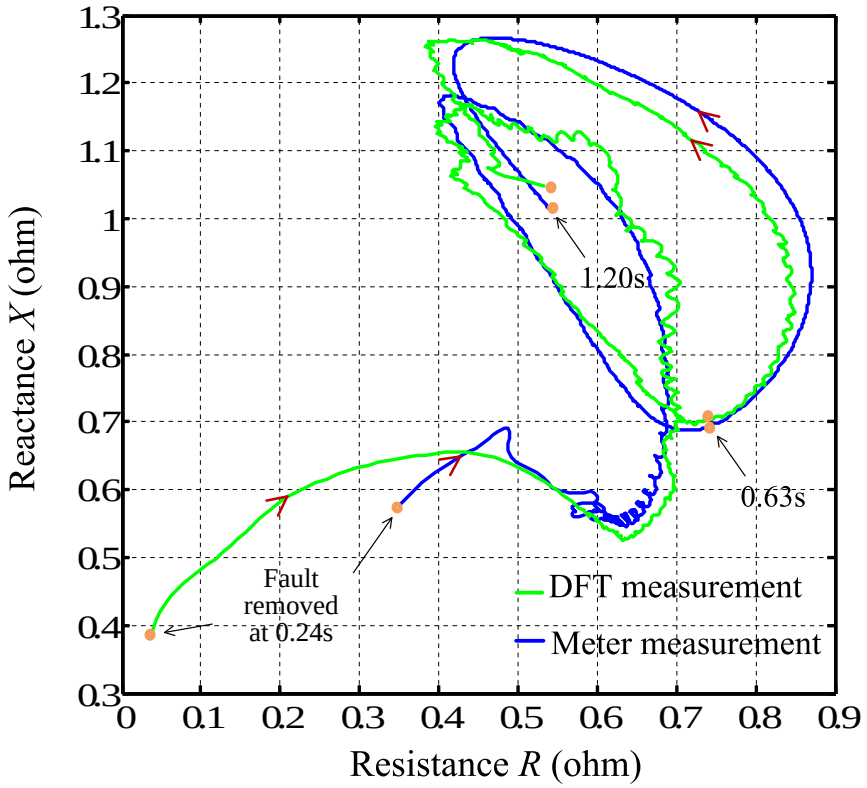

Figure 5.40: DFT compared to RMS meter on impedance measurement of distance relay R98 under power swing in the modified WSCC system.

measured impedance trajectories as shown in Figure 5.40. The calculated COD R^2 is 0.85 when the DFT calculation is treated as the regression and the RMS meter measurement is treated as the observation.

5.7 Summary

This chapter discussed the TZB method in detail using the electromagnetic simulation with RTDS. The practical issues were taken into consideration using the RTDS simulations. The modified WSCC system was developed in the Draft module in RSCAD.

The transmission lines were modeled as the travelling wave lines in kilometers by using

the TLINE program instead of the lumped parameters representations in per unit. The DFT simulation blocks were used for obtaining the phasor values for the local electrical quantities for the TZB calculation method.

The off-nominal frequency of operation of synchronous machines was taken into account in the studies. The generator frequency is determined by the sum of the torques acting on the total inertia of the machine. The TZB method was tested for different stable power swing cases scenarios which were generated by applying the three-phase to ground faults at different locations in the test system. The TZB method for detecting out-of-step condition was also discussed. This chapter discussed several simulation results for validating the effectiveness of the TZB method for blocking Zone 3.

The relative speed ω_r values calculated with the proposed TZB method was compared with the commonly used SEM for stability studies, and the finding was that the two speeds values obtained matched well. The impedance values calculated with the DFT filter were also verified.

Chapter 6

Summary and Conclusions

6.1 Summary

Chapter 1 discussed the impact of power system outages, power system stability, power swings, distance relaying, Zone 3 blocking, etc, which was followed by a discussion on research objectives and thesis organization. Distance relays provide protection to transmission lines by measuring the impedance at the relay location which is proportional to the distance to the fault point. Distance relays have advantages over its counterparts, such as greater trip coverage, greater sensitivity, ease of setting, fixed zone of protection, relatively independent of system and load changes.

Under a steady state operating condition, a power balance exists between generated and consumed active and reactive electrical powers in a power system. When a large disturbance happens, there is a sudden and large change in electrical power values, which results in power swing, i.e. the variation of power flows when the internal voltage of generators at different locations of the power system start slipping relative to each other. As discussed in the thesis it is important to block the third zone protection quickly so that the power system could be kept secure. On the other hand, if it is an unstable power swing, i.e. out-of-step phenomenon, portions of the grid need to be isolated at optimal locations to minimize its impact on the system.

Chapter 2 discussed various methodologies for power swing identification. The methodologies were categorized under broad headings: the methods based on finding ***Energy Equilibrium***, ***Impedance Trajectory Tracking methods***, ***Pattern Recognition ap-***

proaches. The methods which use *Energy Equilibrium* analysis were *Equal Area Criteria (EAC), Time Domain EAC, Extended EAC, Adaptive Extended EAC, State Plane Analysis method, Wavelet Transform method, State Deviation method*, and *Swing-Centre Voltage (SCV) method*, etc. The methods about *Impedance Trajectory Tracking* were *Blinder based schemes, Concentric Characteristics schemes, Basic Characteristic Repositioning methods, Continuous Impedance Calculation method*, and *R-dot method*, etc. *Pattern Recognition approaches* include *Support Vector Machine method, Fuzzy Inference System method, Artificial Neural Network detection method*, etc. Chapter 2 also discussed the recent researches that have appeared in the literature on Zone 3 protection and blocking methods. It is clear from the past research works reported that Zone 3 protection is more vulnerable than Zone 1 and Zone 2 to misoperation due to power swings.

In Chapter 3, the proposed TZB method was discussed. It was based on the assumption that a complex power network can be approximated by a SMIB system at the relay location [39]. The phase one of the algorithm was to calculate the SMIB system impedance employing the locally measured electrical quantities only. With the calculated system impedance, the phase two of the algorithm was calculating the fictitious synchronous machine relative speed in real time. A stable power swing or an out-of-step phenomenon was determined tracking the relative speed variation of the fictitious synchronous machine rotor. If it went through a FZC then it was a stable swing; if it went down and then started increasing without a zero crossing or if it increased continuously then it was an unstable swing. The proposed TZB method (fictitious synchronous machine relative speed calculations) was illustrated using SIMB system simulations (PSCAD/EMTDC simulations). The fictitious machine relative speed was also compared with the generator relative speed value obtained from PSCAD/EMDTC simulations to verify the correctness of the TZB approach.

In Chapter 4, the proposed TZB method was tested on a modified WSCC system utilizing phasor based simulations in a PSAT environment. The sample results for two different distance relays at two different locations in the system were shown in the chapter. The test results demonstrated the effectiveness of the TZB method that it can be applied in real-time. The FZCs could be detected much before the impedance locus enters into Zone 3 of

the distance relay, and the relay could be safely blocked and not misoperate during stable power swings. The TZB method was also compared with a conventional distance relay blocking method (a Double Polygon Blinder scheme), and the advantages of the proposed TZB method were discussed. The calculation of the current for the distance relay was also verified in the final section of Chapter 4.

In Chapter 5, the TZB method was verified using electromagnetic simulations in RTDS for the modified WSCC system. DFT was used for deriving the local phasors of currents and voltages from their instantaneous values just like how they are obtained in a digital/numerical relay. The results for TZB for the stable power swings as well as a sample of the out-of-step condition results were given. The relative speed calculations using the proposed method were compared with those obtained using the classical electro-mechanical Swing Equation Method (SEM).

6.2 Research Contributions

The broader contribution of this research work is developing a power swing identification, and a blocking methodology for blocking Zone 3 distance relays purely from local measurements. The contributions made in the thesis are summarized below:

- *SMIB equivalenting method:* The new method proposed in the thesis is to find a simplified SMIB representation of a complex power system network at every sampling instant using the power-angle equations and the purely local voltage and current measurements. The voltage and current phasors are obtained by doing a DFT of a full cycle of voltage and currrent samples.

- *Stable or Unstable Power Swing Identification:* The proposed algorithm is to find the FZC of the calculated relative speed ω_r. Stable or unstable power swings can be explicitly distinguished by detecting whether the calculated relative speed ω_r goes through a zero crossing or not. The proposed TZB method has been compared with a conventional Double Polygon Blinder scheme widely used in research literatures and

industries.

6.3 Conclusions

The following conclusions can be drawn from the research work:

- The proposed TZB method is a reliable methodology to block distance relays during a power swing. It does not require offline studies to determine the parameters. It identifies power swings using system equilibrium principles, and there is no need to do extensive stability analyses beforehand.
- The TZB is a more practical approach. The inputs to TZB method are local measurements available at the distance relay location, and the scheme is more suited for protection compared to a wide area based scheme.
- The TZB method can be applied to any sized system without prior knowledge of the existing network, so the method can be easily adapted to any configuration of the system.

6.4 Future Work

The following are future recommended works:

- *Testing TZB method on a MRO or an AESO system:* The TZB method was tested with a standard SMIB system and a modified WSCC 10-bus system, respectively. The scheme was also tested with the PSAT phasor based simulations and the more accurate real-time based electromagnetic simulations using RTDS. Testing the proposed scheme with the Canadian utility system such as Midwest Reliability Organization (MRO) or Alberta Electric System Operator (AESO) system would give an opportunity to verify the practical usefulness of the approach.

- *Hardware-in-the-loop testing in RTDS:* Offline studies were used for testing the approach in this thesis work. The proposed algorithm could be implemented in a DSP or FPGA hardware and tested with RTDS in a hardware-in-the-loop fashion just like an actual numerical relay.

- *Further investigation during out-of-step conditions:* The focus of the current research work was on power swing identification and blocking of the third zone distance relay. The TZB method was able to quickly find stable or unstable power swings and quickly find the FZC of the relative speed for the fictitious machine relative speed variation. The magnitude of ω_r was found to be larger than the value obtained from a SEM during out-of-step conditions. The proposed TZB algorithm could be improved further to get a more accurate prediction of the relative machine speed.

- *Investigation on AURORA:* After a major disturbance event happens, the power grid separates into islands due to out-of-step conditions. Before any automatic reclosing happens there needs to be an adequate precaution in place to Avoid Unwanted Reclosing On Rotating Apparatus (AURORA) to eliminate the possibility of the damage of rotating electrical equipment from reconnection [90]. AURORA is a very hot topic in IEEE Power System Relaying Committee (PSRC) and power utility industries. Investigations on AURORA type scheme utilizing the TZB type method could be a good topic for the further research.

References

[1] R. Gokaraju, *EE868 Digital techniques for power system protection course notes.* Department of Electrical & Computer Engineering University of Saskatchewan, 2011.

[2] P. M. Anderson and A. A. Fouad, *Power System Control and Stability.* John Wiley & Sons, Inc., 2004.

[3] "IEEE guide for protective applications to transmission lines," The Institute of Electrical and Electronics Engineer, Inc., Tech. Rep., September 1999.

[4] W. A. Elmore, *Protective Relaying Theory and Applications.* Marcel Dekker, Inc., 2004.

[5] S. Paudyal, "Out-of-Step Protection Using Energy Equilibrium Criterion in The Time Domain," Master's thesis, University of Saskatchewan, Saskatchewan, Canada, 2008.

[6] M. McDonarld and et al., "Power swing and out-of-step considerations on transmission lines," IEEE PSRC Working Group D6, Tech. Rep., Jun 2005.

[7] Binod Shrestha, "A Fast Method for Out-of-Step Protection Using State Plane Trajectories Analysis," Master's thesis, University of Saskatchewan, Saskatchewan, Canada, 2011.

[8] J. Blumschein, Y. Yelgin, and M. Kereit, "Blackout prevention by power swing detection and out-of-step protection," *Journal of Power and Energy Engineering*, vol. 2, pp. 694–704, April 2014.

[9] W. Rebizant and K. Feser, "Fuzzy logic application to out-of-step protection of generators," in *Power Engineering Society Summer Meeting, 2001*, Vancouver, Canada, July 2001.

[10] A. Y. Abdelaziz, M. R. Irving, M. M. Mansour, A. M. EI-Arabaty, and A. I. Nosseir, "Adaptive protection strategies for detecting power system out-of-step conditions using neural networks," *IEE Proceedings - Generation, Transmission and Distribution*, vol. 145, no. 4, pp. 387–394, July 1998.

[11] G. Benmouyal, E. O. Schweitzer, and A. Guzman, "Synchronized phasor measurement in protective relays for protection, control, and analysis of electric power systems," Schweitzer Engineering Laboratories, Inc., Tech. Rep., 2002.

[12] D. Kang and R. Gokaraju, "A new method for blocking third-zone distance relay during stable power swings," *IEEE Transactions on Power Delivery*, vol. 31, no. 4, pp. 1836–1843, January 2016.

[13] W. Stevenson, *Elements of Power System Analysis*. McGraw-Hill Book Company, 1982.

[14] "Application of overreaching distance relays," IEEE PSRC Working Group D4, Tech. Rep., 2009.

[15] J. C. Tan, P. A. Crossley, P. G. McLaren, P. F. Gale, I. Hall, and J. Farrell, "Application of a wide area backup protection expert system to prevent cascading outages," *IEEE Transactions on Power Delivery*, vol. 17, no. 2, pp. 375–380, April 2002.

[16] J. L. Blackburn and T. J. Domin, *Protective Relaying Principles and Applications*. Marcel Dekker, Inc., 1987.

[17] V. Madani, D. Novosel, S. Horowitz, M. Adamiak, J. Amantegui, D. Karlsson, S. Imai, and A. Apostolov, "IEEE PSRC Report on global industry experiences with system integrity protection schemes (SIPS)," *IEEE Transactions on Power Delivery*, vol. 25, no. 4, pp. 2143–2155, October 2010.

[18] A. G. Phadke and J. S. Thorp, *Computer Relaying for Power Systems*. Wiley India Pvt. Ltd., 2012.

[19] S. H. Horowitz and A. G. Phadke, *Power System Relaying*. John Wiley and Sons, Ltd, 2008.

[20] "ANSI/IEEE C37.90 IEEE Standard for relays and relay systems associated with electric power apparatus," The Institute of Electrical and Electrionics Engineers, Inc., Tech. Rep., 1989.

[21] R. K. Aggarwal and et al., *Power System Protection*. The Institution of Electrical Engineers, London, United Kingdom, 1997.

[22] S. Raman, R. Gokaraju, and A. Jain, "An adaptive fuzzy mho relay for phase backup protection with infeed from statcom," *IEEE Transactions on Power Delivery*, vol. 28, no. 1, pp. 120–128, January 2013.

[23] K. K. Li, L. L. Lai, and A. K. David, "Stand along intelligent digital distance relay," *IEEE Transactions on Power Systems*, vol. 15, no. 1, pp. 137–142, February 2000.

[24] *Applicatioon manual REL 531*2.3 High speed line distance protection terminal*. ABB Automation Technology Products AB, 2003.

[25] "Wide area protection of emergency control," IEEE PES-PSRC-SPS Working Group C6, Tech. Rep., May 2003.

[26] N. Kosterev, W. Taylor, and A. Mittelstadt, "Model validation for the August 10, 1996 WSCC system outage," *IEEE Transactions on Power Systems*, vol. 14, no. 3, August 1999.

[27] S. Lim, C. Liu, S. Lee, M. Choi, and S. Rim, "Blocking of zone 3 relays to prevent cascaded events," *IEEE Transactions on Power Systems*, vol. 23, no. 2, pp. 747–754, May 2008.

[28] S. H. Horowitz and A. G. Phadke, "Third zone revisited," *IEEE Transactions on Power Delivery*, vol. 21, no. 1, pp. 23–29, January 2006.

[29] "August 14, 2003 Blackout: NERC Actions to prevent and mitigate the impacts of future cascading blackouts," North American Electrical Reliability Council, Princeton, NJ, Tech. Rep., February 10, 2004.

[30] "Final report on the August 14, 2003 blackout in the United States and Canada: Causes and recommendations," U.S.-Canada Power System Outage Task Force, Tech. Rep., April, 2004.

[31] G. Benmouyal, D. Tziouvaras, and D. Hou, "Zero-setting power-swing blocking protection," in *Proceedings of the 31st Annual Western Protective Relay Conference*, Spohane,WA, October 2004.

[32] J. Mooney and N. Fischer, "Application guidelines for power swing detection on transmission systems," Schweitzer Engineering Laboratories, Inc., Tech. Rep., 2005.

[33] C. W. Taylor, J. M. Haner, L. A. Hill, W. A. Mitttelstadt, and R. L. Cresap, "A new out-of-step relay with rate of change of apparent resistance augmentation," *IEEE Transactions on Power Apparatus and Systems*, vol. 102, no. 3, pp. 631–639, March 1983.

[34] S. Brahma, "Use of wavelets for out-of-step blocking function of distance relays," in *Power Energy Society General Meeting*, Canada, June 2006.

[35] K. Seethalekshmi, S. N. Singh, and S. C. Srivastava, "SVM based power swing identification scheme for distance relays," in *IEEE Power and Energy Society General Meeting*, Minneapolis, USA, 2010.

[36] A. K. Jain, J. Mao, and K. M. Mohiuddin, "Artificial neural networks: A tutorial," *IEEE Computer*, pp. 31–44, March 1996.

[37] K. P. Nayak, K. A. Pradhan, and P. Bajpai, "Secured zone 3 protection during stressed condition," *IEEE Transactions on Power Delivery*, vol. 30, no. 1, pp. 89–96, February 2015.

[38] A. G. Phadke and J. S. Thorp, *Synchronized Phasor Measurements and Their Applications*. Springer Science+Business Media, LLC., 2008.

[39] Y. Xue, T. V. Cutsem, and M. Ribbens Pavella, "Extended equal area criterion justifications, generalizations, applications." *IEEE Transactions on Power Systems*, vol. 4, no. 1, pp. 44–52, Feburary 1989.

[40] V. Centeno, A. G. Phadke, A. Edris, J. Benton, M. Gaudi, and G. Michel, "An adaptive out-of-step relay," *IEEE Transactions on Power Delivery*, vol. 12, no. 1, pp. 61–67, January 1997.

[41] M. Ariff and B. C. Pal, "Adaptive protection and control in the power system for wide-area blackout prevention," *IEEE Transactions on Power Delivery*, vol. 31, no. 4, August 2016.

[42] B. Shrestha, R. Gokaraju, and M. Sachdev, "Out-of-step protection using state-plane trajectories analysis," *IEEE Transactions on Power Delivery*, vol. 28, no. 2, April 2013.

[43] C. Sriram, D. R. Kumar, and G. S. Raju, "Blocking the distance relay operation in third zone during power swing using polynomial curve fitting method," in *2014 International Conference on Smart Electric Grid(ISEG)*, Guntar, India, 2014.

[44] S. Paudyal, R. Gokaraju, and S. M. Sachdev, "Application of equal area criterion conditions in the time domain for out-of-step protection," *IEEE Transactions on Power Delivery*, vol. 25, no. 2, pp. 600–609, January 2010.

[45] *IEEE Guide for AC Generator Protection*. IEEE Power Engineering Sociaty, 2007.

[46] M. A. M. Ariff, B. C. Pal, and A. K. Singh, "Estimating dynamic model parameters for adaptive protection and control in power system," *IEEE Transactions on Power Systems*, vol. 30, no. 2, March 2015.

[47] M. A. M. Ariff and B. C. Pal, "Coherency identification in interconnected power system-an independent component analysis approach," *IEEE Transactions on Power Systems*, vol. 28, no. 2, May 2013.

[48] Y. Cui, R. Kavasseri, and S. Brahma, "Dynamic state estimation assisted out-of-step detection for generators using angular difference," *IEEE Transactions on Power Delivery*, October 2016.

[49] S. H. Zak, *System and Control*. Oxford University Press, Inc, 2003.

[50] P. Sharma, "Fast Methods for Transient Stability Prediction in Large Power Systems and Wind Integrated Power Systems," Master's thesis, University of Saskatchewan, Saskatchewan, Canada, 2013.

[51] J. Machowski and D. Nelles, "New power swing blocking method," in *Developments in Power System Protection*, United Kingdom, March 1997.

[52] S. M. Brahma, "Distance relay with out-of-step blocking function using wavelet transform," *IEEE Transactions on Power Delivery*, vol. 22, no. 3, pp. 1360–1366, July 2007.

[53] H. A. Osman and P. O. Malik, "Transmission line distance protection based on wavelet transform," *IEEE Transactions on Power Delivery*, vol. 19, no. 2, pp. 515–523, April 2004.

[54] K. P. Nayak, G. J. Rao, P. Kundu, K. A. Pradhan, and P. Bajpai, "A comparative assessment of power swing detection techniques," in *Joint International Conference on Power Electronics, Drive and Energy Systems*, India, December 2010.

[55] M. J. Domzalski, P. K. Nickerson, and R. P. Rosen, "Application of mho and quadrilateral distance characteristics in power systems." in *7th Conference of Developments in Power System Protection*, Amsterdam, Netherland, 2001.

[56] G. Multilin, *D60 Line Distance Relay Instruction Manual r4.8x*. GE Multilin, 2005.

[57] J. M. Haner, T. D. Laugh, and C. W. Taylor, "Experience with the r-rdot out-of-step relay," *IEEE Transactions on Power Delivery*, vol. 1, no. 2, pp. 35–39, April 1986.

[58] Z. D. Gao and G. B. Wang, "A new power swing block in distance protection based on a microcomputer principle and performance analysis," in *in Proc. International Confer-*

ence on Advances in Power System Control Operation and Management, Hong Kong, 1991, pp. 623–628.

[59] F. Dernoncourt, "Introduction to fuzzy logic," Massachusetts Institute of Technology, Tech. Rep., January 2013.

[60] A. G. Phadke, J. S. Thorp, and M. G. Adamiak, "A new measurement technique for tracking voltage phasors, local system frequency, and rate of change of frequency," *IEEE Transactions on Power Apparatus and Systems*, vol. PAS-102, no. 5, pp. 1025–1038, May 1983.

[61] *IEEE Standard for Synchrophasors for Power Systems.* IEEE Power Engineering Sociaty, 2005.

[62] P. Kundu and K. A. Pradhan, "Synchrophasor-assisted zone 3 operation," *IEEE Transactions on Power Delivery*, vol. 29, no. 2, pp. 660–667, April 2014.

[63] A. El Hadidy and C. Rehtanz, "A new algorithm to improve the operation of distance relays zone 3 by using synchronized phasor measurements," in *Modern Electric Power Systems 2010*, Wroclaw, Poland, 2010.

[64] V. Centeno, J. De-la Ree, A. G. Phadke, G. Michel, J. Murphy, and R. Burnett, "Adaptive out-of-step relaying using phasor measurement techniques," *IEEE Computer Applications in Power*, vol. 6, no. 4, pp. 12–17, October 1993.

[65] "Application consideration of IEC 61850/UCA 2 for substation ethernet local area network communication for protection and control," IEEE PSRC Working Group H6, Tech. Rep., May 2005.

[66] "IEC 61850 Communication networks and systems in substations," International Electrotechnical Commission, Tech. Rep., 2003.

[67] "IEC 61968 Application integration at electric utilities - system interfaces for distribution management," International Electrotechnical Commission, Tech. Rep., 2003.

[68] "IEC 61970 Energy management system application program interface," International Electrotechnical Commission, Tech. Rep., 2006.

[69] "Final report on the August 14, 2003 blackout in the united states and canada: causes and recommendations," U.S.-Canada Power System Outage Task Force, Tech. Rep., April 2004.

[70] M. S. Sachdev and M. A. Baribeau, "A new algorithm for digital impedance relays," *IEEE Transactions on Power Apparatus and Systems*, vol. PAS-98, no. 6, November 1979.

[71] "Increase line loadability by enabling load encroachment functions of digital relays," North American Electrical Reliability Council, Princeton, NJ, Tech. Rep., December 7, 2005.

[72] Si Chen, "Network Reduction in Power System Analysis," Master's thesis, Technical University of Denmark, Lynby, Denmark, 2009.

[73] *PSCAD Visual Simulation FOR POWER SYSTEMS - PSCAD X4 Online Help.* Manitoba HVDC Research Centre, 2013.

[74] *EMTDC Transient Analysis for PSCAD Power System Simulation.* Manitoba HVDC Research Centre Inc., April 2005.

[75] *PSCAD Power System Computer Aided Design.* Manitoba HVDC Research Centre Inc., April 2005.

[76] R. H. Park, "Two-reaction theory of synchronous machines-generalized method of analysis part i," *Transactions of the American Intitute of Electrical Engineers*, vol. 48, no. 3, pp. 716–727, July 1929.

[77] C. Concordia, "Two-reaction theory of synchronous machines with any balanced terminal impedance," *Electrical Engineering*, vol. 56, no. 9, pp. 1124–1127, September 1937.

[78] F. Milano, "An open source power system analysis toolbox," *IEEE Transactions on Power Systems*, vol. 20, no. 3, Auguest 2005.

[79] Federico Milano, *PSAT Power System Analysis Toolbox*. University of Waterloo, Canada, 2008.

[80] D. Hou, S. Chen, and S. Turner, *SEL-321-5 relay out-of-step logic*. Schweitzer Engineering Laboratories, Inc. Application Guide AG97-13, July 1997.

[81] F. Plumpire, S. Brettschneider, A. Hiebert, M. Thompson, and M. Mynam, "Validation of out-of-step protection with a Real Time Digital Simulator," BC Hydro, Cegertec, BC Transmission Corporation, and Schweitzer Engineering Laboratories, Inc., Tech. Rep., 2006.

[82] P. Forsyth and R. Kuffel, "Utility applications of a RTDS Simulator," in *The 8th International Power Engineering Conference, (IPEC2007)*, Singapore, 2007, p. 6.

[83] *RTDS HAREWARE MANUAL*. RTDS Technologies Inc., January 2012.

[84] *REAL TIME DIGITAL SIMULATOR POWER SYSTEM USER'S MANUAL*. RTDS Technologies Inc., December 2012.

[85] *RTDS OVERHEAD LINE CONSTANTS MANUAL*. RTDS Technologies Inc., OCTOBER 2014.

[86] *REAL TIME DIGITAL SIMULATOR TUTORIAL MANUAL*. RTDS Technologies Inc., JUNE 2015.

[87] *REAL TIME DIGITAL SIMULATOR CONTROL LIBRARY MANUAL*. RTDS Technologies Inc., JULY 2013.

[88] *Aluminum Conductor Steel Reinforced ACSR Cables*. Alcan Products Corporation, January 2008.

[89] S. A. Glantz and B. K. Slinker, *Primer of Applied Regressin and Analysis of Variance*. McGraw-Hill, Inc, 1990.

[90] M. Reichard and et al., "Avoiding unwanted reclosing on rotating apparatus (aurora)," IEEE PSRC Working Group J7, Tech. Rep., Jan 2017.

[91] W. H. Press, S. A. Teukolski, W. T. Vetterling, and B. P. Flannery, *Numerial Receipes in Fortran77*. Press Syndicate of the University of Cambridge, 1992.

[92] W. Press, S. A. Teukolski, W. T. Vetterling, and B. P. Flannery, *Numerial Receipes in Fortran90*. Press Syndicate of the University of Cambridge, 1996.

[93] H. Moller, "Convergence and visualization of laguerre's rootfinding algorithm," *https://wwwmath.uni-muenster.de/u/mollerh/data/LaguerreMoeller.pdf*, 2014.

[94] A. E. Fitzgerald, C. Kingsley, and S. D. Umans, *Electric Machinery*. McGraw Hill, Inc., 1983.

[95] E. W. Kimbark, *Power System Stability*. John Wiley & Sons, Inc., 1964.

[96] P. Kundur, *Power System Stability and Control*. Tata McGraw-Hill Companies, Inc., 1994.

Appendix A

Digital Techniques for Power System Protection

A.1 SMIB system representation

The basic formulation is introduced in [39] on SMIB system representation of a complex power network as the followings. The motion of a multi-machine system is described by

$$\frac{d\delta_i}{dt} = \omega_i, \quad M_i \frac{d\omega_i}{dt} = P_{mi} - P_{ei}, \tag{A.1}$$

where

$$P_{ei} = {E_i}^2 Y_{ii} \cos\theta_{ii} + \sum_{j=1, j\neq i}^{n} E_i E_j Y_{ij} \cos(\delta_i - \delta_j - \theta_{ij}), \tag{A.2}$$

and the notation in the formulas are listed as the following:

δ_i	the rotor angle
$\frac{d\delta_i}{dt}$	the rotor speed
M_i	the inertia constant
$P_{mi}(P_{ei})$	the mechanical input (electrical output) power
E_i	the voltage behind the direct axis transient reactance
Y	the admittance matrix reduced at the internal generator nodes
$Y_{ij}(\theta_{ij})$	the modulus (argument) of the ij^{th} element of Y

where M_i, P_{mi} and E_i are regarded as constants throughout the transients, and loads are modelled as constant impedances. With the basic formulation, the multi-machine system can be reduced into an equivalent two-machine aggregated model. If the following notations are defined

s	the specific critical cluster consist of critical machine only
A	the set of all remaining machines
a	one machine equivalent of all remaining machines

The partial center of angles (PCOA) of remaining machines is given as

$$\delta_a = \sum_{k \in A} \frac{M_k \delta_k}{M_a}; \quad M_a = \sum_{k \in A} M_k; \tag{A.3}$$

and the motion of the equivalent machine of the remaining machines becomes

$$M_a \frac{d^2 \delta_a}{dt^2} = \sum_{k \in A} (P_{mk} - P_{ek}) \tag{A.4}$$

Upon assuming

$$\delta_k = \delta_a \quad \forall k \in A \tag{A.5}$$

we have

$$P_{ek} = {E_k}^2 Y_{kk} \cos\theta_{kk} + E_k E_s Y_{ks} \cos(\delta_a - \delta_s - \theta_{ks}) + \sum_{j \in A, j \neq k} E_k E_j Y_{kj} \cos\theta_{kj}, \tag{A.6}$$

For the specific candidate critical machine, we get

$$M_s \frac{d^2 \delta_s}{dt^2} = (P_{ms} - P_{es}) \tag{A.7}$$

$$P_{es} = {E_s}^2 Y_{ss} \cos\theta_{ss} + \sum_{k \in A} E_s E_k Y_{sk} \cos(\delta_s - \delta_a - \theta_{sk}) \tag{A.8}$$

The two machine aggregated model can be further reduced to an equivalent SMIB system with a single-machine parameter δ, ω, M, P_m, P_e. Making

$$\delta \triangleq \delta_s - \delta_a \tag{A.9}$$

The motion of equivalent SMIB system can be described by the following formula

$$M\frac{d^2\delta}{dt^2} = P_m - [P_c + P_{max}\sin(\delta - \phi)] \tag{A.10}$$

where

$$M = \frac{M_s M_a}{M_T}; \quad M_T = \sum_{i=1}^{n} M_i \tag{A.11}$$

$$P_m = \frac{(M_a P_{ms} - M_s \sum_{k\in A} P_{mk})}{M_T} \tag{A.12}$$

$$P_c = \frac{(M_a E_s^2 G_{ss} - M_s \sum_{k,j\in A} E_k E_j G_{kj})}{M_T} \tag{A.13}$$

$$P_{max} = \sqrt{C^2 + D^2}; \quad \phi = -tan^{-1}\frac{C}{D} \tag{A.14}$$

$$C = \frac{(M_a - M_s)}{M_T}\sum_{k\in A} E_s E_k G_{sk}; \quad D = \sum_{k\in A} E_s E_k B_{sk} \tag{A.15}$$

where δ and M are the rotor angle and inertia constant of the equivalent SMIB system; M_T is the sum of the inertia constants of the total number of the generators; P_m and P_e are the mechanical input power and the electrical output power of the equivalent SMIB system, and B and G are the susceptance and conductance of the network, respectively [42].

A.2 Least Squares [1]

The least square method is the standard approach for regression analysis. Given a set of measurements expressed as the following taken at regular intervals,

$$a + b\,t_1 = c_1 \tag{A.16}$$

$$a + b\,t_2 = c_2 \tag{A.17}$$

$$a + b\,t_3 = c_3 \tag{A.18}$$

$$\text{.....} \tag{A.19}$$

$$a + b\,t_n = c_n \tag{A.20}$$

where c is the measurement; t is the time; a and b are the parameters to estimated.

Then, the error of the estimations to the measurements are

$$\bar{a} + \bar{b}\,t_1 - c_1 = d_1 \tag{A.21}$$

$$\bar{a} + \bar{b}\,t_2 - c_2 = d_2 \tag{A.22}$$

$$\bar{a} + \bar{b}\,t_3 - c_3 = d_3 \tag{A.23}$$

$$\text{.....} \tag{A.24}$$

$$\bar{a} + \bar{b}\,t_n - c_n = d_n \tag{A.25}$$

where d is the estimated error; $\bar{a}$ and $\bar{b}$ are the parameters estimated.

Denoted in matrix forms,

$$\big[T\big]\big[\bar{x}\big] - \big[C\big] = \big[D\big] \tag{A.26}$$

where $[T]$ is $\begin{bmatrix} 1 & t_1 \\ 1 & t_2 \\ 1 & t_3 \\ \text{.....} & \\ 1 & t_n \end{bmatrix}$; $[\bar{x}]$ is $\begin{bmatrix} \bar{a} \\ \bar{b} \end{bmatrix}$; $[c]$ is $\begin{bmatrix} c_1 \\ c_2 \\ c_3 \\ \text{.....} \\ c_n \end{bmatrix}$; $[d]$ is $\begin{bmatrix} d_1 \\ d_2 \\ d_3 \\ \text{.....} \\ d_n \end{bmatrix}$.

The sum of error squares is

$$\begin{bmatrix} d_1 & d_2 & d_3 & ... & d_n \end{bmatrix} \begin{bmatrix} d_1 \\ d_2 \\ d_3 \\ ..... \\ d_n \end{bmatrix} = \begin{bmatrix} {d_1}^2 + {d_2}^2 + {d_3}^2 + ... + {d_n}^2 \end{bmatrix} \tag{A.27}$$

It equals to

$$[D]^T[D] = \Big[[T][x] - [C]\Big]^T \Big[[T][x] - [C]\Big] \tag{A.28}$$

$$= \Big[[x]^T[T]^T[T][x]\Big] - 2[x]^T[T]^T[C] + [C]^T[C] \tag{A.29}$$

The sum of the error squares is minimum, if

$$\frac{d}{d[x]}\Big\{[D]^T[D]\Big\} = \frac{d}{d[x]}\Big\{\Big[[x]^T[T]^T[T][x]\Big] - 2[x]^T[T]^T[C] + [C]^T[C]\Big\} = 0 \tag{A.30}$$

Since

$$\frac{d[x]^T}{d[x]} = \frac{d[\bar{a},\ \bar{b}]^T}{d\begin{bmatrix}\bar{a} \\ \bar{b}\end{bmatrix}} = \begin{bmatrix} 1 & 0 \\ 0 & 1 \end{bmatrix} \tag{A.31}$$

Then

$$\frac{d}{d[x]}\Big[2[x]^T[T]^T[C]\Big] = 2[T]^T[C] \tag{A.32}$$

and

$$\frac{d}{d[x]}\Big[[x]^T[T]^T[T][x]\Big] = 2[T]^T[T][x] \tag{A.33}$$

From Equation A.30

$$[T]^T[T][x] = [T]^T[C] \tag{A.34}$$

Therefore

$$[x] = \Big[[T]^T[T]\Big]^{-1}[T]^T[C] \tag{A.35}$$

A.3 Power Flow

The exchange of energy is expressed in terms of the interaction of electric and magnetic fields in the fundamental theory of the transmission of energy, however people are more concerned with the rate of change of energy with respect to time in terms of voltage and current [13]. The instantaneous power delivered to a load is the product of instantaneous voltage and current as the following equation.

$$p(t) = v(t)i(t) = 2VI\cos(\omega t + \theta_v)\cos(\omega t + \theta_i) \tag{A.36}$$

where $v(t) = \sqrt{2}V\cos(\omega t + \theta_v)$; $i(t) = \sqrt{2}I\cos(\omega t + \theta_i)$; V is the root-mean-square value of $v(t)$; I is the root-mean-square value of $i(t)$; θ_v is the voltage phase angle; θ_i is the current phase angle.

Since

$$\cos A\cos B = \frac{1}{2}\cos(A+B) + \frac{1}{2}\cos(A-B) \tag{A.37}$$

Thus,

$$\cos(\omega t + \theta_v)\cos(\omega t + \theta_i) = \frac{1}{2}\cos(\theta_v - \theta_i) + \frac{1}{2}\cos(2\omega t + \theta_v + \theta_i) \tag{A.38}$$

and

$$\cos(2\omega t + \theta_v + \theta_i) = \cos(2\omega t + 2\theta_v)\cos(\theta_v - \theta_i) + \sin(2\omega + 2\theta_v)\sin(\theta_v - \theta_i) \tag{A.39}$$

The instantaneous power will be expressed as

$$p(t) = VI[\cos(\theta_v - \theta_i) + \cos(2\omega t + 2\theta_v)\cos(\theta_v - \theta_i) + \sin(2\omega t + 2\theta_v)\sin(\theta_v - \theta_i)] \tag{A.40}$$

If a phase angle is defined as $\theta = \theta_v - \theta_i$, the Equation A.40 can be rewritten as

$$p(t) = VI\cos\theta[1 + \cos 2(\omega t + \theta_v)] + VI\sin\theta\sin 2(\omega t + \theta_v) \tag{A.41}$$

The first term of Equation A.41 is the instantaneous power on a resistive load. Neglecting its transient variation, the instantaneous power on a resistive load or the active power can

be expressed as

$$P = VI\cos\theta \tag{A.42}$$

The second term of Equation A.41 is the instantaneous power exchanged on an inductive load. Its amplitude is called the reactive power in the formulation of the following,

$$Q = VI\sin\theta \tag{A.43}$$

In the active and the reactive power Equation A.42 and A.43, θ is positive for an inductive load, i.e. the voltage is leading the current by θ, and θ is negative for an capacitive load, i.e. the voltage is lagging the current by θ.

A.4 Numerical Impedance Calculation

In Section 3.2.3 the phase one of TZB algorithm is calculating the SMIB sequivalent system impedance. The Laguerre's method is employed for numerically polynomial root finding, which is finding the impedance Z in Equation 3.17.

In numerical analyses, Laguerre's method can be used to solve the equation $q(z) = 0$ [91] [92]. Laguerre's method is the most straightforward general complex method, which is almost guaranteed to converge to a root of the polynomial from any initial starting point.

The general form of polynomial can be written as

$$q(z) = (z - z_1)(z - z_2)...(z - z_n) \tag{A.44}$$

After taking the natural logarithm on both side of the equation,

$$ln\big|q(z)\big| = ln\big|(z - z_1)\big| + ln\big|(z - z_2)\big| + ... + ln\big|(z - z_n)\big| \tag{A.45}$$

Applying derivative by

$$E = \frac{d}{dz} ln\big|q(z)\big| \tag{A.46}$$

$$= \frac{1}{(z - z_1)} + \frac{1}{(z - z_2)} + ... + \frac{1}{(z - z_n)} \tag{A.47}$$

$$= \frac{q'(z)}{q(z)}, \tag{A.48}$$

The second derivative by

$$F = -\frac{d^2}{dz^2} ln\big|q(z)\big| \tag{A.49}$$

$$= \frac{1}{(z - z_1)^2} + \frac{1}{(z - z_2)^2} + ... + \frac{1}{(z - z_n)^2} \tag{A.50}$$

$$= \left(\frac{q'(z)}{q(z)}\right)^2 - \frac{q''(z)}{q(z)}, \tag{A.51}$$

The assumption is taken that the root z_1 is away from the initial guess z for a distance a, and all other roots are clustered a distance b away from the root. Therefore, Equation

A.46 and A.49 can be written as

$$E = \frac{1}{a} + \frac{n-1}{b}, \tag{A.52}$$

and

$$F = \frac{1}{a^2} + \frac{n-1}{b^2} \tag{A.53}$$

Solving the E and F equations for a,

$$a = \frac{n}{E \pm \sqrt{(n-1)(nF - E^2)}} \tag{A.54}$$

The method operates starting with an initial guess of root z_0. E and F are obtained based on the given z_0. The distance a of the guess root to the actual root z_1 is calculated iteratively unless becoming small enough within tolerance or the maximum number of iteration is reached.

If z is a simple root of polynomial of $q(z)$, it is reported that the Laguerre's method converges cubically [93]. This is a favourable feature well suitable for distance relay timely operation.

Appendix B

Models with System Data and DQ0 Transformation

B.1 SMIB Test System Setup

Table B.1: PSCAD Single Machine Infinite Bus Test System Data

Base MVA	2220
Base kV	24
Generator data	$2220\,MVA$, $24\,kV$, $60\,Hz$, $H = 3.5\,s$, $r_A = 0.00125\,p.u.$, $x_l = 0.163\,p.u.$, $x_d = 1.81\,p.u.$, $x_q = 1.76\,p.u.$, $x'_d = 0.3 p.u.$, $x'_q = 0.65 p.u.$, $x''_d = 0.23 p.u.$, $x''_q = 0.25 p.u.$, $T'_{d0} = 8s$, $T''_{d0} = 0.03s$, $T'_{q0} = 1s$, $T''_{q0} = 0.07s$
Impedance data	$X_1 = j0.15\,p.u.$, $TL_I = j0.5\,p.u.$, $TL_{II} = j1.0\,p.u.$
Infinite Bus Voltage	$0.9\,p.u.$

B.2 SMIB Test System PSAT Model

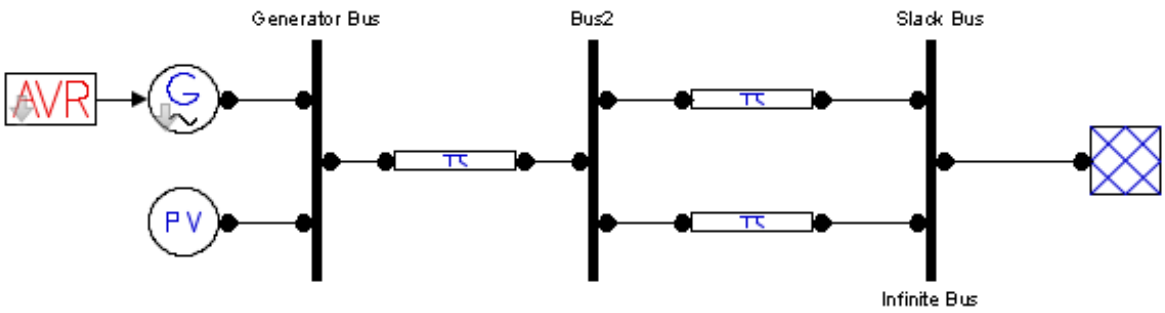

Figure B.1: PSAT Equivalent SMIB system for Load Flow analysis (generated from PSAT^{TM}).

B.3 SMIB Test System Load Flow Data

Table B.2: SMIB Test System Load Flow Analysis Results Data.

Bus No.	Type	Voltage	Load		Generator	
			MW	MVar	MW	MVar
Generator	PV	1.0	0.0	0.0	0.8	4.6
2	PQ	0.97	0.0	0.0	0.0	0.0
Slack	PV	0.9	0.0	0.0	-0.8	-4.1

B.4 SMIB Test System PSCAD Model

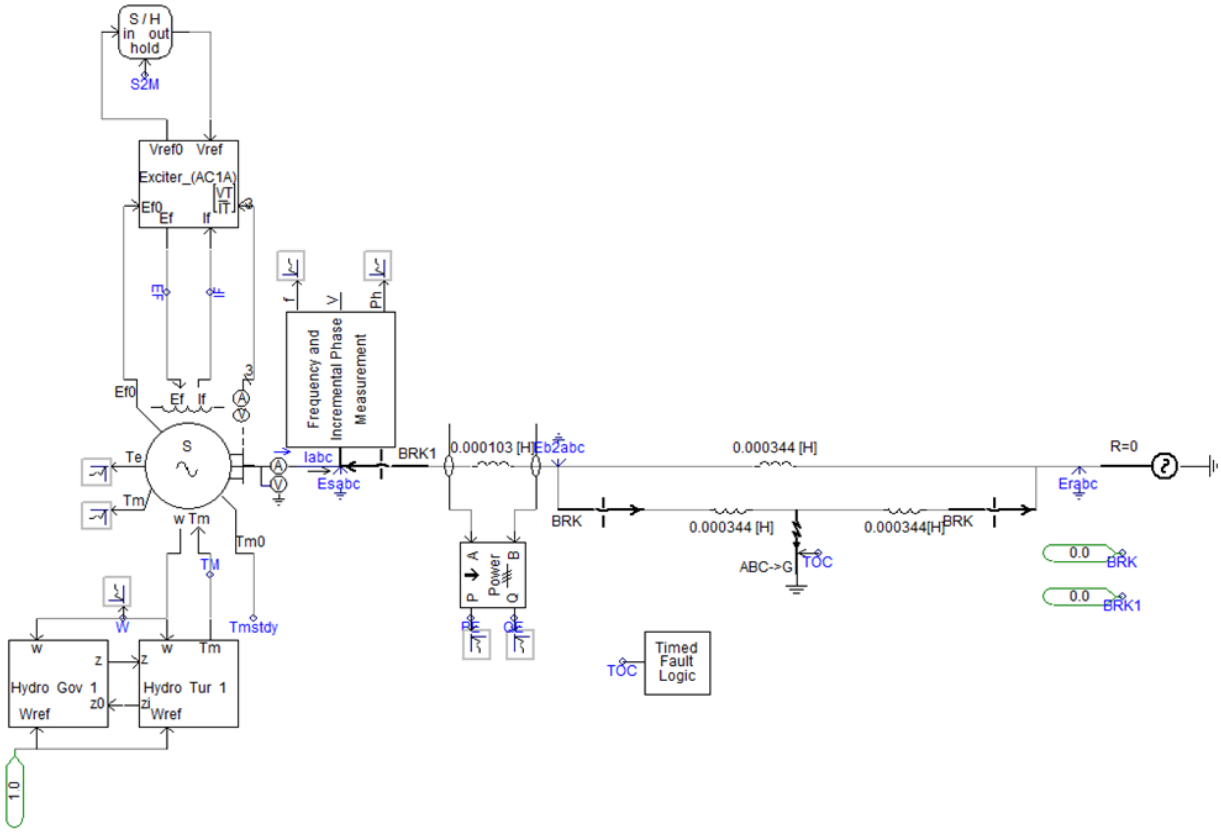

Figure B.2: PSCAD SMIB system for TZB algorithm study (created in PSCAD^{TM}).

B.5 dq0 Transformation

The electrical performance of a synchronous machine is completely described by stator circuit voltage equations, stator flux linkage equations, and rotor circuit flux linkage equations. The inductances in these equations have angle terms changing with time, which induces complexity in machine and power system analyses. $dq0$ transformation converts these complex equations into simple forms of expressions of stator variables.

The stator phase currents are expressed into currents on direct and quadrature axis as follows.

$$i_d = k_d \left[i_a \cos\theta + i_b \cos(\theta - \frac{2\pi}{3}) + i_c \cos(\theta + \frac{2\pi}{3}) \right], \tag{B.1}$$

$$i_q = -k_q \left[i_a \sin\theta + i_b \sin(\theta - \frac{2\pi}{3}) + i_c \sin(\theta + \frac{2\pi}{3}) \right], \tag{B.2}$$

where k_d k_q are the dq constants equal to 2/3.

In a three phase balanced condition,

$$i_a = I_m \sin\omega_s t, \tag{B.3}$$

$$i_b = I_m \sin(\omega_s t - \frac{2\pi}{3}), \tag{B.4}$$

$$i_c = I_m \sin(\omega_s t + \frac{2\pi}{3}), \tag{B.5}$$

i_a i_b i_c are substituted into Equation B.1 and it becomes

$$i_d = k_d \left[I_m \sin\omega_S t \cos\theta + I_m \sin(\omega_S t - \frac{2\pi}{3}) \cos(\theta - \frac{2\pi}{3}) + I_m \sin(\omega_S t + \frac{2\pi}{3}) \cos(\theta + \frac{2\pi}{3}) \right] \tag{B.6}$$

$$= k_d \frac{3}{2} I_m \sin(\omega_s t - \theta) \tag{B.7}$$

$$= I_m \sin(\omega_s t - \theta) \tag{B.8}$$

Similarly, Equation B.2 becomes

$$i_q = -k_q \frac{3}{2} I_m \cos(\omega_s t - \theta) \tag{B.9}$$

$$= -I_m \cos(\omega_s t - \theta) \tag{B.10}$$

The third component is defined as the zero sequence current i_0 expressed as

$$i_0 = \frac{1}{3}(i_a + i_b + i_c), \tag{B.11}$$

where i_0 equals to zero in a balanced condition.

Therefore,

$$\begin{bmatrix} i_d \\ i_q \\ i_0 \end{bmatrix} = \frac{2}{3} \begin{bmatrix} \cos\theta & \cos(\theta - \frac{2\pi}{3}) & \cos(\theta + \frac{2\pi}{3}) \\ \sin\theta & \sin(\theta - \frac{2\pi}{3}) & \sin(\theta + \frac{2\pi}{3}) \\ \frac{1}{2} & \frac{1}{2} & \frac{1}{2} \end{bmatrix} \begin{bmatrix} i_a \\ i_b \\ i_c \end{bmatrix} \tag{B.12}$$

The inverse transformation is expressed as

$$\begin{bmatrix} i_a \\ i_b \\ i_c \end{bmatrix} = \begin{bmatrix} \cos\theta & -\sin\theta & 1 \\ \cos(\theta - \frac{2\pi}{3}) & -\sin(\theta - \frac{2\pi}{3}) & 1 \\ \cos(\theta + \frac{2\pi}{3}) & -\sin(\theta + \frac{2\pi}{3}) & 1 \end{bmatrix} \begin{bmatrix} i_d \\ i_q \\ i_0 \end{bmatrix} \tag{B.13}$$

From Equation B.13

$$i_a = I_m \sin\omega_s t \tag{B.14}$$

$$= I_m \sin(\omega_s t - \theta)\cos\theta + I_m \cos(\omega_s t - \theta)\sin\theta \tag{B.15}$$

$$= i_d \cos\theta - i_q \sin\theta \tag{B.16}$$

The same transformations can be applied to stator flux linkage and voltage equations such as derived in [94] [95] and [96].

The resulting $dq0$ and flux linkage equations are given as the followings

$$\Psi_d = -L_d i_d + L_{af} i_f \tag{B.17}$$

$$\Psi_q = -L_q i_q \tag{B.18}$$

$$\Psi_f = -\frac{3}{2} L_{af} i_d + L_{ff} i_f \tag{B.19}$$

$$\Psi_0 = -L_0 i_0 \tag{B.20}$$

where Ψ_d Ψ_q Ψ_0 are the armature flux linkages reflecting on $dq0$ axis; Ψ_f is the rotor circuit flux linkage; L_d is the direct-axis armature inductance; L_q is the quadrature-axis armature inductance; L_0 is the zero-sequence inductance; L_{af} is the mutual inductance between the field winding and the phase a; L_{ff} is the field winding self-inductance.

The resulting $dq0$ and rotor circuit voltage equations are given as the followings

$$e_d = \dot{\Psi}_d - \Psi_q \omega - R_a i_d \tag{B.21}$$

$$e_q = \dot{\Psi}_q + \Psi_d \omega - R_a i_q \tag{B.22}$$

$$e_0 = \dot{\Psi}_0 - R_a i_0 \tag{B.23}$$

$$e_f = \dot{\Psi}_f + R_f i_f \tag{B.24}$$

where e_d e_q e_0 are the armature voltages reflecting on $dq0$ axis; e_f is the rotor circuit voltage; R_a is the armature resistance; ω is the angular velocity of the machine rotor.

The rotor angular motion can be expressed with Swing Equation as

$$\dot{\delta} = \omega \tag{B.25}$$

$$\dot{\omega} = \frac{1}{2H}(T_m - T_e) \tag{B.26}$$

where δ is the synchronous machine power angle; T_m is the machine mechanical torque supplied by the prime mover; $T_e = \Psi_d i_q - \Psi_q i_d$, the net electrical or electromagnetic torque; H is the inertia H constant.

The dynamics of a synchronous machine can be fully expressed with the aforementioned equations.

B.6 PSAT Modified WSCC Test System

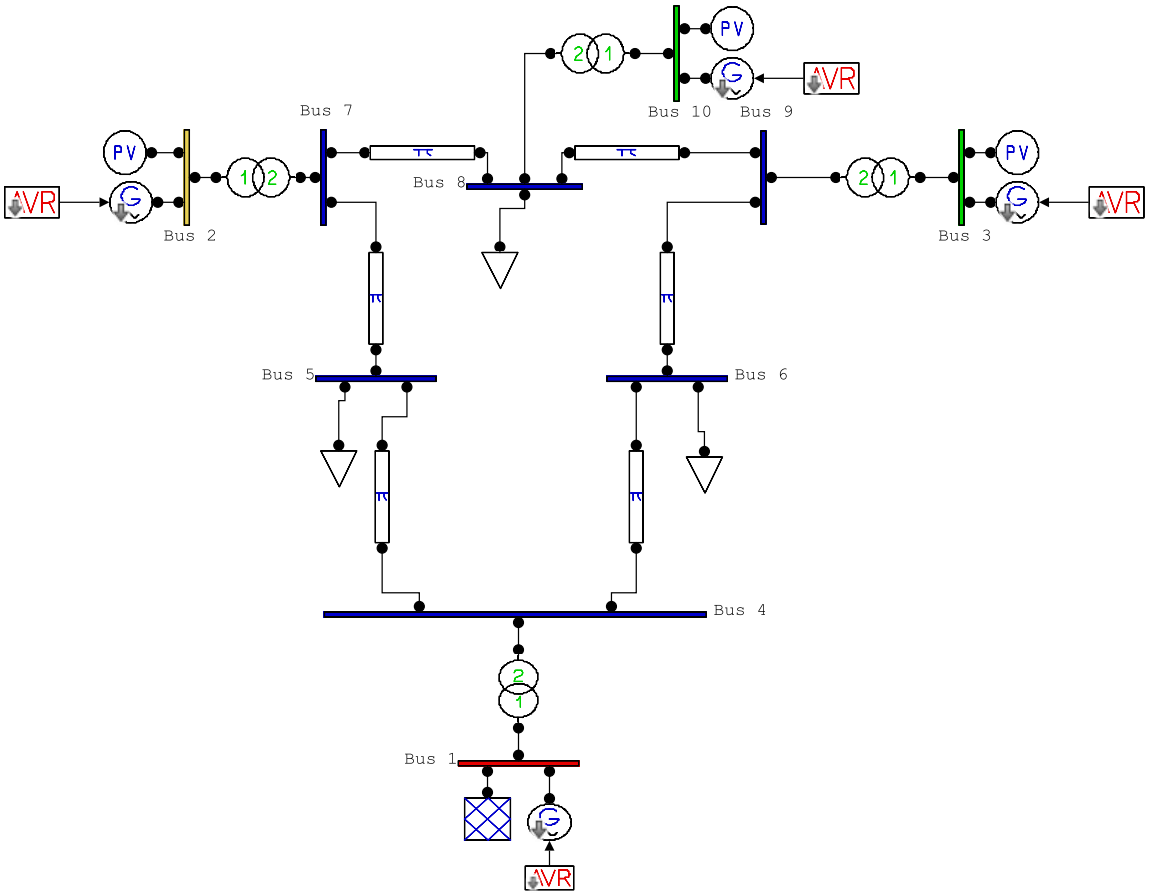

Figure B.3: PSAT Modified WSCC Test system for TZB algorithm study(created in PSAT^{TM}).

B.7 PSAT Modified WSCC Test System Setup

Table B.3: Parameters of Generators and Transformers For Modified WSCC System in PSAT.

Base MVA	100			
Base kV	230			
		Generator		
No.	1	2	3	4
Rated MVA	60.5	60.0	60.0	250.0
Voltage (kV)	16.5	18.0	13.8	13.8
Type	hydro	steam	steam	steam
Speed (r/min)	1800	3600	3600	3600
$x_d(pu)$	0.1460	0.8958	1.3125	1.3125
$x'_d(pu)$	0.0608	0.1198	0.1813	0.1813
$x_q(pu)$	0.0969	0.8645	1.2578	1.2578
$x'_q(pu)$	0.0969	0.1969	0.25	0.25
$x_l(pu)$ (leakage)	0.0336	0.0521	0.0742	0.0742
$r'_{d0}(pu)$	8.96	6.00	5.89	5.89
$r'_{q0}(pu)$	0	0.535	0.600	0.600
		Transformer		
No.	1	2	3	4
Voltage (kV)	16.5/230	18.0/230	13.8/230	13.8/230
$x_T(pu)$	0.576	0.0625	0.0586	0.0586

Table B.4: Parameters of Transmission Lines and Loads in relay R98 study For Modified WSCC System in PSAT.

Base MVA	100					
Base kV	230					
T-Lines						
No.	1	2	3	4	5	6
Bus Connection	9 - 8	7 - 8	9 - 6	7 - 5	5 - 4	6 - 4
$x_L(pu)$	0.1008	0.288	0.170	0.161	0.085	0.092
$r_L(pu)$	0.0119	0.034	0.039	0.032	0.010	0.017
$B/2(pu)$	0.1045	0.298	0.179	0.153	0.088	0.079
Loads						
No.	1		2		3	
$Q_{LD}(pu)$	0.30		0.35		0.50	
$P_{LD}(pu)$	0.90		1.00		1.25	

Table B.5: Parameters of Transmission Lines and Loads in relay R78 study For Modified WSCC System in PSAT.

Base MVA	100					
Base kV	230					
T-Lines						
No.	1	2	3	4	5	6
Bus Connection	9 - 8	7 - 8	9 - 6	7 - 5	5 - 4	6 - 4
$x_L(pu)$	0.3024	0.0720	0.170	0.161	0.085	0.092
$r_L(pu)$	0.0357	0.0085	0.039	0.032	0.010	0.017
$B/2(pu)$	0.3135	0.0745	0.179	0.153	0.088	0.079
Loads						
No.	1		2		3	
$Q_{LD}(pu)$	0.30		0.35		0.50	
$P_{LD}(pu)$	0.90		1.00		1.25	

B.8 RTDS Modified WSCC Test System

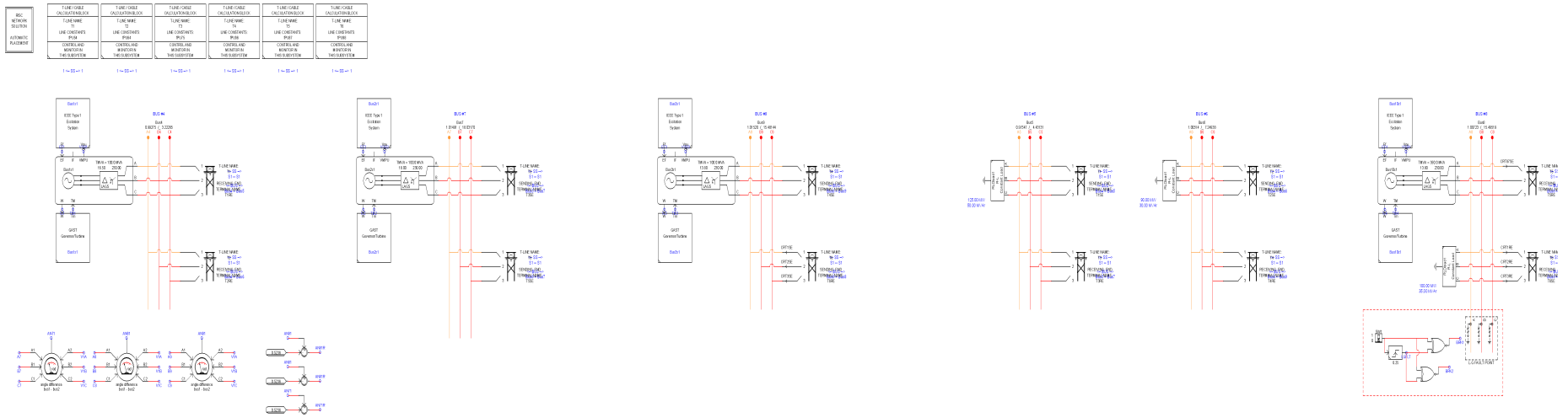

Figure B.4: RTDS Modified WSCC Test system for TZB algorithm study(created in RTDS^{TM}).

B.9 RTDS Modified WSCC Test System Setup

Table B.6: Parameters of Generators and Transformers For Modified WSCC System in RTDS.

Base MVA	100			
Base kV	230			
		Generator		
No.	1	2	3	4
Rated MVA	60.5	60.0	60.0	400.0
Voltage (kV)	16.5	18.0	13.8	13.8
Type	gas	gas	gas	gas
Speed (r/min)	1800	3600	3600	3600
$x_d(pu)$	0.1460	0.8958	1.3125	1.3125
$x'_d(pu)$	0.0608	0.1198	0.1813	0.1813
$x_q(pu)$	0.0969	0.8645	1.2578	1.2578
$x'_q(pu)$	0.0969	0.1969	0.25	0.25
$x_l(pu)$ (leakage)	0.0336	0.0521	0.0742	0.0742
$r'_{d0}(pu)$	8.96	6.00	5.89	5.89
$r'_{q0}(pu)$	0	0.535	0.600	0.600
		Transformer		
No.	1	2	3	4
Voltage (kV)	16.5/230	18.0/230	13.8/230	13.8/230
$x_T(pu)$	0.576	0.0625	0.0586	0.0586

Table B.7: Parameters of Transmission Lines and Loads For Modified WSCC System in RTDS.

Base MVA	100					
Base kV	230					
CHUKAR Transmission Lines						
No.	1	2	3	4	5	6
Bus Connection	9 - 8	7 - 8	9 - 6	7 - 5	5 - 4	6 - 4
Length(km)	230.4	658.5	388.7	368.1	194.4	210.4
Loads						
No.	1		2		3	
$R_{LD}(ohm)$	422.5		422.5		661.3	
$L_{LD}(H)$	17.0		17.0		264.5	

Appendix C

Modified WSCC system Load Flow Data and DFT Transform

C.1 RTDS Modified WSCC Test System Load Flow Data

Table C.1: RTDS Modified WSCC Test System Load Flow Analysis Results.

Bus No.	Type	Voltage	Load		Generator		Unit No.
			MW	MVar	MW	MVar	
1	PV	1.00	0.00	0.00	71.63	27.92	Gen1
2	PV	1.00	0.00	0.00	163.00	4.90	Gen2
3	PV	1.00	0.00	0.00	85.00	-11.45	Gen3
4	PQ	0.99	0.00	0.00	0.00	0.00	
5	PQ	1.00	68.96	32.00	0.00	0.00	
6	PQ	1.02	124.98	4.98	0.00	0.00	
7	PQ	1.01	0.00	0.00	0.00	0.00	
8	PQ	1.01	124.98	4.98	0.00	0.00	
9	PQ	1.02	0.00	0.00	0.00	0.00	
10	PV	1.00	0.00	0.00	85.00	-11.45	Gen4

C.2 PSAT Modified WSCC Test System Load Flow Data

Table C.2: PSAT Modified WSCC Test System Load Flow Analysis Results.

Bus No.	Type	Voltage	Load		Generator		Unit No.
			MW	MVar	MW	MVar	
1	PV	1.040	0.00	0.00	87.76	25.56	Gen1
2	PV	1.025	0.00	0.00	163.00	29.07	Gen2
3	PV	1.025	0.00	0.00	85.00	-9.98	Gen3
4	PQ	1.027	0.00	0.00	0.00	0.00	
5	PQ	0.996	125.00	50.00	0.00	0.00	
6	PQ	1.015	90.00	30.00	0.00	0.00	
7	PQ	1.028	0.00	0.00	0.00	0.00	
8	PQ	1.015	200.00	35.00	0.00	0.00	
9	PQ	1.015	0.00	0.00	0.00	0.00	
10	PV	1.032	0.00	0.00	85.00	19.68	Gen4

C.3 Discrete Fourier Transform Technique

The Fourier Transform (FT) technique is applied for estimating the magnitude and phase angle of a phasor in the continuous domain, such as:

$$I_p \cos(\theta) = \frac{1}{\pi} \int_0^{2\pi} I_p \sin(\omega t + \theta) \big[\sin(\omega t) \big] d\omega t \tag{C.1}$$

$$I_p \sin(\theta) = \frac{1}{\pi} \int_0^{2\pi} I_p \sin(\omega t + \theta) \big[\cos(\omega t) \big] d\omega t \tag{C.2}$$

The above formulations can be derived by the following trigonometric manipulation

$$\sin(\omega t + \theta) \sin(\omega t) = \frac{1}{2} \big[\cos\theta - \cos(2\omega t + \theta) \big] \tag{C.3}$$

and

$$\frac{1}{\pi} \int_0^{2\pi} I_p \sin(\omega t + \theta) \big[\sin(\omega t) \big] d\omega t = \frac{1}{\pi} \int_0^{2\pi} \frac{1}{2} I_p \big[\cos\theta - \cos(2\omega t + \theta) \big] d\omega t \tag{C.4}$$

$$= I_p \cos\theta \tag{C.5}$$

The equations can be represented in the discrete form by replacing integration by summation. The real and the imaginary component of the phasor can be expressed as

$$I_p \cos(\theta) = \frac{2}{N} \sum_{k=m-N}^{k=m-1} i_k \sin \big[(k + N - m) \omega \Delta t) \big] \tag{C.6}$$

$$I_p \sin(\theta) = \frac{2}{N} \sum_{k=m-N}^{k=m-1} i_k \cos \big[(k + N - m) \omega \Delta t) \big] \tag{C.7}$$

where N is the number of samples in a data window; m is the present sample number; i_k is the instantaneous value of the phasor. The magnitude and phase angle of the phasor can be therefore obtained.